Structure-preserving simulation of highly flexible slender structures via port-Hamiltonian systems

Zur Erlangung des akademischen Grades eines

DOKTORS DER INGENIEURWISSENSCHAFTEN (Dr.-Ing.)

von der KIT-Fakultät für
Bauingenieur-, Geo- und Umweltwissenschaften des
Karlsruher Instituts für Technologie (KIT)

genehmigte

DISSERTATION

von

P. L. Kinon, M. Sc.
aus Neuwied

Tag der mündlichen Prüfung: 22.05.2026

Hauptreferent: Prof. Dr.-Ing. habil. Peter Betsch
Korreferent: Prof. Dr. Robert Altmann

Karlsruhe 2026

Die Löcher sind die Hauptsache
An einem Sieb.

— J. Ringelnatz

Abstract

Highly flexible slender structures occur in many engineering applications and in nature. However, the accurate and efficient simulation of their dynamics remains a challenging task. Due to geometric nonlinearities and complex material behavior, conventional numerical methods may violate fundamental physical principles, such as the conservation of total energy. This can lead to numerical instabilities and reduced accuracy in long-term simulations. To address this issue, this thesis employs the port-Hamiltonian (pH) framework and exploits its unifying structure to develop novel modeling and discretization approaches with guaranteed energetic consistency.

First, the fundamental properties of pH systems are discussed, and a general framework capable of representing nonlinear partial differential-algebraic equations is established. Within this unified setting, novel formulations for the dynamics of geometrically exact beams and strings are derived. These formulations rely on independent strain and/or stress variables that are linked to the kinematics via compatibility equations in time-differentiated form. This results in mixed descriptions that naturally prevent numerical problems such as transverse shear locking. The same framework accommodates hyperelastic and viscoelastic material behavior, actuation mechanisms relevant in soft robotics, as well as kinematic constraints.

Second, structure-preserving discretization strategies in space and time are addressed within the pH setting. A mixed Bubnov–Galerkin finite element discretization in space based on standard Lagrange polynomials yields finite-dimensional systems that retain the pH structure. The resulting semi-discrete models, most generally governed by differential-algebraic equations, are objective and preserve the underlying power balance. Concerning time integration, the structural properties of the Hamiltonian — the total energy function — determine the suitable approach. In the case of quadratic Hamiltonians, the implicit midpoint rule is sufficient to ensure exact satisfaction of discrete-time power and momentum balance equations. For general Hamiltonians, newly developed discrete gradient methods provide the same properties.

Overall, the pH formalism provides a new perspective on the dynamics of mechanical systems and related numerical challenges that have been studied for decades. In a unified pH framework, the design of structure-preserving spatial and temporal discretization methods is systematically guided by the underlying power balance. Preserving the pH structure throughout the discretization procedure leads to energetic consistency and improved robustness, making the proposed methods well suited for long-term simulations and future use in advanced control design.

Keywords: Computational dynamics • Nonlinear beam theory • Infinite-dimensional port-Hamiltonian systems • Differential-algebraic equations • Structure-preserving numerical methods • Mixed finite element methods • Discrete gradient schemes • Flexible multibody systems.

Kurzfassung

Hochflexible und schlanke mechanische Strukturen treten in zahlreichen technischen Anwendungen sowie in der Natur auf. Ihre akkurate und zugleich effiziente Simulation stellt jedoch nach wie vor eine erhebliche Herausforderung dar. Geometrische Nichtlinearitäten und komplexes Materialverhalten können dazu führen, dass konventionelle numerische Verfahren grundlegende physikalische Prinzipien, wie die Erhaltung der Gesamtenergie, verletzen. Insbesondere bei Langzeitsimulationen kann dies numerische Instabilitäten und eine verminderte Genauigkeit zur Folge haben. Vor diesem Hintergrund basiert die vorliegende Arbeit auf port-Hamiltonschen (pH) Systemen. Deren vereinheitlichende Struktur dient als Grundlage für die Entwicklung neuartiger, energetisch konsistenter Modellierungs- und Simulationsansätze.

Zunächst werden grundlegende Eigenschaften von pH Systemen erläutert und ein allgemeines pH Modell vorgestellt, das nichtlineare partielle differential-algebraische Gleichungen erfasst. Darauf aufbauend werden neue Formulierungen für geometrisch exakte Balken und Seile entwickelt. Die Modelle verwenden unabhängige Dehnungs- und/oder Spannungsgrößen, die über Kompatibilitätsbedingungen in zeitlich differenzierter Form mit der Kinematik verknüpft sind. Hieraus ergeben sich gemischte Formulierungen, die numerische Probleme wie das transversale Schublocking auf natürliche Weise vermeiden. Des Weiteren lassen sich hyperelastisches und viskoelastisches Materialverhalten, Aktuierungsmechanismen der Soft Robotics sowie kinematische Nebenbedingungen unmittelbar berücksichtigen.

In diesem pH Framework wird anschließend die strukturerhaltende Diskretisierung in Raum und Zeit behandelt. Hierzu wird eine gemischte Bubnov–Galerkin Finite-Elemente-Raumdiskretisierung auf Basis von Lagrange-Polynomen vorgeschlagen, die zu endlichdimensionalen pH Systemen führt. Die resultierenden semidiskreten Modelle, welche im Allgemeinen durch differential-algebraische Gleichungen beschrieben werden, sind objektiv und bewahren die zugrundeliegende Energiebilanz. Für die Zeitintegration von Systemen mit quadratischer Hamilton-Funktion gewährleistet bereits die implizite Mittelpunktregel exakte zeitdiskrete Energie- und Impulsbilanzgleichungen. Bei Systemen mit allgemeineren Hamilton-Funktionen kommen neu gewonnene Diskrete-Gradienten-Verfahren zum Einsatz, die dieselben Eigenschaften besitzen.

Insgesamt führt der pH Formalismus zu einer neuen Perspektive auf dynamische Problemstellungen in der Mechanik und die damit verbundenen numerischen Herausforderungen. Die Entwicklung strukturerhaltender räumlicher und zeitlicher Diskretisierungsmethoden erfolgt dabei konsequent unter Berücksichtigung der zugrundeliegenden Energiebilanz. Die durchgängige Bewahrung der pH Struktur im Diskretisierungsprozess gewährleistet energetische Konsistenz und erhöhte Robustheit. Dadurch eignen sich die vorgeschlagenen Methoden insbesondere für Langzeitsimulationen sowie für zukünftige Anwendungen im Regelungsentwurf.

Schlüsselwörter: Computergestützte Dynamik • Nichtlineare Balkentheorie • Unendlich-dimensionale port-Hamiltonsche Systeme • Differential-algebraische Gleichungen • Strukturerhaltende numerische Methoden • Gemischte Finite-Elemente-Methoden • Diskrete-Gradienten-Verfahren • Flexible Mehrkörpersysteme.

Acknowledgments

I would like to express my gratitude to all those who have accompanied me over the past years.

First, I thank Peter Betsch for supervising this thesis and for his guidance and support throughout my studies and doctoral research. I am especially grateful for the freedom he gave me to pursue my own ideas while always providing insightful advice whenever it was needed. My special thanks go to Robert Altmann for serving as second examiner of this thesis. A memorable part of my doctoral studies was the time spent in Eindhoven. I am grateful to Simon R. Eugster for his hospitality, mentorship, and for providing new perspectives on mechanics. My sincere thanks go to Thomas Seelig for sparking my interest in mechanics, and to Markus Uhlmann for chairing the examination committee and providing insightful lectures that enriched my studies.

Moreover, I am indebted to Tobias Thoma and Paul Kotyczka for the fruitful collaboration through which I learned a great deal about port-Hamiltonian systems. I thank Riccardo Morandin and Philipp Schulze for the enjoyable collaboration and the many insightful discussions on differential-algebraic equations and discrete gradient methods. I would also like to acknowledge Max Herrmann, Maximilian Mogler, Marco Herrmann, Tianxiang Dai, Andrea Brugnoli, Dorothea Hinsen, Giuseppe Capobianco, and Manuel Schaller, as well as many others, for the enjoyable conference experiences and stimulating discussions. A special thank you goes to Lisa Latussek for the many opportunities for mutual learning, both professionally and beyond. I am grateful to Julian Karl Bauer for being a reliable climbing partner and for many engaging discussions on a wide range of topics. My sincere appreciation goes to everyone who took the time to read parts of this thesis and provided valuable comments and corrections. Their careful feedback helped improve the clarity of the work.

In addition, I wish to express my gratitude to the team of the Institute of Mechanics. In particular, I thank Marvin May, Moritz Hille, Alexander Janz, Mark Schiebl, and Bianca Seith for their collegiality and for contributing to a pleasant working atmosphere throughout the years. My sincere thanks go to the organizers and participants of the multinational doctoral college workshops on port-Hamiltonian systems for fostering a vibrant community in which ideas, experiences, and knowledge could be shared openly. Likewise, I am grateful to the other GAMM Juniors and the members of the GAMM Student Chapter in Karlsruhe for creating opportunities for scientific and personal exchange. Special thanks also go to my colleagues in Eindhoven for creating a welcoming and stimulating research environment. I would like to acknowledge my student assistants. Working with them has been a valuable experience, and I have learned much through our exchange.

Finally, I would like to express my deepest gratitude to those who support my personal development and well-being. I am grateful to my friends for their support and encouragement, and for reminding me that life consists of much more than research, deadlines, and debugging sessions. I would like to thank my parents for their unconditional support from the very beginning. Dear Soph, thank you for being such a reliable partner with whom I have shared both the successes and challenges of the past, and with whom I look forward to the future.

Karlsruhe, June 2026 P. L. Kinon

Contents

1. Introduction

Flexible multibody systems play a central role in many engineering applications and in nature. When such systems include slender and highly flexible components, their dynamics become strongly nonlinear due to geometric effects and complex material behavior, posing significant challenges for modeling, simulation, and control strategies. Despite extensive research, the accurate and efficient simulation of such systems remains difficult. A key challenge lies in the development of structure-preserving numerical methods that respect fundamental physical principles of the underlying problem, thereby improving the quality of long-term simulations. Within this context, the present thesis investigates the notion of port-Hamiltonian systems, a promising framework from systems and control theory, as an alternative approach to the design of reliable simulation methods for highly flexible slender structures.

This chapter introduces the background and context of the research conducted in this thesis, and identifies existing research gaps. It formulates the emanating research aims, and outlines the main contributions of the work.

1.1. Background

The scope of this thesis lies at the intersection of three research areas: *Highly flexible slender structures*, *port-Hamiltonian systems*, and *structure-preserving discretization* methods, see Figure 1.1. From a broader perspective, this combination provides a coherent approach for tackling the challenges posed by multifaceted flexible multibody systems. Given the breadth of the involved research areas, this section presents the essential background and main context for this thesis by reviewing existing literature and

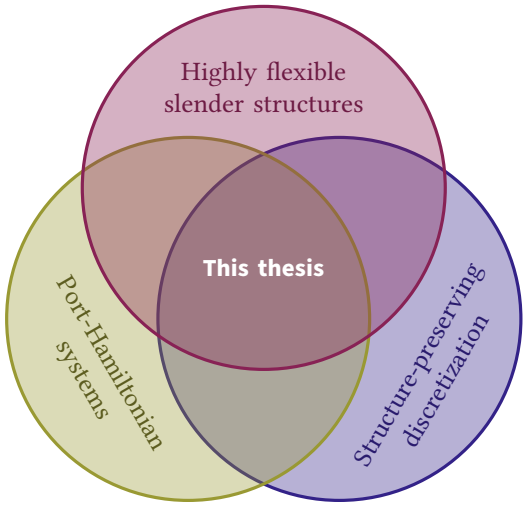

Figure 1.1.: Schematic illustration of the scope and research areas related to this thesis (inspired by [119]).

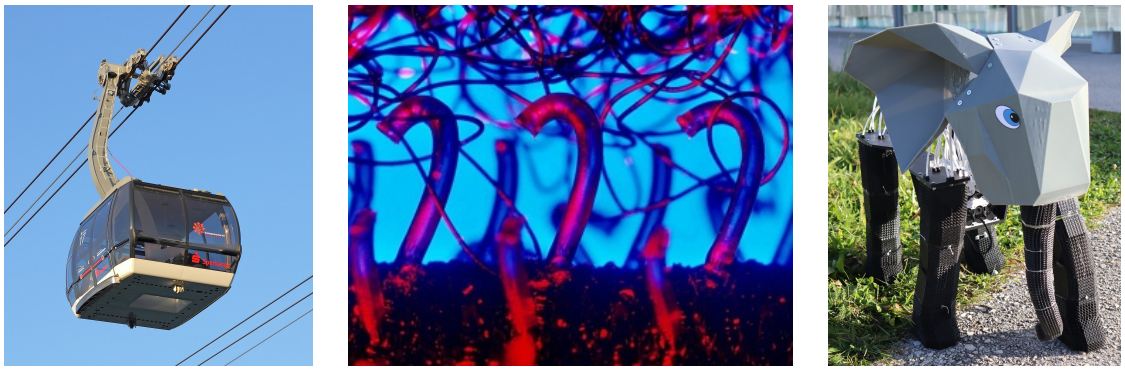

Figure 1.2.: A modern ropeway in Koblenz, Germany [198], the microstructure of a hook-and-loop fastener ("Velcro") [175], and a lattice structure elephant robot [95].

explaining relevant terminology. More comprehensive introductions and detailed literature reviews are provided in the main chapters.

Highly flexible slender structures. A multibody system can be understood as "a collection of bodies and interconnection elements", in which "joints constrain the relative motion of pairs of bodies" [203]. More specifically, *flexible* multibody systems are characterized by the presence of *deformable* bodies. These systems can be found in almost every part of our natural and technical environments. Examples include micro robotics [123] and soft robotics [2], textile manufacturing processes [233], sub-marine cables [238], cable-driven parallel robots [40], as well as numerous other applications from areas such as civil-engineering or aerospace technology. Exemplarily, Figure 1.2 shows the three examples of a ropeway system, a hook-and-loop fastener, and a musculoskeletal robot, all of which admit an interpretation as flexible multibody systems with deformable slender components.

The analysis of multibody systems is a well-established field that is documented in various textbooks [20, 203, 239]. Although models that are based on three-dimensional continuum mechanics accurately capture the behavior of flexible multibody components [82], their high computational cost often renders them unsuitable for practical use. Instead, slender structures, such as *beams* or *strings* [10], extend along a single spatial dimension[1], thus enabling more efficient computations while fully capturing their three-dimensional dynamics. Their slenderness and low resistance towards bending, potentially combined with complex material models and large deformations, render their dynamic behavior highly nonlinear and sensitive to modeling assumptions.

Correspondingly, it is not surprising that the mathematical description and numerical treatment of such highly flexible slender structures is particularly challenging and has attracted considerable interest[2]. Besides floating-frame-of-reference models (FFRM) [202], and absolute-nodal-coordinate formulations (ANCF) [83], also so-called *geometrically exact beam models* [10] have become particularly relevant for nonlinear structural and multibody dynamics[3]. While FFRM assume small elastic deformations relative to a rigid-body reference motion, ANCF beams may be more susceptible to numerical inaccuracies due to their volume-based modeling approach. In contrast, geometrically exact beam models accurately

[1] "A theory of rods is the characterization of the motion of slender solid bodies by a finite number of equations in which there is but one independent spatial variable. (The theory of strings [...] is thus an example of a theory of rods.)" [10, p. 95]

[2] The relevance of this field is, for instance, underlined by the recent foundation of the International Conference on Highly Flexible Slender Structures (HFSS).

[3] These models are also referred to as *Simo–Reissner beams* [187, 209] or *special Cosserat rods* [10]. Throughout this work, the terms *Cosserat rod* and *geometrically exact beam* are used interchangeably.

capture large displacements and rotations without assuming small strains a priori. Accordingly, we refer to them as *fully nonlinear* beam models, that accommodate both geometrical and material nonlinearities. Owing to these properties, geometrically exact beams have become highly influential [31, 33, 34, 53, 59, 61, 67, 69, 94, 102, 104, 105, 114, 133, 134, 139, 141, 143, 193, 235]. Beyond classical engineering applications, these models have lately gained increasing attention in soft and continuum robotics [3, 70, 195, 220]. To address the specific needs of this application, the models have been extended to include viscoelastic effects [75, 140, 144, 236], as well as actuation mechanisms based on pneumatic chambers and tendons [3, 70, 195, 220].

Port-Hamiltonian systems. As with any mechanical problem, a central aspect of highly flexible slender structures is the presence of a power balance[4]. It states that changes of the total energy of a system $\mathcal{H}$, also called *Hamiltonian*, over time t arise solely from the dissipation and interaction with the environment, i.e.,

$$\frac{\mathrm{d}}{\mathrm{d}t}\mathcal{H} = P_R + P_u. \tag{1.1}$$

Therein, $P_R \leq 0$ denotes the dissipated power of the system and P_u the power exchanged with the environment. Modeling approaches and numerical methods that violate this principle can lead to numerical instabilities and unphysical results, especially in long-term simulations. Ensuring energetic consistency, i.e., the satisfaction of a balance equation in the sense of (1.1), is therefore not merely a matter of numerical elegance, but a practical advantage for reliable simulations and control design.

Over the past two decades, the port-Hamiltonian (pH) framework [63, 224] has emerged as a promising paradigm for modeling interconnected dynamical systems across a wide range of domains. In particular, pH systems are well suited to meeting not only the demands of energy-consistent modeling but also of state-of-the-art simulation and control strategies. By adopting energy as a unifying quantity, the pH framework achieves remarkable generality: systems arising in power networks [76], fluid mechanics [226] and reactive flows [5], electromechanics [148], electromagnetics [7], magnetohydrodynamics [170], chemical reaction networks [227] and poroelastic networks [4], as well as quantum mechanics [230] and economics [149], can all be described within this framework. Moreover, the pH formalism has been extended to capture irreversible processes through the notion of *irreversible pH systems* [182]. Additionally, it should be noted that the evolution of pH systems is strongly connected to the bond graph formalism [63, 173]. For further comprehensive studies, the reader is referred to the review articles [162, 183] and the theses [41, 128, 165].

Regardless of the specific application, a pH system combines elements that store energy, dissipate energy, or transfer it to the environment within a unified and systematic mathematical structure, see Figure 1.3 for a schematic illustration. This structure, called *Dirac structure* [58], embodies the power balance (1.1) by means of the relation between power-conjugated variables. This structure comes with insightful mathematical formulations, which do not only enhance physical intuition but also provide a solid foundation for the design of simulation and control methods. Importantly, this structure is preserved under interconnection: the appropriate coupling of pH systems yields a new system of the same form. As a result, complex systems can be assembled from simpler subsystems, while maintaining an overall power balance — a property that is particularly valuable for flexible multibody systems.

The notion of pH systems was originally introduced for finite-dimensional systems [158] — i.e., systems described by a finite number of variables and governed by ordinary differential equations (ODEs) or

[4] While oftentimes the term *energy balance* is preferred, some research communities predominantly refer to it as a *power* balance, since terms of physical dimension of power are equated. In this work the latter terminology is adopted.

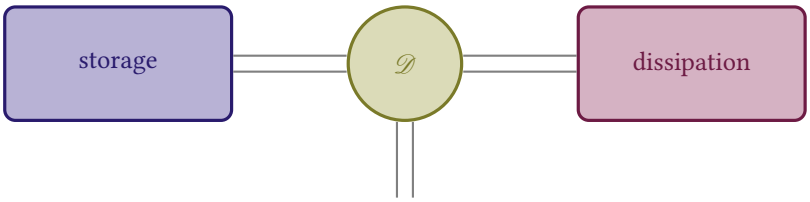

Figure 1.3.: Graphical depiction of a Dirac structure $\mathscr{D}$ that distributes energy between storage and dissipation elements and the environment of a dynamical physical system [224, Figure 2.2].

differential-algebraic equations (DAEs). The framework was later extended to infinite-dimensional systems[5] governed by partial differential equations (PDEs) or partial differential-algebraic equations (PDAEs), with Stokes–Dirac structures providing the underlying mathematical foundation [135, 225]. Due to their intrinsic modularity, pH systems often involve algebraic constraints, and the particularities of pH DAEs have been extensively studied in the works [23, 161, 162, 165, 223]. More recently, further generalizations have been proposed [6, 7, 24, 49, 228].

In line with this evolution, pH formulations for the description of structural dynamics were initially developed for linear structural elements such as the vibrating string [225], the Euler–Bernoulli beam [169], the Timoshenko beam [151], St. Venant torsion [234], and interconnected systems thereof [234]. However, the restriction to linear models is a significant limitation in the context of flexible multibody systems with highly flexible slender structures. Over the past decade, increasingly complex — nonlinear and constrained — pH formulations have therefore been proposed, including models for plates [42, 43], beams undergoing moderate deformations [48, 177, 179], and geometrically exact strings [218]. Geometrically nonlinear pH beam models have been studied in the works [15, 16, 86, 152]. Interconnected flexible multibody systems are addressed in the articles [11, 153, 221], while finite-dimensional pH multibody formulations are discussed in newer publications [25, C4, 147]. Furthermore, a floating-frame formulation has been presented [44], and recent contributions [47, 107, 180, 184, 219] explore the pH framework for continuum mechanics.

Structure-preserving discretization. The equations governing the dynamics of a system — be it ODEs, DAEs, PDEs or PDAEs — are typically too complex to admit analytical solutions, making numerical methods indispensable for simulating dynamical systems. In computational mechanics, the demand for reliable and accurate simulations has long driven the development of numerical schemes that preserve fundamental physical principles at the discrete level [35, 97]. Within the energy-based pH framework, such structure-preserving discretizations are essential to retain the power balance equation (1.1) after discretization, ultimately aiming to fully exploit the advantages of pH systems in simulation and control. For infinite-dimensional pH systems, various structure-preserving spatial discretization techniques have been proposed to obtain finite-dimensional systems that retain the pH structure — overviews can be found in the works [128, 183]. These techniques include finite difference and finite volume methods, but most prominently the finite element (FE) method, which is also the standard tool for spatial discretization in computational mechanics [115, 243].

In this context, *mixed* formulations are particularly known for addressing numerical pathologies like locking[6] (cf. theses [119, 174] and references therein), and providing coarse mesh accuracies [36,

[5] In the context of computational mechanics, the terminology *discrete* vs. *continuous* system is also common, whereas control systems communities may refer to *lumped* vs. *distributed parameter systems*.

[6] Locking describes the presence of unrealistically small deformations of a mechanical model that are due to an inappropriate numerical discretization strategy.

37, 232]. Such formulations are characterized by the inclusion of additional unknowns, which may reduce the level of nonlinearity and thus enhance the performance of the numerical solution procedure [1, 119]. This fact has been underlined by impressive numerical studies [37, Section 7]. Prominent element formulations, such as enhanced assumed strain elements [206] and assumed stress elements [176], introduce additional unknowns that are linked to the displacement field through compatibility conditions. In mechanics, a pH approach naturally leads to mixed formulations, as the energy-based modeling introduces stress or strain variables alongside kinematic quantities. Mixed FE methods [39] — sometimes also called *partitioned FE methods* [54] by the pH community — thus play a central role in pH structural mechanics [44, 48, 234]. For the spatial discretization of geometrically exact beams, mixed FE formulations have been proposed outside the pH framework [57, 92, 104, 122, 196, 231, 244]. Here, a key motivation is the prevention of numerical problems such as *transverse shear locking*, which is commonly handled using selectively reduced integration in purely displacement-based formulations [33, 193, 213].

After spatial discretization, the resulting finite-dimensional system of ODEs or DAEs can be treated with time integration schemes that respect the underlying structure of the dynamical system [35, 97]. The development of structure-preserving time integration methods, sometimes also called geometric integration methods, has a long tradition in computational mechanics, driven by the need for long-term stability and accuracy. So-called energy–momentum (EM) methods are typically based on discrete gradients [88, 90, 160, 207] and have been tailored to geometrically exact beams in the works [34, 141, 193, 208, 213]. However, their combination with mixed formulations (see above) is still a relatively new endeavor [36, 119]. Galerkin-projection methods [8, 9, 29, 30, 32, 65], symplectic methods [138], variational integrators [142, 156], Lie-group integrators [56] and combinations thereof [38, 105, 136, 139] offer alternative routes to the structure-preserving discretization in time.

Compared to classical computational mechanics, the structure-preserving time integration of pH systems is still a relatively young field[7]. A key requirement when integrating pH systems numerically is to account for the energy distribution in the system, which leads to a discrete-time power balance mimicking equation (1.1). Approaches that achieve this oftentimes draw from the developments for mechanical systems and include collocation methods [127, 161], Galerkin-projection methods [84], and splitting schemes [17, 18, 164]. A particularly important class of methods — and a focus of this thesis — are discrete gradient methods [12, 55, 72, 91, 201]. Typically of second-order convergence, these methods are attractive, because they can enforce an exact discrete-time energy balance for general energy functions, while remaining relatively simple to implement. Recent developments have also explored higher-order and derivative-free discrete gradient methods [66, 168]. A key advantage of developing structure-preserving methods for general pH systems is that they can be applied universally, thus decoupling the particular physical modeling from numerical approximation.

1.2. Research gaps and aims

As we have seen, geometrically exact models for highly flexible slender structures, pH formulations, and structure-preserving discretization methods each constitute a vital area of research. Port-Hamiltonian models exist for various structural elements and structure-preserving spatial and temporal discretizations have been proposed in specific contexts. Nevertheless, the overarching aim of this thesis is to connect these research areas and unify their approaches. In doing so, relevant research gaps (**RG**s) can

[7] The studies [72, 91] appear to be among the first to address this topic.

be exposed, as discussed in the following. Hereto, each gap is introduced individually, followed by an overarching statement.

It is well established that the pH framework is particularly well-suited for interconnected dynamical systems such as flexible multibody systems [11, 44, 153, 221], where geometrically exact beams represent an important model for slender components [10]. Existing strain-based pH formulations for geometrically exact beams [15, 16, 152] can describe the dynamics of geometrically exact beams, but generally require reconstructing absolute positions and orientations. This is consistent with approaches developed outside the pH framework [57, 244]. Moreover, the pH framework [152] enables a rigorous Lie-group-based description of finite rotations, yet this rigor entails a higher level of mathematical complexity. Importantly, it is unclear if the above-mentioned existing formulations are amenable to FE discretizations designed to preserve the pH structure in simulation and control. Furthermore, while selectively reduced integration of displacement-based formulations is a popular solution to transverse shear locking [33, 193, 213], its treatment using mixed formulations is rarely discussed, see exceptions [104, 122, 196] in the static scenario and [41] in the pH context. In this context, also the increased robustness and stability of mixed frameworks have not been fully investigated yet. A related question is also how to include kinematic side-conditions, like shear-rigidity. As a result, a coordinate-based, mixed pH formulation for the dynamics of geometrically exact beams is still lacking.

Research gap 1: *Coordinate-based, mixed pH modeling of geometrically exact beams.*

Linear elastic material is commonly employed in formulations for structural mechanics, and many related pH formulations have been developed [16, 42–44, 152, 153, 177, 218, 219, 234]. Eventually, these approaches provide a solid basis for structure-preserving simulations of linear elastic flexible multibody systems. Despite these advances, pH representations of mechanical systems with nonlinear strain energy functions — relevant for applications with soft materials [2] — remain largely unexplored. Similarly, pH formulations for viscoelastic materials described by the generalized-Maxwell model [204] have not been developed so far. In summary, pH PDE and pH PDAE formulations that incorporate complex material behavior are still an open topic.

Research gap 2: *Infinite-dimensional pH mechanical models with hyperelastic and viscoelastic material behavior.*

When it comes to the spatial discretization, it is established that mixed FE methods can be used to discretize pH systems governed by PDEs while preserving their structure [42, 43, 48, 234]. However, existing approaches primarily focus on linear structural elements or geometrically nonlinear elements assuming moderate deformations [48, 177, 179]. An application of a mixed FE approach to fully nonlinear pH models of geometrically exact beams and strings, possibly requiring the satisfaction of algebraic constraint equations, remains an open problem. Challenges in this context include the property of objectivity, the appropriate choice of FE spaces that respect the pH structure, and the prevention of numerical pathologies such as shear and membrane locking.

Research gap 3: *Structure-preserving space discretization for geometrically exact models of highly flexible slender structures formulated as nonlinear pH PDE or PDAE systems.*

Unlike geometric nonlinearities, the presence of material nonlinearities, see **RG 2**, requires specialized time-integration methods for consistent simulation of the dynamical system, such as discrete gradient

schemes [87, 160]. For pH systems with non-quadratic total energy governed by ODEs, a variety of methods have been developed [12, 55, 72, 80, 91, 166]. These approaches can exactly enforce a power balance equation in discrete time for general Hamiltonian functions and are well-established for systems, in which the gradient of the Hamiltonian appears explicitly in the governing ODEs. However, for pH ODEs of more general form and for pH DAEs, the gradient of the Hamiltonian may only appear implicitly, preventing the direct application of existing structure-preserving integrators [C4, 201]. Developing suitable time-integration schemes for such systems remains an open problem.

Research gap 4: *Structure-preserving time integration for nonlinear pH ODE systems with implicit appearance of the gradient of the Hamiltonian and semi-explicit pH DAE systems.*

Moreover, closing this gap jointly with **RG 1** can further enhance the numerical stability of the simulation framework compared to a displacement-based time integration approach. To the best of the author's knowledge, no such approach has yet been developed for geometrically exact beams.

A brief intermediate summary. Addressing **RG 1**–**RG 4** can enable more accurate, robust and energetically consistent simulations of highly flexible slender structures. Closing these gaps through missing pH formulations may avoid numerical problems such as shear locking, accommodate complex material behavior — including nonlinear and inelastic effects — and leverage the structural insight of the pH framework for mixed descriptions with improved stability properties. Moreover, a unifying pH formulation provides a yet unexplored perspective on the development and extension of structure-preserving discretization methods, with the additional potential to support the design of related control strategies.

To this end, this thesis' purpose is to address two main research aims (**RA**s), which are stated as follows.

Research aim 1: *Development of geometrically exact models for highly flexible slender structures in a unified, fully nonlinear pH framework.*

Pursuing this aim addresses **RG 1** and **RG 2** and provides a solid modeling foundation. The second aim is concerned with the structure-preserving discretization, aiming to offset the possible additional modeling effort by exploiting the benefits of structure preservation.

Research aim 2: *Design of structure-preserving numerical methods in space and time for geometrically exact models of highly flexible slender structures based on a unified pH model.*

With this aim, we address **RG 3** and **RG 4**. The two high-level goals, **RA 1** and **RA 2**, represent a canonical division between modeling and discretization. However, addressing the associated aspects requires an interrelated approach. To achieve these goals, this thesis presents a set of contributions (**C**s) to the research community, each detailed in the following section and addressed in the research papers presented in Chapters 3 to 6. For a schematic overview illustrating the relationships between the identified research gaps, the posed research aims, and the derived contributions, see Figure 1.4.

1.3. Contributions

Modeling contributions. First, this thesis establishes a unified pH framework for highly flexible slender structures, thus realizing RA 1. From the wide variety of existing pH formulations, we therefore identify one, which embraces mechanical problems exhibiting

i) nonlinear material behavior,

ii) geometric nonlinearities, and

iii) kinematic constraints.

The corresponding pH formalism must allow for i) a non-quadratic Hamiltonian, ii) state-dependent system matrices reflecting the geometric nonlinearities, and iii) the seamless inclusion of models governed by DAEs and PDAEs.

Contribution 1: *Identification of a recently introduced finite-dimensional pH framework [23, 161, 162] with a sufficient level of generality to accommodate highly flexible slender structures. Application of this framework in an infinite-dimensional setting on a one-dimensional domain.*

Building on this general framework, novel pH formulations for geometrically exact strings [10] and beams [10, 186, 209] are developed and extended to capture hyperelastic material laws and kinematic constraints. The related contributions address the corresponding mechanical modeling tasks. For the beam models, we first consider the planar case, where rotations can be described canonically by an orientation angle $\varphi \in \mathbb{R}$ that does not exhibit singularities. We then proceed to the spatial case, which is severely more complex due to the non-trivial treatment of finite spatial rotations.

The key step in deriving the pH formulation is the interpretation of strains or stresses (or both) as independent variables, just in the spirit of a Hu–Washizu or Hellinger–Reissner variational principle. These additional fields are linked to the kinematics via compatibility conditions in time-differentiated form. This time-differentiation is induced by the requirement to represent the system within the pH structure identified in C 1. To the best of the author's knowledge, this procedure is novel in the context of computational mechanics. By means of a compatibility relation in compliance form, kinematic constraints such as shear-rigidity or inextensibility can be realized in a straightforward way.

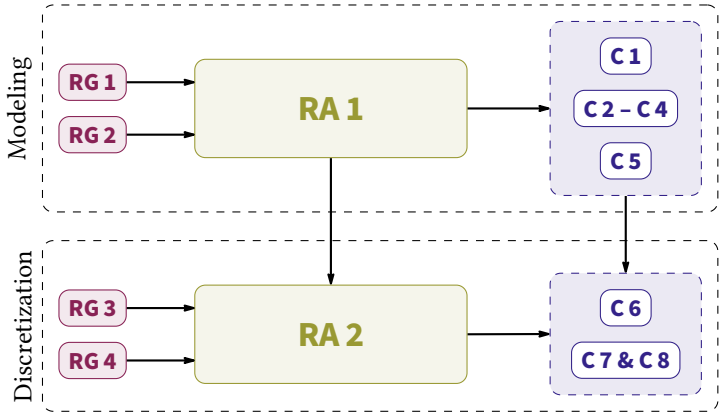

Figure 1.4.: Traceability between research gaps (RGs), research aims (RAs), and contributions (Cs). Although modeling and discretization aspects are grouped separately, RA 2 is strongly connected to RA 1 and the realization of the discretization contributions heavily depends on the pH modeling approach.

Contributions 2 – 4:

C 2: *Proposition of a novel infinite-dimensional pH PDE formulation for geometrically exact planar beams with independent strain measures, fitting into the general framework from* ***C 1****. The formulation features a quadratic Hamiltonian due to linear elasticity.*

C 3: *Deduction of a novel infinite-dimensional pH PDE formulation for geometrically exact strings within the general framework from* ***C 1****. A hyperelastic strain energy is explicitly accounted for by means of a non-quadratic Hamiltonian.*

C 4: *Reformulation of a director-based formulation [33, 193] for geometrically exact 3D beams as a pH PDAE system, fitting into the general framework from* ***C 1****. The formalism is equipped with a compliance formulation [104], thereby allowing for the inclusion of kinematic constraints.*

Eventually, with **C 5**, the formulations are generalized to account for the modeling of slender structures in soft robotics applications.

Contribution 5: *Extension of the beam and string models in the pH framework to include actuation via tendons and pneumatic chambers [70, 195, 220] and dissipative material behavior via generalized Maxwell models [75, 140, 204, 236]. The analysis reveals that this extension can be interpreted as a power-preserving interconnection of an elastic pH system with a purely dissipative pH system.*

Owing to their unified pH formulation, the derived models can be systematically discretized using a wide range of pH-based discretization methods, thereby providing a foundation for numerous future research directions. Moreover, the pH formulation constitutes the essential basis for the discretization methods proposed in this thesis.

Discretization contributions. The contributions addressing **RA 2** are formulated separately for spatial and temporal discretization, reflecting the sequential approach that predominates in the literature for mechanical systems. Building on the developed modeling framework, these contributions focus on the structure-preserving discretization of nonlinear pH PDE and PDAE systems. The generality of the pH framework is exploited to derive discretization schemes that preserve the underlying system structure. While such methods have previously been developed for individual structural elements in isolation, a unified approach that can be systematically extended to other elements has so far been lacking.

For the spatial discretization, straightforward mixed FE methods [44, 48, 234] are applied, which are based on Lagrange polynomials. The mixed quantities (i.e., strains or stresses or both) are approximated discontinuously and independently from the kinematic variables with a polynomial degree that is one order lower. The resulting finite-dimensional models fit again into a pH framework, which motivates the terminology "structure-preserving" in this context, and are invariant under coordinate transformation, fulfilling the property of objectivity.

Contribution 6: *Development of an objective, structure-preserving mixed FE discretization strategy for pH formulations of slender structures, yielding finite-dimensional systems that possess again a pH structure. For beams, these FE models naturally prevent locking.*

With respect to time discretization, the pH structure and its interpretability provide a priori guidance on how individual terms should be discretized in time to ensure structure preservation. Particularly, the form of the Hamiltonian plays a crucial role here, leading to two distinct contributions.

Contributions 7 & 8:

C 7: *Proposition of a straightforward midpoint time integration method for systems with quadratic Hamiltonian. The scheme possesses structure-preserving properties, like ensuring exact discrete-time power and momentum balances.*

C 8: *Design of discrete-gradient-based time integration methods [87, 97, 160] for implicit pH ODEs and semi-explicit pH DAE systems with non-quadratic Hamiltonian, ensuring exact discrete-time power balances.*

The discrete-time results obtained with the proposed methods are additionally kinematically consistent if the respective constraint functions are of quadratic form. Once more, it is worth emphasizing that the derived discretization strategies are not tightly tied to the underlying physical problem and can therefore be adapted to other pH models across different physical disciplines.

The above eight contributions are provided in the individual research papers that constitute this thesis, see also the introductory sections in Chapters 3 to 6. Taken together, **C 1**–**C 8** close **RG 1**–**RG 4** and realize **RA 1** and **RA 2**, see Figure 1.4. To not overextend the scope of this work and focus on the achievement of the discussed contributions, some limitations are imposed.

1.4. Limitations

The introductory chapter, cf. Chapter 2, provides an intuitive overview of pH systems for readers with limited prior exposure. To avoid unnecessary mathematical complexity, we restrict the presentation of Dirac structures to the finite-dimensional setting. Stokes–Dirac structures, which underpin infinite-dimensional pH systems, are therefore not discussed. Nevertheless, we derive a specific class of infinite-dimensional pH systems from the finite-dimensional definition. As such, this chapter serves to introduce the concept of pH systems and convey the central foundations of this thesis.

We restrict our attention to modeling and simulation aspects based on geometrically exact beam and string models with homogeneous material and geometric properties. Other flexible multibody components may introduce additional requirements for the pH framework. While the proposed approaches are expected to extend to elements such as shells or continua, a detailed treatment is beyond the scope of this thesis. Likewise, the focus is further limited to single structural elements. The interconnection of multiple elements into complex multibody systems is considered through a numerical example.

For three-dimensional geometrically exact beams, cf. Chapter 4, a single parametrization of finite rotations is considered, namely using directors [33, 193]. While this choice leads to a comparatively simple structure — characterized by a constant mass matrix and quadratic strain measures — it introduces six additional algebraic constraints. As it is common for geometrically exact beams, we assume St. Venant–Kirchhoff type material leading to linear stress-strain relations. Hyperelastic material behavior is, however, addressed in the context of geometrically exact strings, cf. Chapter 6, and in the chapter devoted to the development of discrete gradient methods, cf. Chapter 5.

Concerning discretization, we emphasize generality arising from the pH formulation while deliberately restricting the methodological scope. Specifically, we consider mixed FE methods with standard Lagrange polynomials in space and midpoint-based discrete gradient methods of at most second order in time. Other structure-preserving techniques are not addressed. The resulting governing equations typically take the form of implicit ODEs or semi-explicit DAEs. While we focus on the discrete preservation of the power balance equation, most of the discrete time formulations also preserve the balance of total angular momentum. However, this is only peripheral in the context of this thesis. The pH-based control design for highly flexible slender structures based on the proposed formulations is left for future research.

More specific limitations are outlined in the respective chapters presenting the individual research papers. The interested reader is also referred to Section 7.2, where future research directions imposed by the deliberately chosen limitations are discussed.

1.5. Outline

We now provide an overview of the structure of this thesis. While Chapter 2 is a newly written introduction, the remaining chapters are based on previously published work. In particular, Chapters 3 to 6 correspond to standalone research articles and are written to be self-contained. To ensure coherence, some elements have been adapted and the notation has been unified as much as possible to align with the overall focus of this work[8]. Each chapter begins with a reference to the corresponding publication, and the contributions discussed in the preceding section are distributed across all chapters.

Chapter 2 provides a brief introduction to pH systems and develops **C 1**.

> The underlying concept of Dirac structures is explained, two definitions of pH systems are given together with their properties. We illustrate the content using representative mechanical examples. The chapter thus offers the necessary background for readers unfamiliar with the pH framework and introduces a general pH model suitable for highly flexible slender structures and flexible multibody systems in general.

Chapter 3 is based on the article [A2] and (partially) develops **C 2**, **C 6** and **C 7**.

> Here, planar geometrically exact beams are modeled within the pH framework using independent displacements, velocities and strains. We develop a structure-preserving spatial mixed FE method and temporal midpoint discretization strategy, yielding an EM scheme. Additionally, the mixed FE approach naturally prevents transverse shear locking and is comparably robust compared to a displacement-based EM formulation, demonstrating the advantages of the pH-based modeling and discretization strategy.

Chapter 4 is based on the article [A4] and (partially) develops **C 4**, **C 5**, **C 6** and **C 7**.

> The pH model is extended to three-dimensional geometrically exact beams, employing a director-based parametrization to handle large rotations. A mixed FE formulation using displacement, velocity and stresses as independent quantities, is applied and covers the DAE case. Shear-rigid and inextensible rod formulations are seamlessly integrated due to a compliance formulation. The formulation is further generalized to include viscoelastic material behavior and non-standard actuation, demonstrating the pH framework's flexibility. The same midpoint time integrator as

[8] The software engineer Phil Karlton is known for the famous words "There are only two hard things in Computer Science: cache invalidation and naming things" [121]. Apparently, the latter issue arises also for mathematical notation.

in Chapter 3 is used. Due to quadratic strain measures, the corresponding evolution equations are variationally exactly integrated.

Chapter 5 is based on the article [A3] and develops **C 8**.

With the aim to simulate geometrically exact structures with nonlinear material behavior, we develop discrete gradient-based time integration schemes for nonlinear pH DAEs. The methods ensure exact discrete power balance for non-quadratic Hamiltonian functions and pH models, in which the gradient of the Hamiltonian appears implicitly, extending structure-preserving integration to a broader class of systems.

Chapter 6 is based on the article [A1] and (partially) develops **C 3**, **C 5**, **C 6**, and **C 8**.

This chapter introduces a pH formulation for geometrically exact strings with hyperelastic and viscoelastic material behavior, using the same generalized Maxwell model as in Chapter 4. We discuss the extension of the pH formulation for PDEs with implicitly appearing general Hamiltonian, which requires the discrete gradient time integrators developed in Chapter 5. It is demonstrated how the generalized Maxwell viscoelasticity can be understood as power-preserving interconnection of smaller pH sub-models, thus benefiting from the pH modeling paradigm. Useful background details originally developed in the closely related work [C2] are contained in Appendix 6.C.

Chapter 7 concludes this thesis with a summary and an outlook.

2. Preliminaries on port-Hamiltonian systems

This chapter provides a brief introduction to port-Hamiltonian (pH) systems, illustrating key concepts through mechanical example systems. It begins with the standard formulation most commonly used in the literature, followed by a discussion of Dirac structures, which form the mathematical foundation underlying all pH system definitions. To address limitations of the standard formulation, we further present a generalized formulation of pH systems, which is central to the remainder of this work. Finally, it is discussed how the framework extends to infinite-dimensional systems on a one-dimensional spatial domain.

Parts of the material presented here are based on the monographs [41, 63, 128, 224], which are also recommended for further reading.

2.1. An ODE representation of port-Hamiltonian systems

Consider a dynamical system evolving over time $t \in \mathbb{T}$, where the time interval of interest is defined as

$$\mathbb{T} = [0, t_{\text{end}}] \subset \mathbb{R}, \qquad t_{\text{end}} > 0. \tag{2.1}$$

The system dynamics are described by equations formulated in terms of the state $\boldsymbol{x} \in \mathscr{C}^\infty(\mathbb{T}, \mathscr{X})$, i.e., $\boldsymbol{x}$ is a smooth function of time[1]. The space $\mathscr{X}$, referred to as the *state space*, is taken in this thesis to be $\mathscr{X} = \mathbb{R}^n$, so that the state is represented by an n-tuple of real numbers uniquely characterizing the system configuration. In the following, we omit the explicit time dependence for notational convenience and include it only where deemed necessary. In particular, we write

$$\boldsymbol{x}(t) \in \mathscr{X}, \qquad \text{or simply} \qquad \boldsymbol{x} \in \mathscr{X}, \tag{2.2}$$

with all equations understood to hold pointwise in time.

In the pH literature, the state variables are also often called *energy variables* [223], as they uniquely determine the system's total energy, described by the *Hamiltonian* function $\mathcal{H} \in \mathscr{C}^1(\mathscr{X}, \mathbb{R})$. Port-Hamiltonian systems can be viewed as a generalization of classical Hamiltonian systems [137] that incorporate external influences through a known input vector $\boldsymbol{u} \in \mathbb{R}^m$. Correspondingly, an output vector $\boldsymbol{y} \in \mathbb{R}^m$ may be defined. Within this setting, we now present the most commonly employed definition of a pH system governed by ordinary differential equations (ODEs).

Definition 2.1 (pH ODE system [223, 224])**.** *A port-Hamiltonian ODE system is a state-space model of the form*

$$\dot{\boldsymbol{x}} = \big(\boldsymbol{J}(\boldsymbol{x}) - \boldsymbol{R}(\boldsymbol{x})\big)\nabla\mathcal{H}(\boldsymbol{x}) + \boldsymbol{B}(\boldsymbol{x})\boldsymbol{u}, \tag{2.3a}$$

$$\boldsymbol{y} = \boldsymbol{B}(\boldsymbol{x})^\top \nabla\mathcal{H}(\boldsymbol{x}), \tag{2.3b}$$

[1] With $\mathscr{C}(\mathscr{A}, \mathscr{B})$ we identify continuous functions mapping from $\mathscr{A}$ to $\mathscr{B}$. We specify that a function is at least k-times continuously differentiable by writing $\mathscr{C}^k(\mathscr{A}, \mathscr{B})$. A *smooth* function $\boldsymbol{f} \in \mathscr{C}^\infty(\mathscr{A}, \mathscr{B})$ is continuously differentiable and possesses as many derivatives as required to justify the mathematical manipulations, rather than infinitely many [10, p. 4].

together with a Hamiltonian function $\mathcal{H} \in \mathscr{C}^1(\mathscr{X}, \mathbb{R})$*, if the structure matrix* $\boldsymbol{J} \in \mathscr{C}(\mathscr{X}, \mathbb{R}^{n\times n})$ *is skew-symmetric and the dissipation matrix* $\boldsymbol{R} \in \mathscr{C}(\mathscr{X}, \mathbb{R}^{n\times n})$ *is symmetric positive semi-definite,*

$$\boldsymbol{J}(\boldsymbol{x}) = -\boldsymbol{J}(\boldsymbol{x})^\top, \qquad \boldsymbol{R}(\boldsymbol{x}) = \boldsymbol{R}(\boldsymbol{x})^\top \succeq 0, \tag{2.3c}$$

for all $\boldsymbol{x} \in \mathscr{X}$*. Moreover,* $\boldsymbol{B} \in \mathscr{C}(\mathscr{X}, \mathbb{R}^{n\times m})$ *is called the* port *matrix.* ♤

Here, $\nabla\mathcal{H} \in \mathscr{C}(\mathscr{X}, \mathbb{R}^n)$ denotes the gradient of $\mathcal{H}$, understood as a column vector, and the notation $\dot{\square} := \frac{\mathrm{d}}{\mathrm{d}t}\square$ is used for the time derivative.

Note that Definition 2.1 not only prescribes a specific structure for the time-invariant (i.e., *autonomous*) state dynamics as ODEs, but also restricts the admissible output to be collocated and power-conjugated with the input. In this context, (2.3a) is referred to as *dynamical equation* and (2.3b) is the *output equation*. By means of the latter it can be understood why the input and output variables have the same dimension and are power-conjugated. Accordingly, the quantity $P_u := \boldsymbol{y}^\top\boldsymbol{u}$ has the physical dimension of power. See the upcoming example Example 2.3 for an illustration of this aspect. Furthermore, from a physical perspective, the matrix $\boldsymbol{J}$ contains purely conservative terms associated with internal energy-routing processes that neither generate nor dissipate energy, whereas $\boldsymbol{R}$ represents purely dissipative effects. Mathematically this is reflected in the properties (2.3c) of the two matrices.

This energy-based interpretation of pH systems is further supported by the power balance equation for the Hamiltonian, which is satisfied by design by every trajectory $(\boldsymbol{x}, \boldsymbol{u}, \boldsymbol{y})$ fulfilling Definition 2.1. Applying the chain rule yields

$$\dot{\mathcal{H}} = \nabla\mathcal{H}(\boldsymbol{x})^\top\dot{\boldsymbol{x}} = \nabla\mathcal{H}(\boldsymbol{x})^\top\boldsymbol{J}(\boldsymbol{x})\nabla\mathcal{H}(\boldsymbol{x}) - \nabla\mathcal{H}(\boldsymbol{x})^\top\boldsymbol{R}(\boldsymbol{x})\nabla\mathcal{H}(\boldsymbol{x}) + \nabla\mathcal{H}(\boldsymbol{x})^\top\boldsymbol{B}(\boldsymbol{x})\boldsymbol{u}, \tag{2.4}$$

where (2.3a) has been used. Due to the skew-symmetry of $\boldsymbol{J}$, cf. (2.3c), the first term vanishes. Invoking (2.3b) then leads to

$$\dot{\mathcal{H}} = -\nabla\mathcal{H}(\boldsymbol{x})^\top\boldsymbol{R}(\boldsymbol{x})\nabla\mathcal{H}(\boldsymbol{x}) + \boldsymbol{y}^\top\boldsymbol{u}. \tag{2.5}$$

This expression shows that the time rate of change of the Hamiltonian, i.e., the total energy, is entirely determined by dissipation power and power supplied through external influences (e.g., control actuation). More precisely, since $\boldsymbol{R}$ is positive semi-definite (2.3c), the dissipation power $P_R := \nabla\mathcal{H}(\boldsymbol{x})^\top\boldsymbol{R}(\boldsymbol{x})\nabla\mathcal{H}(\boldsymbol{x}) \geq 0$ contained in (2.5) is non-negative. Consequently, the so-called *dissipation inequality*

$$\dot{\mathcal{H}} \leq \boldsymbol{y}^\top\boldsymbol{u} \tag{2.6}$$

can be deduced. It states that the time rate of change of the Hamiltonian is bounded by the power P_u induced by the input $\boldsymbol{u}$.

In Figure 2.1, we provide an overview of different classifications of dynamical systems [224, Chapter 7]. In view of the dissipation inequality (2.6), the pH ODE system introduced in Definition 2.1 is *passive*, meaning that the system cannot actively generate energy. In the special case $\boldsymbol{R} = \boldsymbol{0}$, the system is *lossless*, since any change in the total energy is entirely due to input power. If, in addition, the system is closed ($\boldsymbol{u} = \boldsymbol{0}$), it is *energy-conserving*. All of these properties can be understood as special cases of *dissipativity* [237], where the time rate of change of the energy is bounded by a supply rate function $w \in \mathscr{C}(\mathbb{T}, \mathbb{R})$. While energy conservation is often the focus in computational mechanics, passivity constitutes a more general property and plays a central role in modern control design [222].

We now illustrate Definition 2.1 of a pH system by means of two examples that should resonate with readers with a mechanics background.

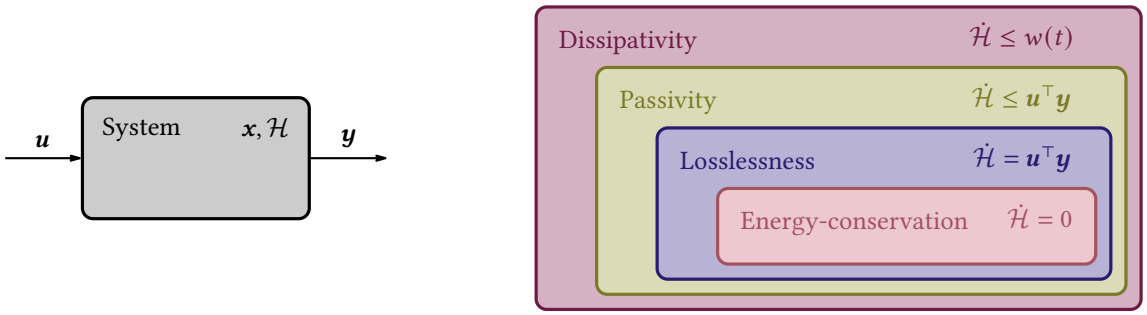

Figure 2.1.: Graphical depiction of a system with state $\boldsymbol{x}$, Hamiltonian (or total energy) function $\mathcal{H}$, input $\boldsymbol{u}$ and output $\boldsymbol{y}$ and classification in a system-theoretic sense [224, 237].

Example 2.2 (Hamiltonian mechanical systems [85, 137])**.** *Consider a Newtonian mechanical system with position coordinates $\boldsymbol{q} \in \mathbb{R}^d$ and conjugate momenta $\boldsymbol{p} := \boldsymbol{M}\dot{\boldsymbol{q}}$, where $\boldsymbol{M} \in \mathbb{R}^{d\times d}$ is a constant, symmetric, and positive definite mass matrix and $U \in \mathscr{C}^1(\mathbb{R}^d, \mathbb{R})$ denotes the potential energy function. The governing equations $\dot{\boldsymbol{q}} = \boldsymbol{M}^{-1}\boldsymbol{p}$ and $\dot{\boldsymbol{p}} = -\nabla U(\boldsymbol{q})$ represent the kinematics equations and balance of momentum, respectively. These ODEs can be rewritten in canonical form as*

$$\begin{bmatrix}\dot{\boldsymbol{q}}\\ \dot{\boldsymbol{p}}\end{bmatrix} = \begin{bmatrix}0 & \boldsymbol{I}\\ -\boldsymbol{I} & 0\end{bmatrix}\begin{bmatrix}\nabla U(\boldsymbol{q})\\ \boldsymbol{M}^{-1}\boldsymbol{p}\end{bmatrix}, \tag{2.7}$$

where $\boldsymbol{I}$ denotes an identity matrix of appropriate dimension and $\boldsymbol{0}$ a matrix full of zeros. Eventually, the present system (2.7) is a special case of pH ODE systems according to Definition 2.1 with

$$\boldsymbol{x} = (\boldsymbol{q}, \boldsymbol{p}) \in \mathbb{R}^{2d}, \qquad \mathcal{H}(\boldsymbol{x}) = \frac{1}{2}\boldsymbol{p}^\top \boldsymbol{M}^{-1}\boldsymbol{p} + U(\boldsymbol{q}), \qquad \text{and} \qquad \boldsymbol{J} = \begin{bmatrix}0 & \boldsymbol{I}\\ -\boldsymbol{I} & 0\end{bmatrix}, \tag{2.8}$$

as well as $\boldsymbol{R} = \boldsymbol{0}$ and $\boldsymbol{u} = \boldsymbol{0}$. Note that the Hamiltonian is here a separable function given by the sum of kinetic and potential energy. Moreover, we have introduced the shorthand notation $\boldsymbol{x} = (\boldsymbol{q}, \boldsymbol{p})$, corresponding to $\boldsymbol{x} = [\boldsymbol{q}^\top, \boldsymbol{p}^\top]^\top \in \mathbb{R}^{2d}$. Notably, the conservation of the Hamiltonian follows immediately from (2.5), that is, $\dot{\mathcal{H}} = 0$. ◇

The previous example highlights that the pH framework can be understood as a natural extension of Hamiltonian dynamics that incorporates dissipative effects and external influences. The next example will play a more prominent role and can be regarded as prototypical for nonlinear elastodynamical systems, including the infinite-dimensional models considered in later parts of this thesis.

Example 2.3 (Nonlinear viscoelastic pendulum [36, C4, 130])**.** *Consider a spring pendulum consisting of a point mass $m > 0$ with position $\boldsymbol{q} \in \mathbb{R}^3$ and a nonlinear elastic spring of natural length $l_0 > 0$ and stiffness parameter $k > 0$, fixed to a revolute joint as depicted in Figure 2.2. The spring is assumed to have negligible mass. In parallel, a viscous dashpot with dynamic viscosity parameter $\eta > 0$ is attached. The related viscous forces[2] have the form $\boldsymbol{f}_{vis} = -\boldsymbol{V}(\boldsymbol{q})\boldsymbol{v}$ with symmetric positive semi-definite $\boldsymbol{V}$ for all $\boldsymbol{q}$. For the point mass, we define the conjugate momentum $\boldsymbol{p} = m\dot{\boldsymbol{q}} \in \mathbb{R}^3$, and the spring elongation is described using a nonlinear strain $C \in \mathbb{R}$, which is related to the position of the point mass via*

$$C = \tilde{C}(\boldsymbol{q}) = \frac{1}{l_0^2}\boldsymbol{q}^\top\boldsymbol{q}. \tag{2.9}$$

[2] Complying with the usual notion of a linear dashpot element, we restrict our attention to viscous forces that are linearly proportional to the radial component of the velocity of the point mass and have radial direction. This can be realized with forces of the form $\boldsymbol{f}_{\text{vis}} = -\eta v\frac{\boldsymbol{q}}{||\boldsymbol{q}||}$, where the velocity component into radial direction is given by $v = \dot{\boldsymbol{q}}^\top\frac{\boldsymbol{q}}{||\boldsymbol{q}||}$ such that $\boldsymbol{V}(\boldsymbol{q}) = \frac{\eta}{||\boldsymbol{q}||^2}\boldsymbol{q}\boldsymbol{q}^\top$.

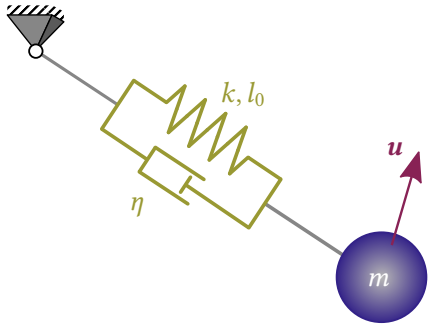

Figure 2.2.: Nonlinear viscoelastic spring pendulum, see Example 2.3.

This strain measure can be interpreted in analogy to the right Cauchy–Green strain from continuum mechanics [111]. The potential energy associated with the spring, $W \in \mathscr{C}^1(\mathbb{R},\mathbb{R})$, may be generally nonlinear, and we consider an additional potential energy $V \in \mathscr{C}^1(\mathbb{R}^3,\mathbb{R})$ related to the mass position, for example due to gravity. Furthermore, the point mass may be subject to external (known) forces $\boldsymbol{u} \in \mathbb{R}^3$.

The governing equations can be derived from the Lagrange–d'Alembert principle [157] as

$$\dot{\boldsymbol{q}} = \frac{1}{m}\boldsymbol{p}, \qquad \dot{\boldsymbol{p}} = -\nabla V(\boldsymbol{q}) - W'(\tilde{C}(\boldsymbol{q}))\nabla\tilde{C}(\boldsymbol{q}) + \boldsymbol{f}_{vis}(\boldsymbol{q},\boldsymbol{p}) + \boldsymbol{u}, \tag{2.10}$$

where W' denotes the derivative of the univariate, scalar-valued function W. The first equation in (2.10) *expresses the kinematic relation, while the second represents the balance of linear momentum for the point mass, in which the first two terms correspond to the potential and elastic forces, respectively. With the correspondences $\boldsymbol{M} := m\boldsymbol{I} \in \mathbb{R}^{3\times3}$ and $U(\boldsymbol{q}) = V(\boldsymbol{q}) + W(\tilde{C}(\boldsymbol{q}))$, this system can be aligned with the previous example, cf. Example 2.2.*

However, in the spirit of the pH modeling paradigm, we treat the strain C as an independent state variable, since it directly contributes to the Hamiltonian of the system. To obtain an pH ODE (2.3) *we consider the time derivative of the strain [C4], which gives*

$$\dot{C} = \frac{\mathrm{d}}{\mathrm{d}t}\tilde{C}(\boldsymbol{q}) = \nabla\tilde{C}(\boldsymbol{q})^\top\frac{1}{m}\boldsymbol{p} = \frac{2}{l_0^2}\boldsymbol{q}^\top\frac{1}{m}\boldsymbol{p}, \tag{2.11}$$

where we have used the kinematic relations (2.9) *and* (2.10)*. The governing dynamics are then composed of the original ODEs* (2.10)*, recast in this extended (mixed) form, together with the kinematic compatibility equation* (2.11) *such that*

$$\begin{bmatrix}\dot{\boldsymbol{q}}\\ \dot{\boldsymbol{p}}\\ \dot{C}\end{bmatrix} = \begin{bmatrix}0 & \boldsymbol{I} & 0\\ -\boldsymbol{I} & -\boldsymbol{V}(\boldsymbol{q}) & -\frac{2}{l_0^2}\boldsymbol{q}\\ 0 & \frac{2}{l_0^2}\boldsymbol{q}^\top & 0\end{bmatrix}\begin{bmatrix}\nabla V(\boldsymbol{q})\\ \frac{1}{m}\boldsymbol{p}\\ W'(C)\end{bmatrix} + \begin{bmatrix}0\\ \boldsymbol{I}\\ 0\end{bmatrix}\boldsymbol{u}. \tag{2.12}$$

Note that for this extended representation with independent strain state C, the compatibility relation (2.11) *must be expressed in time-differentiated form. In contrast to this ODE formulation, directly imposing $C - \tilde{C}(\boldsymbol{q}) = 0$ would result in a DAE of differential index 1. System* (2.12) *can be seen to be a pH ODE system* (2.3a) *with state $\boldsymbol{x} = (\boldsymbol{q},\boldsymbol{p},C) \in \mathbb{R}^7$, state-dependent structure and dissipation matrix*

$$\boldsymbol{J}(\boldsymbol{x}) = \begin{bmatrix}0 & \boldsymbol{I} & 0\\ -\boldsymbol{I} & 0 & -\frac{2}{l_0^2}\boldsymbol{q}\\ 0 & \frac{2}{l_0^2}\boldsymbol{q}^\top & 0\end{bmatrix} = -\boldsymbol{J}(\boldsymbol{x})^\top, \qquad \boldsymbol{R}(\boldsymbol{x}) = \operatorname{diag}(\boldsymbol{0},\boldsymbol{V}(\boldsymbol{q}),\boldsymbol{0}) = \boldsymbol{R}(\boldsymbol{x})^\top \succeq 0. \tag{2.13}$$

Note that the state-dependence of the structure matrix is due to the quadratic, i.e., nonlinear strain function (2.9)*. This reflects the geometric nonlinearity of the problem at hand. Moreover, the constant input matrix is given by* $\boldsymbol{B} = [\boldsymbol{0}, \boldsymbol{I}, \boldsymbol{0}]^\top \in \mathbb{R}^{7\times 3}$*, and the associated Hamiltonian reads*

$$\mathcal{H}(\boldsymbol{q}, \boldsymbol{p}, C) = \frac{1}{2m}\boldsymbol{p}^\top \boldsymbol{p} + V(\boldsymbol{q}) + W(C). \tag{2.14}$$

The output quantity, as prescribed by (2.3b) *is given by the velocity of the point mass,*

$$\boldsymbol{y} = \begin{bmatrix} 0 & \boldsymbol{I} & 0 \end{bmatrix} \begin{bmatrix} \nabla V(\boldsymbol{q}) \\ \frac{1}{m}\boldsymbol{p} \\ W'(C) \end{bmatrix} = \frac{1}{m}\boldsymbol{p}. \tag{2.15}$$

The input force $\boldsymbol{u}$ *and output velocity* $\boldsymbol{y}$ *act at the same location and form a power-conjugate pair.* ◊

Before highlighting potential limitations of the introduced pH framework according to Definition 2.1, and motivating a more general one, let us briefly discuss the underlying mathematical notion: Dirac structures. They provide a geometric viewpoint on the system dynamics and offer a deeper appreciation of the intrinsic elegance of pH systems. That said, for understanding the subsequent chapters, it is perfectly fine to skip the upcoming section if desired.

2.2. The geometric point of view: Dirac structures

The mathematical concept underlying every pH system is that of a Dirac structure [58]. This unifying framework encompasses (abstract) elements that store, dissipate, and exchange energy with the environment, without necessarily corresponding to physical sub-components of the system. A Dirac structure encodes the power balance (2.5) through relations between power-conjugated variables, namely *effort* variables $\boldsymbol{e}$ and *flow* variables $\boldsymbol{f}$, collectively referred to as *port* variables $(\boldsymbol{e}, \boldsymbol{f})$. Their specific physical interpretation depends on the domain — for example, force and velocity in translational mechanics, torque and angular velocity in rotational mechanics, voltage and current in electrical systems, or volumetric flow and pressure in hydrodynamics [63].

A Dirac structure is defined on the vector spaces of efforts $\boldsymbol{e} \in \mathscr{E}$ and flows $\boldsymbol{f} \in \mathscr{F}$, with $\mathscr{B} = \mathscr{E} \times \mathscr{F}$ denoting the space of port variables. Eventually, the Dirac structure $\mathscr{D}$ will be a specific subspace of the space of port variables, i.e., $\mathscr{D} \subset \mathscr{B}$. The physical property of power conjugacy between efforts and flows is captured mathematically by the fact that they reside in dual spaces, $\mathscr{E} = \mathscr{F}^*$. Accordingly, elements of one space act as linear functionals on the other, thus mapping to the real numbers $\mathbb{R}$. The corresponding duality pairing is denoted by $\langle \square, \square \rangle : \mathscr{B} \to \mathbb{R}$ and the dimension of $\mathscr{E}$ and $\mathscr{F}$ needs to be equal. For nonlinear pH systems, the dynamics may further depend on the state $\boldsymbol{x} \in \mathscr{X}$ (see the state-dependent structure matrix in Example 2.3). In this case, the Dirac structure itself becomes state-dependent: the relation between flows and efforts varies over the state space, and the Dirac structure is said to be *modulated* by the state.

Definition 2.4 (Dirac structure [58, 223, 224, 246])**.** *Let* $\boldsymbol{x} \in \mathscr{X}$ *denote the state, and* $\mathscr{B} = \mathscr{E} \times \mathscr{F}$ *the space of port variables. Then, a modulated Dirac structure* $\mathscr{D}$ *on* $\mathscr{X}$ *is a family of subspaces* $\mathscr{D}(\boldsymbol{x}) \subset \mathscr{B}$ *such that*

(i) $\langle \boldsymbol{e}, \boldsymbol{f} \rangle = 0 \qquad \forall\, (\boldsymbol{e}, \boldsymbol{f}) \in \mathscr{D}(\boldsymbol{x})$,

(ii) $\dim(\mathscr{D}(\boldsymbol{x})) = \dim(\mathscr{E})$,

for all $\boldsymbol{x} \in \mathscr{X}$. The state-dependence of $\mathscr{D}$ is required to be smooth. ♤

As discussed in Section 2.1, it is sufficient for the purposes of this work to assume $\mathscr{X} = \mathbb{R}^n$. Likewise, we can assume $\mathscr{E} = \mathbb{R}^p$, $\mathscr{F} = (\mathbb{R}^p)^* = \mathbb{R}^p$, and consequently $\mathscr{D}(\boldsymbol{x}) \subset \mathscr{B} = \mathbb{R}^p \times \mathbb{R}^p$ for some p. In this case, Property (i) of a Dirac structure reduces to the standard scalar product of two column vectors. Accordingly, the total power is given by

$$P = \boldsymbol{e}^\top \boldsymbol{f} = 0, \tag{2.16}$$

which expresses power conservation. Regarding Property (ii), it can be shown that any $\mathscr{D}(\boldsymbol{x})$ satisfying Property (i) has maximal dimension $\dim(\mathscr{E})$ [223].

Let us introduce one of the most important realizations of a (modulated) Dirac structure, which is given by the graph $\mathscr{D}_{\text{graph}}(\boldsymbol{x})$ of a modulated skew-symmetric mapping [223, 224], that is given by $\tilde{\boldsymbol{J}}(\boldsymbol{x})(\square) : \mathscr{E} \to \mathscr{F}$ with pointwise satisfaction of $\tilde{\boldsymbol{J}}(\boldsymbol{x}) = -\tilde{\boldsymbol{J}}(\boldsymbol{x})^\top$. Correspondingly, the graph of that mapping is defined as

$$\mathscr{D}_{\text{graph}}(\boldsymbol{x}) = \operatorname{graph} \tilde{\boldsymbol{J}}(\boldsymbol{x}) := \left\{ (\boldsymbol{e}, \boldsymbol{f}) \in \mathscr{B} \,\middle|\, \boldsymbol{f} = \tilde{\boldsymbol{J}}(\boldsymbol{x})\boldsymbol{e} \right\}. \tag{2.17}$$

We now verify that this subspace defines a Dirac structure according to Definition 2.4. With $\boldsymbol{f} = \tilde{\boldsymbol{J}}(\boldsymbol{x})\boldsymbol{e}$, Property (i) holds since

$$\boldsymbol{e}^\top \boldsymbol{f} = \boldsymbol{e}^\top \tilde{\boldsymbol{J}}(\boldsymbol{x})\boldsymbol{e} = 0,$$

by skew-symmetry of $\tilde{\boldsymbol{J}}(\boldsymbol{x})$. Property (ii) follows because, if $\mathscr{E}$ has dimension p, each $\boldsymbol{e} \in \mathscr{E}$ uniquely determines $\boldsymbol{f} = \tilde{\boldsymbol{J}}(\boldsymbol{x})\boldsymbol{e} \in \mathscr{F}$, so no additional dimensions exist and

$$\dim(\mathscr{D}_{\text{graph}}(\boldsymbol{x})) = p.$$

It is not surprising that also the graph of skew-symmetric maps from $\mathscr{F}$ to $\mathscr{E}$, e.g., inducing $\boldsymbol{e} = \boldsymbol{\omega}(\boldsymbol{x})\boldsymbol{f}$ for $\boldsymbol{\omega}(\boldsymbol{x}) = -\boldsymbol{\omega}(\boldsymbol{x})^\top$ for all $\boldsymbol{x} \in \mathscr{X}$, represents a Dirac structure. Actually, both scenarios can be traced back to the special case of Dirac structures in kernel representation [223, 224] with one coefficient matrix being the identity and the other one a skew-symmetric matrix.

With this understanding of Dirac structures as subspaces of spaces of port variables, we can draw a connection to the underlying physics. Recall the intuitive picture of a system composed of interconnected elements that store, dissipate, or transfer energy to the environment (see Figure 2.3, also introduced in Chapter 1). We can formalize this by assigning a set of port variables to each bond between elements. For instance, the bond between the central energy-routing element and the storage element has port variables $(\boldsymbol{e}_S, \boldsymbol{f}_S)$, the bond to the dissipation element has $(\boldsymbol{e}_R, \boldsymbol{f}_R)$, and the bond to the external environment has $(\boldsymbol{e}_P, \boldsymbol{f}_P)$. In this representation, the central energy-routing element corresponds to a Dirac structure $\mathscr{D}$, with total effort and flow vectors

$$\boldsymbol{e} = (\boldsymbol{e}_S, \boldsymbol{e}_R, \boldsymbol{e}_P) \in \mathbb{R}^p, \qquad \boldsymbol{f} = (\boldsymbol{f}_S, \boldsymbol{f}_R, \boldsymbol{f}_P) \in \mathbb{R}^p.$$

Property (i) then implies that the net power across the interconnection vanishes, see (2.16),

$$P = \begin{bmatrix} \boldsymbol{e}_S \\ \boldsymbol{e}_R \\ \boldsymbol{e}_P \end{bmatrix}^\top \begin{bmatrix} \boldsymbol{f}_S \\ \boldsymbol{f}_R \\ \boldsymbol{f}_P \end{bmatrix} = \boldsymbol{e}_S^\top \boldsymbol{f}_S + \boldsymbol{e}_R^\top \boldsymbol{f}_R + \boldsymbol{e}_P^\top \boldsymbol{f}_P = 0. \tag{2.18}$$

This picture allows us to interpret the ports and provides a foundation for defining pH systems in terms of Dirac structures. To this end, let us elaborate more on the individual ports.

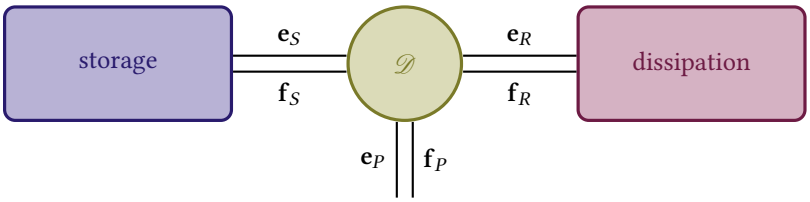

Figure 2.3.: Graphical depiction of a Dirac structure $\mathscr{D}$ with related ports [224, Figure 2.2].

Energy storage. Following the discussion in Section 2.1, an energy-storing element is described by energy variables (states) $\boldsymbol{x} \in \mathscr{X} = \mathbb{R}^n$, which determine its Hamiltonian $\mathcal{H}$, i.e., the total amount of stored energy. The associated port variables are

$$\boldsymbol{f}_S = -\dot{\boldsymbol{x}} \in \mathbb{R}^n, \qquad \boldsymbol{e}_S = \nabla\mathcal{H}(\boldsymbol{x}) \in \mathbb{R}^n, \tag{2.19}$$

where the signs are chosen so that the resulting power

$$P_S = \boldsymbol{e}_S^\top \boldsymbol{f}_S = -\nabla\mathcal{H}(\boldsymbol{x})^\top \dot{\boldsymbol{x}} = -\dot{\mathcal{H}} \tag{2.20}$$

represents the power extracted from the storage element.

Energy dissipation. For a dissipative element with effort $\boldsymbol{e}_R \in \mathbb{R}^{n_R}$ and flow $\boldsymbol{f}_R \in \mathbb{R}^{n_R}$ we introduce a (possibly modulated) resistive structure $\mathscr{R}(\boldsymbol{x})$, [224, Section 2.4]. Such a structure can be any subset $\mathscr{R}(\boldsymbol{x}) \subset \mathbb{R}^{n_R} \times \mathbb{R}^{n_R}$, such that

$$(\boldsymbol{e}_R, \boldsymbol{f}_R) \in \mathscr{R}(\boldsymbol{x}) \;\Rightarrow\; P_R = \boldsymbol{e}_R^\top \boldsymbol{f}_R \leq 0, \tag{2.21}$$

for every $\boldsymbol{x} \in \mathscr{X}$. The state-dependence of $\mathscr{R}$ is required to be smooth. By (2.21), every effort-flow pair from a resistive structure dissipates (or at most preserves) power. A typical example is given by the linear relation $\boldsymbol{e}_R = -\bar{\boldsymbol{R}}(\boldsymbol{x})\boldsymbol{f}_R$ for some pointwise symmetric and positive semi-definite $\bar{\boldsymbol{R}}(\boldsymbol{x}) = \bar{\boldsymbol{R}}(\boldsymbol{x})^\top \succeq 0$.

Port to the environment. The port variables associated with the system's interaction with the environment are typically represented by the input vector $\boldsymbol{u} \in \mathbb{R}^m$ and the collocated, power-conjugated output vector $\boldsymbol{y} \in \mathbb{R}^m$. In the literature, either

$$(\boldsymbol{e}_P, \boldsymbol{f}_P) = (\boldsymbol{u}, \boldsymbol{y}) \quad \text{or} \quad (\boldsymbol{e}_P, \boldsymbol{f}_P) = (\boldsymbol{y}, \boldsymbol{u}) \tag{2.22}$$

are used. In either case, the transmitted power amounts to $P_u = \boldsymbol{u}^\top \boldsymbol{y}$.

With these considerations we may now implicitly define a pH system by means of its underlying Dirac structure.

Definition 2.5 (Implicit pH system [224])**.** *A pH system is defined by the dynamics implicitly induced by*

$$(\nabla\mathcal{H}(\boldsymbol{x}), \boldsymbol{e}_R, \boldsymbol{e}_P, -\dot{\boldsymbol{x}}, \boldsymbol{f}_R, \boldsymbol{f}_P) \in \mathscr{D}(\boldsymbol{x}), \quad (\boldsymbol{e}_R, \boldsymbol{f}_R) \in \mathscr{R}(\boldsymbol{x}) \tag{2.23}$$

on the state variables $\boldsymbol{x} \in \mathbb{R}^n$ at all times t. Here $\mathscr{D}(\boldsymbol{x}) \subset \mathbb{R}^n \times \mathbb{R}^{n_R} \times \mathbb{R}^m \times \mathbb{R}^n \times \mathbb{R}^{n_R} \times \mathbb{R}^m$ represents a modulated Dirac structure as defined in Definition 2.4 and $\mathscr{R}(\boldsymbol{x}) \subset \mathbb{R}^{n_R} \times \mathbb{R}^{n_R}$ is a resistive structure, defined through (2.21). ♤

As a consequence of Property (i) of Dirac structures, we can now specify the related power balance equation (2.18) by means of the port relations (2.19), (2.21) and (2.22) such that

$$\begin{bmatrix} \nabla\mathcal{H}(\boldsymbol{x}) \\ \boldsymbol{e}_R \\ \boldsymbol{u} \end{bmatrix}^\top \begin{bmatrix} -\dot{\boldsymbol{x}} \\ \boldsymbol{f}_R \\ \boldsymbol{y} \end{bmatrix} = 0 \quad \Leftrightarrow \quad \dot{\mathcal{H}} = \boldsymbol{e}_R^\top \boldsymbol{f}_R + \boldsymbol{u}^\top \boldsymbol{y} \leq \boldsymbol{u}^\top \boldsymbol{y}. \tag{2.24}$$

Correspondingly, even without explicitly specifying the structure of the governing equations, a similar power balance arises, as already discussed for pH ODEs in (2.5). In this context, the defining property of the resistive structure (2.21) induces a dissipation inequality, consistent with the one obtained from the ODE case (2.6). By construction, *all* pH systems are passive, cf. Figure 2.1.

This equivalence motivates us to link the two viewpoints. In particular, one can show that pH ODE systems from Definition 2.1 admit an underlying Dirac structure, given by the graph of a specific skew-symmetric mapping (2.17). In particular, we consider the relation $\boldsymbol{f} = \tilde{\boldsymbol{J}}(\boldsymbol{x})\boldsymbol{e}$ to be specified in block form as

$$\begin{bmatrix} -\dot{\boldsymbol{x}} \\ \boldsymbol{f}_R \\ \boldsymbol{y} \end{bmatrix} = \begin{bmatrix} -\boldsymbol{J}(\boldsymbol{x}) & -\boldsymbol{G}_R(\boldsymbol{x}) & -\boldsymbol{B}(\boldsymbol{x}) \\ \boldsymbol{G}_R(\boldsymbol{x})^\top & 0 & 0 \\ \boldsymbol{B}(\boldsymbol{x})^\top & 0 & 0 \end{bmatrix} \begin{bmatrix} \nabla\mathcal{H}(\boldsymbol{x}) \\ \boldsymbol{e}_R \\ \boldsymbol{u} \end{bmatrix}, \tag{2.25}$$

cf. [223, Equation 2.42]. Therein, the skew-symmetry of $\tilde{\boldsymbol{J}}(\boldsymbol{x})$ follows directly from its block structure and the skew-symmetry of $\boldsymbol{J}(\boldsymbol{x})$. It remains to identify suitable $\boldsymbol{G}_R \in \mathbb{R}^{n \times n_R}$, which can be interpreted as a linear coupling between storage and resistive port variables. In particular, an admissible choice for $\boldsymbol{G}_R$ ensures that the dissipation matrix $\boldsymbol{R}(\boldsymbol{x})$ in the pH ODE representation is consistent with a resistive structure, defined by the linear relation $\boldsymbol{e}_R = -\bar{\boldsymbol{R}}(\boldsymbol{x})\boldsymbol{f}_R$. This leads eventually to the equivalence condition

$$\boldsymbol{R}(\boldsymbol{x}) = \boldsymbol{G}_R(\boldsymbol{x})\bar{\boldsymbol{R}}(\boldsymbol{x})\boldsymbol{G}_R(\boldsymbol{x})^\top, \tag{2.26}$$

for every $\boldsymbol{x} \in \mathscr{X}$. Thus, $\boldsymbol{G}_R(\boldsymbol{x})$ must be chosen in such a way that its column space contains the image of $\boldsymbol{R}(\boldsymbol{x})$. In the simplest case, $\boldsymbol{G}_R = \boldsymbol{I}$ so that $\boldsymbol{R}(\boldsymbol{x}) = \bar{\boldsymbol{R}}(\boldsymbol{x})$. In general, however, only a partition of the storage effort $\boldsymbol{e}_S = \nabla\mathcal{H}(\boldsymbol{x})$ is directly linked to the resistive structure, and $\boldsymbol{G}_R$ may therefore be rectangular.

Let us examine this case in more detail in the subsequent example, where we construct the underlying Dirac structure of the pendulum introduced in Example 2.3.

Example 2.6 (Nonlinear viscoelastic spring pendulum, continued)**.** *Let us revisit the viscoelastic spring-pendulum in Example 2.3 and decompose it into three subsystems that store energy, one that dissipates energy, and one for the interaction with the environment.*

- *The first energy-storing subsystem is associated with the potential energy of the point mass, with state $\boldsymbol{x}_1 = \boldsymbol{q} \in \mathbb{R}^3$ and Hamiltonian $\mathcal{H}_1(\boldsymbol{x}_1) = V(\boldsymbol{q})$. In view of* (2.19)*, this yields the flow $\boldsymbol{f}_1 = -\dot{\boldsymbol{q}} \in \mathbb{R}^3$ and the effort[3] $\boldsymbol{e}_1 = \nabla\mathcal{H}_1(\boldsymbol{x}_1) = \nabla V(\boldsymbol{q}) \in \mathbb{R}^3$, reflecting the power conjugation of velocity and force as flow and effort, respectively.*
- *The second energy-storing subsystem corresponds to the kinetic energy of the point mass, with state $\boldsymbol{x}_2 = \boldsymbol{p} \in \mathbb{R}^3$ and Hamiltonian $\mathcal{H}_2(\boldsymbol{x}_2) = \frac{1}{2m}\boldsymbol{p}^\top\boldsymbol{p}$. The associated port variables are $\boldsymbol{f}_2 = -\dot{\boldsymbol{p}} \in \mathbb{R}^3$ and $\boldsymbol{e}_2 = \nabla\mathcal{H}_2(\boldsymbol{x}_2) = \frac{1}{m}\boldsymbol{p} \in \mathbb{R}^3$.*

[3] This notation should not be confused with basis vectors of a Euclidean frame.

- *The third energy-storing subsystem represents the elastic potential energy of the spring, with state* $x_3 = C \in \mathbb{R}$ *and Hamiltonian* $\mathcal{H}_3(x_3) = W(C)$*. Its corresponding flow and effort are* $f_3 = -\dot{C} \in \mathbb{R}$ *and* $e_3 = W'(C) \in \mathbb{R}$*, respectively.*
- *In addition, the system contains a resistive subsystem modeling viscous dissipation. Here, the flow is given by the velocity of the point mass,* $\boldsymbol{f}_R = \boldsymbol{v} \in \mathbb{R}^3$*, and the effort corresponds to the viscous force,* $\boldsymbol{e}_R = \boldsymbol{f}_{\text{vis}} \in \mathbb{R}^3$*. Since we have assumed the viscous behavior to be governed by* $\boldsymbol{f}_{\text{vis}} = -\boldsymbol{V}(\boldsymbol{q})\boldsymbol{v}$ *with* $\boldsymbol{V} = \boldsymbol{V}^\top \succeq 0$ *for all* $\boldsymbol{q}$*, this is consistent with a resistive structure of the form* $\boldsymbol{e}_R = -\bar{\boldsymbol{R}}\boldsymbol{f}_R$*, where* $\bar{\boldsymbol{R}} = \boldsymbol{V}$*.*
- *Finally, the port describing the interaction with the environment is given by the effort-flow pair* $(\boldsymbol{e}_P, \boldsymbol{f}_P) = (\boldsymbol{u}, \boldsymbol{v})$*, where* $\boldsymbol{u}$ *is an external force on the point mass that has velocity* $\boldsymbol{v}$*.*

We can now show that the underlying Dirac structure is actually an embodiment of the governing physics. First, the velocity of the point mass needs to be identical in all representations and the strain rate of the spring, see relation (2.11)*, can be calculated accordingly. This yields the conditions*

$$\boldsymbol{f}_1 = -\boldsymbol{e}_2 = -\boldsymbol{f}_R = -\boldsymbol{f}_P, \qquad \text{and} \qquad f_3 = -\frac{2}{l_0^2}\boldsymbol{q}^\top \boldsymbol{e}_2. \tag{2.27}$$

Second, the dynamics must comply with the balance of linear momentum, i.e.,

$$-\boldsymbol{f}_2 = -\boldsymbol{e}_1 - \frac{2}{l_0^2}\boldsymbol{q}\, e_3 + \boldsymbol{e}_R + \boldsymbol{e}_P. \tag{2.28}$$

Rewriting those equations as

$$\begin{bmatrix} \boldsymbol{f}_1 \\ \boldsymbol{f}_2 \\ f_3 \\ \boldsymbol{f}_R \\ \boldsymbol{f}_P \end{bmatrix} = \begin{bmatrix} 0 & -\boldsymbol{I} & 0 & 0 & 0 \\ \boldsymbol{I} & 0 & \frac{2}{l_0^2}\boldsymbol{q} & -\boldsymbol{I} & -\boldsymbol{I} \\ 0 & -\frac{2}{l_0^2}\boldsymbol{q}^\top & 0 & 0 & 0 \\ 0 & \boldsymbol{I} & 0 & 0 & 0 \\ 0 & \boldsymbol{I} & 0 & 0 & 0 \end{bmatrix} \begin{bmatrix} \boldsymbol{e}_1 \\ \boldsymbol{e}_2 \\ e_3 \\ \boldsymbol{e}_R \\ \boldsymbol{e}_P \end{bmatrix} \tag{2.29}$$

provides the skew-symmetric map (2.25) *with* $\boldsymbol{B}^\top = \boldsymbol{G}_R^\top = [\boldsymbol{0}\ \boldsymbol{I}\ \boldsymbol{0}] \in \mathbb{R}^{3\times 7}$*. The resulting ODEs are identical to* (2.12) *where we make use of the overall state* $\boldsymbol{x} = (\boldsymbol{x}_1, \boldsymbol{x}_2, \boldsymbol{x}_3) = (\boldsymbol{q}, \boldsymbol{p}, C) \in \mathbb{R}^7$*, together with the total Hamiltonian* $\mathcal{H} = \mathcal{H}_1 + \mathcal{H}_2 + \mathcal{H}_3$ *and thus* $\nabla\mathcal{H}(\boldsymbol{x}) = (\nabla V(\boldsymbol{q}), \frac{1}{m}\boldsymbol{p}, W'(C))$*. Lastly, the dissipation matrix in* (2.13) *can be recovered using* (2.26) *as* $\boldsymbol{R} = \boldsymbol{G}_R \bar{\boldsymbol{R}} \boldsymbol{G}_R^\top = \operatorname{diag}(\boldsymbol{0}, \boldsymbol{V}(\boldsymbol{q}), \boldsymbol{0}) \in \mathbb{R}^{7\times 7}$*.* ◇

Thus, it is not surprising that the class of pH systems implicitly defined through Dirac structures, see Definition 2.5, extends well beyond those admitting the ODE representation of Definition 2.1. Correspondingly, we proceed by introducing a more general formulation for pH systems.

2.3. A generalized DAE representation of port-Hamiltonian systems

We seek to generalize the notion of port-Hamiltonian systems (see Definition 2.1) for later use in this thesis. To this end, we allow for the presence of an additional matrix $\boldsymbol{E}$ multiplying the time derivative of the state variables, which provides greater flexibility for modeling purposes. Notably, this extension entails that the gradient of the Hamiltonian $\nabla\mathcal{H}$ no longer enters the dynamical equations explicitly. Instead, an additional equation is required to close the system. Moreover, the matrix $\boldsymbol{E}$ is not even required to be regular, which allows the framework to encompass differential-algebraic equations (DAEs). Enriching DAEs with input and output variables gives rise to the terminology of *descriptor* systems [23, Section 1].

Definition 2.7 (pH DAE system [A3, 161])**.** *A port-Hamiltonian descriptor system, shorthand* pH DAE system*, is a state-space model of the form*

$$\boldsymbol{E}(\boldsymbol{x})\dot{\boldsymbol{x}} = \big(\boldsymbol{J}(\boldsymbol{x}) - \boldsymbol{R}(\boldsymbol{x})\big)\boldsymbol{z}(\boldsymbol{x}) + \boldsymbol{B}(\boldsymbol{x})\boldsymbol{u}, \tag{2.30a}$$

$$\boldsymbol{y} = \boldsymbol{B}(\boldsymbol{x})^\top \boldsymbol{z}(\boldsymbol{x}), \tag{2.30b}$$

together with a Hamiltonian $\mathcal{H} \in \mathscr{C}^1(\mathscr{X}, \mathbb{R})$*, where* $\boldsymbol{E}, \boldsymbol{J}, \boldsymbol{R} \in \mathscr{C}(\mathscr{X}, \mathbb{R}^{n\times n})$*,* $\boldsymbol{B} \in \mathscr{C}(\mathscr{X}, \mathbb{R}^{n\times m})$*, and* $\boldsymbol{z} \in \mathscr{C}(\mathscr{X}, \mathbb{R}^n)$ *satisfy the properties* $\boldsymbol{J}(\boldsymbol{x}) = -\boldsymbol{J}(\boldsymbol{x})^\top$*,* $\boldsymbol{R}(\boldsymbol{x}) = \boldsymbol{R}(\boldsymbol{x})^\top \succeq 0$ *for all* $\boldsymbol{x} \in \mathscr{X}$*. Moreover,* $(\boldsymbol{E}, \boldsymbol{z})$ *is a gradient pair for* $\mathcal{H}$*, which means that*

$$\boldsymbol{E}(\boldsymbol{x})^\top \boldsymbol{z}(\boldsymbol{x}) = \nabla\mathcal{H}(\boldsymbol{x}) \tag{2.30c}$$

for all $\boldsymbol{x} \in \mathscr{X}$*. Here* $\boldsymbol{E}, \boldsymbol{J}, \boldsymbol{R}$ *are called the descriptor, structure, and dissipation matrix, respectively, and* $\boldsymbol{z}$ *is called the costate function.* ♤

As stated above, the gradient of the Hamiltonian no longer appears explicitly in the dynamical equation (2.30a), but is replaced by the costate function. These two quantities are linked through the so-called *gradient-pair* relation (2.30c), which is an additional building block of this formalism that ensures its pH structure. The output equation (2.30b) is modified accordingly.

Notably, this definition encompasses the pH ODE representation in Definition 2.1 as a special case, which can be recovered by setting $\boldsymbol{E} = \boldsymbol{I}$. Correspondingly, the relation (2.30c) then yields $\boldsymbol{z}(\boldsymbol{x}) = \nabla\mathcal{H}(\boldsymbol{x})$. In general, however, the descriptor matrix $\boldsymbol{E}$ may even be singular, which allows for the inclusion of algebraic constraints in the system. Let us illustrate this case by means of Hamiltonian mechanical systems, as seen in Example 2.2, now with additional holonomic constraints.

Example 2.8 (Hamiltonian mechanical systems, continued)**.** *We reconsider the Hamiltonian dynamics of a mechanical system as already introduced in Example 2.2. The system is now subject to* r *independent, holonomic constraints*

$$\boldsymbol{g} \in \mathscr{C}^1(\mathbb{R}^d, \mathbb{R}^r), \qquad \boldsymbol{g}(\boldsymbol{q}) = \boldsymbol{0}, \tag{2.31}$$

which render the coordinates $\boldsymbol{q} \in \mathbb{R}^d$ *redundant. Accordingly, Lagrange multipliers* $\boldsymbol{\lambda} \in \mathbb{R}^r$ *appear together with the constraint Jacobian* $\mathrm{D}\boldsymbol{g}(\boldsymbol{q})$ *in the form of constraint forces in the momentum balance. To match the pH DAE structure of the dynamical equation* (2.30a)*, the constraints* (2.31) *are imposed at velocity level as*

$$\mathrm{D}\boldsymbol{g}(\boldsymbol{q})\dot{\boldsymbol{q}} = \boldsymbol{0}, \tag{2.32}$$

thereby restricting admissible velocities. In contrast to the classical formulation, this reduces the differential index from 3 to 2. Neglecting again external forces $\boldsymbol{u}$ *for clarity, the resulting pH DAE system reads*

$$\begin{bmatrix} \boldsymbol{I} & 0 & 0 \\ 0 & \boldsymbol{I} & 0 \\ 0 & 0 & \boldsymbol{0} \end{bmatrix} \begin{bmatrix} \dot{\boldsymbol{q}} \\ \dot{\boldsymbol{p}} \\ \dot{\boldsymbol{\lambda}} \end{bmatrix} = \left(\begin{bmatrix} 0 & \boldsymbol{I} & 0 \\ -\boldsymbol{I} & 0 & -\mathrm{D}\boldsymbol{g}(\boldsymbol{q})^\top \\ 0 & \mathrm{D}\boldsymbol{g}(\boldsymbol{q}) & 0 \end{bmatrix} \right) \begin{bmatrix} \nabla U(\boldsymbol{q}) \\ \boldsymbol{M}^{-1}\boldsymbol{p} \\ \boldsymbol{\lambda} \end{bmatrix} \tag{2.33}$$

and can be understood in the framework of Definition 2.7 using the singular descriptor matrix $\boldsymbol{E} = \mathrm{diag}(\boldsymbol{I}, \boldsymbol{I}, \boldsymbol{0})$*. In this context, we have introduced the Jacobian* $\mathrm{D}\boldsymbol{g}(\boldsymbol{q})$*, intended as a matrix function whose rows transposed are the gradients of the entries* g_i $(i = 1, \ldots, r)$*, cf. Equation* (5.1) *for completeness. The associated Hamiltonian of the system coincides with that of the unconstrained case* (2.8)*, but the state vector is extended to* $\boldsymbol{x} = (\boldsymbol{q}, \boldsymbol{p}, \boldsymbol{\lambda})$*. One has to additionally check the gradient-pair relation* (2.30c) *in order to asses the pH structure of the system. Since the Lagrange multipliers do not enter the Hamiltonian, this property can be verified directly. Lastly, note that the use of time-differentiated algebraic constraints is analogous to the strain evolution discussed in Example 2.3. This pH model can also be extended to*

non-constant mass matrices [B6, 216] or even more general Lagrangian settings [B6]. More details on the derivations of the governing equations may be found for example in the textbook [110, Chapter 1]. A similar model will be revisited in Section 5.5.1 later in this work. ◊

As anticipated, the extended formulation (2.30) for pH DAEs also satisfies an underlying power balance equation, because it has an associated Dirac structure. Using the chain rule and subsequently inserting (2.30c) and (2.30a) yields

$$\dot{\mathcal{H}} = \nabla\mathcal{H}(\boldsymbol{x})^\top \dot{\boldsymbol{x}} = \boldsymbol{z}(\boldsymbol{x})^\top \boldsymbol{E}(\boldsymbol{x})\dot{\boldsymbol{x}} = \boldsymbol{z}(\boldsymbol{x})^\top \Big(\big(\boldsymbol{J}(\boldsymbol{x}) - \boldsymbol{R}(\boldsymbol{x})\big)\boldsymbol{z}(\boldsymbol{x}) + \boldsymbol{B}(\boldsymbol{x})\boldsymbol{u} \Big). \tag{2.34}$$

Exploiting the skew-symmetry of $\boldsymbol{J}$ and inserting (2.30b) then leads to the power balance equation

$$\dot{\mathcal{H}} = -\boldsymbol{z}(\boldsymbol{x})^\top \boldsymbol{R}(\boldsymbol{x})\boldsymbol{z}(\boldsymbol{x}) + \boldsymbol{y}^\top \boldsymbol{u}. \tag{2.35}$$

Identifying the non-negative dissipation power here as $P_R := \boldsymbol{z}(\boldsymbol{x})^\top \boldsymbol{R}(\boldsymbol{x})\boldsymbol{z}(\boldsymbol{x}) \geq 0$, we can again infer the dissipation inequality $\dot{\mathcal{H}} \leq \boldsymbol{y}^\top \boldsymbol{u}$. Consequently, the system is passive. Further, it is lossless when $\boldsymbol{R} = \boldsymbol{0}$, and energy-conserving when additionally $\boldsymbol{u} = \boldsymbol{0}$, cf. Figure 2.1.

We now turn to the underlying Dirac and resistive structures related to pH descriptor systems from Definition 2.7. To this end, we first consider the so-called *Dirac–dissipative representation* (shorthand *DDR*) [165], which provides an equivalent formulation of the equations (2.30) as

$$\begin{bmatrix} \nabla\mathcal{H}(\boldsymbol{x}) \\ \boldsymbol{0} \\ \boldsymbol{y} \end{bmatrix} + \begin{bmatrix} 0 & -\boldsymbol{E}(\boldsymbol{x})^\top & 0 \\ \boldsymbol{E}(\boldsymbol{x}) & \boldsymbol{J}(\boldsymbol{x}) - \boldsymbol{R}(\boldsymbol{x}) & \boldsymbol{B}(\boldsymbol{x}) \\ 0 & -\boldsymbol{B}(\boldsymbol{x})^\top & 0 \end{bmatrix} \begin{bmatrix} -\dot{\boldsymbol{x}} \\ \boldsymbol{z}(\boldsymbol{x}) \\ \boldsymbol{u} \end{bmatrix} = 0. \tag{2.36}$$

The individual block rows of the DDR (2.36) correspond to the gradient-pair relation (2.30c), the dynamical equation (2.30a), and the output equation (2.30b), respectively. As the name suggests, this representation combines a Dirac structure, as introduced in Definition 2.4, with a resistive structure (cf. Equation (2.21)) into a single formulation. To disentangle these two components, we proceed along the lines of Morandin [165, Theorem 3.2.13]. To this end, we introduce the port variables

$$(\boldsymbol{e}_S, \boldsymbol{f}_S) = (\nabla\mathcal{H}(\boldsymbol{x}), -\dot{\boldsymbol{x}}), \tag{2.37a}$$
$$(\boldsymbol{e}_P, \boldsymbol{f}_P) = (\boldsymbol{y}, \boldsymbol{u}), \tag{2.37b}$$
$$(\boldsymbol{e}_{R,1}, \boldsymbol{f}_{R,1}) = (\boldsymbol{0}, \boldsymbol{z}(\boldsymbol{x})), \tag{2.37c}$$
$$(\boldsymbol{e}_{R,2}, \boldsymbol{f}_{R,2}) = (-\boldsymbol{f}_{R,1}, -\boldsymbol{R}(\boldsymbol{x})\boldsymbol{e}_{R,2}), \tag{2.37d}$$

where the port relations (2.37a) are associated with energy storage, see (2.19). Relation (2.37b) corresponds to the interconnection to the environment, consistently with (2.22). Moreover, (2.37c) and (2.37d) constitute dissipative ports that form the resistive structure

$$\begin{bmatrix} \boldsymbol{e}_{R,1} \\ \boldsymbol{f}_{R,2} \end{bmatrix} + \begin{bmatrix} 0 & 0 \\ 0 & \boldsymbol{R}(\boldsymbol{x}) \end{bmatrix} \begin{bmatrix} \boldsymbol{f}_{R,1} \\ \boldsymbol{e}_{R,2} \end{bmatrix} = 0. \tag{2.38}$$

The defining property of a resistive structure, cf. (2.21), namely $P_R = \boldsymbol{e}_R^\top \boldsymbol{f}_R \leq 0$, can be proven as

$$P_R = \begin{bmatrix} \boldsymbol{e}_{R,1} \\ \boldsymbol{e}_{R,2} \end{bmatrix}^\top \begin{bmatrix} \boldsymbol{f}_{R,1} \\ \boldsymbol{f}_{R,2} \end{bmatrix} = \begin{bmatrix} \boldsymbol{0} \\ \boldsymbol{e}_{R,2} \end{bmatrix}^\top \begin{bmatrix} \boldsymbol{z}(\boldsymbol{x}) \\ -\boldsymbol{R}(\boldsymbol{x})\boldsymbol{e}_{R,2} \end{bmatrix} = -\boldsymbol{z}(\boldsymbol{x})^\top \boldsymbol{R}(\boldsymbol{x})\boldsymbol{z}(\boldsymbol{x}) \leq 0 \tag{2.39}$$

for all $\boldsymbol{x} \in \mathscr{X}$, where we ultimately used $\boldsymbol{e}_{R,2} = -\boldsymbol{f}_{R,1} = -\boldsymbol{z}(\boldsymbol{x})$, see (2.37c) and (2.37d). Furthermore, one can expose the underlying Dirac structure by combining the DDR (2.36) with the port definitions (2.37) to obtain

$$\begin{bmatrix} \boldsymbol{e}_S \\ \boldsymbol{e}_{R,1} \\ \boldsymbol{e}_{R,2} \\ \boldsymbol{e}_P \end{bmatrix} + \begin{bmatrix} 0 & -\boldsymbol{E}(\boldsymbol{x})^\top & 0 & 0 \\ \boldsymbol{E}(\boldsymbol{x}) & \boldsymbol{J}(\boldsymbol{x}) & -\boldsymbol{I} & \boldsymbol{B}(\boldsymbol{x}) \\ 0 & \boldsymbol{I} & 0 & 0 \\ 0 & -\boldsymbol{B}(\boldsymbol{x})^\top & 0 & 0 \end{bmatrix} \begin{bmatrix} \boldsymbol{f}_S \\ \boldsymbol{f}_{R,1} \\ \boldsymbol{f}_{R,2} \\ \boldsymbol{f}_P \end{bmatrix} = \boldsymbol{0} \qquad \Leftrightarrow \qquad \boldsymbol{e} + \tilde{\boldsymbol{J}}(\boldsymbol{x})\boldsymbol{f} = \boldsymbol{0}. \tag{2.40}$$

It can be seen that this Dirac structure again relates to the graph of a skew-symmetric map (2.17). Note that the power balance equation (2.35) related to pH descriptor systems can be equivalently derived by means of the fundamental property of Dirac structures $\boldsymbol{e}^\top \boldsymbol{f} = 0$ together with the definitions (2.37).

As discussed above, the pH formalism (2.30) not only accommodates DAE systems, but also provides increased modeling flexibility even when $\boldsymbol{E}$ is regular. We study this formally by means of state transformations. In particular, the pH descriptor formulation can be understood as being naturally induced by a state transformation of a pH ODE system. Consider a pH ODE with state $\boldsymbol{x}$ and Hamiltonian $\mathcal{H}$ governed by (2.3), such that $\dot{\boldsymbol{x}} = (\boldsymbol{J}(\boldsymbol{x}) - \boldsymbol{R}(\boldsymbol{x}))\nabla\mathcal{H}(\boldsymbol{x}) + \boldsymbol{B}(\boldsymbol{x})\boldsymbol{u}$ and $\boldsymbol{y} = \boldsymbol{B}(\boldsymbol{x})^\top \nabla\mathcal{H}(\boldsymbol{x})$. Suppose we seek a representation in new state variables $\tilde{\boldsymbol{x}}$, related to the original ones via a diffeomorphism, that is defined together with its Jacobian as

$$\boldsymbol{x} = \boldsymbol{\varphi}(\tilde{\boldsymbol{x}}), \quad \mathrm{D}\boldsymbol{\varphi}(\tilde{\boldsymbol{x}}) =: \boldsymbol{E}(\tilde{\boldsymbol{x}}). \tag{2.41}$$

Additionally, we introduce a new Hamiltonian $\tilde{\mathcal{H}}$ as the composition of the state transformation and the original Hamiltonian such that

$$\tilde{\mathcal{H}}(\tilde{\boldsymbol{x}}) = \mathcal{H}(\boldsymbol{\varphi}(\tilde{\boldsymbol{x}})) \quad \Rightarrow \quad \nabla\tilde{\mathcal{H}}(\tilde{\boldsymbol{x}}) = \mathrm{D}\boldsymbol{\varphi}(\tilde{\boldsymbol{x}})^\top \nabla\mathcal{H}(\boldsymbol{x})\big|_{\boldsymbol{x}=\boldsymbol{\varphi}(\tilde{\boldsymbol{x}})}, \tag{2.42}$$

where we have used the chain rule. Defining the costate function of the emanating pH DAE as $\boldsymbol{z}(\tilde{\boldsymbol{x}}) := \nabla\mathcal{H}(\boldsymbol{x})|_{\boldsymbol{x}=\boldsymbol{\varphi}(\tilde{\boldsymbol{x}})}$, and inserting the Jacobian $\boldsymbol{E}$ into (2.42), yields the gradient-pair relation (2.30c) of the emanating pH DAE

$$\boldsymbol{E}(\tilde{\boldsymbol{x}})^\top \boldsymbol{z}(\tilde{\boldsymbol{x}}) = \nabla\tilde{\mathcal{H}}(\tilde{\boldsymbol{x}}). \tag{2.43}$$

Eventually, the original dynamical equation and the output equation can be evaluated at $\boldsymbol{x} = \boldsymbol{\varphi}(\tilde{\boldsymbol{x}})$ as well and by means of the newly defined costate and $\dot{\boldsymbol{x}} = \boldsymbol{E}(\tilde{\boldsymbol{x}})\,\dot{\tilde{\boldsymbol{x}}}$ we obtain

$$\boldsymbol{E}(\tilde{\boldsymbol{x}})\dot{\tilde{\boldsymbol{x}}} = \big(\boldsymbol{J}(\boldsymbol{\varphi}(\tilde{\boldsymbol{x}})) - \boldsymbol{R}(\boldsymbol{\varphi}(\tilde{\boldsymbol{x}}))\big)\boldsymbol{z}(\tilde{\boldsymbol{x}}) + \boldsymbol{B}(\boldsymbol{\varphi}(\tilde{\boldsymbol{x}}))\boldsymbol{u}, \quad \boldsymbol{y} = \boldsymbol{B}(\boldsymbol{\varphi}(\tilde{\boldsymbol{x}}))^\top \boldsymbol{z}(\tilde{\boldsymbol{x}}), \tag{2.44}$$

which corresponds to (2.30a) and (2.30b), respectively.

Note that no transformation of the system matrices is required in the procedure above. Instead, it suffices to compose the original mappings $\boldsymbol{J}$, $\boldsymbol{R}$, and $\boldsymbol{B}$ with the state transformation $\boldsymbol{\varphi}$. Conversely, any pH descriptor system (2.30) with regular descriptor matrix $\boldsymbol{E}$ can be transformed into an equivalent pH ODE system [C4, Remark 2.2]. Moreover, the reader is referred to Mehrmann and Morandin [161] for the illustration of structure-preserving state transformations between pH DAE systems of the form (2.30). Let us now illustrate the state transformation using the earlier viscoelastic spring pendulum example.

Example 2.9 (Nonlinear viscoelastic spring pendulum, continued)**.** *We reconsider the system previously studied in Examples 2.3 and 2.6. Up to this point, the state variables have been chosen as* $\boldsymbol{x} = (\boldsymbol{q}, \boldsymbol{p}, C) \in \mathbb{R}^7$. *We now perform a state transformation as outlined above and investigate the dynamics in terms of the new state*

$$\tilde{\boldsymbol{x}} = (\boldsymbol{q}, \boldsymbol{v}, \varepsilon) \in \mathbb{R}^7,$$

where $\boldsymbol{v} = \dot{\boldsymbol{q}} = m^{-1}\boldsymbol{p} \in \mathbb{R}^3$ *denotes the velocity of the point mass and* $\varepsilon \in \mathbb{R}$*, satisfying*

$$\varepsilon = \tilde{\varepsilon}(\boldsymbol{q}) = \frac{1}{2}\left(\frac{\boldsymbol{q}^\top \boldsymbol{q}}{l_0^2} - 1\right), \tag{2.45}$$

is an alternative strain measure, which can be interpreted as the Green–Lagrangian strain known from continuum mechanics [36, 111]. The original state is related to the new one by a diffeomorphism (2.41) *that is given, together with the associated Jacobian, as*

$$\boldsymbol{\varphi}(\tilde{\boldsymbol{x}}) = \begin{bmatrix} \boldsymbol{q} \\ m\boldsymbol{v} \\ 2\varepsilon + 1 \end{bmatrix}, \qquad \text{and} \qquad \boldsymbol{E} = \mathrm{D}\boldsymbol{\varphi}(\tilde{\boldsymbol{x}}) = \operatorname{diag}(\boldsymbol{I}, m\boldsymbol{I}, 2). \tag{2.46}$$

Substituting these relations into the Hamiltonian expressed in the original variables (2.14) *yields the transformed Hamiltonian*

$$\tilde{\mathcal{H}}(\tilde{\boldsymbol{x}}) = \frac{1}{2} m\boldsymbol{v}^\top \boldsymbol{v} + V(\boldsymbol{q}) + W_\varepsilon(\varepsilon).$$

Here, W_ε *denotes the hyperelastic strain energy expressed in terms of the new strain variable, under the condition that* $W_\varepsilon(\tilde{\varepsilon}(\boldsymbol{q})) = W(\tilde{C}(\boldsymbol{q}))$*. Using the relation* (2.43)*, the costate function* $\boldsymbol{z}(\tilde{\boldsymbol{x}})$ *can be computed, and the equations of motion in the transformed variables follow directly from* (2.44) *as*

$$\begin{bmatrix} \boldsymbol{I} & 0 & 0 \\ 0 & m\boldsymbol{I} & 0 \\ 0 & 0 & 2 \end{bmatrix} \begin{bmatrix} \dot{\boldsymbol{q}} \\ \dot{\boldsymbol{v}} \\ \dot{\varepsilon} \end{bmatrix} = \begin{bmatrix} 0 & \boldsymbol{I} & 0 \\ -\boldsymbol{I} & -\boldsymbol{V}(\boldsymbol{q}) & -\frac{2}{l_0^2}\boldsymbol{q} \\ 0 & \frac{2}{l_0^2}\boldsymbol{q}^\top & 0 \end{bmatrix} \begin{bmatrix} \nabla V(\boldsymbol{q}) \\ \boldsymbol{v} \\ \frac{1}{2}W_\varepsilon'(\varepsilon) \end{bmatrix} + \begin{bmatrix} 0 \\ \boldsymbol{I} \\ 0 \end{bmatrix} \boldsymbol{u}, \tag{2.47}$$

where the expressions for $\boldsymbol{J}(\tilde{\boldsymbol{x}})$ *and* $\boldsymbol{R}(\tilde{\boldsymbol{x}})$ *are obtained by inserting the state transformation into the matrix functions of the original dynamical equation* (2.12)*. In the present example, both matrices depend only on the position* $\boldsymbol{q}$*, which remains unchanged under the transformation. We have omitted the output equation for the sake of simplicity.* ◇

As already indicated above, the pH formalism discussed in this section offers increased flexibility for modeling purposes. This becomes apparent from the following considerations. So far, the costate $\boldsymbol{z}$ appearing in the dynamical equation (2.30a) has been interpreted as a function of the state, that is, $\boldsymbol{z} \in \mathscr{C}(\mathscr{X}, \mathbb{R}^n)$. For (2.30) to define a descriptor system, the costate function and the descriptor matrix must form a gradient pair for the Hamiltonian, meaning that (2.30c) has to be satisfied for all $\boldsymbol{x} \in \mathscr{X}$. In this context, the equations (2.30a) and (2.30b) constitute $n + m$ equations for $(\boldsymbol{x}, \boldsymbol{y}) \in \mathbb{R}^{n+m}$. If, in addition, (2.30c) holds, the system has a pH structure. By contrast, the costate (or partitions thereof) may instead be treated as an independent set of unknowns. For regular $\boldsymbol{E}$, the quantity $\boldsymbol{z} \in \mathbb{R}^n$ constitutes additional unknowns, and the $2n + m$ equations

$$\boldsymbol{E}(\boldsymbol{x})\dot{\boldsymbol{x}} = \big(\boldsymbol{J}(\boldsymbol{x}) - \boldsymbol{R}(\boldsymbol{x})\big)\boldsymbol{z} + \boldsymbol{B}(\boldsymbol{x})\boldsymbol{u}, \tag{2.48a}$$

$$\boldsymbol{y} = \boldsymbol{B}(\boldsymbol{x})^\top \boldsymbol{z}, \tag{2.48b}$$

$$\boldsymbol{E}(\boldsymbol{x})^\top \boldsymbol{z} = \nabla \mathcal{H}(\boldsymbol{x}). \tag{2.48c}$$

have to be solved for $(\boldsymbol{x}, \boldsymbol{y}, \boldsymbol{z}) \in \mathbb{R}^{2n+m}$. Importantly, system (2.48) is equivalent to (2.30), since the new variable $\boldsymbol{z}$ is uniquely determined by the gradient-pair condition (2.48c).

Another option arises when the descriptor matrix has a block-diagonal structure, $\boldsymbol{E} = \operatorname{diag}(\boldsymbol{E}_{11}, \boldsymbol{E}_{22})$, with the state correspondingly partitioned as $\boldsymbol{x} = (\boldsymbol{x}_1, \boldsymbol{x}_2)$. In this setting, the costate can be decomposed as $\boldsymbol{z} = (\boldsymbol{z}_1(\boldsymbol{x}), \boldsymbol{z}_2)$, where the first component is treated as a function of the state and the second entry

represents an additional set of unknowns. This decomposition requires the explicit inclusion of the gradient-pair relation in the sense of (2.48c), namely $\boldsymbol{E}_{22}^{\top} \boldsymbol{z}_2 = \nabla_{\boldsymbol{x}_2} \mathcal{H}$, into the governing equations. For $\boldsymbol{z}_1(\boldsymbol{x})$, the gradient-pair condition (2.30c) can be verified to establish the pH structure. This approach is employed in Chapter 5 for the construction of structure-preserving time integrators for semi-explicit pH DAEs, where $\boldsymbol{E}_{22} = \boldsymbol{0}$. Let us illustrate this concept in the following example — see also the formulation (2.53) further below dealing with the DAE case.

Example 2.10 (Nonlinear viscoelastic spring pendulum, continued)**.** *For the pendulum considered in the previous Example 2.9, the costate can be partitioned as* $\boldsymbol{z} = (\boldsymbol{z}_1(\boldsymbol{x}), z_2)$*, where* $\boldsymbol{z}_1(\boldsymbol{x}) = (\nabla V(\boldsymbol{q}), \boldsymbol{v}) \in \mathscr{C}(\mathscr{X}, \mathbb{R}^6)$ *is treated as a function of the state, and* $z_2 := \sigma \in \mathbb{R}$ *is an independent unknown. Consequently, the dynamical equation* (2.47) *can be rewritten as*

$$\begin{bmatrix} \boldsymbol{I} & \boldsymbol{0} & \boldsymbol{0} \\ \boldsymbol{0} & m\boldsymbol{I} & \boldsymbol{0} \\ \boldsymbol{0} & \boldsymbol{0} & 1 \end{bmatrix} \begin{bmatrix} \dot{\boldsymbol{q}} \\ \dot{\boldsymbol{v}} \\ \dot{\varepsilon} \end{bmatrix} = \begin{bmatrix} \boldsymbol{0} & \boldsymbol{I} & \boldsymbol{0} \\ -\boldsymbol{I} & -\boldsymbol{V}(\boldsymbol{q}) & -\frac{1}{l_0^2}\boldsymbol{q} \\ \boldsymbol{0} & \frac{1}{l_0^2}\boldsymbol{q}^{\top} & 0 \end{bmatrix} \begin{bmatrix} \nabla V(\boldsymbol{q}) \\ \boldsymbol{v} \\ \sigma \end{bmatrix} + \begin{bmatrix} \boldsymbol{0} \\ \boldsymbol{I} \\ \boldsymbol{0} \end{bmatrix} \boldsymbol{u}, \tag{2.49a}$$

$$\sigma = W_{\varepsilon}'(\varepsilon), \tag{2.49b}$$

and must be solved for $(\boldsymbol{q}, \boldsymbol{v}, \varepsilon, \sigma)$*. These equations differ from those induced by a Hu–Washizu principle [36, Equation 9] only in the time-differentiated form of the compatibility condition, i.e., the third row of* (2.49a)*. As discussed above, the procedure necessitates additional equations relating the new unknowns to the corresponding component of the Hamiltonian gradient. In this context, the constitutive relation* (2.49b) *is induced by Equation* (2.48c)*.* ◊

Notably, the formulation of pH systems in this section encompasses the DAE case, characterized by a singular descriptor matrix $\boldsymbol{E}$, as a limit case. This can be achieved by means of *velocity-stress* formulations [47, 219], which assume linear-elastic material behavior, that is, a quadratic Hamiltonian[4]. In such formulations, the compatibility conditions between independent stress variables and kinematic quantities appear in compliance form, involving inverse stiffness parameters that can be set to zero. This property is particularly relevant for mechanical systems subject to additional kinematic constraints, such as inextensibility of strings [218, Appendix A] or the shear rigidity in beam models [104, A4] — see also Chapter 4. We illustrate this aspect again using the pendulum example.

Example 2.11 (Nonlinear viscoelastic spring pendulum, continued)**.** *Let us revisit the viscoelastic spring-pendulum governed by the pH formulation* (2.49)*. Assume a quadratic strain energy function*

$$W_{\varepsilon}(\varepsilon) = \frac{1}{2} k l_0^2 \varepsilon^2, \tag{2.50}$$

corresponding to a St. Venant–Kirchhoff type material model. From the relation (2.49b)*, we obtain the linear and invertible stress-strain mapping* $\sigma = k l_0^2 \varepsilon$ *such that*

$$\varepsilon = c\sigma, \qquad \text{where} \qquad c := k^{-1} l_0^{-2}$$

[4] Note that this is a common assumption for geometrically exact beam and shell models. Despite the presence of large rotations, displacements, and deformations, the strain field can typically be assumed to remain moderate at the local level, which motivates the use of a St. Venant–Kirchhoff material law.

describes an inverse stiffness parameter, called compliance parameter. This relation allows us to eliminate the strain variable and reformulate the dynamical system (2.49a) *in velocity-stress form with the state variables* $\boldsymbol{x} = (\boldsymbol{q}, \boldsymbol{v}, \sigma) \in \mathbb{R}^7$ *as*

$$\begin{bmatrix} \boldsymbol{I} & 0 & 0 \\ 0 & m\boldsymbol{I} & 0 \\ 0 & 0 & c \end{bmatrix} \begin{bmatrix} \dot{\boldsymbol{q}} \\ \dot{\boldsymbol{v}} \\ \dot{\sigma} \end{bmatrix} = \begin{bmatrix} 0 & \boldsymbol{I} & 0 \\ -\boldsymbol{I} & -\boldsymbol{V}(\boldsymbol{q}) & -\frac{1}{l_0^2}\boldsymbol{q} \\ 0 & \frac{1}{l_0^2}\boldsymbol{q}^\top & 0 \end{bmatrix} \begin{bmatrix} \nabla V(\boldsymbol{q}) \\ \boldsymbol{v} \\ \sigma \end{bmatrix} + \begin{bmatrix} 0 \\ \boldsymbol{I} \\ 0 \end{bmatrix} \boldsymbol{u}. \tag{2.51}$$

The related Hamiltonian reads

$$\mathcal{H}(\boldsymbol{x}) = \frac{1}{2} m \boldsymbol{v}^\top \boldsymbol{v} + V(\boldsymbol{q}) + W^\star(\sigma). \tag{2.52}$$

This formulation admits a variational interpretation in terms of a Hellinger–Reissner principle and the complementary strain energy function $W^\star(\sigma) = \frac{1}{2} c \sigma^2$ *is obtained via a Legendre transformation of the strain-based energy function* (2.50)*. Moreover, the last block of* (2.51) *still represents a compatibility relation between the strain (expressed in terms of the stress) and the kinematic variables. Using the compliance parameter* c*, this relation may be referred to as a time-differentiated compliance equation.*

An important advantage of the velocity-stress formulation (2.51) *is that kinematic constraints can be imposed in a straightforward manner. In particular, by letting* $k \to \infty$*, the compliance is set to zero, such that* $c = 0$ *in* (2.51)*. In this limit, the spring behaves as a rigid link, and the system reduces to the model of a mathematical pendulum governed by*

$$\begin{bmatrix} \boldsymbol{I} & 0 & 0 \\ 0 & m\boldsymbol{I} & 0 \\ 0 & 0 & 0 \end{bmatrix} \begin{bmatrix} \dot{\boldsymbol{q}} \\ \dot{\boldsymbol{v}} \\ \dot{\sigma} \end{bmatrix} = \begin{bmatrix} 0 & \boldsymbol{I} & 0 \\ -\boldsymbol{I} & -\boldsymbol{V}(\boldsymbol{q}) & -\frac{1}{l_0^2}\boldsymbol{q} \\ 0 & \frac{1}{l_0^2}\boldsymbol{q}^\top & 0 \end{bmatrix} \begin{bmatrix} \nabla V(\boldsymbol{q}) \\ \boldsymbol{v} \\ \sigma \end{bmatrix} + \begin{bmatrix} 0 \\ \boldsymbol{I} \\ 0 \end{bmatrix} \boldsymbol{u}. \tag{2.53}$$

In this setting, the stress $\sigma \in \mathbb{R}$ *acts as a Lagrange multiplier, which enforces the kinematic relation*

$$\frac{1}{l_0^2}\boldsymbol{q}^\top \boldsymbol{v} = 0 \qquad \Leftrightarrow \qquad \frac{\mathrm{d}}{\mathrm{d}t}\tilde{\varepsilon}(\boldsymbol{q}) = 0 \tag{2.54}$$

based on (2.45)*, at all times. Thus,* $\tilde{\varepsilon}(\boldsymbol{q}) = const.$ *can be regarded as a holonomic constraint function, similar to* (2.31) *in Example 2.8. Consequently,* (2.53) *is a DAE with differential index 2 that accounts for holonomic constraints on velocity-level, cf. also* (2.32)*.* ♢

Going back to the bigger picture, this example has shown that the description of DAEs — appearing as limit case — directly fits into the above framework (2.30) without any modeling modifications. Therefore, taking into account the considerations from this section, Definition 2.7 for pH DAEs is more general and versatile than the ODE framework from Definition 2.1. It will be taken up frequently throughout this thesis, and we introduce an adaption for infinite-dimensional systems in the upcoming section.

Remark 2.12. *As a consequence of the modularity of Dirac structures [63, Chapter 2.5], the structure of pH systems is invariant under power-preserving interconnections. Thus, the appropriate coupling of two systems of the pH form* (2.30)*, yields a bigger pH system with the same structure. This constitutes a highly relevant aspect, which can be exploited for the modular modeling of flexible multibody systems [44, B6]. To not overextend the scope of this introductory chapter, however, we refrain from an in-depth exploration of that topic.* ♧

2.4. Infinite-dimensional port-Hamiltonian systems

Motivated by the goal to deal with highly flexible slender structures, we now turn our attention to infinite-dimensional pH systems, in which partial differential equations (PDEs), or more generally partial differential-algebraic equations (PDAEs), govern the evolution of variables distributed over a spatial domain. In contrast to the finite-dimensional case, energy storage, dissipation, and interaction with the environment are no longer localized at discrete points. As a result, the system variables become elements of function spaces — i.e., infinite-dimensional vector spaces — and spatial derivatives naturally enter the governing equations.

While the mathematical description of infinite-dimensional pH systems appears to be more involved than in the finite-dimensional case, the underlying physical principles remain unchanged [246]. In particular, the skew-symmetric structure matrix $\boldsymbol{J}$ that characterizes finite-dimensional pH systems (cf. Definitions 2.1 and 2.7) is replaced by a *differential operator* in the infinite-dimensional setting. This operator exhibits an analogous structural property, ensuring that infinite-dimensional pH systems satisfy a power balance equation by construction as well. This structural correspondence provides a natural extension of the finite-dimensional theory and leads to a definition of infinite-dimensional pH descriptor systems that generalizes Definition 2.7 from the previous section.[5]

We focus specifically on pH systems defined on one-dimensional spatial domains. From a mechanical perspective, such systems describe slender structures, where the governing equations evolve along a single spatial dimension that is significantly larger than the other two. Accordingly, we introduce the one-dimensional spatial domain $\Omega = [0, L] \subset \mathbb{R}$, where $L > 0$, being parameterized by the material coordinate $s \in \Omega$. The partial derivative with respect to the variable s is denoted by $\partial_s \square$, where the symbol $\square$ represents a placeholder. Moreover, the boundary of Ω consists of the points at $s = 0$ and $s = L$, so we write $\partial\Omega = \{0, L\}$.

Having specified the spatial domain, we now introduce the variables of the infinite-dimensional system. In general, such variables depend on both the spatial variable $s \in \Omega$ and time $t \in \mathbb{T}$. Exemplarily, the state variables are formally defined as $\boldsymbol{x} \in \mathscr{C}^\infty(\Omega \times \mathbb{T}, \mathscr{X})$, where $\mathscr{X} = \mathbb{R}^n$. Analogously to the finite-dimensional setting (see Section 2.1), we suppress the explicit time dependence in order to focus on the spatial structure of the system. Accordingly, for each $t \in \mathbb{T}$, we consider

$$\boldsymbol{x}(\cdot, t) \in \mathscr{C}^\infty(\Omega, \mathscr{X}), \qquad \text{or simply} \qquad \boldsymbol{x} \in \mathscr{C}^\infty(\Omega, \mathscr{X}). \tag{2.55}$$

All equations are then understood to hold pointwise in time.

To simplify the notation, we begin by introducing the following inner products. For vector-valued functions[6] $\boldsymbol{v}, \boldsymbol{w} \in \mathscr{L}^2(\Omega, \mathbb{R}^n)$ we define the expressions

$$(\boldsymbol{v}, \boldsymbol{w})_\Omega := \int_\Omega \boldsymbol{v}^\top \boldsymbol{w} \, \mathrm{d}s, \qquad [\boldsymbol{v}, \boldsymbol{w}]_{\partial\Omega} := \left[\boldsymbol{v}^\top \boldsymbol{w}\right]_{s=0}^{L}. \tag{2.56}$$

The dimension is clear from the context and is therefore omitted in the notation of the inner product. Moreover, we present the integration-by-parts formula for $\boldsymbol{v}, \boldsymbol{w} \in \mathscr{C}^1(\Omega, \mathbb{R}^n)$ as

$$(\partial_s \boldsymbol{v}, \boldsymbol{w})_\Omega + (\boldsymbol{v}, \partial_s \boldsymbol{w})_\Omega = [\boldsymbol{v}, \boldsymbol{w}]_{\partial\Omega}. \tag{2.57}$$

[5] Some of the content in this section is presented similarly in the thesis by Brugnoli [41], which provides a clear introduction, and also draws on the textbook [189]. Here, we adapt the material to our context, including illustrative examples and basic explanations for readers with limited prior exposure.

[6] An $\mathscr{L}^2$ function on Ω is a function $\boldsymbol{v} : \Omega \to \mathbb{R}^n$ such that the following integral exists and is finite, i.e., $\int_\Omega \boldsymbol{v}^\top \boldsymbol{v} \, \mathrm{d}s < \infty$ [10, Equation 8.1]. In other words, nothing "pathological" happens when computing the integral. The space of all such functions is denoted by $\mathscr{L}^2(\Omega, \mathbb{R}^n)$ and is called the space of square-integrable functions.

Further, we denote by $\mathscr{C}_0^\infty(\Omega, \mathbb{R}^n)$ the space of *test functions*, i.e., smooth vector-valued functions with compact support[7] in the domain Ω [189, Definition 5.1]. In particular, functions in $\mathscr{C}_0^\infty(\Omega, \mathbb{R}^n)$ vanish near the boundary $\partial\Omega$, and so do all of their derivatives. Consequently, they satisfy homogeneous boundary conditions,

$$\boldsymbol{w} \in \mathscr{C}_0^\infty(\Omega, \mathbb{R}^n) \qquad \Rightarrow \qquad \boldsymbol{w} \in \mathscr{C}^\infty(\Omega, \mathbb{R}^n) \quad \text{and} \quad \boldsymbol{w}(s=0,t) = \boldsymbol{w}(s=L,t) = \boldsymbol{0}. \tag{2.58}$$

This property will be used repeatedly below.

As noted at the beginning of this section, in infinite-dimensional dynamical systems, matrices representing linear mappings between finite-dimensional vector spaces are replaced by *differential operators*. These operators may depend on additional parameters. For the description of dynamical systems these parameters are typically given by the state variables $\boldsymbol{x} \in \mathscr{C}^\infty(\Omega, \mathscr{X})$. In this case, we say the operator is *modulated* by the state. For example, consider

$$\begin{aligned} \mathcal{A}(\boldsymbol{x}) : \mathscr{C}^\infty(\Omega, \mathbb{R}^n) &\to \mathscr{C}^\infty(\Omega, \mathbb{R}^m), \\ \boldsymbol{v} &\mapsto \boldsymbol{w} = \mathcal{A}(\boldsymbol{x})\boldsymbol{v}, \end{aligned} \tag{2.59}$$

which maps between functional spaces (here for simplicity $\mathscr{C}^\infty$). For each $\boldsymbol{x} \in \mathscr{C}^\infty(\Omega, \mathscr{X})$, the components of $\boldsymbol{w}$ are linear combinations of the components of $\boldsymbol{v}$ and spatial derivatives thereof — see also more formal definitions [41, Section 2.2.1], [189, Equations (2.5)–(2.9)]. We now proceed with two illustrative examples.

Example 2.13 (Geometrically exact string [10])**.** *Consider a geometrically exact string with constant mass density $\rho > 0$, cross-sectional area $A > 0$ and position vector $\boldsymbol{r} \in \mathscr{C}^\infty(\Omega, \mathbb{R}^3)$. The balance of linear momentum in the absence of external loads reads [10, Equation 2.9]*

$$\rho A\, \partial_{tt}^2 \boldsymbol{r}(s,t) = \boldsymbol{f}^{\text{int}}(s,t), \tag{2.60}$$

where the internal force vector $\boldsymbol{f}^{\text{int}} \in \mathscr{C}^\infty(\Omega, \mathbb{R}^3)$ is given by[8]

$$\boldsymbol{f}^{\text{int}}(s,t) = \partial_s\big(S(s,t)\,\boldsymbol{t}(s,t)\big), \qquad \boldsymbol{t}(s,t) = \partial_s \boldsymbol{r}(s,t). \tag{2.61}$$

Therein, $S \in \mathscr{C}^\infty(\Omega, \mathbb{R})$ is a scalar stress measure and $\boldsymbol{t} \in \mathscr{C}^\infty(\Omega, \mathbb{R}^3)$ is the field of non-unit tangent vectors on the string. Equivalently, equation (2.61) *can be rewritten as*

$$\boldsymbol{f}^{\text{int}} = \mathcal{A}(\boldsymbol{t})\, S, \qquad \text{with} \qquad \mathcal{A}(\boldsymbol{t}) := \partial_s(\boxdot\, \boldsymbol{t}) \tag{2.62}$$

being a modulated differential operator $\mathcal{A}(\boldsymbol{t}) : \mathscr{C}^\infty(\Omega, \mathbb{R}) \to \mathscr{C}^\infty(\Omega, \mathbb{R}^3)$, mapping the scalar tension to the internal force vector. A related operator may also be found in Thoma and Kotyczka [218]. For a detailed description of the mechanical model we refer to Antman [10, Chapter 2, Section 2] and Chapter 6 of this thesis. ♢

The matrices in the finite-dimensional pH setting exhibited properties such as skew-symmetry that are essential for the pH structure, cf. Sections 2.1 to 2.3. Therefore, we now introduce the concept of *formal adjoints* of differential operators, which forms the basis for the corresponding concepts in infinite-dimensional systems.

[7] The support of a function is defined as the closure of the set on which the function is non-zero [10, p. 4]. With respect to the spatial variable $s \in \Omega$, for $\boldsymbol{w} \in \mathscr{C}_0^\infty(\Omega, \mathbb{R}^n)$ there exists a compact (i.e., bounded and closed), proper subset $K \subset \Omega$ such that $\boldsymbol{w}(s,t) = \boldsymbol{0}\ \forall\, s \notin K$ and $\forall\, t \in \mathbb{T}$ [189, Definition 5.1].

[8] In (2.61), we have deviated from the common literature [10, Equation 2.10b], see Section 6.C.1 for the connecting arguments.

Definition 2.14 (Formal adjoint [189])**.** *The formal adjoint $\mathcal{A}^*(\boldsymbol{x}) : \mathscr{C}^\infty(\Omega, \mathbb{R}^m) \to \mathscr{C}^\infty(\Omega, \mathbb{R}^n)$ of a state-modulated differential operator $\mathcal{A}(\boldsymbol{x})$ according to* (2.59) *is defined by the relation*

$$(\mathcal{A}(\boldsymbol{x})\boldsymbol{v}, \boldsymbol{w})_\Omega = (\boldsymbol{v}, \mathcal{A}^*(\boldsymbol{x})\boldsymbol{w})_\Omega \tag{2.63}$$

for all $\boldsymbol{x} \in \mathscr{C}^\infty(\Omega, \mathscr{X})$ and all test functions $\boldsymbol{v} \in \mathscr{C}_0^\infty(\Omega, \mathbb{R}^n)$, $\boldsymbol{w} \in \mathscr{C}_0^\infty(\Omega, \mathbb{R}^m)$, see also [189, Equation (5.169)]. ♤

In contrast to the operator adjoint in a broader sense [71, p. 732], the attribute "formal" refers to the operator obtained by applying integration by parts, while neglecting boundary contributions [189, p.164], [41, Remark 1]. This is justified by restricting Definition 2.14 to smooth functions $\boldsymbol{v}, \boldsymbol{w}$ with compact support in Ω. For first-order differential operators, however, the integration-by-parts formula (2.57) has to be performed only once, such that the satisfaction of homogeneous boundary conditions (2.58) would technically be sufficient.

Example 2.15. *Let us revisit Example 2.13 and assume $\boldsymbol{v} \in \mathscr{C}_0^\infty(\Omega, \mathbb{R}^3)$, $S \in \mathscr{C}_0^\infty(\Omega, \mathbb{R})$ with compact support in Ω such that homogeneous boundary conditions* (2.58) *are satisfied. Then, for the modulated differential operator* (2.62)*, one can deduce its formal adjoint $\mathcal{A}^*(\boldsymbol{t}) : \mathscr{C}^\infty(\Omega, \mathbb{R}^3) \to \mathscr{C}^\infty(\Omega, \mathbb{R})$ via*

$$(\mathcal{A}(\boldsymbol{t})S, \boldsymbol{v})_\Omega = (\partial_s(S\,\boldsymbol{t}), \boldsymbol{v})_\Omega = \left(S, -\boldsymbol{t}^\top \partial_s \boldsymbol{v}\right)_\Omega = (S, \mathcal{A}^*(\boldsymbol{t})\boldsymbol{v})_\Omega\,, \qquad \text{where} \qquad \mathcal{A}^*(\boldsymbol{t}) = -\boldsymbol{t}^\top \partial_s \square\,, \tag{2.64}$$

for all $\boldsymbol{t} \in \mathscr{C}^\infty(\Omega, \mathbb{R}^3)$. For the second equality in (2.64)*, we have used integration by parts* (2.57) *once. Further, the presence of homogeneous boundary conditions has been taken into account, which is sufficient here, since $\mathcal{A}$ is only a first-order differential operator.* ♢

With this, we can introduce the notion of *formally skew-adjoint* differential operators, in analogy with skew-symmetric matrices, which have played a central role in the finite-dimensional pH setting, cf. Definitions 2.1 and 2.7.

Definition 2.16 (Formally skew-adjoint operator [41])**.** *A state-modulated differential operator $\mathcal{A}(\boldsymbol{x})$ is called formally skew-adjoint if $\mathcal{A}(\boldsymbol{x}) = -\mathcal{A}^*(\boldsymbol{x})$ or using* (2.63) *equivalently*

$$(\mathcal{A}(\boldsymbol{x})\boldsymbol{v}, \boldsymbol{w})_\Omega + (\boldsymbol{v}, \mathcal{A}(\boldsymbol{x})\boldsymbol{w})_\Omega = 0, \tag{2.65}$$

for all $\boldsymbol{x} \in \mathscr{C}^\infty(\Omega, \mathscr{X})$ and all $\boldsymbol{v}, \boldsymbol{w} \in \mathscr{C}_0^\infty(\Omega, \mathbb{R}^n)$. ♤

Condition (2.65) can understood in analogy to the identity $(\boldsymbol{A}\boldsymbol{v})^\top \boldsymbol{w} + \boldsymbol{v}^\top \boldsymbol{A}\boldsymbol{w} = 0$ for a skew-symmetric matrix $\boldsymbol{A} = -\boldsymbol{A}^\top$ in the finite-dimensional case. Let us now illustrate this concept with the example of the geometrically exact string from before.

Example 2.17. *The dynamics of the geometrically exact string from Example 2.13 can be represented in a mixed velocity-stress formulation, similar to the pendulum problem in Example 2.11. Hereto, we introduce an independent velocity vector $\boldsymbol{v}$, a Green–Lagrangian strain function $\varepsilon = \tilde{\varepsilon}(\boldsymbol{t}) = \frac{1}{2}(\boldsymbol{t}^\top \boldsymbol{t} - 1)$, cf.* (6.4)*, and assume a linear constitutive relation $S = EA\varepsilon$ of St. Venant–Kirchhoff type, where $E > 0$ can be interpreted as Young's modulus. Find further details in Remark 6.5. Eventually, the governing PDEs are given by $\partial_t \boldsymbol{r} = \boldsymbol{v}$ and*

$$\begin{bmatrix} \rho A \boldsymbol{I} & 0 \\ 0 & (EA)^{-1} \end{bmatrix} \begin{bmatrix} \partial_t \boldsymbol{v} \\ \partial_t S \end{bmatrix} = \begin{bmatrix} 0 & \partial_s(\square\,\boldsymbol{t}) \\ \boldsymbol{t}^\top \partial_s \square & 0 \end{bmatrix} \begin{bmatrix} \boldsymbol{v} \\ S \end{bmatrix}, \tag{2.66}$$

where $\boldsymbol{t} = \partial_s \boldsymbol{r}$, cf. (2.61)*, has been used to derive $\partial_t \boldsymbol{t} = \partial_s \boldsymbol{v}$. Particularly, on the right hand side of* (2.66)*, we can identify the modulated differential operator*

$$\mathcal{L}(\boldsymbol{t}) = \begin{bmatrix} 0 & \mathcal{A}(\boldsymbol{t})\square \\ -\mathcal{A}^*(\boldsymbol{t})\square & 0 \end{bmatrix}, \tag{2.67}$$

with $\mathcal{A}(\boldsymbol{t})$ *and its formal adjoint* $\mathcal{A}^*(\boldsymbol{t})$ *defined in* (2.62) *and* (2.64)*, respectively. It can be shown in a straightforward manner that* $\mathcal{L}(\boldsymbol{t}) : \mathscr{C}^\infty(\Omega, \mathbb{R}^4) \to \mathscr{C}^\infty(\Omega, \mathbb{R}^4)$ *from* (2.67) *is formally skew-adjoint. To this end, consider* $\boldsymbol{v}_1, \boldsymbol{v}_2 \in \mathscr{C}_0^\infty(\Omega, \mathbb{R}^3)$ *and* $S_1, S_2 \in \mathscr{C}_0^\infty(\Omega, \mathbb{R})$ *and verify* (2.65) *as*

$$\left(\begin{bmatrix} 0 & \mathcal{A}(\boldsymbol{t})\square \\ -\mathcal{A}^*(\boldsymbol{t})\square & 0 \end{bmatrix} \begin{bmatrix} \boldsymbol{v}_1 \\ S_1 \end{bmatrix}, \begin{bmatrix} \boldsymbol{v}_2 \\ S_2 \end{bmatrix} \right)_\Omega + \left(\begin{bmatrix} \boldsymbol{v}_2 \\ S_2 \end{bmatrix}, \begin{bmatrix} 0 & \mathcal{A}(\boldsymbol{t})\square \\ -\mathcal{A}^*(\boldsymbol{t})\square & 0 \end{bmatrix} \begin{bmatrix} \boldsymbol{v}_1 \\ S_1 \end{bmatrix} \right)_\Omega = 0, \tag{2.68}$$

for all $\boldsymbol{t} \in \mathscr{C}^\infty(\Omega, \mathbb{R}^3)$*. Therein, we have used the block structure of the operator and the symmetry of the inner products. Notably, the proof was largely facilitated by the prior knowledge from Example 2.15, which helped us identify the particular structure of the operator* (2.67)*. Alternatively, the formal skew-adjointness could have been verified directly for the representation on the right-hand side of* (2.66)*.* ◇

In summary, the property of formal skew-adjointness is directly connected to the integration-by-parts formula (2.57). In higher-dimensional spatial domains, this concept extends to generalized Stokes' theorem (or *divergence theorem*). This connection explains the prefix "Stokes" in *Stokes–Dirac structures*, which are used to define infinite-dimensional port-Hamiltonian systems [135], [41, Section 2.2.2].

Conversely, if the vector functions in (2.65) do not have compact support, the resulting terms arise solely from the boundary. This fact is closely related to the aim to describe *open* physical systems actuated at their boundaries, thus providing us with the necessary tools to describe the boundary behavior of infinite-dimensional pH systems. To this end, we formalize integration by parts in an abstract form as

$$(\boldsymbol{w}, \mathcal{A}(\boldsymbol{x})\boldsymbol{w})_\Omega = (\mathcal{B}_\partial(\boldsymbol{x})\boldsymbol{w})^\top \mathcal{C}_\partial(\boldsymbol{x})\boldsymbol{w}, \tag{2.69}$$

for some formally skew-adjoint operator $\mathcal{A} = -\mathcal{A}^*$. Here, $\mathcal{B}_\partial(\boldsymbol{x}), \mathcal{C}_\partial(\boldsymbol{x}) \colon \mathscr{C}^\infty(\Omega, \mathbb{R}^n) \to \mathscr{C}^\infty(\partial\Omega, \mathbb{R}^m)$ denote boundary operators, that may be modulated as well. They are directly associated with the operator $\mathcal{A}$ and act by performing certain manipulations of their arguments combined with an evaluation at the boundaries. Interestingly, the choice of boundary operators is not unique, as will be seen in the upcoming example. In fact this ambiguity corresponds to different boundary conditions for an infinite-dimensional physical system.

Example 2.18. *Consider again the formally skew-adjoint differential operator* (2.67)*, which is modulated by* $\boldsymbol{t} \in \mathscr{C}^\infty(\Omega, \mathbb{R}^3)$*, appearing in the description of geometrically exact strings. For* $\boldsymbol{w} = (\boldsymbol{v}, S)$ *and* $\boldsymbol{v} \in \mathscr{C}^\infty(\Omega, \mathbb{R}^3)$ *and* $S \in \mathscr{C}^\infty(\Omega, \mathbb{R})$*, which explicitly do not satisfy homogeneous boundary conditions, one obtains*

$$\left(\begin{bmatrix} \boldsymbol{v} \\ S \end{bmatrix}, \begin{bmatrix} 0 & \partial_s(\square \boldsymbol{t}) \\ \boldsymbol{t}^\top \partial_s \square & 0 \end{bmatrix} \begin{bmatrix} \boldsymbol{v} \\ S \end{bmatrix} \right)_\Omega = [\boldsymbol{v}, S\boldsymbol{t}]_{\partial\Omega} = \left[\boldsymbol{v}(s,t)^\top S(s,t) \boldsymbol{t}(s,t) \right]_{s=0}^{L} \tag{2.70}$$

after integration by parts (2.57)*. As a consequence, one can infer many pairs of boundary operators by comparison of* (2.70) *with the abstract relation* (2.69)*, e.g.,*

$$(1) \qquad \mathcal{B}_\partial^{(1)} = \begin{bmatrix} \square(L,t) & 0 \\ \square(0,t) & 0 \end{bmatrix}, \qquad \mathcal{C}_\partial^{(1)} = \begin{bmatrix} 0 & \square(L,t)\boldsymbol{t}(L,t) \\ 0 & -\square(0,t)\boldsymbol{t}(0,t) \end{bmatrix}, \tag{2.71a}$$

$$(2) \qquad \mathcal{B}_\partial^{(2)} = \begin{bmatrix} 0 & \square(L,t)\boldsymbol{t}(L,t) \\ 0 & -\square(0,t)\boldsymbol{t}(0,t) \end{bmatrix}, \qquad \mathcal{C}_\partial^{(2)} = \begin{bmatrix} \square(L,t) & 0 \\ \square(0,t) & 0 \end{bmatrix}, \tag{2.71b}$$

$$(3) \qquad \mathcal{B}_\partial^{(3)} = \begin{bmatrix} \square(L,t) & 0 \\ 0 & -\square(0,t)\boldsymbol{t}(0,t) \end{bmatrix}, \qquad \mathcal{C}_\partial^{(3)} = \begin{bmatrix} 0 & \square(L,t)\boldsymbol{t}(L,t) \\ \square(0,t) & 0 \end{bmatrix}, \tag{2.71c}$$

$$(4) \qquad \mathcal{B}_\partial^{(4)} = \begin{bmatrix} 0 & \square(L,t)\boldsymbol{t}(L,t) \\ \square(0,t) & 0 \end{bmatrix}, \qquad \mathcal{C}_\partial^{(4)} = \begin{bmatrix} \square(L,t) & 0 \\ 0 & -\square(0,t)\boldsymbol{t}(0,t) \end{bmatrix}, \tag{2.71d}$$

In fact, the choice (2.71a) *corresponds to pure Dirichlet boundary conditions (prescribed velocity input),* (2.71b) *to pure Neumann boundary conditions (prescribed stress input), and* (2.71c) *and* (2.71d) *to mixed boundary conditions.* ◇

The interpretation of different boundary operators corresponding to different boundary conditions leads, in the pH interpretation, to different causal assignments of input and output variables [129, p. 446]. This becomes clearer in Definition 2.19 for infinite-dimensional pH systems, see in particular (2.74c) and (2.74d).

Before proceeding, we discuss the final cornerstone in the definition of pH systems, the description of energy storage. For infinite-dimensional systems, the total energy is distributed over the entire spatial domain. Accordingly, the Hamiltonian function of finite-dimensional pH systems is replaced by a functional

$$\mathcal{H}\colon \mathscr{C}^\infty(\Omega, \mathscr{X}) \to \mathbb{R}, \qquad \mathcal{H}(\boldsymbol{x}) = \int_\Omega h(\boldsymbol{x}(s,\cdot))\,\mathrm{d}s, \tag{2.72}$$

which is defined as the integral of a Hamiltonian density $h \in \mathscr{C}^1(\mathscr{X}, \mathbb{R})$ over the domain [41, 128]. Analogous to the gradient in finite dimensions, we introduce the variational derivative $\delta_{\boldsymbol{x}}\mathcal{H}$, obtained from a Taylor expansion of the Hamiltonian functional

$$\mathcal{H}(\boldsymbol{x} + \delta\boldsymbol{x}) = \mathcal{H}(\boldsymbol{x}) + (\delta_{\boldsymbol{x}}\mathcal{H}, \delta\boldsymbol{x})_\Omega + o(\delta\boldsymbol{x}), \tag{2.73}$$

where $\delta\boldsymbol{x}$ are admissible, arbitrary variations of the state variables, and $o(\delta\boldsymbol{x})$ collects terms of order higher than one in $\delta\boldsymbol{x}$. If the Hamiltonian density h, as in (2.72), does not depend on spatial derivatives of the state, then the variational derivative reduces to the gradient of the density [41, 128],

$$\delta_{\boldsymbol{x}}\mathcal{H} = \nabla h(\boldsymbol{x}).$$

With these ingredients, we are now ready to define an infinite-dimensional pH (descriptor) system. This definition exhibits string analogies to the finite-dimensional pH DAE system from Definition 2.7.

Definition 2.19 (pH PDAE system)**.** *An infinite-dimensional port-Hamiltonian descriptor system, shorthand* pH PDAE *system, on a one-dimensional spatial domain Ω is a state-space model of the form*

$$\left.\begin{aligned} \mathcal{E}(\boldsymbol{x})\partial_t\boldsymbol{x} &= \big(\mathcal{J}(\boldsymbol{x}) - \mathcal{R}(\boldsymbol{x})\big)\boldsymbol{z}(\boldsymbol{x}) + \mathcal{B}_\Omega(\boldsymbol{x})\boldsymbol{u}_\Omega, && (2.74a)\\ \boldsymbol{y}_\Omega &= \mathcal{B}_\Omega^\top(\boldsymbol{x})\boldsymbol{z}(\boldsymbol{x}), && (2.74b)\end{aligned}\right\} \quad \text{on} \quad \Omega,$$

$$\left.\begin{aligned} \boldsymbol{u}_\partial &= \mathcal{B}_\partial(\boldsymbol{x})\boldsymbol{z}(\boldsymbol{x}), && (2.74c)\\ \boldsymbol{y}_\partial &= \mathcal{C}_\partial(\boldsymbol{x})\boldsymbol{z}(\boldsymbol{x}), && (2.74d)\end{aligned}\right\} \quad \text{on} \quad \partial\Omega,$$

together with $\mathcal{H}$, a Hamiltonian functional (2.72)*, if*

(i) the differential operator $\mathcal{J}$, called structure operator, is formally skew-adjoint and the dissipation matrix $\mathcal{R} \in \mathscr{C}(\mathscr{X}, \mathbb{R}^{n\times n})$ is symmetric, positive semi-definite and such that $\mathcal{J}(\boldsymbol{x}) = -\mathcal{J}^*(\boldsymbol{x})$ and $\mathcal{R}(\boldsymbol{x}) = \mathcal{R}(\boldsymbol{x})^\top \succeq 0$,

(ii) the descriptor matrix $\mathcal{E} \in \mathscr{C}(\mathscr{X}, \mathbb{R}^{n\times n})$ and the costate function $\boldsymbol{z} \in \mathscr{C}(\mathscr{X}, \mathbb{R}^n)$ satisfy

$$\mathcal{E}(\boldsymbol{x})^\top\boldsymbol{z}(\boldsymbol{x}) = \delta_{\boldsymbol{x}}\mathcal{H}(\boldsymbol{x}), \tag{2.74e}$$

(iii) and the boundary operators $\mathcal{B}_\partial, \mathcal{C}_\partial$ are related to the structure operator $\mathcal{J}$ via the abstract integration-by-parts formula (2.69)*,*

for all state variables $\boldsymbol{x} \in \mathscr{C}^\infty(\Omega \times \mathbb{T}, \mathscr{X})$. Moreover, $\mathcal{B}_\Omega \in \mathscr{C}(\mathscr{X}, \mathbb{R}^{n\times m})$ is a distributed port matrix, $(\boldsymbol{u}_\Omega, \boldsymbol{y}_\Omega)$ are the distributed input and output and $(\boldsymbol{u}_\partial, \boldsymbol{y}_\partial)$ the boundary input and output. ♤

Note that Definition 2.19 not only prescribes a specific structure for the time-invariant state dynamics, but also restricts the admissible output to be collocated with the input. In this setting, (2.74a) is referred to as the *dynamical equation*, whereas (2.74b) is called the *distributed output equation*. In analogy to finite-dimensional pH DAEs, see Definition 2.7, the descriptor matrix $\mathcal{E}$ may be singular. Hence, (2.74a) encompasses both PDEs and PDAEs. Moreover, the Hamiltonian enters the dynamical equation implicitly through the costate function $\boldsymbol{z}$, linked by the gradient-pairing relation (2.74e). In contrast to the finite-dimensional case, admissible boundary inputs and outputs must additionally be specified via (2.74c) and (2.74d), respectively. Both are directly related to the formally skew-adjoint operator $\mathcal{J}$ through Property (iii). Finally, note that this definition assumes $\mathcal{E}$, $\mathcal{R}$ and $\mathcal{B}_\Omega$ to be matrix-valued functions. The case, in which $\mathcal{B}_\Omega$ is a differential operator, can be found in Section 6.2.1. A further generalization, in which $\mathcal{E}$ and $\mathcal{R}$ are differential operators would be possible as well [216]. However, this is not required for the purposes of this thesis.

As in the finite-dimensional pH case, a power balance equation follows by construction. To this end, applying the chain rule and using the gradient-pairing relation (2.74e) associated with Property (ii) yields

$$\dot{\mathcal{H}} = (\delta_{\boldsymbol{x}}\mathcal{H}, \partial_t \boldsymbol{x})_\Omega = \left(\mathcal{E}(\boldsymbol{x})^\top \boldsymbol{z}(\boldsymbol{x}), \partial_t \boldsymbol{x}\right)_\Omega = (\boldsymbol{z}(\boldsymbol{x}), \mathcal{E}(\boldsymbol{x})\partial_t \boldsymbol{x})_\Omega \,. \tag{2.75}$$

Substituting the dynamical equation (2.74a) gives rise to

$$\begin{aligned} \dot{\mathcal{H}} &= \left(\boldsymbol{z}(\boldsymbol{x}), \left(\mathcal{J}(\boldsymbol{x}) - \mathcal{R}(\boldsymbol{x})\right)\boldsymbol{z}(\boldsymbol{x}) + \mathcal{B}_\Omega(\boldsymbol{x})\boldsymbol{u}_\Omega\right)_\Omega \\ &= -\left(\boldsymbol{z}(\boldsymbol{x}), \mathcal{R}(\boldsymbol{x})\boldsymbol{z}(\boldsymbol{x})\right)_\Omega + \left(\mathcal{B}_\Omega(\boldsymbol{x})^\top \boldsymbol{z}(\boldsymbol{x}), \boldsymbol{u}_\Omega\right)_\Omega + \left(\mathcal{B}_\partial \boldsymbol{z}(\boldsymbol{x})\right)^\top \mathcal{C}_\partial \boldsymbol{z}(\boldsymbol{x}), \end{aligned} \tag{2.76}$$

where we have made use of the abstract integration-by-parts formula (2.69), which is induced by Properties (i) and (iii). Lastly, we insert the definitions of the distributed output (2.74b) and the boundary input (2.74c) and output (2.74d), to obtain

$$\dot{\mathcal{H}} = -\left(\boldsymbol{z}(\boldsymbol{x}), \mathcal{R}(\boldsymbol{x})\boldsymbol{z}(\boldsymbol{x})\right)_\Omega + \left(\boldsymbol{y}_\Omega, \boldsymbol{u}_\Omega\right)_\Omega + \boldsymbol{y}_\partial^\top \boldsymbol{u}_\partial. \tag{2.77}$$

This power balance equation for the infinite-dimensional pH descriptor system can be directly compared to the finite-dimensional counterpart (2.35), showing that the time rate of change of the total energy is entirely due to the dissipated power $P_R(\boldsymbol{x}) := \left(\boldsymbol{z}(\boldsymbol{x}), \mathcal{R}(\boldsymbol{x})\boldsymbol{z}(\boldsymbol{x})\right)_\Omega \geq 0$ (cf. Property (i)) and the power supplied by the inputs. Moreover, this relation leads directly to the dissipation inequality

$$\dot{\mathcal{H}} \leq \left(\boldsymbol{y}_\Omega, \boldsymbol{u}_\Omega\right)_\Omega + \boldsymbol{y}_\partial^\top \boldsymbol{u}_\partial, \tag{2.78}$$

which reveals the passivity of the system. For $\mathcal{R} = \boldsymbol{0}$, the system is lossless. If additionally $\boldsymbol{u}_\Omega = \boldsymbol{0}$ and $\boldsymbol{u}_\partial = \boldsymbol{0}$, it is energy-conserving.

At this stage, we do not further explore the underlying Stokes–Dirac structure and instead refer to the literature, cf. [135, 246] and [41, Section 2.2.2]. Ultimately, this definition is closely related to the Dirac structure introduced in Section 2.2 and naturally incorporates an additional boundary port with port variables $(\boldsymbol{u}_\partial, \boldsymbol{y}_\partial)$, see (2.74c) and (2.74d), along with the abstract integration-by-parts formula (2.69).

Remark 2.20. *Since the procedure of structure-preserving discretization in space and time is treated in detail in the subsequent chapters, we omit a detailed discussion here for the sake of conciseness. In particular, the spatial discretization using mixed finite elements is presented in Sections 3.4.1, 4.4.1 and 6.3.1. The time discretization via discrete gradients is covered comprehensively in Chapter 5 and Section 6.3.2 and the special case employing the simple implicit midpoint rule for systems with quadratic Hamiltonian can be seen in Sections 3.4.2 and 4.4.2.* ♧

With the background concepts introduced in this chapter, the reader should be well prepared to proceed to the following chapters, which focus on the pH modelling of highly flexible structures and structure-preserving discretization strategies.

3. Energy–momentum-consistent simulation of planar geometrically exact beams in a port-Hamiltonian framework

This chapter is based on:*
Kinon PL, Betsch P, and Eugster SR. "Energy-momentum-consistent simulation of planar geometrically exact beams in a port-Hamiltonian framework". In: *Multibody System Dynamics*, 2025. DOI: 10.1007/s11044-025-10087-9

Abstract: We propose a new, port-Hamiltonian formulation for the highly nonlinear dynamics of planar geometrically exact beams, which are amenable to arbitrary large deformations and rotations. A structure-preserving spatial and temporal discretization procedure - using mixed finite elements and second-order time-stepping methods - is proposed. It is observed that the present approach is objective, locking-free and provides an exact discrete representation of the energy and angular momentum balance. By comparing the approach to a classical displacement-based scheme from the literature it is shown that the port-Hamiltonian formulation paves new ways for the design of energy–momentum schemes in computational mechanics. Numerical examples underline the applicability to flexible multibody systems and beneficial numerical performance.

Keywords: Planar Simo–Reissner beam • Port-Hamiltonian systems • Flexible multibody systems • Structure-preserving discretization • Mixed finite elements • Locking.

3.1. Introduction

Highly flexible slender structures, such as beams, strings, rods, or shells, are ubiquitous in complex natural and technical systems. Typically, they function as sub-modules within larger flexible multibody systems, which may also include rigid components or joints [20, 202]. The dynamic behavior of such systems can be highly complex due to nonlinear geometry and intricate material properties. Accurately simulating these systems is crucial, particularly for long-term behavior, where numerical dissipation or energetic inconsistencies can lead to unphysical results.

A central approach to describing large deformations in thin, highly flexible structures is the use of geometrically exact beam (GEB) models, also known as Simo–Reissner beams [187, 209] or special Cosserat rods [10]. These highly popular models [34, 53, 59, 67, 133, 134, 141] accurately capture large displacements and rotations without relying on linear approximations and remain a highly active research topic [102, 105, 139, 235]. For a comprehensive overview on beam modeling, see [163].

The port-Hamiltonian (pH) framework has proven to be a powerful method for modeling and controlling dynamical systems [63, 224]. By ensuring energetic consistency and enabling modular interconnections,

the pH framework allows interactions between different physical domains — such as mechanics, electronics, and thermodynamics — to be unified within a single formalism. This approach has been successfully applied to infinite-dimensional dynamical systems [118, 183, 225] and various structural elements such as strings [C2, A1, 218], plates [42, 43], and beams [86, 151, 152, 179]. In the context of finite strain elasticity, velocity-stress formulations have been developed in [47, 219]. In [44] the application to a floating frame formulation is discussed. Starting from a discrete Lagrangian description, the pH approach is exploited in [50] for energy-shaping control.

Furthermore, structure-preserving discretization methods are crucial for the successful application of the pH framework in flexible multibody simulations. These methods ensure that the underlying energy balance equation is maintained at the discrete level, preventing numerical dissipation and energy inconsistencies. In particular, the spatial discretization of pH systems is commonly handled using the mixed finite element methods [44, 48, 54, C2, 234]. Similarly, time discretization plays a crucial role in capturing the evolution of system dynamics while preserving energetic consistency. Energy-preserving time discretization schemes, such as midpoint type methods, discrete gradient approaches or projection-based schemes ensure that energy flows within the system are correctly simulated, which is particularly vital for long-term stability and control applications.

Schemes capable of preserving both energy and momentum are commonly termed EM schemes. Being a popular tool for the simulation of mechanical systems, notable works dealing with geometrically exact beams are for example [116, 141, 213].

Research Gap. Despite the extensive research on both GEB models and the pH framework, there has been no prior work integrating these two approaches. This is surprising given that the pH framework is particularly well-suited for flexible multibody systems, where GEB formulations are often used. The combination of these two methodologies could provide a powerful tool for accurate and energy-consistent simulations of such systems.

Another critical challenge in the numerical simulation of slender mechanical structures is the phenomenon of transverse shear locking. This numerical stiffening effect arises during discretization, leading to unrealistically small deformations. While popular solutions such as selectively reduced integration [213] and mixed finite elements exist, shear locking has received little attention in the pH context. The only reference we are aware of is [41], which discusses mixed finite elements for Mindlin plates but does not address GEBs.

Additionally, existing geometrically nonlinear pH beam formulations [86, 152] rely on Lie group representations for rotations, which, while mathematically elegant, require a deep understanding of differential geometry. This limits accessibility for engineers and practitioners unfamiliar with these advanced mathematical concepts. A coordinate-based formulation would be more approachable and widely applicable in engineering practice.

Contributions. To bridge these gaps, our work contributes to the field in the following key areas:

C1) We propose a novel, infinite-dimensional pH formulation for planar GEBs, which naturally accommodates large deformations and rotations while ensuring intrinsic energy consistency. This formulation allows for seamless interconnection with other pH systems.

C2) We analyze the structure-preserving spatial and temporal discretization using mixed finite elements and second-order time-stepping methods. Our approach yields a new energy–momentum

(EM) scheme and thus ensures exact discrete representations of the energy and angular momentum balance, enhancing long-term simulation accuracy.

C3) We demonstrate that the mixed finite element approach, naturally induced by the pH framework, prevents shear locking for planar GEBs.

In our previous work, we applied an analogous pH-based approach to geometrically exact strings [C2] and incorporated energy-consistent dissipation models [A1], see also Chapter 6 of this work. Therein, the specific pH framework [23, C4, 161, 162] has been proven useful also in the finite-dimensional setting. Here, we adopt this formulation for planar beams, addressing the specific challenges associated with their nonlinear geometry and deformation behavior.

Assumptions. We exclusively consider planar problems here to avoid additional challenges related to the parametrization of spatial rotations. For simplicity, we also assume the cross-section as well as material parameters of the beam to be constant along its centerline. Although the kinematical description is entirely nonlinear in this work, thus allowing large rotations and displacements, it is sensible to locally assume small deformations. To this end, we restrict ourselves to a linear St. Venant–Kirchhoff type stress-strain relation at some point throughout the discretization procedure. Nevertheless, nonlinear constitutive laws may be included in a straightforward manner, effecting only the necessary time discretization. Analogously to the previous works [C2, A1] one could exemplarily use discrete gradients to obtain EM schemes in that case, see also Chapter 6 of this work. More details on discrete gradient methods in general can be found in Chapter 5.

Notation. Vector-valued functions are denoted using bold faces, e.g. $\boldsymbol{a}, \boldsymbol{b} \in \mathbb{R}^2$. Scalars assume italic fonts, e.g. $c, d \in \mathbb{R}$. Moreover, we write $\boldsymbol{a} = \sum_{\alpha=1}^{2} a_\alpha \boldsymbol{e}_\alpha$, where $\boldsymbol{e}_\alpha$ denotes a unit vector of a Euclidean inertial frame in $\mathbb{R}^2$. The scalar product of two vector-valued quantities is denoted by, e.g. $\boldsymbol{a}^\top \boldsymbol{b} = a_1 b_1 + a_2 b_2$. We define the result of a cross-product of two vectors from $\mathbb{R}^2$ as $c = \boldsymbol{a} \times \boldsymbol{b} = a_1 b_2 - a_2 b_1$. For simplicity we introduce a representation using a constant, skew-symmetric matrix $\boldsymbol{S} \in \mathbb{R}^{2\times 2}$ such that

$$\boldsymbol{a} \times \boldsymbol{b} = \boldsymbol{a}^\top \boldsymbol{S} \boldsymbol{b} = (\boldsymbol{S}^\top \boldsymbol{a})^\top \boldsymbol{b}, \quad \text{where} \quad \boldsymbol{S} := \begin{bmatrix} 0 & 1 \\ -1 & 0 \end{bmatrix}. \tag{3.1}$$

Partial derivatives of sufficiently smooth vector functions are denoted by $\partial_s \boldsymbol{n}(s,t) = \partial \boldsymbol{n}(s,t)/\partial s$. Second partial derivatives are written as, e.g., $\partial^2_{ss} \boldsymbol{n}(s,t) = \partial^2 \boldsymbol{n}(s,t)/\partial s^2$ or $\partial^2_{st} \boldsymbol{n}(s,t) = \partial^2 \boldsymbol{n}(s,t)/\partial s \partial t$. For the inner product over a one-dimensional domain parameterized by an arc-length coordinate s, we denote

$$(\boldsymbol{a}, \boldsymbol{b})_\Omega := \int_\Omega \boldsymbol{a}^\top \boldsymbol{b} \, \mathrm{d}s, \quad (c, d)_\Omega := \int_\Omega c\, d \, \mathrm{d}s, \quad [\boldsymbol{a}, \boldsymbol{b}]_{\partial\Omega} := \left[\boldsymbol{a}^\top \boldsymbol{b}\right]_{s=0}^{L}, \quad [c, d]_{\partial\Omega} := \left[c\, d\right]_{s=0}^{L}, \tag{3.2}$$

always taking into account the dimension of the respective quantities. Identity matrices are denoted by $\boldsymbol{I}$ and matrices full of zeros by $\boldsymbol{0}$, their dimension being clear from the context. The square $\square$ represents a placeholder and will be used for instance in differential operator matrices.

Outline. The remainder of this work is structured as follows: In Section 3.2 we introduce the initial boundary value problem (IBVP) connected to planar GEB dynamics. Section 3.3 starts by reformulating this IBVP as an infinite-dimensional pH system and analyzes underlying conservation principles. In Section 3.4, the structure-preserving discretization in space and time is demonstrated, also showing that discrete versions of the conservation properties can be obtained. We also show that the newly

devised EM scheme distinguishes itself from previously developed EM schemes. Section 3.5 contains numerical results for example problems. A conclusion is given in Section 3.6. Derivations and details, which are not crucial for the bulk part of the work, are comprised in Appendices 3.A to 3.E.

3.2. Problem description

Consider a one-dimensional material beam configuration $\Omega = [0, L]$, with length $L \in \mathbb{R}$, such that the motion of each material point on the centerline (also referred to as *backbone* or *line of centroids*) is described via the position vector $\boldsymbol{r}(s,t) \in \Omega_t \subset \mathbb{R}^2$. Here, the independent quantities are the material (arc-length) coordinate $s \in \Omega$ which parametrizes the centerline of the stress-free initial configuration $\Omega_0 = \{\boldsymbol{r}(s,0) = s\boldsymbol{e}_1 | s \in \Omega\}$, and time $t \in \mathbb{T} = [0, t_{\text{end}}] \subset \mathbb{R}$, see Figure 3.1. Allowing a geometrically exact description of the kinematics, every cross-section remains planar during motion and its orientation is described by means of an angle $\varphi : \Omega \times \mathbb{T} \to \mathbb{R}$, which parametrizes a local rotation matrix

$$\boldsymbol{\Lambda}(\varphi(s,t)) = \begin{bmatrix} \cos\varphi(s,t) & -\sin\varphi(s,t) \\ \sin\varphi(s,t) & \cos\varphi(s,t) \end{bmatrix} \tag{3.3}$$

from $SO(2)$, the special orthogonal group in two dimensions. Hence, it holds that $\boldsymbol{\Lambda}^\top = \boldsymbol{\Lambda}^{-1}$ and $\det(\boldsymbol{\Lambda}) = 1$. In the following, the explicit dependence on the spatial and temporal domains is omitted and only mentioned where deemed necessary. It can be easily verified that the relationships

$$\partial_s \boldsymbol{\Lambda} = \partial_s \varphi \, \boldsymbol{S}^\top \boldsymbol{\Lambda}, \qquad \partial_t \boldsymbol{\Lambda} = \partial_t \varphi \, \boldsymbol{S}^\top \boldsymbol{\Lambda} \tag{3.4}$$

hold, where the skew-symmetric matrix $\boldsymbol{S}$ has been introduced in (3.1). To quantify the strain in the beam we use two material strain measures. The first one is given by

$$\boldsymbol{\Gamma} = \begin{bmatrix} \Gamma_1 \\ \Gamma_2 \end{bmatrix} = \boldsymbol{\Lambda}^\top \partial_s \boldsymbol{r} - \begin{bmatrix} 1 \\ 0 \end{bmatrix}, \tag{3.5}$$

where $\partial_s \boldsymbol{r}$ is the spatial tangent vector to the deformed centerline of the beam. Consequently, Γ_1 can be linked to a dilation and Γ_2 to the transverse shear strain. Additionally, we consider the curvature measure

$$\kappa = \partial_s \varphi, \tag{3.6}$$

which can be interpreted as the rate of change of orientation when moving along the beam. Note that for the straight initial configuration, relations (3.5) and (3.6) induce $\boldsymbol{\Gamma}(s,0) = \boldsymbol{0}$ and $\kappa(s,0) = 0$, for all $s \in \Omega$. Moreover, the rotation matrix can be expressed in terms of unit directors $\{\boldsymbol{d}_\alpha\}_{\alpha=1}^2$, where $\boldsymbol{d}_1$ is

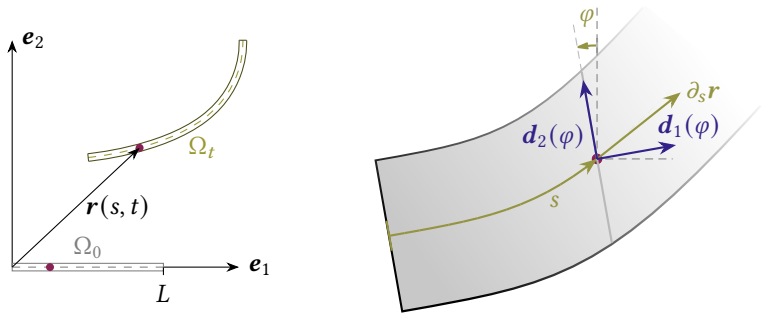

Figure 3.1.: Planar geometrically exact beam kinematics.

normal to each cross section and $\boldsymbol{d}_2$ transverse to it, such that $\boldsymbol{\Lambda} = [\boldsymbol{d}_1, \boldsymbol{d}_2]$. Now, the physical nature of the strain quantities can be underlined since $\Gamma_1 = \boldsymbol{d}_1^\top \partial_s \boldsymbol{r} - 1$ and $\Gamma_2 = \boldsymbol{d}_2^\top \partial_s \boldsymbol{r}$. We further remark that one may write $\boldsymbol{d}_\alpha = \boldsymbol{\Lambda} \boldsymbol{e}_\alpha$, $\alpha \in \{1, 2\}$.

The kinetic energy of the beam is defined as the functional

$$\mathcal{T}(\boldsymbol{r}, \varphi) = \int_\Omega \left(\frac{1}{2} \rho A \partial_t \boldsymbol{r}^\top \partial_t \boldsymbol{r} + \frac{1}{2} \rho I (\partial_t \varphi)^2 \right) \mathrm{d}s, \tag{3.7}$$

where the mass density per unit length is denoted as $\rho A \geq 0$ and the rotational inertia per unit length is $\rho I \geq 0$. Additionally, the constitutive behavior is assumed to be governed by an elastic potential that enters the total potential energy

$$\mathcal{V}(\boldsymbol{r}, \varphi) = \int_\Omega W(\boldsymbol{\Gamma}, \kappa) \, \mathrm{d}s. \tag{3.8}$$

Therein, W denotes the strain energy density function. The material stress resultants are defined as partial derivatives of the strain energy density, i.e.,

$$\boldsymbol{N} = \partial_{\boldsymbol{\Gamma}} W \quad \text{and} \quad M = \partial_\kappa W. \tag{3.9}$$

Their spatial counterparts can be determined by $\boldsymbol{n} = \boldsymbol{\Lambda} \boldsymbol{N}$ for the spatial internal force vector and $m = M$ for the spatial internal moment. Note that $\boldsymbol{N}$ contains both the normal and shear force while M denotes the material bending moment.

Remark 3.1. *For a linear-elastic material model, one can assume a St. Venant–Kirchhoff type quadratic potential* $W(\boldsymbol{\Gamma}, \kappa) = \frac{1}{2} \boldsymbol{\Gamma}^\top \boldsymbol{D}_{\mathrm{ts}} \boldsymbol{\Gamma} + \frac{1}{2} EI \kappa^2$ *with*

$$\boldsymbol{D}_{\mathrm{ts}} = \begin{bmatrix} EA & 0 \\ 0 & kGA \end{bmatrix}. \tag{3.10}$$

Therein, the cross-sectional area A, the elastic modulus E, the shear modulus G and shear stiffness correction factor k appear. Correspondingly, (3.9) *gives rise to* $\boldsymbol{N} = \boldsymbol{D}_{\mathrm{ts}} \boldsymbol{\Gamma}$ *and* $M = EI\kappa$. ♧

Using Hamilton's principle one can derive the following partial differential equations (PDEs), which can be recognized as local balance equations for angular and linear momentum [10, 187], i.e.,

$$\begin{aligned} \rho A \partial_{tt}^2 \boldsymbol{r}(s,t) &= \partial_s (\boldsymbol{\Lambda} \boldsymbol{N})(s,t) + \overline{\boldsymbol{n}}(s,t), \\ \rho I \partial_{tt}^2 \varphi(s,t) &= \partial_s M(s,t) + \partial_s \boldsymbol{r}(s,t) \times (\boldsymbol{\Lambda} \boldsymbol{N})(s,t) + \overline{m}(s,t), \end{aligned} \tag{3.11}$$

where external distributed forces $\overline{\boldsymbol{n}}$ and torques $\overline{m}$ have been introduced.

The nonlinear IBVP at hand is completed by possibly mixed boundary conditions on $\partial\Omega = \{0, L\} = \partial\Omega_{\mathrm{D}} \cup \partial\Omega_{\mathrm{N}}$, e.g.,

$$\begin{aligned} \boldsymbol{r}(s=0,t) &= \boldsymbol{r}_{\mathrm{D}}(t), & \boldsymbol{n}(s=L,t) &= \boldsymbol{n}_{\mathrm{N}}(t), \\ \varphi(s=0,t) &= \varphi_{\mathrm{D}}(t), & m(s=L,t) &= m_{\mathrm{N}}(t), \end{aligned} \tag{3.12}$$

where $\partial\Omega_{\mathrm{D}}$ at $s = 0$ denotes the Dirichlet boundary, $\partial\Omega_{\mathrm{N}}$ refers to the Neumann boundary at $s = L$ and $(\square)_{\mathrm{D/N}}$ indicates a prescribed quantity on the respective boundary. Lastly, appropriate initial values

$$\begin{aligned} \boldsymbol{r}(s,0) &= \boldsymbol{r}_0(s) \quad \text{on} \quad \Omega, \\ \varphi(s,0) &= \varphi_0(s) \quad \text{on} \quad \Omega, \end{aligned} \tag{3.13}$$

with prescribed data $(\square)_0$, are required. Eventually, the IBVP looks for solutions $(\boldsymbol{r}^*, \varphi^*)$ of the PDEs (3.11) along with the constitutive closure relations (3.9), such that (3.12) and (3.13) are satisfied.

3.3. Mixed formulation as a port-Hamiltonian system

We propose a pH formulation for planar geometrically exact beam dynamics and subsequently develop a structure-preserving spatial and temporal discretization approach. In a first step, this involves a reformulation of the above IBVP as outlined in the following.

3.3.1. Reformulation as infinite-dimensional port-Hamiltonian system

To rewrite the above IBVP (3.11) for geometrically exact beams as an infinite-dimensional pH system [225], we introduce an extended set of variables. Besides the state variables from the Lagrangian formulation, also the strains $(\boldsymbol{\Gamma}, \kappa)$ and velocities

$$\boldsymbol{v} := \partial_t \boldsymbol{r}, \qquad \omega := \partial_t \varphi \tag{3.14}$$

are introduced as independent variables. Thus, the state is now given by

$$\boldsymbol{x} = (\boldsymbol{r}, \varphi, \boldsymbol{v}, \omega, \boldsymbol{\Gamma}, \kappa). \tag{3.15}$$

The total energy, also referred to as *Hamiltonian* functional (2.72), of the beam is given by

$$\mathcal{H}(\boldsymbol{x}) = \int_\Omega h(\boldsymbol{x}) \,\mathrm{d}s = \int_\Omega \Big(\frac{1}{2}\rho A \boldsymbol{v}^\top \boldsymbol{v} + \frac{1}{2}\rho I \omega^2 + W(\boldsymbol{\Gamma}, \kappa)\Big)\mathrm{d}s, \tag{3.16}$$

being the sum of kinetic energy (3.7) and the internal potential energy[1] (3.8). Additionally, we have introduced the Hamiltonian density per unit length h in equation (3.16). We moreover require evolution equations for the strains, which can be deduced from their definitions (3.5) and (3.6) as well as (3.4), such that

$$\begin{aligned} \partial_t \boldsymbol{\Gamma} &= \omega \boldsymbol{\Lambda}^\top \boldsymbol{S}\, \partial_s \boldsymbol{r} + \boldsymbol{\Lambda}^\top \partial_s \boldsymbol{v}, \\ \partial_t \kappa &= \partial_s \omega. \end{aligned} \tag{3.17}$$

Now, it is possible to formulate the IBVP from the previous section equivalently in terms of the extended state (3.15) as a set of PDEs

$$\partial_t \boldsymbol{r} = \boldsymbol{v}, \tag{3.18a}$$
$$\partial_t \varphi = \omega, \tag{3.18b}$$
$$\rho A \partial_t \boldsymbol{v} = \partial_s(\boldsymbol{\Lambda N}) + \overline{\boldsymbol{n}}, \tag{3.18c}$$
$$\rho I \partial_t \omega = \partial_s M + \partial_s \boldsymbol{r}^\top \boldsymbol{S \Lambda N} + \overline{m}, \tag{3.18d}$$
$$\partial_t \boldsymbol{\Gamma} = \omega \boldsymbol{\Lambda}^\top \boldsymbol{S}\, \partial_s \boldsymbol{r} + \boldsymbol{\Lambda}^\top \partial_s \boldsymbol{v}, \tag{3.18e}$$
$$\partial_t \kappa = \partial_s \omega. \tag{3.18f}$$

along with the constitutive closure relations (3.9) and appropriate initial and boundary conditions, conforming with (3.12) and (3.13).

[1] Note that the potential of external loads is not included in (3.16). Instead, external distributed forces and torques essentially take the role of inputs acting on the system.

To highlight the pH structure of the above PDEs and to show that the problem at hand is an infinite-dimensional pH system [161, 162, 225], we make use of a matrix operator notation such that

$$\mathcal{E}\partial_t \begin{bmatrix} \boldsymbol{r} \\ \varphi \\ \boldsymbol{v} \\ \omega \\ \boldsymbol{\Gamma} \\ \kappa \end{bmatrix} = \begin{bmatrix} 0 & 0 & \boldsymbol{I} & 0 & 0 & 0 \\ 0 & 0 & 0 & 1 & 0 & 0 \\ -\boldsymbol{I} & 0 & 0 & 0 & \partial_s(\boldsymbol{\Lambda}(\varphi)\square) & 0 \\ 0 & -1 & 0 & 0 & \partial_s \boldsymbol{r}^\top \boldsymbol{S}\boldsymbol{\Lambda}(\varphi)\square & \partial_s\square \\ 0 & 0 & \boldsymbol{\Lambda}(\varphi)^\top \partial_s\square & \square\boldsymbol{\Lambda}(\varphi)^\top \boldsymbol{S}\,\partial_s \boldsymbol{r} & 0 & 0 \\ 0 & 0 & 0 & \partial_s\square & 0 & 0 \end{bmatrix} \begin{bmatrix} 0 \\ 0 \\ \boldsymbol{v} \\ \omega \\ \boldsymbol{N} \\ M \end{bmatrix} + \begin{bmatrix} 0 & 0 \\ 0 & 0 \\ \boldsymbol{I} & 0 \\ 0 & 1 \\ 0 & 0 \\ 0 & 0 \end{bmatrix} \begin{bmatrix} \overline{\boldsymbol{n}} \\ \overline{m} \end{bmatrix}, \tag{3.19}$$

where $\mathcal{E} = \operatorname{diag}(\boldsymbol{I}, 1, \rho A\boldsymbol{I}, \rho I, \boldsymbol{I}, 1)$ is the block-diagonal *descriptor* matrix. The above equation can be written in the compact form

$$\mathcal{E}\partial_t \boldsymbol{x} = \mathcal{J}(\boldsymbol{x})\boldsymbol{z}(\boldsymbol{x}) + \mathcal{B}_\Omega \boldsymbol{u}_\Omega, \tag{3.20}$$

which is a specific description of a pH system going back to Mehrmann and co-workers [161, 162], see also related works such as [44, C2, 219] for other infinite-dimensional mechanical systems. Similar models dealing with spatial geometrically exact beams and strings can be found in Chapter 4 and Chapter 6, respectively. A detailed definition of infinite-dimensional port-Hamiltonian descriptor systems is given in Definition 2.19 contained in Chapter 2 of this work. One major benefit of this specific formulation is that it may integrate constraints leading to partial differential-algebraic systems. In the pH state differential equation (3.20), $\mathcal{E}$ is a symmetric and constant coefficient matrix, $\mathcal{B}$ is referred to as *control* or *input* matrix operator, which is also constant. The distributed *control input* $\boldsymbol{u} = (\overline{\boldsymbol{n}}, \overline{m})$ contains the external distributed forces and torques per unit length. We have moreover introduced the so-called *costate* function $\boldsymbol{z}$ being dependent on the state $\boldsymbol{x}$ given by (3.15). The differential *structure* matrix operator $\mathcal{J}$ is *formally skew-adjoint* (see also the upcoming Section 3.3.2 and particularly Remark 3.2), and state-dependent. The state-dependence here reflects the geometric nonlinearity of the problem at hand. This property is discussed in Chapter 2 of the present work by means of a finite dimensional model problem, cf. Example 2.3. Corresponding to the distributed control input, power-conjugated and collocated output quantities are defined through

$$\boldsymbol{y}_\Omega = \mathcal{B}_\Omega^\top \boldsymbol{z}(\boldsymbol{x}) = \begin{bmatrix} \boldsymbol{v} \\ \omega \end{bmatrix}. \tag{3.21}$$

It is known that (3.20) enjoys a pH structure, if and only if

$$\mathcal{E}^\top \boldsymbol{z}(\boldsymbol{x}) = \delta_{\mathrm{x}} \mathcal{H}(\boldsymbol{x}), \tag{3.22}$$

where $\delta_{\mathrm{x}} H$ represents the variational derivative of the Hamiltonian functional, see its definition in (2.73). In the present case, the Hamiltonian density h does not depend on derivatives of the state. Accordingly, one obtains

$$\delta_{\mathrm{x}} \mathcal{H}(\boldsymbol{x}) = \nabla h(\boldsymbol{x}) = (\boldsymbol{0}, 0, \rho A\boldsymbol{v}, \rho I\omega, \partial_\Gamma W, \partial_\kappa W)\,, \tag{3.23}$$

such that (3.22) holds true in view of the constitutive laws (3.9).

3.3.2. Energy balance and passivity

The formal skew-adjointness of $\mathcal{J}$ is crucial for the energy balance, which in general takes into account the power transmitted into the system across its boundary. To see this, we consider

$$\dot{\mathcal{H}} = (\delta_{\mathrm{x}} \mathcal{H}, \partial_t \boldsymbol{x})_\Omega = \left(\mathcal{E}^\top \boldsymbol{z}, \partial_t \boldsymbol{x}\right)_\Omega = (\boldsymbol{z}, \mathcal{E}\partial_t \boldsymbol{x})_\Omega = (\boldsymbol{z}, \mathcal{J}\boldsymbol{z})_\Omega + (\boldsymbol{z}, \mathcal{B}_\Omega \boldsymbol{u}_\Omega)_\Omega\,, \tag{3.24}$$

where we have subsequently inserted (3.22) and (3.20). After a straightforward calculation, the first term on the right-hand side of the last equation yields

$$(\boldsymbol{z}, \mathcal{J}\boldsymbol{z})_\Omega = (\boldsymbol{v}, \partial_s \boldsymbol{n})_\Omega + (\boldsymbol{n}, \partial_s \boldsymbol{v})_\Omega + (\omega, \partial_s M)_\Omega + (M, \partial_s \omega)_\Omega + (\partial_s \boldsymbol{r}, \omega \boldsymbol{S}\boldsymbol{n})_\Omega + (\boldsymbol{n}, \omega \boldsymbol{S}\partial_s \boldsymbol{r})_\Omega \,. \tag{3.25}$$

Integration by parts implies the following relationships

$$\begin{aligned} (\boldsymbol{v}, \partial_s \boldsymbol{n})_\Omega &= -(\boldsymbol{n}, \partial_s \boldsymbol{v})_\Omega + [\boldsymbol{v}, \boldsymbol{n}]_{\partial\Omega} \,, \\ (\omega, \partial_s M)_\Omega &= -(M, \partial_s \omega)_\Omega + [\omega, M]_{\partial\Omega} \,. \end{aligned} \tag{3.26}$$

Inserting from (3.26) into (3.25) and canceling out the last two terms in (3.25) due to the skew-symmetry of $\boldsymbol{S}$ yields

$$(\boldsymbol{z}, \mathcal{J}\boldsymbol{z})_\Omega = [\boldsymbol{v}, \boldsymbol{n}]_{\partial\Omega} + [\omega, M]_{\partial\Omega} \,. \tag{3.27}$$

The last relation can be understood as an embodiment of the abstract integration-by-parts formula (2.69) contained in Chapter 2 of this work. Moreover, the second term on the right-hand side of (3.24) can be recast in the form

$$(\boldsymbol{z}, \mathcal{B}_\Omega \boldsymbol{u}_\Omega)_\Omega = \left(\boldsymbol{u}_\Omega, \mathcal{B}_\Omega^\top \boldsymbol{z}\right)_\Omega = \left(\boldsymbol{u}_\Omega, \boldsymbol{y}_\Omega\right)_\Omega \,, \tag{3.28}$$

where definition (3.21) of the output $\boldsymbol{y}_\Omega$ has been taken into account. Thus, (3.24) can eventually be written as

$$\dot{\mathcal{H}} = [\boldsymbol{v}, \boldsymbol{n}]_{\partial\Omega} + [\omega, M]_{\partial\Omega} + \left(\boldsymbol{u}_\Omega, \boldsymbol{y}_\Omega\right)_\Omega \,. \tag{3.29}$$

The last equation complies with the balance law for energy. In particular, the boundary terms on the right-hand side account for the power transmitted across the boundary of the system. Depending on the specific boundary conditions, (3.29) can be recast in the form

$$\dot{\mathcal{H}} = \boldsymbol{u}_\partial^\top \boldsymbol{y}_\partial + \left(\boldsymbol{u}_\Omega, \boldsymbol{y}_\Omega\right)_\Omega \,, \tag{3.30}$$

where $(\boldsymbol{u}_\partial, \boldsymbol{y}_\partial)$ is the boundary input-output pair. For example, in the case of the mixed boundary conditions (3.12), one has

$$\boldsymbol{u}_\partial = \begin{bmatrix} \boldsymbol{v}_\mathrm{D}(t) \\ \omega_\mathrm{D}(t) \\ \boldsymbol{n}_\mathrm{N}(t) \\ m_\mathrm{N}(t) \end{bmatrix} \text{ and } \boldsymbol{y}_\partial = \begin{bmatrix} -\boldsymbol{n}(0,t) \\ -m(0,t) \\ \boldsymbol{v}(L,t) \\ \omega(L,t) \end{bmatrix} . \tag{3.31}$$

Note that the balance law for energy (3.30) automatically ensures conservation of energy for closed systems (i.e., for $\boldsymbol{u}_\Omega = \boldsymbol{0}$, $\boldsymbol{u}_\partial = \boldsymbol{0}$) and demonstrates the property of passivity. This property lies at the core of pH systems and can be exploited for advanced control design. Later, when it comes to the numerical discretization, we aim to preserve the pH structure to retain this property in simulations.

Remark 3.2. *The property of formal skew-adjointness is basically an extension of skew-symmetry for matrices to differential matrix operators. Loosely speaking, this means that the computation of $(\boldsymbol{z}, \mathcal{J}\boldsymbol{z})_\Omega$ may only yield boundary terms after integration by parts, see* (3.27)*. This property can be briefly written as $\mathcal{J} = -\mathcal{J}^*$. For more details, see Definition 2.16 in Chapter 2 of this work.* ♧

Remark 3.3. *The underlying mathematical notion is that of a Stokes–Dirac structure, which defines so-called* flow *and* effort *variables on respective dual spaces. This Stokes–Dirac structure is modulated by the state, which can be seen from the state-dependence of the structure matrix operator $\mathcal{J}(\boldsymbol{x})$. For more detailed explanations on this topic, the interested reader is referred to Chapter 4 in [63], or related works like [42], [44] or [41]. An introduction to the mathematical notion of Dirac structures is given in Section 2.2 of this work.* ♧

Remark 3.4. *Dissipative material behavior can be easily incorporated into the formulation as, e.g., already demonstrated in [A1]. This procedure is also detailed for similar mechanical models in Chapters 4 and 6 of this work. Eventually, the pH differential equations are modified such that*

$$\mathcal{E}\partial_t \boldsymbol{x} = (\mathcal{J}(\boldsymbol{x}) - \mathcal{R}(\boldsymbol{x}))\, \boldsymbol{z}(\boldsymbol{x}) + \mathcal{B}_\Omega \boldsymbol{u}_\Omega, \tag{3.32}$$

where $\mathcal{R} = \mathcal{R}^*$ is a self-adjoint, positive semi-definite dissipation matrix operator containing dissipative terms. The pH system remains passive and moreover exhibits dissipation, i.e.,

$$\dot{\mathcal{H}} = (\delta_{\boldsymbol{x}}\mathcal{H}(\boldsymbol{x}), \partial_t \boldsymbol{x})_\Omega = (\boldsymbol{z}, \mathcal{J}(\boldsymbol{x})\boldsymbol{z})_\Omega - (\boldsymbol{z}, \mathcal{R}\boldsymbol{z})_\Omega + \left(\boldsymbol{y}_\Omega, \boldsymbol{u}_\Omega\right)_\Omega \leq \boldsymbol{y}_\partial^\top \boldsymbol{u}_\partial + \left(\boldsymbol{y}_\Omega, \boldsymbol{u}_\Omega\right)_\Omega \tag{3.33}$$

since $(\boldsymbol{z}(\boldsymbol{x}), \mathcal{R}(\boldsymbol{x})\boldsymbol{z}(\boldsymbol{x}))_\Omega \geq 0$ for all $\boldsymbol{x}$.

♧

3.3.3. Weak formulation

The weak form of the IBVP can be derived in a straightforward manner from the differential form. Accordingly, pre-multiplying (3.19) on both sides by appropriate test functions $(\boldsymbol{w}^{\boldsymbol{r}}, w^{\varphi}, \boldsymbol{w}^{\boldsymbol{v}}, w^{\omega}, \boldsymbol{w}^{\boldsymbol{\Gamma}}, w^{\kappa})$, integrating over the spatial domain Ω and applying integration by parts yields

$$(\boldsymbol{w}^{\boldsymbol{r}}, \partial_t \boldsymbol{r} - \boldsymbol{v})_\Omega = 0, \tag{3.34a}$$
$$(w^{\varphi}, \partial_t \varphi - \omega)_\Omega = 0, \tag{3.34b}$$
$$\left(\boldsymbol{w}^{\boldsymbol{v}}, \rho A \partial_t \boldsymbol{v}\right)_\Omega + \left(\partial_s(\boldsymbol{w}^{\boldsymbol{v}}), \boldsymbol{\Lambda}\boldsymbol{N}\right)_\Omega - \left[(\boldsymbol{w}^{\boldsymbol{v}})^\top \boldsymbol{n}_{\mathrm{N}}\right]_{\partial\Omega_{\mathrm{N}}} - \left(\boldsymbol{w}^{\boldsymbol{v}}, \overline{\boldsymbol{n}}\right)_\Omega = 0, \tag{3.34c}$$
$$(w^{\omega}, \rho I \partial_t \omega)_\Omega + (\partial_s(w^{\omega}), M)_\Omega - \left(w^{\omega}, \partial_s \boldsymbol{r}^\top \boldsymbol{S}\boldsymbol{\Lambda}\boldsymbol{N}\right)_\Omega - \left[w^{\omega}\, m_{\mathrm{N}}\right]_{\partial\Omega_{\mathrm{N}}} - (w^{\omega}, \overline{m})_\Omega = 0, \tag{3.34d}$$
$$\left(\boldsymbol{w}^{\boldsymbol{\Gamma}}, \partial_t \boldsymbol{\Gamma}\right)_\Omega - \left(\boldsymbol{w}^{\boldsymbol{\Gamma}}, \omega \boldsymbol{\Lambda}^\top \boldsymbol{S}\, \partial_s \boldsymbol{r}\right)_\Omega - \left(\boldsymbol{w}^{\boldsymbol{\Gamma}}, \boldsymbol{\Lambda}^\top \partial_s \boldsymbol{v}\right)_\Omega = 0, \tag{3.34e}$$
$$(w^{\kappa}, \partial_t \kappa - \partial_s \omega)_\Omega = 0, \tag{3.34f}$$

for all test functions from appropriate spaces.

To obtain (3.34c) and (3.34d) vanishing test functions on the Dirichlet boundary have been taken into account. Note that the constitutive relations (3.9) will be required in a weak sense as well. Correspondingly, we write

$$\left(\boldsymbol{w}^{\boldsymbol{N}}, \boldsymbol{N} - \partial_{\boldsymbol{\Gamma}} W\right)_\Omega = 0, \tag{3.34g}$$
$$\left(w^{M}, M - \partial_{\kappa} W\right)_\Omega = 0, \tag{3.34h}$$

introducing additional test functions $\boldsymbol{w}^{\boldsymbol{N}}$ and w^{M}.

Remark 3.5. *The weak form* (3.34) *is valid if the Dirichlet boundary conditions are considered in the space of admissible test functions. However, if the Dirichlet boundary conditions are to be enforced in a weak sense, the weak form must be slightly modified, e.g., by introducing additional Lagrange multipliers and accounting for the prescribed boundary values. In general, enforcing non-homogeneous mixed boundary conditions for pH systems requires additional care, see, for example, [45, 46, 217, 218].* ♧

Remark 3.6. *The inclusion of the constitutive laws in the weak form* (3.34) *may appear unconventional at first. However, this will be handy later on in the structure-preserving discretization procedure. Additionally,*

this highlights the close connection of the present weak form with a 8-field Hu–Washizu-like variational principle $\delta S_{\mathrm{HW}}(\boldsymbol{r}, \varphi, \boldsymbol{v}, \omega, \boldsymbol{\Gamma}, \kappa, \boldsymbol{N}, M) = 0$ *[243]. To this end, choose the test functions as*

$$\boldsymbol{w}^{\boldsymbol{r}} = \rho A \delta \boldsymbol{v}, \quad w^{\varphi} = \rho I \delta \omega, \quad \boldsymbol{w}^{\boldsymbol{v}} = \delta \boldsymbol{r}, \quad w^{\omega} = \delta \varphi, \quad \boldsymbol{w}^{\boldsymbol{\Gamma}} = \delta \boldsymbol{N}, \quad w^{\kappa} = \delta M, \quad \boldsymbol{w}^{\boldsymbol{N}} = \delta \boldsymbol{\Gamma}, \quad w^{M} = \delta \kappa. \tag{3.35}$$

Furthermore, instead of the rate form of the strain-displacement relationships in (3.34e) *and* (3.34f)*, the variational principle yields the strain-displacement relationships* (3.5) *and* (3.6)*. For the details, see Appendix 3.A.* ♧

3.3.4. Balance of total angular momentum

The total angular momentum of the planar beam relative to the origin of the coordinate frame is defined by

$$J = \int_{\Omega} \left(\boldsymbol{r}^{\top} \boldsymbol{S} \rho A \boldsymbol{v} + \rho I \omega \right) \, \mathrm{d}s. \tag{3.36}$$

Assuming a pure Neumann problem (i.e., no Dirichlet boundary conditions), the following choice of admissible test functions

$$\boldsymbol{w}^{\boldsymbol{r}} = \boldsymbol{S}^{\top} \rho A \boldsymbol{v}, \quad \boldsymbol{w}^{\boldsymbol{v}} = \boldsymbol{S}^{\top} \boldsymbol{r}, \quad \text{and} \quad w^{\omega} = 1, \tag{3.37}$$

can be made in the weak form (3.34). Accordingly, inserting these functions into (3.34a), (3.34c) and (3.34d) and subsequently adding the resulting equations yields

$$\begin{aligned} \left(\boldsymbol{S}^{\top} \rho A \boldsymbol{v}, \partial_t \boldsymbol{r} \right)_{\Omega} + \left(\boldsymbol{S}^{\top} \boldsymbol{r}, \rho A \partial_t \boldsymbol{v} \right)_{\Omega} + \left(1, \rho I \partial_t \omega \right)_{\Omega} = \\ \left(\boldsymbol{S}^{\top} \rho A \boldsymbol{v}, \boldsymbol{v} \right)_{\Omega} - \left(\partial_s (\boldsymbol{S}^{\top} \boldsymbol{r}), \boldsymbol{\Lambda} \boldsymbol{N} \right)_{\Omega} + \left[\boldsymbol{S}^{\top} \boldsymbol{r}^{\top} \boldsymbol{n}_{\mathrm{N}} \right]_{\partial \Omega_{\mathrm{N}}} + \left(\boldsymbol{S}^{\top} \boldsymbol{r}, \overline{\boldsymbol{n}} \right)_{\Omega} \\ + \left(1, \partial_s \boldsymbol{r}^{\top} \boldsymbol{S} \boldsymbol{\Lambda} \boldsymbol{N} \right)_{\Omega} + \left[m_{\mathrm{N}} \right]_{\partial \Omega_{\mathrm{N}}} + \left(1, \overline{m} \right)_{\Omega}. \end{aligned} \tag{3.38}$$

While the first term on the right-hand side of the last equation vanishes due to the skew-symmetry of matrix $\boldsymbol{S}$, it can be shown that the second and fifth term cancel each other. Moreover, the left-hand side can be identified as the temporal derivative of the total angular momentum (3.36). Thus, we arrive at the balance equation

$$\partial_t J = \int_{\Omega} \left(\boldsymbol{r}^{\top} \boldsymbol{S} \overline{\boldsymbol{n}} + \overline{m} \right) \, \mathrm{d}s + \left[\boldsymbol{r}^{\top} \boldsymbol{S} \boldsymbol{n}_{\mathrm{N}} + m_{\mathrm{N}} \right]_{\partial \Omega_{\mathrm{N}}}. \tag{3.39}$$

This demonstrates that the time rate of change of the total angular momentum is equal to the angular momentum exerted on the system by distributed input forces and torques as well as Neumann boundary conditions. In the special case of closed systems, the total angular momentum is preserved.

Remark 3.7. *Note that the balance equation for the total energy can also be proven by employing a similar approach. In particular, choosing* $\boldsymbol{w}^{\boldsymbol{v}} = \boldsymbol{v}$, $w^{\omega} = \omega$, $\boldsymbol{w}^{\boldsymbol{\Gamma}} = \boldsymbol{N}$ *and* $w^{\kappa} = M$ *in weak form* (3.34)*, subsequently adding the equations resulting from* (3.34c)-(3.34f)*, and taking into account* (3.34g) *and* (3.34h) *with* $\boldsymbol{w}^{\boldsymbol{N}} = \partial_t \boldsymbol{\Gamma}$ *and* $w^{M} = \partial_t \kappa$*, one arrives at relation* (3.30). ♧

3.4. Structure-preserving discretization

The numerical discretization of the pH system is based on the structure-preserving mixed finite element method and energy-consistent time-stepping schemes. Crucial properties of the infinite-dimensional pH system can be carried over to the discrete setting. The methodology is summarized in the following sections.

3.4.1. Discretization in space

The pH system for the geometrically exact beam dynamics (3.19) is readily available for spatial discretization via its weak form (3.34). Specifically, we employ a mixed finite element approach and divide the beam domain into n_e finite elements, i.e., $\Omega = \cup_{e=1}^{n_\mathrm{e}} \Omega^e$. Similar approaches for related mechanical models can be found in the subsequent Chapters 4 and 6. Since we make use of 2-node finite elements (see Figure 3.2), the total amount of nodes is $n_\mathrm{n} = n_\mathrm{e} + 1$. Displacement and velocity quantities $(\boldsymbol{r}, \varphi, \boldsymbol{v}, \omega)$ are approximated with C^0-continuous, piecewise linear Lagrangian shape functions, while strain and stress type quantities $(\boldsymbol{\Gamma}, \kappa, \boldsymbol{N}, M)$ use piecewise constant discontinuous approximations. We denote by

$$\mathcal{V}_\mathrm{h} \subset H^1(\Omega, \mathbb{R}^2), \quad \mathcal{W}_\mathrm{h} \subset H^1(\Omega, \mathbb{R}), \quad \mathcal{G}_\mathrm{h} \subset L^2(\Omega, \mathbb{R}^2), \quad \mathcal{K}_\mathrm{h} \subset L^2(\Omega, \mathbb{R}), \tag{3.40}$$

finite-dimensional subspaces of the Sobolev spaces of square-integrable C^0-continuous functions and of the spaces of square-integrable, piecewise constant functions. Choosing a specific basis within the Bubnov–Galerkin method, the approximation is expressed as

$$\begin{aligned}
\boldsymbol{r}_\mathrm{h}(s,t) &= \boldsymbol{\Phi}_2(s)\hat{\boldsymbol{r}}(t) \in \mathcal{V}_\mathrm{h}, & \boldsymbol{v}_\mathrm{h}(s,t) &= \boldsymbol{\Phi}_2(s)\hat{\boldsymbol{v}}(t) \in \mathcal{V}_\mathrm{h}, \\
\varphi_\mathrm{h}(s,t) &= \boldsymbol{\Phi}_1(s)\hat{\boldsymbol{\varphi}}(t) \in \mathcal{W}_\mathrm{h}, & \omega_\mathrm{h}(s,t) &= \boldsymbol{\Phi}_1(s)\hat{\boldsymbol{\omega}}(t) \in \mathcal{W}_\mathrm{h}, \\
\boldsymbol{\Gamma}_\mathrm{h}(s,t) &= \boldsymbol{\Psi}_2(s)\hat{\boldsymbol{\Gamma}}(t) \in \mathcal{G}_\mathrm{h}, & \boldsymbol{N}_\mathrm{h}(s,t) &= \boldsymbol{\Psi}_2(s)\hat{\boldsymbol{N}}(t) \in \mathcal{G}_\mathrm{h}, \\
\kappa_\mathrm{h}(s,t) &= \boldsymbol{\Psi}_1(s)\hat{\boldsymbol{\kappa}}(t) \in \mathcal{K}_\mathrm{h}, & M_\mathrm{h}(s,t) &= \boldsymbol{\Psi}_1(s)\hat{\boldsymbol{M}}(t) \in \mathcal{K}_\mathrm{h},
\end{aligned} \tag{3.41}$$

where $\square_\mathrm{h}$ denotes an approximation of the field quantity $\square$ and the nodal-unknown vector $\hat{\square}$ contains entries from all finite elements and the respective nodes. Moreover, for the approximation of the corresponding test function $\boldsymbol{w}_\mathrm{h}^{\square}$ consider the same basis as for $\square_\mathrm{h}$. In this context, the above ansatz matrices contain the linear Lagrangian shape functions or the piecewise constant functions, e.g.,

$$\boldsymbol{r}_\mathrm{h}(s,t) = \boldsymbol{\Phi}_2(s)\hat{\boldsymbol{r}}(t) = \sum_{i=1}^{n_\mathrm{n}} N_i(s)\boldsymbol{r}_i(t), \tag{3.42a}$$

$$\boldsymbol{\Gamma}_\mathrm{h}(s,t) = \boldsymbol{\Psi}_2(s)\hat{\boldsymbol{\Gamma}}(t) = \sum_{i=1}^{n_\mathrm{e}} \tilde{N}_i(s)\boldsymbol{\Gamma}_i(t), \tag{3.42b}$$

for more details see Appendix 3.B. The basis functions are depicted in Figure 3.3. We follow common finite element procedures, see e.g., [240, 243], which also includes an assembly of the global system matrices and vectors accounting for the respective nodal indices and degrees of freedom, such that e.g., $\boldsymbol{r}_2^{e+1} = \boldsymbol{r}_1^e$ are the same degree of freedom. The degrees of freedom of one finite element are depicted in Figure 3.2. Additionally, we perform all computations on element level and consider the isoparametric concept to transform all calculations to a standard reference element with $\xi \in \hat{\Omega} = [-1, 1]$, see Figure 3.3.

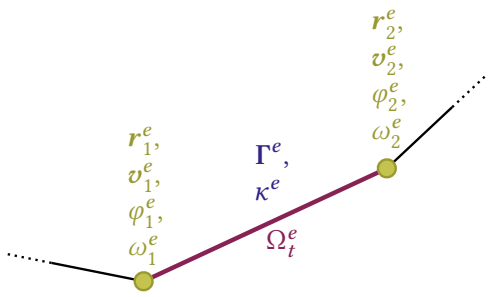

Figure 3.2.: Degrees of freedom of one finite element.

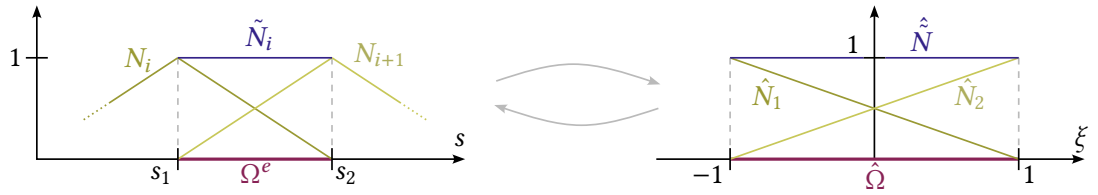

Figure 3.3.: Ansatz functions and reference element.

Eventually, the finite-dimensional version of the state (3.15) contains the degrees of freedom of all finite elements and is given by

$$\hat{\boldsymbol{x}} = (\hat{\boldsymbol{r}}, \hat{\boldsymbol{\varphi}}, \hat{\boldsymbol{v}}, \hat{\boldsymbol{\omega}}, \hat{\boldsymbol{\Gamma}}, \hat{\boldsymbol{\kappa}}). \tag{3.43}$$

Inserting the ansatz (3.41) into (3.16) gives rise to the approximated Hamiltonian. Note that we henceforth assume linear-elastic constitutive relations (see Remark 3.1) for the ease of notation. The discrete Hamiltonian reads

$$\hat{\mathcal{H}}(\hat{\boldsymbol{x}}) = \frac{1}{2}\hat{\boldsymbol{v}}^\top \rho A \boldsymbol{M}_2 \hat{\boldsymbol{v}} + \frac{1}{2}\hat{\boldsymbol{\omega}}^\top \rho I \boldsymbol{M}_1 \hat{\boldsymbol{\omega}} + \frac{1}{2}\hat{\boldsymbol{\Gamma}}^\top \boldsymbol{D}_2 \hat{\boldsymbol{\Gamma}} + \frac{1}{2}\hat{\boldsymbol{\kappa}}^\top \boldsymbol{D}_1 \hat{\boldsymbol{\kappa}}, \tag{3.44}$$

where the system matrices can be found in Appendix 3.C . The corresponding discrete system dynamics are obtained by approximating the weak form (3.34) with the ansatz spaces (3.40). The discrete system dynamics are given by

$$\left(\boldsymbol{w}_\mathrm{h}^{\boldsymbol{r}}, \partial_t \boldsymbol{r}_\mathrm{h} - \boldsymbol{v}_\mathrm{h}\right)_\Omega = 0, \tag{3.45a}$$
$$\left(w_\mathrm{h}^{\varphi}, \partial_t \varphi_\mathrm{h} - \omega_\mathrm{h}\right)_\Omega = 0, \tag{3.45b}$$
$$\left(\boldsymbol{w}_\mathrm{h}^{\boldsymbol{v}}, \rho A \partial_t \boldsymbol{v}_\mathrm{h}\right)_\Omega + \left(\partial_s \boldsymbol{w}_\mathrm{h}^{\boldsymbol{v}}, \boldsymbol{\Lambda}(\varphi_\mathrm{h}) \boldsymbol{N}_\mathrm{h}\right)_\Omega - \left[(\boldsymbol{w}_\mathrm{h}^{\boldsymbol{v}})^\top \boldsymbol{n}_\mathrm{N}\right]_{\partial\Omega_\mathrm{N}} - \left(\boldsymbol{w}_\mathrm{h}^{\boldsymbol{v}}, \overline{\boldsymbol{n}}\right)_\Omega = 0, \tag{3.45c}$$
$$\left(w_\mathrm{h}^{\omega}, \rho I \partial_t \omega_\mathrm{h}\right)_\Omega + \left(\partial_s w_\mathrm{h}^{\omega}, M_\mathrm{h}\right)_\Omega - \left(w_\mathrm{h}^{\omega}, (\partial_s \boldsymbol{r}_\mathrm{h})^\top \boldsymbol{S}\boldsymbol{\Lambda}(\varphi_\mathrm{h}) \boldsymbol{N}_\mathrm{h}\right)_\Omega - \left[w_\mathrm{h}^{\omega}\, m_\mathrm{N}\right]_{\partial\Omega_\mathrm{N}} - \left(w_\mathrm{h}^{\omega}, \overline{m}\right)_\Omega = 0, \tag{3.45d}$$
$$\left(\boldsymbol{w}_\mathrm{h}^{\boldsymbol{\Gamma}}, \partial_t \boldsymbol{\Gamma}_\mathrm{h}\right)_\Omega - \left(\boldsymbol{w}_\mathrm{h}^{\boldsymbol{\Gamma}}, \omega_\mathrm{h} \boldsymbol{\Lambda}(\varphi_\mathrm{h})^\top \boldsymbol{S} \partial_s \boldsymbol{r}_\mathrm{h}\right)_\Omega - \left(\boldsymbol{w}_\mathrm{h}^{\boldsymbol{\Gamma}}, \boldsymbol{\Lambda}(\varphi_\mathrm{h})^\top \partial_s \boldsymbol{v}_\mathrm{h}\right)_\Omega = 0, \tag{3.45e}$$
$$\left(w_\mathrm{h}^{\kappa}, \partial_t \kappa_\mathrm{h} - \partial_s \omega_\mathrm{h}\right)_\Omega = 0, \tag{3.45f}$$
$$\left(\boldsymbol{w}_\mathrm{h}^{\boldsymbol{N}}, \boldsymbol{N}_\mathrm{h} - \boldsymbol{D}_\mathrm{ts} \boldsymbol{\Gamma}_\mathrm{h}\right)_\Omega = 0, \tag{3.45g}$$
$$\left(w_\mathrm{h}^{M}, M_\mathrm{h} - EI\kappa_\mathrm{h}\right)_\Omega = 0. \tag{3.45h}$$

With the chosen basis functions from (3.41) it is possible to transform the above variational formulation into a finite-dimensional pH system in terms of differential equations, assuming the arbitrariness of the test functions. We arrive at the discrete pH system governed by

$$\begin{bmatrix} \boldsymbol{M}_2 & 0 & 0 & 0 & 0 & 0 \\ 0 & \boldsymbol{M}_1 & 0 & 0 & 0 & 0 \\ 0 & 0 & \rho A \boldsymbol{M}_2 & 0 & 0 & 0 \\ 0 & 0 & 0 & \rho I \boldsymbol{M}_1 & 0 & 0 \\ 0 & 0 & 0 & 0 & \boldsymbol{C}_2 & 0 \\ 0 & 0 & 0 & 0 & 0 & \boldsymbol{C}_1 \end{bmatrix} \frac{\mathrm{d}}{\mathrm{d}t} \begin{bmatrix} \hat{\boldsymbol{r}} \\ \hat{\boldsymbol{\varphi}} \\ \hat{\boldsymbol{v}} \\ \hat{\boldsymbol{\omega}} \\ \hat{\boldsymbol{\Gamma}} \\ \hat{\boldsymbol{\kappa}} \end{bmatrix} = \tag{3.46}$$

$$\begin{bmatrix} 0 & 0 & \boldsymbol{M}_2 & 0 & 0 & 0 \\ 0 & 0 & 0 & \boldsymbol{M}_1 & 0 & 0 \\ -\boldsymbol{M}_2^\top & 0 & 0 & 0 & -\boldsymbol{G}_2(\hat{\boldsymbol{\varphi}}) & 0 \\ 0 & -\boldsymbol{M}_1^\top & 0 & 0 & \boldsymbol{V}(\hat{\boldsymbol{r}}, \hat{\boldsymbol{\varphi}}) & -\boldsymbol{G}_1 \\ 0 & 0 & \boldsymbol{G}_2(\hat{\boldsymbol{\varphi}})^\top & -\boldsymbol{V}(\hat{\boldsymbol{r}}, \hat{\boldsymbol{\varphi}})^\top & 0 & 0 \\ 0 & 0 & 0 & \boldsymbol{G}_1^\top & 0 & 0 \end{bmatrix} \begin{bmatrix} \boldsymbol{0} \\ \boldsymbol{0} \\ \hat{\boldsymbol{v}} \\ \hat{\boldsymbol{\omega}} \\ \hat{\boldsymbol{N}} \\ \hat{\boldsymbol{M}} \end{bmatrix} + \begin{bmatrix} \boldsymbol{B}_\partial & \boldsymbol{B}_\Omega \end{bmatrix} \begin{bmatrix} \boldsymbol{u}_\partial(t) \\ \hat{\boldsymbol{u}}_\Omega(t) \end{bmatrix}.$$

along with the algebraic constraints for the stress resultants

$$\boldsymbol{C}_2\hat{\boldsymbol{N}} = \boldsymbol{D}_2\hat{\boldsymbol{\Gamma}}, \quad \text{and} \quad \boldsymbol{C}_1\hat{\boldsymbol{M}} = \boldsymbol{D}_1\hat{\boldsymbol{\kappa}}, \tag{3.47}$$

emerging from (3.45g) and (3.45h). These relations can be used to express the unknowns for the stress resultants in terms of unknowns for the strains, e.g., $\hat{\boldsymbol{N}} = \hat{\boldsymbol{N}}(\hat{\boldsymbol{\Gamma}})$. For the detailed definitions of the system matrices see Appendix 3.C. For the implementation details concerning the input vectors and matrices, which deal with both distributed and boundary inputs, we refer to Appendix 3.D. Note that the system output $\hat{\boldsymbol{y}}$ contains both angular and translational velocities in the domain and at the boundary, i.e.,

$$\hat{\boldsymbol{y}} = \begin{bmatrix} \boldsymbol{y}_\partial \\ \hat{\boldsymbol{y}}_\Omega \end{bmatrix} = \begin{bmatrix} \boldsymbol{B}_\partial^\top \\ \boldsymbol{B}_\Omega^\top \end{bmatrix} \hat{\boldsymbol{z}}(\hat{\boldsymbol{x}}), \tag{3.48}$$

see also the definition in the continuous setting (3.31). Analogously to the infinite-dimensional version (3.20), we can recast the semi-discrete set of equations in the spirit of a pH framework as in [23, 161, 162] given by

$$\begin{aligned} \boldsymbol{E}\frac{\mathrm{d}}{\mathrm{d}t}\hat{\boldsymbol{x}} &= \boldsymbol{J}(\hat{\boldsymbol{x}})\hat{\boldsymbol{z}}(\hat{\boldsymbol{x}}) + \boldsymbol{B}\hat{\boldsymbol{u}}, \\ \hat{\boldsymbol{y}} &= \boldsymbol{B}^\top\hat{\boldsymbol{z}}(\hat{\boldsymbol{x}}), \end{aligned} \tag{3.49}$$

where the output equation has been appended. For further details, see also Section 2.3 for a detailed introduction to such a pH formulation and in particular Definition 2.7.

Analogously to (3.20), $\boldsymbol{E}$ is a symmetric coefficient matrix and $\boldsymbol{J}(\hat{\boldsymbol{x}}) = -\boldsymbol{J}(\hat{\boldsymbol{x}})^\top$ denotes a skew-symmetric and state-dependent structure matrix, reflecting the geometric nonlinearity of the problem at hand. As in the infinite-dimensional case, the system (3.49) is pH if and only if

$$\boldsymbol{E}^\top\hat{\boldsymbol{z}}(\hat{\boldsymbol{x}}) = \nabla\hat{\mathcal{H}}(\hat{\boldsymbol{x}}) \tag{3.50}$$

holds true. In view of the discrete Hamiltonian (3.44) this can be verified by using the discrete constitutive relations (3.47). Note that the input term $\boldsymbol{B}\hat{\boldsymbol{u}}$ contains both distributed and boundary input terms, i.e., distributed forces and torques as well as boundary quantities emanating from the Neumann boundary conditions. Moreover, $\hat{\boldsymbol{z}}$ is the discretized costate function. As already shown in the infinite-dimensional setting, one core property of the pH formulation is that it satisfies a formalized energy balance, see (3.30). This property is inherited by the semi-discrete system (3.49) such that

$$\frac{\mathrm{d}}{\mathrm{d}t}\hat{\mathcal{H}} = \nabla\hat{\mathcal{H}}(\hat{\boldsymbol{x}})^\top\frac{\mathrm{d}}{\mathrm{d}t}\hat{\boldsymbol{x}} = \hat{\boldsymbol{z}}(\hat{\boldsymbol{x}})^\top\boldsymbol{E}\partial_t\hat{\boldsymbol{x}} = \hat{\boldsymbol{z}}(\hat{\boldsymbol{x}})^\top(\boldsymbol{J}(\hat{\boldsymbol{x}})\hat{\boldsymbol{z}}(\hat{\boldsymbol{x}}) + \boldsymbol{B}\hat{\boldsymbol{u}}) = \hat{\boldsymbol{y}}^\top\hat{\boldsymbol{u}}, \tag{3.51}$$

where the skew-symmetry of the structure-matrix has been taken into account. This relation highlights the passivity of the finite-dimensional system and energy-conservation is obtained for closed system. The semi-discrete pH system (3.49) is the basis for the structure-preserving time discretization in the next section.

3.4.2. Discretization in time

We aim at a structure-preserving time discretization of the semi-discrete pH system (3.49) with the equivalent variational formulation (3.45). To this end, we apply an implicit one-step scheme which is based on the implicit mid-point rule. Let $\hat{\boldsymbol{x}}^n \approx \hat{\boldsymbol{x}}(t^n)$ at time instance t^n and consider an equidistant time-grid such that $\mathbb{T} = \cup_{n=0}^{N}[t^n, t^{n+1}]$ with N time steps of constant size $h = t^{n+1} - t^n$.

The time-stepping scheme we propose, given the pH system (3.49), can now be written in the form

$$\begin{aligned} \mathbf{E}\left(\hat{\mathbf{x}}^{n+1} - \hat{\mathbf{x}}^{n}\right) &= h\,\mathbf{J}(\hat{\boldsymbol{x}}^{n+1/2})\hat{\mathbf{z}}(\hat{\boldsymbol{x}}^{n+1/2}) + h\,\mathbf{B}\hat{\mathbf{u}}^{n+1/2}, \\ \hat{\mathbf{y}}^{n+1/2} &= \mathbf{B}^{\top}\hat{\mathbf{z}}(\hat{\boldsymbol{x}}^{n+1/2}), \end{aligned} \tag{3.52}$$

for $n = 0, \dots, N-1$, where $\hat{\boldsymbol{x}}^{n+1/2} = \frac{1}{2}(\hat{\mathbf{x}}^{n+1} + \hat{\mathbf{x}}^{n})$, While we assume that $\hat{\mathbf{u}}^{n+1/2}$ is the evaluation of the (possibly discontinuous) input function at $t^{n+1/2}$, this must not be necessarily the case. It could also be the evaluation at some other point within the time interval of interest or an average value. Additionally, the time-discrete costate $\hat{\mathbf{z}}(\hat{\boldsymbol{x}}^{n+1/2})$ satisfies

$$\mathbf{E}^{\top}\hat{\mathbf{z}}(\hat{\boldsymbol{x}}^{n+1/2}) = \nabla\hat{\mathcal{H}}(\hat{\mathbf{x}}^{n+1/2}). \tag{3.53}$$

Additionally, the discrete-time output $\hat{\boldsymbol{y}}^{n+1/2}$ is an approximation for $\hat{\boldsymbol{y}}(t^{n+1/2})$. For at most quadratic Hamiltonians, like here (3.44), the midpoint-evaluated gradient satisfies the directionality property[2]

$$\nabla\hat{\mathcal{H}}(\hat{\mathbf{x}}^{n+1/2})^{\top}\left(\hat{\mathbf{x}}^{n+1} - \hat{\mathbf{x}}^{n}\right) = \hat{\mathcal{H}}(\hat{\mathbf{x}}^{n+1}) - \hat{\mathcal{H}}(\hat{\mathbf{x}}^{n}). \tag{3.54}$$

The structure-preserving scheme is energy-consistent and second-order accurate. It ensures an exact energy balance in discrete time, i.e., making use of directionality property (3.54) we obtain

$$\begin{aligned} \hat{\mathcal{H}}^{n+1} - \hat{\mathcal{H}}^{n} = \hat{\mathbf{z}}(\hat{\boldsymbol{x}}^{n+1/2})^{\top}\mathbf{E}\left(\hat{\mathbf{x}}^{n+1} - \hat{\mathbf{x}}^{n}\right) &= \hat{\mathbf{z}}(\hat{\boldsymbol{x}}^{n+1/2})^{\top} h\left(\mathbf{J}(\hat{\boldsymbol{x}}^{n+1/2})\hat{\mathbf{z}}(\hat{\boldsymbol{x}}^{n+1/2}) + \mathbf{B}\hat{\mathbf{u}}^{n+1/2}\right) \\ &= h\,(\hat{\mathbf{u}}^{n+1/2})^{\top}\hat{\boldsymbol{y}}^{n+1/2}, \end{aligned} \tag{3.55}$$

where we have used the skew-symmetry of $\boldsymbol{J}$. This relation is a time-discrete counterpart of (3.51). This proves that the present time-stepping scheme exhibits passivity and losslessness (which includes energy-conservation in the case of vanishing inputs).

Remark 3.8. *Note that analogously to [C2, A1] discrete gradients may be employed in the case of nonlinear materials to obtain energy-consistency in that case. The application of discrete gradients ensures the directionality condition* (3.54) *to be true for all Hamiltonians.* ♧

The time-stepping scheme (3.52), (3.53) corresponds to an approximation of the weak form (3.45) after choosing the above-mentioned basis functions. A direct discretization of this weak form in an equivalent manner yields

$$\left(\boldsymbol{w}_{\mathrm{h}}^{\boldsymbol{r}}, \boldsymbol{r}_{\mathrm{h}}^{n+1} - \boldsymbol{r}_{\mathrm{h}}^{n} - h\boldsymbol{v}_{\mathrm{h}}^{n+1/2}\right)_{\Omega} = 0, \tag{3.56a}$$

$$\left(w_{\mathrm{h}}^{\varphi}, \varphi_{\mathrm{h}}^{n+1} - \varphi_{\mathrm{h}}^{n} - h\omega_{\mathrm{h}}^{n+1/2}\right)_{\Omega} = 0, \tag{3.56b}$$

$$\begin{aligned} &\left(\boldsymbol{w}_{\mathrm{h}}^{\boldsymbol{v}}, \rho A(\boldsymbol{v}_{\mathrm{h}}^{n+1} - \boldsymbol{v}_{\mathrm{h}}^{n})\right)_{\Omega} + \left(\partial_s \boldsymbol{w}_{\mathrm{h}}^{\boldsymbol{v}}, h\boldsymbol{\Lambda}(\varphi_{\mathrm{h}}^{n+1/2})\boldsymbol{N}_{\mathrm{h}}^{n+1/2}\right)_{\Omega} \\ &\qquad - h\left[(\boldsymbol{w}_{\mathrm{h}}^{\boldsymbol{v}})^{\top}\boldsymbol{n}_{\mathrm{N}}^{n+1/2}\right]_{\partial\Omega_{\mathrm{N}}} - h\left(\boldsymbol{w}_{\mathrm{h}}^{\boldsymbol{v}}, \overline{\boldsymbol{n}}^{n+1/2}\right)_{\Omega} = 0, \end{aligned} \tag{3.56c}$$

$$\begin{aligned} &\left(w_{\mathrm{h}}^{\omega}, \rho I(\omega_{\mathrm{h}}^{n+1} - \omega_{\mathrm{h}}^{n})\right)_{\Omega} + \left(\partial_s w_{\mathrm{h}}^{\omega}, hM_{\mathrm{h}}^{n+1/2}\right)_{\Omega} \\ &\qquad - \left(w_{\mathrm{h}}^{\omega}, h(\partial_s \boldsymbol{r}_{\mathrm{h}}^{n+1/2})^{\top}S\boldsymbol{\Lambda}(\varphi_{\mathrm{h}}^{n+1/2})\boldsymbol{N}_{\mathrm{h}}^{n+1/2}\right)_{\Omega} - h\left[w_{\mathrm{h}}^{\omega} m_{\mathrm{N}}^{n+1/2}\right]_{\partial\Omega_{\mathrm{N}}} - h\left(w_{\mathrm{h}}^{\omega}, \overline{m}^{n+1/2}\right)_{\Omega} = 0, \end{aligned} \tag{3.56d}$$

$$\left(\boldsymbol{w}_{\mathrm{h}}^{\Gamma}, \boldsymbol{\Gamma}_{\mathrm{h}}^{n+1} - \boldsymbol{\Gamma}_{\mathrm{h}}^{n}\right)_{\Omega} - \left(\boldsymbol{w}_{\mathrm{h}}^{\Gamma}, h\omega_{\mathrm{h}}^{n+1/2}\boldsymbol{\Lambda}(\varphi^{n+1/2})^{\top}S\partial_s \boldsymbol{r}_{\mathrm{h}}^{n+1/2}\right)_{\Omega} - \left(\boldsymbol{w}_{\mathrm{h}}^{\Gamma}, h\boldsymbol{\Lambda}(\varphi_{\mathrm{h}}^{n+1/2})^{\top}\partial_s \boldsymbol{v}_{\mathrm{h}}^{n+1/2}\right)_{\Omega} = 0, \tag{3.56e}$$

[2] This property can be directly extended for more general Hamiltonians by means of discrete gradients [87, 97, C4]. This is discussed for the case of geometrically exact strings in Chapter 6 of this work. More details on discrete gradients can be found in Chapter 5.

$$\left(w_{\mathrm{h}}^{\kappa}, \kappa_{\mathrm{h}}^{n+1} - \kappa_{\mathrm{h}}^{n} - h\partial_s \omega_{\mathrm{h}}^{n+1/2}\right)_{\Omega} = 0, \quad (3.56\mathrm{f})$$

$$\left(\boldsymbol{w}_{\mathrm{h}}^{N}, \boldsymbol{N}_{\mathrm{h}}^{n+1/2} - \boldsymbol{D}_{\mathrm{ts}}\boldsymbol{\Gamma}_{\mathrm{h}}^{n+1/2}\right)_{\Omega} = 0, \quad (3.56\mathrm{g})$$

$$\left(w_{\mathrm{h}}^{M}, M_{\mathrm{h}}^{n+1/2} - EI\kappa_{\mathrm{h}}^{n+1/2}\right)_{\Omega} = 0. \quad (3.56\mathrm{h})$$

The weak representation (3.56) also facilitates the following derivations.

3.4.3. Discrete balance of total angular momentum

Here, we show that the proposed discretization approach inherits the balance of angular momentum (3.39) in a discrete sense. To this end, one proceeds in very similar way to the continuous case, see Section 3.3.4. The discrete total angular momentum is defined as

$$J_{\mathrm{h}}^{n} = \int_{\Omega} \left((\boldsymbol{r}_{\mathrm{h}}^{n})^{\top} \boldsymbol{S} \rho A \boldsymbol{v}_{\mathrm{h}}^{n} + \rho I \omega_{\mathrm{h}}^{n} \right) \mathrm{d}s \quad (3.57)$$

for $n = 0, \ldots, N$. It is then stated that the identity

$$J_{\mathrm{h}}^{n+1} - J_{\mathrm{h}}^{n} = \int_{\Omega} \left((\boldsymbol{r}_{\mathrm{h}}^{n+1/2})^{\top} \boldsymbol{S} \rho A (\boldsymbol{v}_{\mathrm{h}}^{n+1} - \boldsymbol{v}_{\mathrm{h}}^{n}) + (\boldsymbol{r}_{\mathrm{h}}^{n+1} - \boldsymbol{r}_{\mathrm{h}}^{n})^{\top} \boldsymbol{S} \rho A \boldsymbol{v}_{\mathrm{h}}^{n+1/2} + \rho I (\omega_{\mathrm{h}}^{n+1} - \omega_{\mathrm{h}}^{n}) \right) \mathrm{d}s \quad (3.58)$$

holds true. Now, from all admissible test functions we set

$$\boldsymbol{w}_{\mathrm{h}}^{r} = \boldsymbol{S}^{\top} \rho A \boldsymbol{v}_{\mathrm{h}}^{n+1/2}, \quad \boldsymbol{w}_{\mathrm{h}}^{v} = \boldsymbol{S}^{\top} \boldsymbol{r}_{\mathrm{h}}^{n+1/2}, \quad \text{and} \quad w_{\mathrm{h}}^{\omega} = 1, \quad (3.59)$$

and add up the discrete-time weak forms (3.56a), (3.56c) and (3.56d). Eventually, the right-hand side of (3.58) can be identified in the result, such that

$$J_{\mathrm{h}}^{n+1} - J_{\mathrm{h}}^{n} = \int_{\Omega} \left((\boldsymbol{r}_{\mathrm{h}}^{n+1/2})^{\top} \boldsymbol{S} \overline{\boldsymbol{n}}^{n+1/2} + \overline{m}^{n+1/2} \right) \mathrm{d}s + \left[(\boldsymbol{r}_{\mathrm{h}}^{n+1/2})^{\top} \boldsymbol{S} (\boldsymbol{n}_{\mathrm{N}})^{n+1/2} + (m_{\mathrm{N}})^{n+1/2} \right]_{\partial\Omega_{\mathrm{N}}} \quad (3.60)$$

remains. Correspondingly, only terms induced by Neumann boundary conditions as well as distributed input forces and torques remain in the discrete balance of angular momentum. This shows that the proposed time-discretization scheme inherits the balance of angular momentum from the continuous setting and the total angular momentum is conserved for closed systems.

Remark 3.9. *Note that the discrete-time balance equation for the total energy* (3.55) *can be proven alternatively by employing a similar approach with appropriate discrete-time test functions.* ♧

3.4.4. Comparison with the usual approach to the design of EM methods

The present pH approach to the design of EM schemes can be distinguished from previously proposed EM methods, which typically impose the strain-displacement relationships (3.5) and (3.6) at the end of each time step. In particular, the present approach relies on the time discretization of the rate form of the strain-displacement relationship (3.17), which is further analyzed in Section 3.4.4.1. This crucial difference is illustrated in Section 3.4.4.2 by comparing the present formulation with the classical work by Stander and Stein [213]. Lastly, we deduce a purely displacement-based version of the pH scheme making use of an internal history variable in Section 3.4.4.3. In what follows, we can focus on the temporal discretization while leaving the spatial discretization apart for the sake of conciseness.

3.4.4.1. Strain-displacement relationships in the time-discrete setting

Second-order EM schemes are commonly based on the application of the mid-point rule to the kinematic displacement-velocity equations. That is, in the present case of the planar beam[3]

$$\boldsymbol{r}^{n+1} - \boldsymbol{r}^n = h\boldsymbol{v}^{n+1/2}, \tag{3.61a}$$

$$\varphi^{n+1} - \varphi^n = h\omega^{n+1/2}, \tag{3.61b}$$

which conforms with (3.56a) and (3.56b), respectively. Our pH approach relies on the discretization of the rate form of the strain-displacement relationship (3.17). Accordingly, application of the mid-point rule yields

$$\boldsymbol{\Gamma}^{n+1} - \boldsymbol{\Gamma}^n = h\omega^{n+1/2}\boldsymbol{\Lambda}(\varphi^{n+1/2})^\top \boldsymbol{S}\,\partial_s\boldsymbol{r}^{n+1/2} + h\boldsymbol{\Lambda}(\varphi^{n+1/2})^\top\partial_s\boldsymbol{v}^{n+1/2}, \tag{3.62a}$$

$$\kappa^{n+1} - \kappa^n = h\partial_s\omega^{n+1/2}, \tag{3.62b}$$

which complies with (3.56e) and (3.56f), respectively. Substituting (3.61b) into (3.62b) yields

$$\kappa^{n+1} - \kappa^n = \partial_s\varphi^{n+1} - \partial_s\varphi^n, \tag{3.63}$$

which implies $\kappa^{n+1} = \partial_s\varphi^{n+1}$, since $\kappa^n = \partial_s\varphi^n$ is given for consistent initial conditions. However, a similar result is not obtained from (3.62a) due to the nonlinearity of the strain-displacement relation (3.5), i.e., $\boldsymbol{\Gamma} = \boldsymbol{\Lambda}(\varphi)^\top\partial_s\boldsymbol{r} - \boldsymbol{e}_1$. Instead, (3.62a) can be recast in the form

$$\boldsymbol{\Gamma}^{n+1} = \boldsymbol{\Gamma}^n + \Delta\varphi\boldsymbol{\Lambda}(\varphi^{n+1/2})^\top\boldsymbol{S}\,\partial_s\boldsymbol{r}^{n+1/2} + \boldsymbol{\Lambda}(\varphi^{n+1/2})^\top\partial_s(\Delta\boldsymbol{r}), \tag{3.64}$$

where use has been made of (3.61) along with the notation

$$\Delta\varphi := \varphi^{n+1} - \varphi^n \quad \text{and} \quad \Delta\boldsymbol{r} := \boldsymbol{r}^{n+1} - \boldsymbol{r}^n. \tag{3.65}$$

Thus (3.64) serves as update formula for the determination of $\boldsymbol{\Gamma}^{n+1}$. Note that this is in sharp contrast to evaluating the strain-displacement relation (3.5) at t^{n+1}.

3.4.4.2. Link to the classical EM scheme by Stander & Stein

To link the present pH EM scheme to the classical EM scheme by Stander & Stein [213], we first provide a modification of (3.64) which enforces the fulfillment of the strain-displacement relation (3.5) at t^{n+1}. This is, as stated above, a typical feature of common EM methods. Accordingly, we consider the modified mid-point rule

$$\boldsymbol{\Gamma}^{n+1} - \boldsymbol{\Gamma}^n = hZ_2(\Delta\varphi)\omega^{n+1/2}\boldsymbol{\Lambda}(\varphi^{n+1/2})^\top\boldsymbol{S}\,\partial_s\boldsymbol{r}^{n+1/2} + hZ_1(\Delta\varphi)\boldsymbol{\Lambda}(\varphi^{n+1/2})^\top\partial_s\boldsymbol{v}^{n+1/2}, \tag{3.66}$$

where

$$Z_1(\Delta\varphi) := \cos\frac{\Delta\varphi}{2} \quad \text{and} \quad Z_2(\Delta\varphi) := \frac{\sin\frac{\Delta\varphi}{2}}{\frac{\Delta\varphi}{2}} \tag{3.67}$$

have been introduced. Since both $Z_1 \to 1$ and $Z_2 \to 1$ for $\Delta\varphi \to 0$, the consistency of the mid-point rule is not affected. Moreover, since Z_1 and Z_2 merely cause a second-order perturbation of the mid-point

[3] The energy-consistent time discretization proposed in [116] for the present planar beam model is an exceptional case which relies on a modification of (3.61b) leading to $2\tan\frac{\varphi^{n+1}-\varphi^n}{2} = h\omega^{n+1/2}$.

rule, the accuracy of the integration rule is not affected. This modification eventually yields an endpoint satisfaction of the kinematic relation such that $\boldsymbol{\Gamma}^{n+1} = \boldsymbol{\Lambda}(\varphi^{n+1})^\top \partial_s \boldsymbol{r}^{n+1} - \boldsymbol{e}_1$. For the detailed derivations, see Appendix 3.E.

We continue with the weak form that lies at the heart of [213]. Specifically, the weak form can be cast in the frame of the principle of virtual work leading to

$$G^{\text{dyn}} + G^{\text{int}} = G^{\text{ext}}, \tag{3.68}$$

where

$$G^{\text{dyn}} = \int_\Omega \left(\delta \boldsymbol{r}^\top \rho A \partial_t \boldsymbol{v} + \delta\varphi \rho I \partial_t \omega\right) \,\mathrm{d}s, \tag{3.69a}$$

$$G^{\text{int}} = \int_\Omega \left(\delta \boldsymbol{\Gamma}^\top \boldsymbol{N} + \delta\kappa M\right) \,\mathrm{d}s, \tag{3.69b}$$

$$G^{\text{ext}} = \int_\Omega \left(\delta \boldsymbol{r}^\top \overline{\boldsymbol{n}} + \delta\varphi \overline{m}\right) \,\mathrm{d}s + \left[\delta \boldsymbol{r}^\top \boldsymbol{n}_{\text{N}} + \delta\varphi \, m_{\text{N}}\right]_{\partial\Omega_{\text{N}}}. \tag{3.69c}$$

Accordingly, G^{dyn} contains the contribution of the inertia terms to the virtual work, G^{int} represents the virtual work due to deformations and G^{ext} accounts for the virtual work of external loads. The mid-point type temporal discretization in [213] can now be written as

$$G^{\text{dyn}}_{\text{mp}} + h G^{\text{int}}_{\text{mp}} = h G^{\text{ext}}_{\text{mp}}, \tag{3.70}$$

where

$$G^{\text{dyn}}_{\text{mp}} = \int_\Omega \left(\delta \boldsymbol{r}^\top \rho A \left(\boldsymbol{v}^{n+1} - \boldsymbol{v}^n\right) + \delta\varphi \rho I \left(\omega^{n+1} - \omega^n\right)\right) \,\mathrm{d}s, \tag{3.71a}$$

$$G^{\text{int}}_{\text{mp}} = \int_\Omega \left(\delta \boldsymbol{\Gamma}_{\text{alg}}^\top \boldsymbol{N}^{n+1/2} + \partial_s(\delta\varphi) M^{n+1/2}\right) \,\mathrm{d}s, \tag{3.71b}$$

$$G^{\text{ext}}_{\text{mp}} = \int_\Omega \left(\delta \boldsymbol{r}^\top \overline{\boldsymbol{n}}^{n+1/2} + \delta\varphi \, \overline{m}^{n+1/2}\right) \,\mathrm{d}s + \left[\delta \boldsymbol{r}^\top (\boldsymbol{n}_{\text{N}})^{n+1/2} + \delta\varphi \, (m_{\text{N}})^{n+1/2}\right]_{\partial\Omega_{\text{N}}}. \tag{3.71c}$$

The two changes compared to the standard mid-point rule concern (i) the introduction of average stress-resultants in (3.71b), and (ii) the definition of $\delta\boldsymbol{\Gamma}_{\text{alg}}$ in (3.71b). Since in [213] St. Venant–Kirchhoff type material is considered (cf. Remark 3.1 in the present work), the average stress-resultants take the form

$$\boldsymbol{N}^{n+1/2} = \boldsymbol{D}_{\text{ts}} \boldsymbol{\Gamma}^{n+1/2} \quad \text{and} \quad M^{n+1/2} = EI\kappa^{n+1/2}, \tag{3.72}$$

where

$$\boldsymbol{\Gamma}^{n+1/2} = \frac{1}{2}\left(\boldsymbol{\Lambda}(\varphi^{n+1})^\top \partial_s \boldsymbol{r}^{n+1} + \boldsymbol{\Lambda}(\varphi^n)^\top \partial_s \boldsymbol{r}^n\right) - \boldsymbol{e}_1 \quad \text{and} \quad \kappa^{n+1/2} = \partial_s \varphi^{n+1/2}. \tag{3.73}$$

The definition of $\delta\boldsymbol{\Gamma}_{\text{alg}}$ can be motivated by the specific form of (3.66) along with (3.61), such that

$$\delta\boldsymbol{\Gamma}_{\text{alg}} := \delta\varphi Z_2(\Delta\varphi) \boldsymbol{\Lambda}(\varphi^{n+1/2})^\top \boldsymbol{S} \, \partial_s \boldsymbol{r}^{n+1/2} + Z_1(\Delta\varphi) \boldsymbol{\Lambda}(\varphi^{n+1/2})^\top \partial_s \delta\boldsymbol{r}. \tag{3.74}$$

Inserting (3.74) into (3.71b), we obtain

$$\begin{aligned} G^{\text{int}}_{\text{mp}} = \int_\Omega \Big(&\delta\varphi Z_2(\Delta\varphi) (\partial_s \boldsymbol{r}^{n+1/2})^\top \boldsymbol{S}^\top \boldsymbol{\Lambda}(\varphi^{n+1/2}) \boldsymbol{N}^{n+1/2} \\ &+ \partial_s(\delta\boldsymbol{r})^\top Z_1(\Delta\varphi) \boldsymbol{\Lambda}(\varphi^{n+1/2}) \boldsymbol{N}^{n+1/2} + \partial_s(\delta\varphi) M^{n+1/2}\Big) \,\mathrm{d}s. \end{aligned} \tag{3.75}$$

It is now a straightforward exercise to show that (3.75) leads to the element internal force vector in equation (17) of [213] associated with a 2-node element based on linear Lagrangian shape functions.

To summarize, the displacement-based EM scheme devised in [213] is based on the fields $(\boldsymbol{r}, \varphi)$ and $(\boldsymbol{v}, \omega)$ and a mid-point type temporal discretization leading to (3.61) along with (3.70). The only modifications made in [213] to the standard mid-point rule are contained in (3.75), resulting in a specific EM scheme. Concerning the spatial discretization in [213], the well-established 2-node element is applied which relies on reduced one-point quadrature to prevent transverse shear locking. Inspired by the investigations in this section, we next reduce our newly devised pH-EM scheme to displacement-based form in order to underline the main differences between our approach and that by Stander & Stein [213].

3.4.4.3. Irreducible pH-EM scheme

The present pH approach to the planar beam formulation leads in a natural way to a mixed formulation that facilitates the straightforward construction of a new EM scheme. In this section, we show that the mixed formulation can be reduced to a displacement-based formulation closely related to the one considered in Section 3.4.4.2. In analogy to (3.61), we consider the standard midpoint rule for $\partial_t \boldsymbol{r} = \boldsymbol{v}$ and $\partial_t \varphi = \omega$. Note that this essentially coincides with the weak counterparts (3.56a) and (3.56b). Furthermore, (3.56c) and (3.56d) can be recast in a form similar to (3.70) leading to

$$G_{\mathrm{mp}}^{\mathrm{dyn}} + h\tilde{G}_{\mathrm{mp}}^{\mathrm{int}} = hG_{\mathrm{mp}}^{\mathrm{ext}}, \tag{3.76}$$

where

$$\tilde{G}_{\mathrm{mp}}^{\mathrm{int}} = \int_{\Omega} \left(\delta\varphi \partial_s (\boldsymbol{r}^{n+1/2})^{\top} \boldsymbol{S}^{\top} \boldsymbol{\Lambda}(\varphi^{n+1/2}) \boldsymbol{N}^{n+1/2} + \partial_s(\delta \boldsymbol{r})^{\top} \boldsymbol{\Lambda}(\varphi^{n+1/2}) \boldsymbol{N}^{n+1/2} + \partial_s(\delta\varphi) M^{n+1/2} \right) \mathrm{d}s. \tag{3.77}$$

Again, the formulas in (3.72) are used to calculate the algorithmic stress-resultants. However, instead of (3.73), the weak form (3.56) gives rise to

$$\boldsymbol{\Gamma}^{n+1/2} = \frac{1}{2}\left(\boldsymbol{\Gamma}^{n} + \boldsymbol{\Gamma}^{n+1}\right) = \boldsymbol{\Gamma}^{n} + \frac{1}{2}\left(\Delta\varphi \boldsymbol{\Lambda}(\varphi^{n+1/2})^{\top} \boldsymbol{S}\, \partial_s \boldsymbol{r}^{n+1/2} + \boldsymbol{\Lambda}(\varphi^{n+1/2})^{\top} \partial_s(\Delta \boldsymbol{r}) \right), \tag{3.78a}$$

$$\kappa^{n+1/2} = \partial_s \varphi^{n+1/2}, \tag{3.78b}$$

see also (3.64). Comparison of (3.78) with (3.73) reveals that a crucial difference between the two EM schemes under consideration lies in the calculation of $\boldsymbol{\Gamma}^{n+1/2}$. Note that in the displacement-based formulation the calculation of $\boldsymbol{\Gamma}^{n+1/2}$ in (3.78a) requires to retrieve $\boldsymbol{\Gamma}^{n}$. Accordingly, $\boldsymbol{\Gamma}^{n}$ can be regarded as history variable for the calculation of the algorithmic stress-resultants. We further stress that the present EM scheme does not necessitate the introduction of the highly-nonlinear correction terms $Z_1(\Delta\varphi)$ and $Z_2(\Delta\varphi)$ featuring in (3.75).

3.5. Numerical examples

In the following, the newly proposed approach is applied to some numerical examples. Since this involves the solution of the implicit set of equations (3.52) and (3.53), Newton's method is used in every time step. The spatial integrals are approximated by means of a full two-point Gaussian quadrature rule. The Dirichlet boundary conditions for the displacements and velocities are incorporated directly

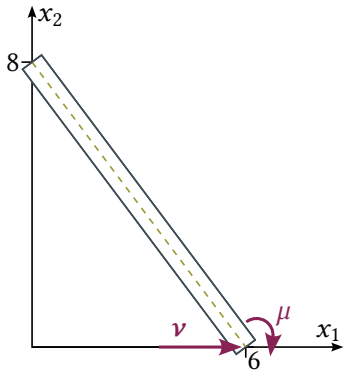

h	t_{end}	n_{e}	L	ρA	ρI	$EA = GA$	EI
0.1	15	10	10	1	10	10000	100

Table 3.1.: Flying spaghetti: Initial configuration, input loads and parameters.

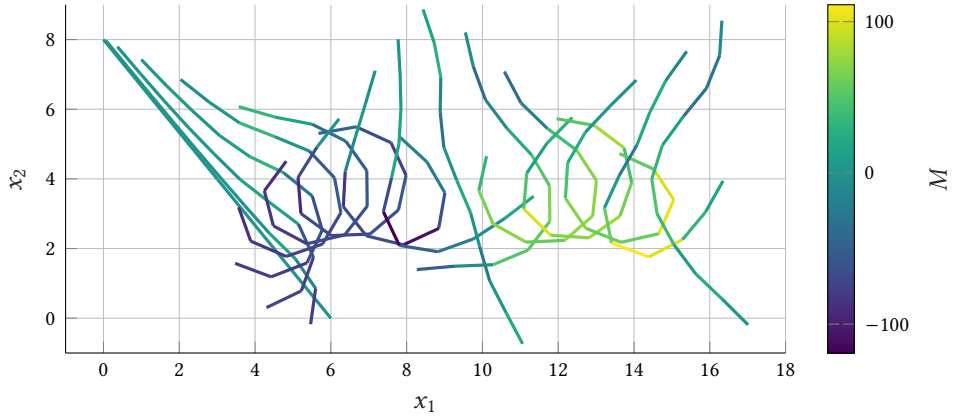

Figure 3.4.: Flying spaghetti: Configuration of the beam at different time instances for $t \leq 7.5$, after each 5 time increments.

into the ansatz functions, see Remark 3.5. The computations have been performed using the finite element code `moofeKIT`, see [79], which can also be used for verification.

The first example is used to verify the discrete conservation properties. The second application demonstrates the ability to perform quasi-static simulations as well and shows that the pH approach prevents numerical locking effects. The last example illustrates the usage of the proposed approach for interconnected flexible multibody systems.

3.5.1. Flying spaghetti

The first example is concerned with the free motion of a tumbling beam. The so-called *flying spaghetti* problem was originally proposed by [205] and analyzed in multiple works, e.g., [81, 113]. The main

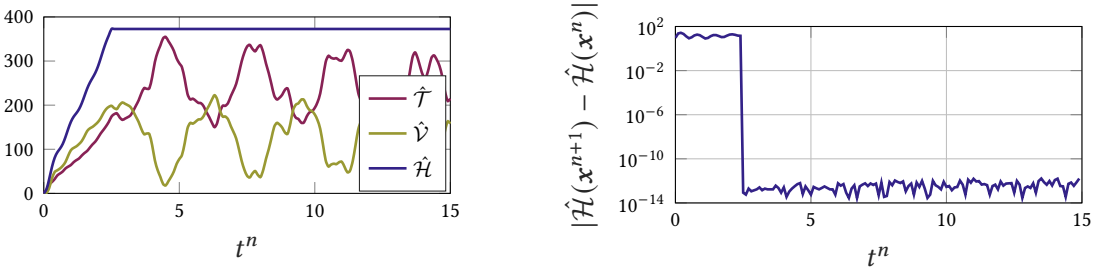

Figure 3.5.: Flying spaghetti: Energetic evolution (left) and discrete-time increments of total energy (right).

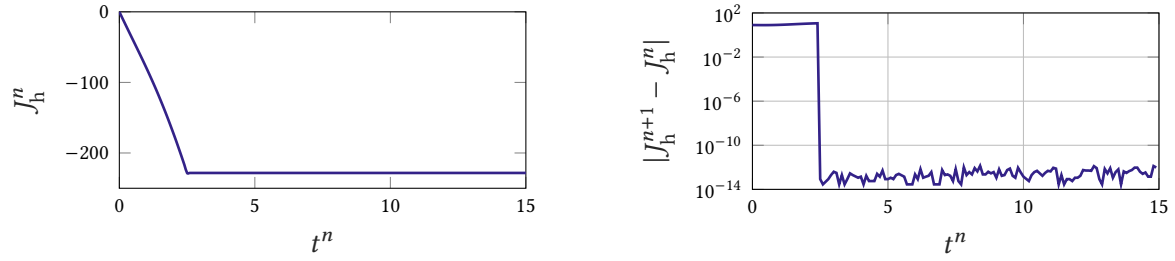

Figure 3.6.: Flying spaghetti: Angular momentum evolution (left) and discrete-time increments (right).

objective here is to validate the time-discrete conservation principles of the proposed method. Initially positioned in an inclined configuration (see depiction in Table 3.1), the beam is released and allowed to move freely in space. The beam is subject to pure Neumann boundary conditions: A free end at $s = 0$ and a nodal force and torque at $s = L$, which is applied for a short period of time, i.e., $\boldsymbol{n}(s = L, t) = \boldsymbol{\nu}$ and $m(s = L, t) = \mu$ with

$$\boldsymbol{\nu} = \begin{cases} 8\boldsymbol{e}_1 & \text{for } t \leq 2.5, \\ 0 & \text{for } t > 2.5, \end{cases} \qquad \mu = \begin{cases} -80 & \text{for } t \leq 2.5, \\ 0 & \text{for } t > 2.5. \end{cases} \tag{3.79}$$

At $t = 2.5$, the system is closed as both boundary inputs become zero and the beam continues with a free flight. Although the original parameters from [205] violate some physical plausibility relations (e.g., $EA/EI \neq \rho A/\rho I$), we use them here for the sake of comparability to many other works in the literature, see Table 3.1.

Firstly, we can verify that the motion is in good agreement with [205, Figure 4], see snapshots in Figure 3.4. Secondly, we can observe the conservation of energy and angular momentum in Figures 3.5 and 3.6, respectively. The accuracy is of the order of machine precision. This verifies our previous findings that as soon as the system is closed both quantities are preserved. Note that also during the loading phase, consistent discrete-time balance equations have been obtained, see (3.55) and (3.60).

3.5.2. Quasi-static roll up

In this example, the ability of the proposed formulation to circumvent shear locking is demonstrated using a widespread benchmark problem, see, e.g., [52, 99, 188, 235]. Moreover, it is shown that the proposed formulation is amenable to quasi-static simulations.

An initially straight cantilever beam, which is clamped at $s = 0$ such that we enforce the Dirichlet boundary conditions

$$\boldsymbol{r}(s = 0, t) = \boldsymbol{0}, \quad \boldsymbol{v}(s = 0, t) = \boldsymbol{0}, \quad \varphi(s = 0, t) = 0, \quad \omega(s = 0, t) = 0, \tag{3.80}$$

is rolled up by applying a quasi-static torque at the free end at $s = L$, see depiction in Table 3.2. A reference solution shows that for a torque of $m_{\text{rollup}} = 2\pi EI/L$, the beam is rolled up to a complete circular arc with constant curvature. For the simulation parameters we have chosen the same values as in [99], see Table 3.2.

h	t_{end}	n_e	L	$\rho A = \rho I$	$EA = GA$	EI
0.01	1	8	10	0	10000	500

Table 3.2.: Quasi-static roll up: Initial configuration, input torque and parameters.

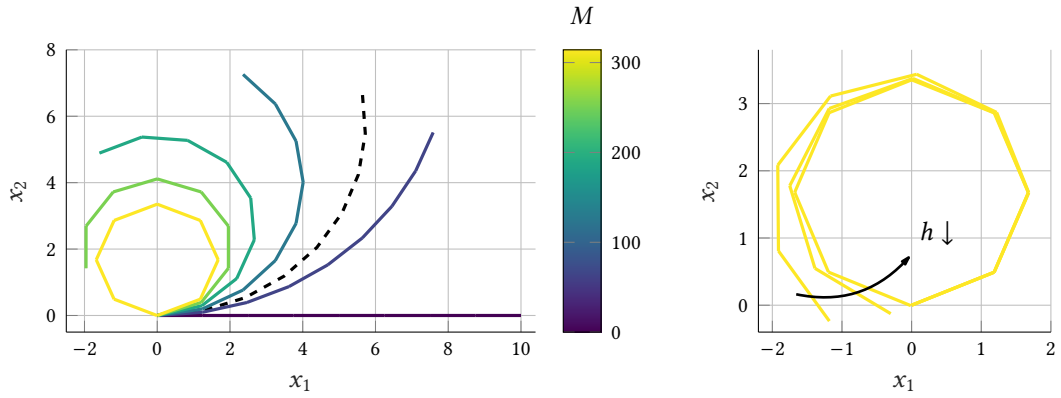

Figure 3.7.: Quasi-static roll up: Configuration of the beam at different load levels $t \in \{0, 0.2, 0.2, 0.6, 0.8, 1\}$ obtained with our formulation and comparison with fully integrated classical formulation [213] (see dashed line) (left) and with different coarser discretization levels, $h \in \{0.02, 0.1, 0.2\}$ (right).

Simulations for this benchmark problem yield incorrect outcomes when the numerical approximation procedure suffers from locking effects [99], since the stiffness is greatly overestimated, resulting in the beam failing to form a complete ring. As this behavior is absent even with the coarse spatial discretization that we have chosen here, it can be concluded that shear locking does not occur in our pH beam model, see Figure 3.7 (left). Contrarily, the final configuration obtained with the classical beam formulation by [213] — see also Section 3.4.4 — and a full two point Gaussian quadrature exhibits locking, see dashed line. This formulation requires a reduced integration with only one integration point to avoid the problem.

Since our pH formulation is intrinsically dynamical, we refrain from introducing a static formulation and instead achieve a quasi-static simulation approach by neglecting inertial terms, such that $\rho = 0$. In this context, velocity-type quantities can then be regarded as *coordinate increments*. Moreover, time $t \in [0, 1]$ now corresponds to a loading factor which is increased in each step such that

$$\mu(t) = t\, m_{\text{rollup}}. \tag{3.81}$$

For $t = 1$, the final state is obtained, yielding a complete roll up of the cantilever beam. Due to the incrementing nature of our solution procedure, where approximation errors are induced in each *pseudo-time* step, a path-dependence becomes present. The approximate solution converges to the analytical solution when choosing sufficiently many pseudo-time steps, highlighting that the present approach is free from the numerical shear locking effect. See, e.g., Figure 3.7 for different configurations throughout the simulation. It can be verified that the beam has a homogeneous internal moment at each step. At the end of the simulation the end moment of $m_{\text{rollup}} = 100\pi$ is exactly reached.

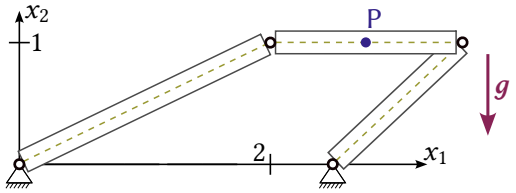

h	t_{end}	n_{e}	L	ρ
0.02	10	$\{10, 6, 6\}$	$\{\sqrt{5}, 1.5, \sqrt{2}\}$	2710
A	I	E	ν	$\boldsymbol{g}$
0.05^2	$0.05^4/12$	$2.1 \cdot 10^{11}$	0.3	$-9.81\rho A\boldsymbol{e}_2$

Table 3.3.: Closed-loop flexible multibody system: Initial configuration and parameters.

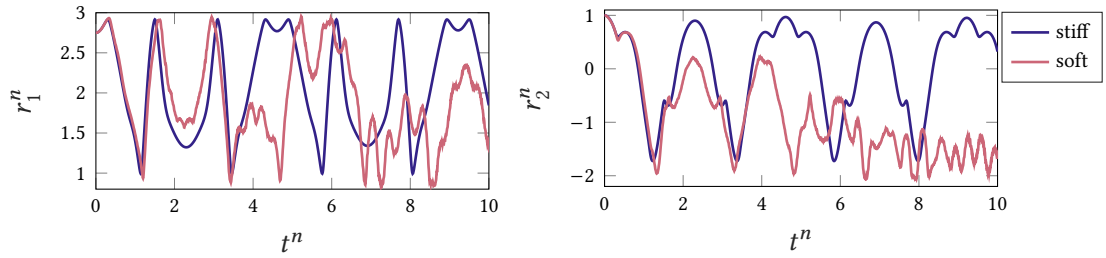

Figure 3.8.: Closed-loop flexible multibody system: Position of P over time.

3.5.3. Closed-loop flexible multibody system

Lastly, the well-known four-bar mechanism as a benchmark problem for flexible multibody systems, see, e.g., [26, 73, 241], is analyzed. The compliant mechanism consists of three flexible beam elements with quadratic cross section and material parameters of steel, see Table 3.3 for details corresponding to [241]. The beams are interconnected by revolute joints, start from being at rest in an initial configuration as depicted in Table 3.3. The system is subject to gravity acting in negative x_2-direction, which is easily incorporated into the proposed pH formulation by setting the distributed input forces to the appropriate constant value, i.e., $\bar{\boldsymbol{n}} = \boldsymbol{g}$. Beam 1 and 3 are connected to the ground via revolute support joints.

We start our analysis by examining the evolution of the position of the center point P of the middle beam, initially located at $\boldsymbol{r}_\mathrm{P}(t=0) = (2.75, 1.5)$, over time. Here, we distinguish between two different scenarios: The first scenario deals with the chosen material parameters as for steel (see Table 3.3, labeled as "stiff"). For the second scenario we have reduced the elastic modulus of the middle beam to $E = 2.1 \cdot 10^8$ (labeled as "soft"), which also required a smaller time step size of $h_\mathrm{soft} = 0.005$. The results depicted in Figure 3.8 show that the flexible mechanism undergoes a periodic swing motion with a period of approximately 4.7 when choosing the stiff material for all beams. Snapshots for the motion are shown in Figure 3.9.

Additionally, convergence studies were performed to investigate the approximation accuracy for the position of point P at $t = 1$ with respect to both temporal and spatial discretization in the stiff scenario. The results in Figure 3.10 show that the relative error

$$e = \frac{||\boldsymbol{r}_\mathrm{P}(t=1) - \boldsymbol{r}_\mathrm{ref,P}(t=1)||}{||\boldsymbol{r}_\mathrm{ref,P}(t=1)||} \tag{3.82}$$

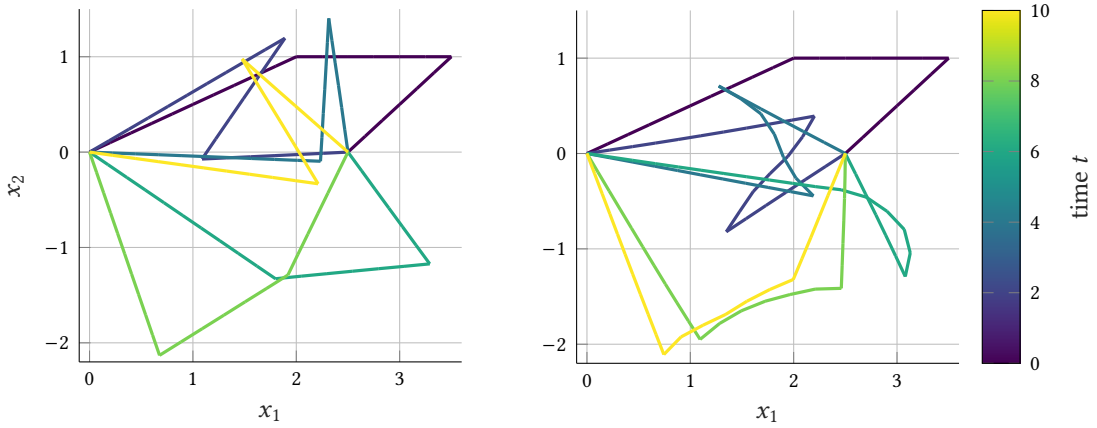

Figure 3.9.: Closed-loop flexible multibody system: Snapshots for $t \in \{0, 2, 4, 6, 8, 10\}$ (left: stiff scenario, right: soft scenario).

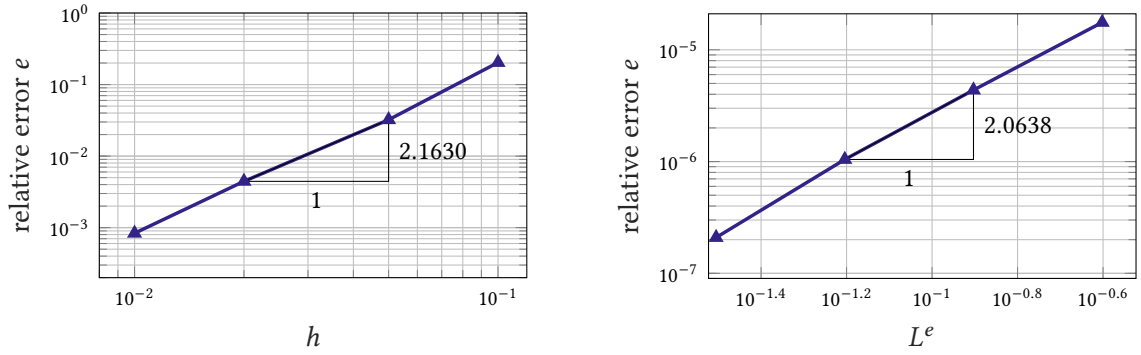

Figure 3.10.: Closed-loop flexible multibody system: Convergence results for accuracy of position of P.

obtained with our approach decreases with order two with increasing temporal resolution, which is in line with the expected behavior for the midpoint-type discretization. For the reference overkill solution, we have chosen $h = 0.005$. The classical method [213] yields very similar results.

Next, the spatial discretization error is investigated by varying the number of elements n_e with reference length L^e, for all beams, see Figure 3.10 (right). The results show that the error decreases with order two with increasing spatial resolution. For the reference overkill solution, we have chosen $n_e = 96$ for beam 2 and $n_e = 160$ for beams 1 and 3.

Lastly, we observed an increased robustness of our mixed EM approach in the pH framework (labeled "pH-EM") compared to the classical scheme [213] (labeled "cl-EM"), resulting in a notably reduced amount of Newton iterations per time step, see Figure 3.11. The mean number of necessary Newton iterations for the classical scheme is 6.464 compared to a number of 4.594 for our mixed approach pH-EM and 6.348 for its irreducible implementation (labeled "pH-EMi", see Section 3.4.4.3). This comparison has been performed with a less strict convergence criterion for the norm of the residual, i.e., $\varepsilon_{\text{Newton}} = 10^{-5}$. For smaller tolerances, cl-EM and pH-EMi do not converge anymore whereas pH-EM converged down to $\varepsilon_{\text{Newton}} = 10^{-11}$. For these investigations we have computed the tangent matrix for Newton's method using a central differences numerical approach.

3.6. Conclusion and outlook

In this work, we introduced a novel port-Hamiltonian (pH) formulation for planar geometrically exact beams, providing a structure-preserving approach to modeling their highly nonlinear dynamics. By

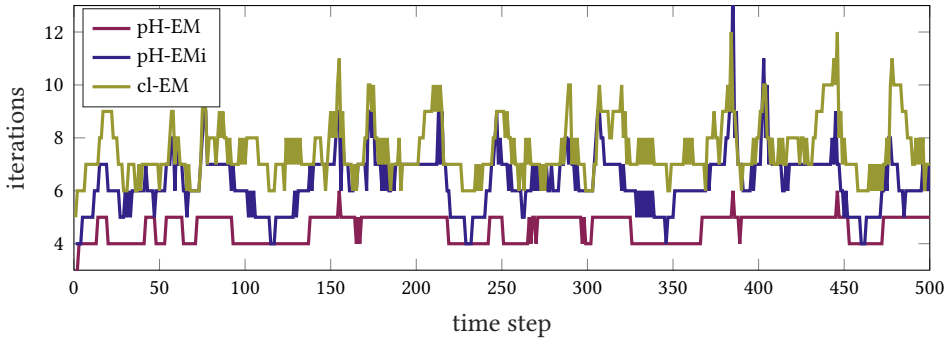

Figure 3.11.: Closed-loop flexible multibody system: Robustness comparison of necessary Newton iterations.

leveraging mixed finite elements and second-order time-stepping methods, we ensured an exact discrete representation of energy and angular momentum balance, addressing a key challenge in the accurate and long-term simulation of flexible multibody systems. The continuous and discretized models are intrinsically passive, highlighting the potential of the pH framework for complex flexible multibody system simulations and advanced control design. We have also shown that the newly devised pH-EM scheme distinguishes itself from previously developed EM schemes. The distinguishing feature of the present pH-EM scheme has been highlighted by reducing the mixed pH-based formulation to an irreducible displacement-based version which shows that the implementation of the new EM scheme relies on the use of history variables. Furthermore, our numerical results have demonstrated that the proposed formulation naturally prevents shear locking, making it a robust and efficient choice for modeling large deformations and rotations in slender structures. Simulations validated the beneficial performance of the pH-based approach, with the energy-consistent discretization ensuring an exact energy balance in discrete time. The formulation accurately captures the nonlinear dynamics of planar geometrically exact beams while maintaining energy consistency and passivity, making it a promising tool for simulating and controlling flexible multibody systems.

Future research directions might explore the beneficial pH properties with respect to the energy-consistent interconnection in a multibody context. Moreover an extension of the pH modeling approach and the related design of an EM scheme to three-dimensional beam problems and other geometrically nonlinear mechanical systems can follow a similar procedure as in the present work. Lastly, also coupling with other fields, e.g., with electrical fields [114] or advanced dissipative terms [75, A1], may be included[4].

Appendix to Chapter 3

3.A. Relation to a Hu–Washizu type variational formulation

The pH formulation dealt with in Section 3.3.1 can be linked to a mixed Hu–Washizu type extension of Hamilton's principle. To this end, we introduce the 8-field variational functional

$$\begin{aligned} S_{\mathrm{HW}}(\boldsymbol{r},\varphi,\boldsymbol{v},\omega,\boldsymbol{\Gamma},\kappa,\boldsymbol{N},M) = &\int_0^T \int_\Omega \left(\frac{1}{2}\rho A \boldsymbol{v}^\top \boldsymbol{v} + \frac{1}{2}\rho I \omega^2 + (\partial_t \boldsymbol{r} - \boldsymbol{v})^\top \rho A \boldsymbol{v} + (\partial_t \varphi - \omega)\rho I \omega \right) \mathrm{d}s\,\mathrm{d}t \\ &- \int_0^T \int_\Omega \left(W(\boldsymbol{\Gamma},\kappa) + \boldsymbol{N}^\top \boldsymbol{g}_1(\boldsymbol{\Gamma},\varphi,\partial_s \boldsymbol{r}) + M g_2(\kappa,\partial_s \varphi) \right) \mathrm{d}s\,\mathrm{d}t \\ &- \int_0^T V_{\mathrm{ext}}(\boldsymbol{r},\varphi)\,\mathrm{d}t. \end{aligned} \tag{3.83}$$

[4] The three-dimensional case and the incorporation of dissipative terms can be found in the remainder of this work, cf. Chapter 4.

Therein, $\boldsymbol{N}$ and M act as Lagrange multipliers enforcing the kinematic constraints defining the strains in (3.5) and (3.6) such that

$$\boldsymbol{g}_1(\boldsymbol{\Gamma}, \varphi, \partial_s \boldsymbol{r}) = \boldsymbol{\Lambda}(\varphi)^\top \partial_s \boldsymbol{r} - \boldsymbol{e}_1 - \boldsymbol{\Gamma} = \boldsymbol{0}, \qquad g_2(\kappa, \partial_s \varphi) = \partial_s \varphi - \kappa = 0, \tag{3.84}$$

and V_{ext} is the potential of external dead loads

$$V_{\text{ext}}(\boldsymbol{r}, \varphi) = -\int_\Omega \left(\overline{\boldsymbol{n}}^\top \boldsymbol{r} + \overline{m}\varphi\right) \,\mathrm{d}s - \left[\boldsymbol{n}_{\text{N}}^\top \boldsymbol{r} + m_{\text{N}}\varphi\right]_{\partial\Omega_N}. \tag{3.85}$$

It can be shown by a straightforward calculation that the stationary condition $\delta S_{\text{HW}} = 0$ of functional (3.83) yields

$$-(\delta\boldsymbol{r}, \rho A \partial_t \boldsymbol{v})_\Omega - (\partial_s(\delta\boldsymbol{r}), \boldsymbol{\Lambda}\boldsymbol{N})_\Omega + \left[\delta\boldsymbol{r}^\top \boldsymbol{n}_{\text{N}}\right]_{\partial\Omega_{\text{N}}} + (\delta\boldsymbol{r}, \overline{\boldsymbol{n}})_\Omega = 0, \tag{3.86a}$$

$$-(\delta\varphi, \rho I \partial_t \omega)_\Omega - (\partial_s(\delta\varphi), M)_\Omega + \left(\delta\varphi, \partial_s \boldsymbol{r}^\top \boldsymbol{S}\boldsymbol{\Lambda}\boldsymbol{N}\right)_\Omega + \left[\delta\varphi\, m_{\text{N}}\right]_{\partial\Omega_{\text{N}}} + (\delta\varphi, \overline{m})_\Omega = 0, \tag{3.86b}$$

$$(\rho A \delta\boldsymbol{v}, \partial_t \boldsymbol{r} - \boldsymbol{v})_\Omega = 0, \tag{3.86c}$$

$$(\rho I \delta\omega, \partial_t \varphi - \omega)_\Omega = 0, \tag{3.86d}$$

$$(\delta\boldsymbol{\Gamma}, \boldsymbol{N} - \partial_{\boldsymbol{\Gamma}} W)_\Omega = 0, \tag{3.86e}$$

$$(\delta\kappa, M - \partial_\kappa W)_\Omega = 0, \tag{3.86f}$$

$$\left(\delta\boldsymbol{N}, \boldsymbol{\Gamma} - \boldsymbol{\Lambda}(\varphi)^\top \partial_s \boldsymbol{r} + \boldsymbol{e}_1\right)_\Omega = 0, \tag{3.86g}$$

$$(\delta M, \kappa - \partial_s \varphi)_\Omega = 0, \tag{3.86h}$$

for all $t \in \mathbb{T}$.

Apart from (3.86e) and (3.86f), which need to be replaced with weak forms of (3.17), these identities formally coincide with the weak form (3.34) of the pH formulation.

3.B. Implementation details for the basis functions and ansatz matrices

In Section 3.4.1 the displacements and velocities $(\boldsymbol{r}, \varphi, \boldsymbol{v}, \omega)$ are approximated in the following fashion:

$$\omega_{\text{h}}(s,t) = \sum_{i=1}^{n_{\text{n}}} N_i(s)\omega_i(t) = \begin{bmatrix} N_1(s) & N_2(s) & \cdots & N_{n_{\text{n}}}(s) \end{bmatrix} \begin{bmatrix} \omega_1(t) \\ \omega_2(t) \\ \vdots \\ \omega_{n_{\text{n}}}(t) \end{bmatrix} = \boldsymbol{\Phi}_1(s)\hat{\boldsymbol{\omega}}(t), \tag{3.87}$$

$$\begin{aligned} \boldsymbol{v}_{\text{h}}(s,t) &= \sum_{i=1}^{n_{\text{n}}} N_i(s)\boldsymbol{v}_i(t) \\ &= \begin{bmatrix} N_1(s) & 0 & N_2(s) & 0 & \cdots & N_{n_{\text{n}}}(s) & 0 \\ 0 & N_1(s) & 0 & N_2(s) & \cdots & 0 & N_{n_{\text{n}}}(s) \end{bmatrix} \begin{bmatrix} \boldsymbol{v}_1(t) \\ \boldsymbol{v}_2(t) \\ \vdots \\ \boldsymbol{v}_{n_{\text{n}}}(t) \end{bmatrix} = \boldsymbol{\Phi}_2(s)\hat{\boldsymbol{v}}(t), \end{aligned} \tag{3.88}$$

cf. (3.41). The nodal basis functions $N_i(s)$ are defined as piecewise linear functions on the interval $[0, L]$, see Figure 3.3. For the element-based degrees of freedom $(\boldsymbol{\Gamma}, \kappa)$ the ansatz is analogous but with piecewise constant basis functions $\tilde{N}_i(s)$, see Figure 3.3. Since the computations are performed on

element level in a reference element, these ansatz matrices have reference-element-related counterparts given by

$$\boldsymbol{\Phi}_1^{(e)}(\xi) = \begin{bmatrix} \hat{N}_1(\xi) & \hat{N}_2(\xi) \end{bmatrix}, \quad \boldsymbol{\Phi}_2^{(e)}(\xi) = \begin{bmatrix} \hat{N}_1(\xi) & 0 & \hat{N}_2(\xi) & 0 \\ 0 & \hat{N}_1(\xi) & 0 & \hat{N}_2(\xi) \end{bmatrix} \tag{3.89}$$

as well as

$$\boldsymbol{\Psi}_1^{(e)}(\xi) = 1 \quad \text{and} \quad \boldsymbol{\Psi}_2^{(e)}(\xi) = \begin{bmatrix} 1 & 0 \\ 0 & 1 \end{bmatrix}. \tag{3.90}$$

3.C. System matrices for the finite-dimensional port-Hamiltonian system

The approximation matrices arising in the spatial discretization procedure in Section 3.4.1 are given by

$$\boldsymbol{M}_\alpha = \int_\Omega \boldsymbol{\Phi}_\alpha^\top \boldsymbol{\Phi}_\alpha \, \mathrm{d}s, \quad \boldsymbol{C}_\alpha = \int_\Omega \boldsymbol{\Psi}_\alpha^\top \boldsymbol{\Psi}_\alpha \, \mathrm{d}s, \quad \boldsymbol{D}_2 = \int_\Omega \boldsymbol{\Psi}_2^\top \boldsymbol{D}_{\mathrm{ts}} \boldsymbol{\Psi}_2 \, \mathrm{d}s, \quad \boldsymbol{D}_1 = \int_\Omega \boldsymbol{\Psi}_1^\top EI \boldsymbol{\Psi}_1 \, \mathrm{d}s \tag{3.91}$$

for $\alpha \in \{1, 2\}$, as well as

$$\boldsymbol{G}_1 = \int_\Omega \partial_s \boldsymbol{\Phi}_1^\top \boldsymbol{\Psi}_1 \, \mathrm{d}s, \quad \boldsymbol{G}_2(\hat{\boldsymbol{\varphi}}) = \int_\Omega \partial_s \boldsymbol{\Phi}_2^\top \boldsymbol{\Lambda}(\varphi_{\mathrm{h}}) \boldsymbol{\Psi}_2 \, \mathrm{d}s, \quad \boldsymbol{V}(\hat{\boldsymbol{r}}, \hat{\boldsymbol{\varphi}}) = \int_\Omega \boldsymbol{\Phi}_1^\top (\partial_s \boldsymbol{r}_{\mathrm{h}})^\top \boldsymbol{S} \boldsymbol{\Lambda}(\varphi_{\mathrm{h}}) \boldsymbol{\Psi}_2 \, \mathrm{d}s. \tag{3.92}$$

3.D. Implementation details for the boundary terms

In the finite-dimensional pH system (3.49), which arises after spatial discretization, the boundary terms require additional attention. The boundary terms are given by

$$\boldsymbol{B}\hat{\boldsymbol{u}}(t) = \begin{bmatrix} \boldsymbol{B}_\partial & \boldsymbol{B}_\Omega \end{bmatrix} \begin{bmatrix} \boldsymbol{u}_\partial(t) \\ \hat{\boldsymbol{u}}_\Omega(t) \end{bmatrix}, \tag{3.93}$$

where for $\boldsymbol{u}_\partial$ we consider a boundary input vector for pure Neumann boundaries similar to the one in (3.31). The corresponding matrix is given by

$$\boldsymbol{B}_\partial = \begin{bmatrix} \boldsymbol{0} & \boldsymbol{0} \\ \boldsymbol{0} & \boldsymbol{0} \\ \boldsymbol{B}_{\partial,\boldsymbol{n}} & \boldsymbol{0} \\ \boldsymbol{0} & \boldsymbol{B}_{\partial,m} \\ \boldsymbol{0} & \boldsymbol{0} \\ \boldsymbol{0} & \boldsymbol{0} \end{bmatrix}, \quad \text{with} \quad \boldsymbol{B}_{\partial,\boldsymbol{n}} = \begin{bmatrix} \boldsymbol{I} & \boldsymbol{0} \\ \boldsymbol{0} & \boldsymbol{0} \\ \vdots & \vdots \\ \boldsymbol{0} & \boldsymbol{0} \\ \boldsymbol{0} & \boldsymbol{I} \end{bmatrix} \in \mathbb{R}^{2(n_{\mathrm{e}}+1)\times 4}, \quad \boldsymbol{B}_{\partial,m} = \begin{bmatrix} 1 & 0 \\ 0 & 0 \\ \vdots & \vdots \\ 0 & 0 \\ 0 & 1 \end{bmatrix} \in \mathbb{R}^{(n_{\mathrm{e}}+1)\times 2}. \tag{3.94}$$

Moreover in (3.93), the distributed input matrix and control input vector are given by

$$\boldsymbol{B}_\Omega = \begin{bmatrix} \boldsymbol{0} & \boldsymbol{0} \\ \boldsymbol{0} & \boldsymbol{0} \\ \boldsymbol{M}_2 & \boldsymbol{0} \\ \boldsymbol{0} & \boldsymbol{M}_1 \\ \boldsymbol{0} & \boldsymbol{0} \\ \boldsymbol{0} & \boldsymbol{0} \end{bmatrix}, \quad \hat{\boldsymbol{u}}_\Omega(t) = \begin{bmatrix} \hat{\boldsymbol{u}}_{\boldsymbol{n},\Omega}(t) \\ \hat{\boldsymbol{u}}_{m,\Omega}(t) \end{bmatrix} \tag{3.95}$$

containing the mass matrices $\boldsymbol{M}_1$ and $\boldsymbol{M}_2$ defined in (3.91). In the last equation, the discrete distributed input vector contains the nodal evaluations of the distributed control inputs (i.e. distributed forces and torques) such that

$$\hat{\boldsymbol{u}}_{\boldsymbol{n},\Omega}(t) = \begin{bmatrix} \overline{\boldsymbol{n}}(s=0,t) \\ \overline{\boldsymbol{n}}(s=\Delta s,t) \\ \vdots \\ \overline{\boldsymbol{n}}(s=n_\mathrm{e}\Delta s,t) \\ \overline{\boldsymbol{n}}(s=L,t) \end{bmatrix}, \quad \text{and} \quad \hat{\boldsymbol{u}}_{m,\Omega}(t) = \begin{bmatrix} \overline{m}(s=0,t) \\ \overline{m}(s=\Delta s,t) \\ \vdots \\ \overline{m}(s=n_\mathrm{e}\Delta s,t) \\ \overline{m}(s=L,t) \end{bmatrix}, \tag{3.96}$$

where Δs is the length of one finite element in the undeformed reference configuration such that $n_\mathrm{e}\Delta s = L$, the undeformed length of the beam. The collocated, and power-conjugated output corresponding to (3.93) can be deduced as

$$\hat{\boldsymbol{y}} = \begin{bmatrix} \boldsymbol{y}_\partial \\ \hat{\boldsymbol{y}}_\Omega \end{bmatrix} = \begin{bmatrix} \boldsymbol{B}_\partial^\top \\ \boldsymbol{B}_\Omega^\top \end{bmatrix} \hat{\boldsymbol{z}}(\hat{\boldsymbol{x}}) = \begin{bmatrix} \boldsymbol{B}_{\partial,\boldsymbol{n}}^\top \hat{\boldsymbol{v}} \\ \boldsymbol{B}_{\partial,m}^\top \hat{\boldsymbol{\omega}} \\ \boldsymbol{M}_2 \hat{\boldsymbol{v}} \\ \boldsymbol{M}_1 \hat{\boldsymbol{\omega}} \end{bmatrix} = \begin{bmatrix} \hat{\boldsymbol{v}}_1 \\ \hat{\boldsymbol{v}}_{n_\mathrm{n}} \\ \hat{\boldsymbol{\omega}}_1 \\ \hat{\boldsymbol{\omega}}_{n_\mathrm{n}} \\ \boldsymbol{M}_2 \hat{\boldsymbol{v}} \\ \boldsymbol{M}_1 \hat{\boldsymbol{\omega}} \end{bmatrix}, \tag{3.97}$$

where the first 4 entries correspond to Neumann boundary inputs and the last 2 entries represent the distributed output depending on the nodal velocities.

3.E. Proof of the result in Section 3.4.4.2

Here, it is demonstrated that the modified midpoint discretization (3.66) yields a fulfillment of the kinematic relation (3.5) in the time endpoint t^{n+1}. Making use of (3.61), (3.66) can be written as

$$\boldsymbol{\Gamma}^{n+1} - \boldsymbol{\Gamma}^n = \Delta\varphi Z_2(\Delta\varphi)\boldsymbol{\Lambda}(\varphi^{n+1/2})^\top \boldsymbol{S}\,\partial_s \boldsymbol{r}^{n+1/2} + Z_1(\Delta\varphi)\boldsymbol{\Lambda}(\varphi^{n+1/2})^\top \partial_s(\Delta\boldsymbol{r}), \tag{3.98}$$

To prove that (3.98) does indeed yield the desired result, we make use of the identities

$$\cos\frac{\Delta\varphi}{2}\boldsymbol{\Lambda}(\varphi^{n+1/2}) = \frac{1}{2}\left(\boldsymbol{\Lambda}^n + \boldsymbol{\Lambda}^{n+1}\right) =: \boldsymbol{\Lambda}^{n+1/2}, \tag{3.99a}$$

$$2\tan\frac{\Delta\varphi}{2}\boldsymbol{S}^\top\boldsymbol{\Lambda}^{n+1/2} = \boldsymbol{\Lambda}^{n+1} - \boldsymbol{\Lambda}^n, \tag{3.99b}$$

where we write shortly $\boldsymbol{\Lambda}^n := \boldsymbol{\Lambda}(\varphi^n)$ and $\boldsymbol{\Lambda}^{n+1} := \boldsymbol{\Lambda}(\varphi^{n+1})$. The validity of (3.99a) and (3.99b) can be shown by using basic relations for the sine and cosine functions. Starting with the *sum-to-product* identities

$$\cos x + \cos y = 2\cos\frac{x+y}{2}\cos\frac{x-y}{2}, \tag{3.100a}$$

$$\sin x - \sin y = 2\cos\frac{x+y}{2}\sin\frac{x-y}{2}, \tag{3.100b}$$

together with $\cos a = \cos(-a)$ and $\sin a = -\sin(-a)$, the validity of (3.99a) can be checked on a component basis. For example, the $(1,1)$ component of (3.99a) coincides with (3.100a) by setting $x = \varphi^n$ and $y = \varphi^{n+1}$. The remaining component equations can be checked similarly. The second identity (3.99b) can be recast in the form

$$\sin\frac{\Delta\varphi}{2}\boldsymbol{S}^\top\left(\boldsymbol{\Lambda}^n + \boldsymbol{\Lambda}^{n+1}\right) = \cos\frac{\Delta\varphi}{2}\left(\boldsymbol{\Lambda}^{n+1} - \boldsymbol{\Lambda}^n\right) \tag{3.101}$$

Again, the validity of the last equation can be checked on a component basis. For example, the $(1,2)$ component of (3.101) can be written as

$$-\sin\frac{y-x}{2}\,(\cos x+\cos y)=\cos\frac{y-x}{2}\,(-\sin y+\sin x)\,, \tag{3.102}$$

where, as before, $x=\varphi^n$ and $y=\varphi^{n+1}$ has been set. Substituting (3.100a) and (3.100b) into the last equation confirms that (3.102) is identically satisfied. The remaining component equations of (3.99b) can be checked analogously.

Now, (3.98) can be rewritten as

$$\begin{aligned}
\boldsymbol{\Gamma}^{n+1}-\boldsymbol{\Gamma}^n &= \Delta\varphi\frac{\sin\frac{\Delta\varphi}{2}}{\frac{\Delta\varphi}{2}}\boldsymbol{\Lambda}(\varphi^{n+1/2})^\top \boldsymbol{S}\,\partial_s\boldsymbol{r}^{n+1/2}+\cos\frac{\Delta\varphi}{2}\boldsymbol{\Lambda}(\varphi^{n+1/2})^\top\partial_s(\Delta\boldsymbol{r})\\
&= 2\frac{\sin\frac{\Delta\varphi}{2}}{\cos\frac{\Delta\varphi}{2}}(\boldsymbol{\Lambda}^{n+1/2})^\top\boldsymbol{S}\,\partial_s\boldsymbol{r}^{n+1/2}+(\boldsymbol{\Lambda}^{n+1/2})^\top\partial_s(\Delta\boldsymbol{r})\\
&= \left((\boldsymbol{\Lambda}^{n+1})^\top-(\boldsymbol{\Lambda}^n)^\top\right)\,\partial_s\boldsymbol{r}^{n+1/2}+(\boldsymbol{\Lambda}^{n+1/2})^\top\partial_s(\Delta\boldsymbol{r})\\
&= (\boldsymbol{\Lambda}^{n+1})^\top\partial_s\boldsymbol{r}^{n+1}-(\boldsymbol{\Lambda}^n)^\top\partial_s\boldsymbol{r}^n.
\end{aligned}$$

Here, in a first step (3.99a) has been used twice and in a second step (3.99b) has been applied. The last equation can be obtained by a direct calculation. Thus, provided that $\boldsymbol{\Gamma}^n=(\boldsymbol{\Lambda}^n)^\top\partial_s\boldsymbol{r}^n-\boldsymbol{e}_1$ is given, we obtain the desired result $\boldsymbol{\Gamma}^{n+1}=(\boldsymbol{\Lambda}^{n+1})^\top\partial_s\boldsymbol{r}^{n+1}-\boldsymbol{e}_1$.

4. Mixed formulation and structure-preserving discretization of Cosserat rod dynamics in a port-Hamiltonian framework

This chapter is based on:*
Kinon PL, Eugster SR, and Betsch P. "Mixed formulation and structure-preserving discretization of Cosserat rod dynamics in a port-Hamiltonian framework". In: *Computer Methods in Applied Mechanics and Engineering*, 458: 118966, 2026. DOI: 10.1016/j.cma.2026.118966

Abstract: An energy-based modeling framework for the nonlinear dynamics of spatial Cosserat rods undergoing large displacements and rotations is proposed. The mixed formulation features independent displacement, velocity and stress variables and is further objective and locking-free. Finite rotations are represented using a director formulation that avoids singularities and yields a constant mass matrix. This results in an infinite-dimensional nonlinear port-Hamiltonian (pH) system governed by partial differential-algebraic equations with a quadratic energy functional. Using a time-differentiated compliance form of the stress-strain relations allows for the imposition of kinematic constraints, such as inextensibility or shear-rigidity. A structure-preserving finite element discretization leads to a finite-dimensional system with pH structure, thus facilitating the design of an energy–momentum-consistent integration scheme. Dissipative material behavior (via the generalized-Maxwell model) and non-standard actuation approaches (via pneumatic chambers or tendons) integrate naturally into the framework. As illustrated by selected numerical examples, the present framework establishes a new approach to energy–momentum-consistent formulations in computational mechanics involving finite rotations.

Keywords: Simo–Reissner beam • Kirchhoff beam • Port-Hamiltonian systems • Differential-algebraic equations • Structure-preserving discretization • Mixed finite elements.

4.1. Introduction

Flexible multibody systems consisting of rigid bodies and flexible components [20] have a plethora of applications, as for example in the fields of soft robotics [2] or cable dynamics [62]. These systems are inherently complex, driven by geometric nonlinearities and intricate material behavior, thus requiring accurate and robust simulation methods [97].

To this end, the present work provides a novel modeling framework for the dynamics of *Cosserat rods* [10], which are a cornerstone in modeling the nonlinear dynamics of thin, flexible structures. Hereto, the governing equations are recast as a *port-Hamiltonian* system [63]. This approach inherently provides a mixed formulation in terms of independent displacement, velocity and stress variables and facilitates the *structure-preserving discretization* in space and time.

Cosserat rods. Cosserat rods are also referred to as Simo–Reissner beams [187, 209] or geometrically exact beams [34, 193].[1] These models have become highly influential [34, 59, 61, 67, 101, 104, 105, 133, 141, 193, 212, 235], as they avoid linear or higher order approximations. Lately, these models appear also more frequently in soft robotics [3, 70, 195, 220].

The complexity of this model is mostly due to its geometric nonlinearity originating from finite rotations, whose parametrization can be approached in various ways [20]. Possible options to parameterize the rotational degrees of freedom include, but are not limited to Euler angles, (projected) unit quaternions or vectors of relative rotation. In this work, a singularity-free parametrization will be considered, which avoids coordinates of rotational nature altogether and yields a constant and diagonal mass matrix — the director framework. Due to its beneficial properties, the director formulation of Cosserat rods has been a popular choice in the design of finite element (FE) methods. The corresponding FE implementations rely either on the imposition of algebraic nodal constraints [31, 33, 34, 67, 141] or on the introduction of nodal rotational degrees of freedom [69, 94, 114, 143, 193]. More details on the choice of rotational parameters can be found in the works [21, 27, 117, 194].

Port-Hamiltonian systems. The port-Hamiltonian (pH) framework provides a unifying approach to modeling, simulation, and control of interconnected dynamical systems [63], ideally suited for flexible multibody systems. The pH description takes into account dissipation and interaction with the environment, and can thus be considered an extension of classical Hamiltonian dynamics.

Originally introduced for finite-dimensional systems in [158], the extension of the pH modeling paradigm to infinite-dimensional systems can be traced back to [225] and has been subject to extensive research in various areas [183]. In the context of structural dynamics, pH formulations have been developed for geometrically exact strings [C2, A1, 218], plates [42, 43] and beams restricted to small or moderate deformations [48, 151, 177, 179, 234]. Nonlinear strain-based beam models have been addressed in [16, 150, 152]. Using a material formulation entirely in a body-fixed frame, these formulations are closely related to Hodges' *intrinsic* description of the Cosserat rod [109]. The equivalence to the description commonly used in structural mechanics has been shown in [192] and the related pH representation is detailed in [15].

Structure-preserving discretization. Port-Hamiltonian formulations inherently provide energy-consistency, thus being ideally suited for the design of structure-preserving discretization methods [97], which guarantee that the underlying power balance is respected at the discrete level. This avoids numerical dissipation and energy inconsistencies, which is particularly critical in long-term simulations and in control-oriented problems [50, 171].

Numerical schemes that preserve both energy and momentum are commonly referred to as EM schemes. Although [208] was the first EM method for spatial Cosserat rods, the important property of objectivity was violated, as has been shown in [59]. The first EM method for spatial Cosserat rods that retains the objectivity is due to [193], see also [31, 34], making use of the above-mentioned director framework.

In the context of infinite-dimensional pH systems, the spatial discretization is likewise achieved through FE methods [54] yielding finite dimensional pH systems, see also [44, 48, C2, A2, 218, 234] for applications in structural dynamics. It is important to note that the typical use of energy variables in the pH approach inherently gives rise to mixed FE formulations, thus incorporating also independent stress and/or strain fields. Similarly, time discretization plays a pivotal role for accurate simulations

[1] Throughout this chapter we use the terms *Cosserat rod* and *beam* interchangeably.

with energetic consistency. Energy-consistent integration schemes for pH systems include discrete gradient formulations [91, C2, A3, C4] and projection-based approaches [84].

4.1.1. Research gaps

To the best of the authors' knowledge, mixed formulations and FE methods for the dynamics of Cosserat rods are still quite rare. Despite the extensive research on this beam formulation and the pH framework, their integration has received only limited attention. The existing strain-based pH formulations [15, 16, 152] require reconstructing absolute position and orientation as it is also frequently the case for contributions outside the pH community [57, 244]. Moreover, the Lie-group setting in [152] introduces additional geometric complexity, and neither discretizations in [15, 16, 152] employ finite elements. Contrarily, proposed formulations from the computational mechanics community are predominantly restricted to the static scenario [92, 104, 122, 154, 196, 231].

Another challenge in the simulation of slender mechanical structures is transverse shear locking. This numerical stiffening effect arises during discretization, leading to unrealistically small deformations. While selectively reduced integration [33, 193] is a popular solution, its treatment using mixed approaches is rarely discussed, see exceptions [104, 122, 196] and [41, A2] in the pH context.

Linear constitutive relations can be naturally included into the pH formulation using a compliance equation based on a Hellinger–Reissner variational principle [92, 104, 122, 196]. So-called *velocity-stress* formulations, which are popular in the pH community [48, 218, 219], are related to this concept and consider the compliance equation in time-differentiated form. However, the connection to the Hellinger–Reissner principle has not been explicitly made in these works. For Cosserat rods, such formulations also bring the advantage of easily preventing certain deformation modes such that also shear-rigid or inextensible beams may be simulated without further modifications of the formulation [104]. However, an application to the dynamics of Cosserat rods, especially in combination with a pH formulation, is still open.

Lastly, both the description of viscoelasticity with the generalized-Maxwell model [75, 140, 236] and the actuation using pneumatic chambers and tendons [3, 70, 195, 220] are central in continuum robotics. Their inclusion into a pH framework remains an open topic.

4.1.2. Contributions

The findings in the previous works [A2, A1] indicate that a mixed pH formulation can advance the development of structure-preserving methods for nonlinear structural dynamics. Therein, the specific pH framework [23, C4, 161, 162] has been proven useful also in the infinite-dimensional setting. In the present work, we adopt this formulation for spatial Cosserat rods, address the specific challenges associated with finite rotations, and bridge the above-mentioned gaps as follows:

C1) We propose a mixed, infinite-dimensional pH formulation for spatial Cosserat rods, which naturally accommodates independent displacement, velocity and stress variables, while ensuring intrinsic energy–momentum consistency. The employed director-parametrization of finite rotations provides constant and diagonal mass matrices.

C2) We show the structure-preserving spatial and temporal discretization using mixed finite elements and second-order time-stepping methods, which are facilitated by the mixed pH formulation. Our approach ensures exact discrete representations of the power and angular momentum balance.

C3) We demonstrate that the FE approach, induced by the pH framework, prevents shear locking and straightforwardly includes shear-rigid and inextensible beam formulations as special cases. This can be easily realized in the context of a compliance equation in time-differentiated form.

C4) We extend the given pH model with respect to viscoelastic material behavior in terms of a generalized-Maxwell model, and actuation by pneumatic chambers and tendons. These extensions fit well into the proposed pH formulation.

4.1.3. Notation

We follow the following notation rules. Scalars $f, g, n, m, s \in \mathbb{R}$ are represented in italic fonts. Vectors and d-tuples are treated equally as one-column matrices, e.g., $\boldsymbol{a}, \boldsymbol{b}, \boldsymbol{c} \in \mathbb{R}^{d\times 1}$, using bold fonts. All 3-dimensional vectors representing physical quantities are expressed directly in coordinates, that is, as triples in $\mathbb{R}^3$ relative to a fixed inertial orthonormal basis. Accordingly, the basis vectors of this inertial frame have the canonical coordinate representations $\boldsymbol{e}_1 = (1,0,0)$, $\boldsymbol{e}_2 = (0,1,0)$ and $\boldsymbol{e}_3 = (0,0,1)$. Making use of the Einstein summation convention for repeated indices, i.e., for Latin indices $i, j, k \in \{1,2,3\}$ and Greek indices $\alpha, \beta \in \{1,2\}$, a 3-dimensional vector can be written as $\boldsymbol{a} = \sum_{i=1}^{3} a_i \boldsymbol{e}_i = a_i \boldsymbol{e}_i = (a_1, a_2, a_3)$. For convenience, a short bracket notation is used to express $[\boldsymbol{a}^\top, \boldsymbol{b}^\top]^\top =: (\boldsymbol{a}, \boldsymbol{b})$. The scalar product is denoted by $\boldsymbol{a}^\top \boldsymbol{b} = a_i b_i$ and the cross-product in $\mathbb{R}^3$ reads $\boldsymbol{c} = \boldsymbol{a} \times \boldsymbol{b} = \varepsilon_{ijk} a_j b_k \boldsymbol{e}_i = \tilde{\boldsymbol{a}}\boldsymbol{b}$, where we made use of the Levi-Civita symbol ε_{ijk} and $\widetilde{\square}$ denotes the mapping between $\mathbb{R}^3$ and the space of skew-symmetric matrices $\mathfrak{so}(3) \subset \mathbb{R}^{3\times 3}$. The Kronecker delta δ_{ij} yields one for $i = j$ and zero for $i \neq j$. Matrices $\boldsymbol{A} \in \mathbb{R}^{n\times m}$ use bold faces and differential matrix operators involving derivatives are denoted as calligraphic uppercase letters $\mathcal{A}$. Matrix transposition is denoted by $\boldsymbol{A}^\top$ and the formal adjoint of an operator $\mathcal{A}^*$. Matrix-vector multiplication and the action of an operator are denoted similarly as $\boldsymbol{A}\boldsymbol{b}$ and $\mathcal{A}\boldsymbol{b}$. Identity matrices are represented as $\boldsymbol{I}$ and matrices full of zeros as $\boldsymbol{0}$, their dimension being clear from the context. The square $\square$ represents a placeholder. The partial derivative of a function f is denoted $\partial_{\square} f$. We introduce further $\square_{,s} := \partial_s \square$ and $\dot{\square} := \partial_t \square$. The inner product on a one-dimensional domain Ω, parameterized by s, is denoted $(\boldsymbol{a}, \boldsymbol{b})_\Omega := \int_\Omega \boldsymbol{a}^\top \boldsymbol{b} \, \mathrm{d}s$ or $(f, g)_\Omega := \int_\Omega f \, g \, \mathrm{d}s$, thus taking into account the correct dimension.

4.1.4. Outline

The remainder of this work is structured as follows: In Section 4.2 we introduce the problem statement connected to spatial Cosserat rod dynamics. In Section 4.3 the model is reformulated as a first-order system and its pH structure is shown, inducing naturally a power balance equation. Facilitated by the pH formulation, this power balance equation can be carried over to the discrete level by means of structure-preserving discretization as shown in Section 4.4. Thereafter, Section 4.5 deals with the extension of the formulation to viscoelasticity and two actuation mechanisms, which are relevant in continuum robotics applications. Ultimately, Section 4.6 contains numerical examples, which verify the properties of the proposed approach. These are further recapitulated in the conclusion in Section 4.7. Derivations and details, which are not crucial to grasp the main arguments, are comprised in Appendices 4.A to 4.E.

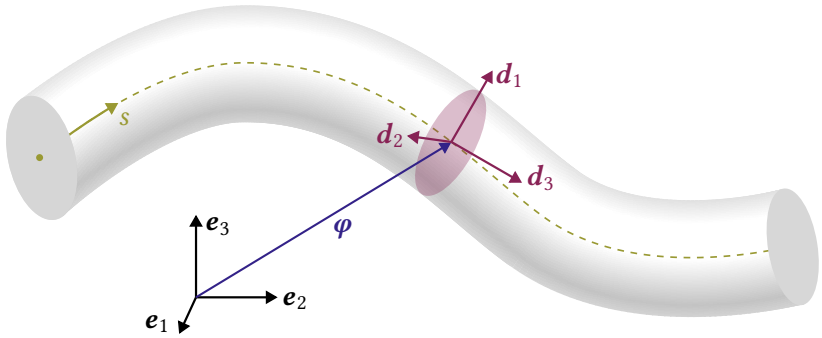

Figure 4.1.: Schematic depiction of a Cosserat rod configuration.

4.2. Problem description

4.2.1. Kinematics

Configuration. The following concepts are based on the models in [33, 193]. Consider a one-dimensional material beam domain $\Omega = [0, L] \subset \mathbb{R}$, with length $L \in \mathbb{R}$, such that the motion of each material point on the centerline (also referred to as *backbone* or *line of centroids*) is described via $\boldsymbol{\varphi}(s,t) \in \mathbb{R}^3$. Here, the material coordinate $s \in \Omega$ is the arc-length parametrization of the centerline of the stress-free initial configuration $\Omega_0 = \{\boldsymbol{\varphi}(s,0) = s\boldsymbol{e}_3 | s \in \Omega\}$ and $t \in \mathbb{T} = [0, t_{\text{end}}] \subset \mathbb{R}$ denotes time. Allowing a geometrically exact description of the kinematics, every cross-section remains plane and rigid during motion and its orientation is described by means of a rotation matrix

$$\boldsymbol{\Lambda}(s,t) = \begin{bmatrix} \boldsymbol{d}_1(s,t) & \boldsymbol{d}_2(s,t) & \boldsymbol{d}_3(s,t) \end{bmatrix} = \boldsymbol{d}_k(s,t)\boldsymbol{e}_k^\top, \tag{4.1}$$

from $SO(3)$, the special orthogonal group. The columns of $\boldsymbol{\Lambda}$ form a local frame of orthonormal directors $\boldsymbol{d}_i(s,t) \in \mathbb{R}^3$ for $i = 1, 2, 3$. See Figure 4.1 for a depiction of the kinematics. The director $\boldsymbol{d}_3(s,t)$ is assumed to be normal to each cross section and $\boldsymbol{d}_1(s,t), \boldsymbol{d}_2(s,t)$ are transverse to it, such that $\boldsymbol{d}_3(s,t) = \boldsymbol{d}_1(s,t) \times \boldsymbol{d}_2(s,t)$. For simplicity, we further assume that $\boldsymbol{d}_1(s,t)$ and $\boldsymbol{d}_2(s,t)$ coincide with the principal axes of inertia of the cross-section at all times. In the following, the explicit dependence on space and time is omitted and only mentioned where deemed necessary. Abusing notation, we also interpret $\boldsymbol{\Lambda} = \boldsymbol{\Lambda}(\boldsymbol{d})$ as function of the vertical concatenation of the directors $\boldsymbol{d} = (\boldsymbol{d}_1, \boldsymbol{d}_2, \boldsymbol{d}_3) \in \mathbb{R}^9$. Furthermore, we call $(\boldsymbol{\varphi}, \boldsymbol{d})$ *displacement* quantities, as they uniquely characterize the displacement of each material point on the beam configuration. Since $\boldsymbol{\Lambda}(\boldsymbol{d}) \in SO(3)$, it holds that $\det(\boldsymbol{\Lambda}(\boldsymbol{d})) = +1$ and $\boldsymbol{\Lambda}(\boldsymbol{d})^\top \boldsymbol{\Lambda}(\boldsymbol{d}) = \boldsymbol{\Lambda}(\boldsymbol{d})\boldsymbol{\Lambda}(\boldsymbol{d})^\top = \boldsymbol{I}$. Consequently, there are 6 orthonormality conditions

$$\boldsymbol{0} = \boldsymbol{g}(\boldsymbol{d}) \in \mathbb{R}^6 \quad \Leftrightarrow \quad \frac{1}{2}\left(\boldsymbol{d}_i^\top \boldsymbol{d}_j - \delta_{ij}\right) = 0, \tag{4.2}$$

for $(i,j) \in \{(1,1), (2,2), (3,3), (1,2), (2,3), (3,1)\}$.

Strains. We make use of the objective, material strain measures $\boldsymbol{\Gamma} = \boldsymbol{\Lambda}^\top \boldsymbol{\varphi}_{,s}$ to describe shear deformation and dilatation and $\widetilde{\boldsymbol{K}} = \boldsymbol{\Lambda}^\top \boldsymbol{\Lambda}_{,s}$ for curvature and torsion, which can be expressed equivalently as

$$\boldsymbol{\Gamma} = (\boldsymbol{d}_k^\top \boldsymbol{\varphi}_{,s})\boldsymbol{e}_k = \begin{bmatrix} \boldsymbol{d}_1^\top \boldsymbol{\varphi}_{,s} \\ \boldsymbol{d}_2^\top \boldsymbol{\varphi}_{,s} \\ \boldsymbol{d}_3^\top \boldsymbol{\varphi}_{,s} \end{bmatrix}, \qquad \boldsymbol{K} = \frac{1}{2}\varepsilon_{ijk}(\boldsymbol{d}_k^\top \boldsymbol{d}_{j,s})\boldsymbol{e}_i = \frac{1}{2}\begin{bmatrix} \boldsymbol{d}_3^\top \boldsymbol{d}_{2,s} - \boldsymbol{d}_2^\top \boldsymbol{d}_{3,s} \\ \boldsymbol{d}_1^\top \boldsymbol{d}_{3,s} - \boldsymbol{d}_3^\top \boldsymbol{d}_{1,s} \\ \boldsymbol{d}_2^\top \boldsymbol{d}_{1,s} - \boldsymbol{d}_1^\top \boldsymbol{d}_{2,s} \end{bmatrix}, \tag{4.3}$$

where we switched to the axial vector of $\widetilde{\boldsymbol{K}}$. Due to the bilinearity of both $\boldsymbol{\Gamma}(\boldsymbol{d}, \boldsymbol{\varphi}_{,s})$ and $\boldsymbol{K}(\boldsymbol{d}, \boldsymbol{d}_{,s})$, one can compactly rewrite them using two different representations each, i.e.,

$$\boldsymbol{\Gamma} = \boldsymbol{\Lambda}(\boldsymbol{d})^\top \boldsymbol{\varphi}_{,s} = \boldsymbol{J}_{\boldsymbol{N}}(\boldsymbol{\varphi}_{,s})^\top \boldsymbol{d}, \qquad \boldsymbol{K} = \boldsymbol{L}(\boldsymbol{d}_{,s})\boldsymbol{d} = -\boldsymbol{L}(\boldsymbol{d})\boldsymbol{d}_{,s}. \tag{4.4}$$

The rotation matrix (4.1) as well as the newly introduced matrices

$$\boldsymbol{J}_{\boldsymbol{N}}(\boldsymbol{\varphi}_{,s}) = \begin{bmatrix} \boldsymbol{\varphi}_{,s} & \boldsymbol{0} & \boldsymbol{0} \\ \boldsymbol{0} & \boldsymbol{\varphi}_{,s} & \boldsymbol{0} \\ \boldsymbol{0} & \boldsymbol{0} & \boldsymbol{\varphi}_{,s} \end{bmatrix} \in \mathbb{R}^{9\times 3}, \qquad \boldsymbol{L}(\boldsymbol{d}) = \frac{1}{2}\begin{bmatrix} \boldsymbol{0} & -\boldsymbol{d}_3^\top & \boldsymbol{d}_2^\top \\ \boldsymbol{d}_3^\top & \boldsymbol{0} & -\boldsymbol{d}_1^\top \\ -\boldsymbol{d}_2^\top & \boldsymbol{d}_1^\top & \boldsymbol{0} \end{bmatrix} \in \mathbb{R}^{3\times 9} \tag{4.5}$$

are linear functions of their arguments. Note that $\boldsymbol{L}(\boldsymbol{d})\boldsymbol{d} = \boldsymbol{0}$ due to (4.2).

Remark 4.1. *We assume straight and stress-free initial configurations that serve as the reference configuration. Thus, the cross-section normal $\boldsymbol{d}_3(s, t = 0)$ aligns with the centerline tangent vector $\boldsymbol{\varphi}_{,s}(s, t = 0)$ implying the homogeneous reference strains $\boldsymbol{\Gamma}_0 := \boldsymbol{\Gamma}(s, t = 0) = (0, 0, 1)$ and $\boldsymbol{K}_0 := \boldsymbol{K}(s, t = 0) = \boldsymbol{0}$. For pre-curved beams, the reference strains would be different, which does not affect the generality of the theoretical framework developed in the remainder of this work. Moreover, $\boldsymbol{\Gamma}$ describes the rate of change of the centerline (i.e., the tangent vector), while $\boldsymbol{K}$ describes the rate of change of orientation when moving along the beam. The fact that $\boldsymbol{K}$ is derived from a skew-symmetric matrix $\widetilde{\boldsymbol{K}}$ can be traced back to taking the derivative of the orthonormality constraints* (4.2) *with respect to s.* ♧

4.2.2. Constitutive modeling

Starting from the general case of hyperelastic material models based on a scalar-valued strain energy function $W = \check{W}(\boldsymbol{\Gamma}, \boldsymbol{K})$ being a function of the strain measures, the corresponding work-conjugated stress quantities are derived as

$$\boldsymbol{N} = \partial_{\boldsymbol{\Gamma}} \check{W}, \qquad \boldsymbol{M} = \partial_{\boldsymbol{K}} \check{W}. \tag{4.6}$$

Here, indicated by an uppercase notation, $\boldsymbol{N} = N_i \boldsymbol{e}_i$ are the material normal and shear forces and $\boldsymbol{M} = M_i \boldsymbol{e}_i$ are the material bending and torsion moments. The spatial stress quantities $\boldsymbol{n}$ and $\boldsymbol{m}$ can be linked to their material counterparts via

$$\boldsymbol{n} = \boldsymbol{\Lambda}(\boldsymbol{d})\boldsymbol{N} = N_i \boldsymbol{d}_i, \qquad \boldsymbol{m} = \boldsymbol{\Lambda}(\boldsymbol{d})\boldsymbol{M} = M_i \boldsymbol{d}_i. \tag{4.7}$$

In the following, we assume linear constitutive laws such that W has quadratic form. This is a common assumption in the literature since locally only small strains are expected. We thus write

$$\check{W}(\boldsymbol{\Gamma}, \boldsymbol{K}) = \frac{1}{2}(\boldsymbol{\Gamma} - \boldsymbol{\Gamma}_0)^\top \boldsymbol{C}_\Gamma (\boldsymbol{\Gamma} - \boldsymbol{\Gamma}_0) + \frac{1}{2}(\boldsymbol{K} - \boldsymbol{K}_0)^\top \boldsymbol{C}_K (\boldsymbol{K} - \boldsymbol{K}_0) \tag{4.8}$$

with constant elasticity matrices $\boldsymbol{C}_\Gamma = \operatorname{diag}(k_{\mathrm{s}1}, k_{\mathrm{s}2}, k_{\mathrm{e}}) \in \mathbb{R}^{3\times 3}$ and $\boldsymbol{C}_K = \operatorname{diag}(k_{\mathrm{b}1}, k_{\mathrm{b}2}, k_{\mathrm{t}}) \in \mathbb{R}^{3\times 3}$ as well as $\boldsymbol{\Gamma}_0$ and $\boldsymbol{K}_0$ according to Remark 4.1.

Compliance form. A quadratic hyperelastic strain energy function can also be expressed in terms of the stresses as *complementary energy function* $W = W^\star(\boldsymbol{N}, \boldsymbol{M})$ such that

$$W^\star(\boldsymbol{N}, \boldsymbol{M}) = \frac{1}{2}\boldsymbol{N}^\top \boldsymbol{C}_N \boldsymbol{N} + \frac{1}{2}\boldsymbol{M}^\top \boldsymbol{C}_M \boldsymbol{M} \tag{4.9}$$

with compliance matrices $\boldsymbol{C}_N = \operatorname{diag}(k_{\mathrm{s1}}^{-1}, k_{\mathrm{s2}}^{-1}, k_{\mathrm{e}}^{-1}) \in \mathbb{R}^{3\times3}$, $\boldsymbol{C}_M = \operatorname{diag}(k_{\mathrm{b1}}^{-1}, k_{\mathrm{b2}}^{-1}, k_{\mathrm{t}}^{-1}) \in \mathbb{R}^{3\times3}$. Note that these matrices are allowed to be singular if some stiffnesses tend to infinity, e.g., $k_{\mathrm{s1}}, k_{\mathrm{s2}} \to \infty$ and thus $\boldsymbol{C}_N = \operatorname{diag}(0, 0, k_{\mathrm{e}}^{-1})$ for shear-stiff beam theories, like the well-known *Kirchhoff*-beam model. Similar to (4.6), the strain measures can be derived by differentiation, such that

$$\boldsymbol{\Gamma} - \boldsymbol{\Gamma}_0 = \partial_{\boldsymbol{N}} W^\star = \boldsymbol{C}_N \boldsymbol{N}, \qquad \boldsymbol{K} - \boldsymbol{K}_0 = \partial_{\boldsymbol{M}} W^\star = \boldsymbol{C}_M \boldsymbol{M}. \tag{4.10}$$

In the case of hyperelastic stress-strain relations that cannot be inverted, a Hu–Washizu type approach [C2, A2] might be required. Such an approach is discussed in Appendix 3.A of the previous chapter for the planar case. Similarly, the pH formulation of hyperelastic strings in Chapter 6 can be linked to a related Hu–Washizu principle. Note that the compliance form employed here, is also explained in an insightful way for the model problem of a spring pendulum, cf. Example 2.11 in Chapter 2 of the present work.

4.2.3. Equations of motion

The partial differential equations governing the dynamics of the Cosserat rod can be derived from the principle of virtual work, see Appendix 4.B, as

$$\rho A \partial_{tt}^2 \boldsymbol{\varphi} = \boldsymbol{n}_{,s} + \bar{\boldsymbol{n}}, \qquad \boldsymbol{I}_\rho \partial_t \boldsymbol{\omega} + \boldsymbol{\omega} \times \boldsymbol{I}_\rho \boldsymbol{\omega} = \boldsymbol{m}_{,s} + \boldsymbol{\varphi}_{,s} \times \boldsymbol{n} + \bar{\boldsymbol{m}}, \tag{4.11}$$

stating the local balance of linear and angular momentum in spatial form, respectively [10, 209]. Here, we introduced the uniformly distributed mass density per unit length $\rho \geq 0$ and cross section area $A > 0$, $\boldsymbol{\omega}(s,t) \in \mathbb{R}^3$ is the spatial angular velocity, $\boldsymbol{I}_\rho \in \mathbb{R}^{3\times3}$ is the spatial representation of the inertia tensor, and $\bar{\boldsymbol{n}}(s,t), \bar{\boldsymbol{m}}(s,t) \in \mathbb{R}^3$ are external distributed forces and moments per unit length.

In contrast to (4.11), we target a formulation in terms of directors as introduced above. Considering the derivations from Appendix 4.B, one obtains the equivalent representation of the Cosserat rod dynamics in the form

$$\rho A \partial_{tt}^2 \boldsymbol{\varphi} = \boldsymbol{n}_{,s} + \bar{\boldsymbol{n}}, \tag{4.12a}$$

$$\boldsymbol{M}_\rho \partial_{tt}^2 \boldsymbol{d} = -\boldsymbol{J}_{\boldsymbol{N}} \boldsymbol{N} - \mathcal{J}_{\boldsymbol{M}} \boldsymbol{M} - \boldsymbol{G}_d^\top \boldsymbol{\lambda} + \boldsymbol{T} \bar{\boldsymbol{m}}, \tag{4.12b}$$

$$\boldsymbol{g}(\boldsymbol{d}) = \boldsymbol{0}, \tag{4.12c}$$

where $\boldsymbol{J}_{\boldsymbol{N}}$ has been introduced in (4.5). Further, we have introduced a constant and diagonal mass matrix $\boldsymbol{M}_\rho = \operatorname{diag}(M_\rho^{11}\boldsymbol{I}, M_\rho^{22}\boldsymbol{I}, \boldsymbol{0}) \in \mathbb{R}^{9\times9}$, and the operator matrix $\mathcal{J}_{\boldsymbol{M}}$, which is defined together with its adjoint $\mathcal{J}_{\boldsymbol{K}} = \mathcal{J}_{\boldsymbol{M}}^*$ as

$$\mathcal{J}_{\boldsymbol{M}}(\boldsymbol{d}, \boldsymbol{d}_{,s})\square = \boldsymbol{L}(\boldsymbol{d}_{,s})^\top \square + \partial_s(\boldsymbol{L}(\boldsymbol{d})^\top \square), \qquad \mathcal{J}_{\boldsymbol{K}}(\boldsymbol{d}, \boldsymbol{d}_{,s})\square = \boldsymbol{L}(\boldsymbol{d}_{,s})\square - \boldsymbol{L}(\boldsymbol{d})\partial_s \square\,. \tag{4.13}$$

Here, $\boldsymbol{L}$ is given in (4.5). Additionally in (4.12b), we have introduced $\boldsymbol{T} \in \mathbb{R}^{9\times3}$ defined as

$$\boldsymbol{T}(\boldsymbol{d}) = -\frac{1}{2}\begin{bmatrix}\tilde{\boldsymbol{d}}_1 \\ \tilde{\boldsymbol{d}}_2 \\ \tilde{\boldsymbol{d}}_3\end{bmatrix}, \qquad \text{with} \qquad \boldsymbol{T}(\boldsymbol{d})^\top = \frac{1}{2}\begin{bmatrix}\tilde{\boldsymbol{d}}_1 & \tilde{\boldsymbol{d}}_2 & \tilde{\boldsymbol{d}}_3\end{bmatrix}, \tag{4.14}$$

which connects angular velocities and director velocities, see (4.85) in Appendix 4.A. Lastly, the constraint Jacobian

$$\boldsymbol{G}_d(\boldsymbol{d}) = \mathrm{D}\boldsymbol{g}(\boldsymbol{d}) = \begin{bmatrix} \boldsymbol{d}_1^\top & \boldsymbol{0} & \boldsymbol{0} \\ \boldsymbol{0} & \boldsymbol{d}_2^\top & \boldsymbol{0} \\ \boldsymbol{0} & \boldsymbol{0} & \boldsymbol{d}_3^\top \\ \frac{1}{2}\boldsymbol{d}_2^\top & \frac{1}{2}\boldsymbol{d}_1^\top & \boldsymbol{0} \\ \boldsymbol{0} & \frac{1}{2}\boldsymbol{d}_3^\top & \frac{1}{2}\boldsymbol{d}_2^\top \\ \frac{1}{2}\boldsymbol{d}_3^\top & \boldsymbol{0} & \frac{1}{2}\boldsymbol{d}_1^\top \end{bmatrix} \in \mathbb{R}^{6\times9} \tag{4.15}$$

and the vector containing all Lagrange multipliers $\boldsymbol{\lambda} \in \mathbb{R}^6$ encode constraint forces in (4.12b). These forces ensure the fulfillment of the orthonormality constraints (4.12c), which are equivalent to (4.2). Note that $\boldsymbol{N}$ and $\boldsymbol{M}$ are calculated by means of $\boldsymbol{\varphi}$ and $\boldsymbol{d}$ via (4.6) and (4.4). The related initial boundary value problem is completed by suitable initial and boundary conditions.

The purely displacement-based formulation (4.12) can be prone to locking and more tedious to deal with in the context of energy–momentum-consistent discretization. We thus target a mixed, port-Hamiltonian description in the following section.

4.3. Port-Hamiltonian formulation

4.3.1. Local form as first order system

Our goal is to rewrite the problem at hand as a set of first-order partial-differential equations with algebraic constraints due to the orthonormality of the directors. To this end, we introduce independent stress and velocity variables, linked via a compliance equation in time-differentiated form, and also consider the orthonormality constraints on velocity level.

Let us introduce independent centerline velocities $\boldsymbol{v}_\varphi = \dot{\boldsymbol{\varphi}}$ and director-related velocities $\boldsymbol{v}_d = \dot{\boldsymbol{d}}$ as well as the displacement and velocity vectors $\boldsymbol{q}, \boldsymbol{v} \in \mathbb{R}^{12}$ such that

$$\boldsymbol{q} = \begin{bmatrix} \boldsymbol{\varphi} \\ \boldsymbol{d} \end{bmatrix}, \quad \boldsymbol{v} = \begin{bmatrix} \boldsymbol{v}_\varphi \\ \boldsymbol{v}_d \end{bmatrix} \qquad \text{with} \qquad \dot{\boldsymbol{q}} = \boldsymbol{v}. \tag{4.16}$$

By making use of the newly introduced velocities, we can rewrite the balance equations (4.12a) and (4.12b) as

$$\rho A \dot{\boldsymbol{v}}_\varphi = \partial_s(\boldsymbol{\Lambda} \boldsymbol{N}) + \bar{\boldsymbol{n}}, \qquad \boldsymbol{M}_\rho \dot{\boldsymbol{v}}_d = -\boldsymbol{J}_{\boldsymbol{N}} \boldsymbol{N} - \mathcal{J}_{\boldsymbol{M}} \boldsymbol{M} - \boldsymbol{G}_d^\top \boldsymbol{\lambda} + \boldsymbol{T} \bar{\boldsymbol{m}}. \tag{4.17}$$

Next, taking the time derivative of the compliance equation (4.10) together with (4.4) we obtain an evolution equation for the stresses as

$$\boldsymbol{C}_N \dot{\boldsymbol{N}} = \boldsymbol{\Lambda}(\boldsymbol{d})^\top \boldsymbol{v}_{\varphi,s} + \boldsymbol{J}_{\boldsymbol{N}}(\boldsymbol{\varphi}_{,s})^\top \boldsymbol{v}_d, \qquad \boldsymbol{C}_M \dot{\boldsymbol{M}} = \mathcal{J}_{\boldsymbol{K}}(\boldsymbol{d}, \boldsymbol{d}_{,s}) \boldsymbol{v}_d. \tag{4.18}$$

Note that we have used the operator matrix $\mathcal{J}_{\boldsymbol{K}}(\boldsymbol{d}, \boldsymbol{d}_{,s})$ in (4.18), which is defined in (4.13). Lastly, the use of directors as independent quantities requires the explicit enforcement of 6 orthonormality constraints (4.12c), which we will also consider in time-differentiated form as

$$\boldsymbol{G}(\boldsymbol{q}) \boldsymbol{v} = \begin{bmatrix} \boldsymbol{0} & \boldsymbol{G}_d(\boldsymbol{d}) \end{bmatrix} \begin{bmatrix} \boldsymbol{v}_\varphi \\ \boldsymbol{v}_d \end{bmatrix} = \boldsymbol{0}, \tag{4.19}$$

where the constraint matrix $\boldsymbol{G}_d(\boldsymbol{d})$ is defined in (4.15). Eventually, together with suitable initial and boundary conditions, equations (4.16), (4.17), (4.18) and (4.19) are the basis for a mixed, pH formulation of the Cosserat rod dynamics. For the sake of brevity, let us introduce

$$\begin{gathered} \boldsymbol{\sigma} = \begin{bmatrix} \boldsymbol{N} \\ \boldsymbol{M} \end{bmatrix}, \quad \boldsymbol{C} = \begin{bmatrix} \boldsymbol{C}_N & \boldsymbol{0} \\ \boldsymbol{0} & \boldsymbol{C}_M \end{bmatrix}, \quad \boldsymbol{M}_o = \begin{bmatrix} \rho A \boldsymbol{I} & \boldsymbol{0} \\ \boldsymbol{0} & \boldsymbol{M}_\rho \end{bmatrix}, \quad \boldsymbol{B}_\Omega(\boldsymbol{q}) = \begin{bmatrix} \boldsymbol{I} & \boldsymbol{0} \\ \boldsymbol{0} & \boldsymbol{T}(\boldsymbol{d}) \end{bmatrix}, \quad \boldsymbol{u}_\Omega = \begin{bmatrix} \bar{\boldsymbol{n}} \\ \bar{\boldsymbol{m}} \end{bmatrix}, \\ \mathcal{J}_{\boldsymbol{\sigma}}(\boldsymbol{q}, \boldsymbol{q}_{,s}) = \begin{bmatrix} \boldsymbol{\Lambda}(\boldsymbol{d})^\top \partial_s \square & \boldsymbol{J}_{\boldsymbol{N}}(\boldsymbol{\varphi}_{,s})^\top \\ \boldsymbol{0} & \mathcal{J}_{\boldsymbol{K}}(\boldsymbol{d}, \boldsymbol{d}_{,s}) \end{bmatrix}, \quad \mathcal{J}_{\boldsymbol{v}}(\boldsymbol{q}, \boldsymbol{q}_{,s}) = \begin{bmatrix} -\partial_s(\boldsymbol{\Lambda}(\boldsymbol{d}) \square) & \boldsymbol{0} \\ \boldsymbol{J}_{\boldsymbol{N}}(\boldsymbol{\varphi}_{,s}) & \mathcal{J}_{\boldsymbol{M}}(\boldsymbol{d}, \boldsymbol{d}_{,s}) \end{bmatrix}, \end{gathered} \tag{4.20}$$

to compactly rewrite (4.17) and (4.18) in the following section.

4.3.2. Port-Hamiltonian representation

The pH representation of the governing partial differential-algebraic equations at hand comprises equations (4.16), (4.17), (4.18) and (4.19). Using the definitions (4.20), we can rewrite them as

$$\begin{bmatrix} \boldsymbol{I} & 0 & 0 & 0 \\ 0 & \boldsymbol{M}_o & 0 & 0 \\ 0 & 0 & \boldsymbol{C} & 0 \\ 0 & 0 & 0 & \boldsymbol{0} \end{bmatrix} \partial_t \begin{bmatrix} \boldsymbol{q} \\ \boldsymbol{v} \\ \boldsymbol{\sigma} \\ \boldsymbol{\lambda} \end{bmatrix} = \begin{bmatrix} 0 & \boldsymbol{I} & 0 & 0 \\ -\boldsymbol{I} & 0 & -\mathcal{J}_{\boldsymbol{v}}(\boldsymbol{q}) & -\boldsymbol{G}(\boldsymbol{q})^\top \\ 0 & \mathcal{J}_{\boldsymbol{\sigma}}(\boldsymbol{q}) & 0 & 0 \\ 0 & \boldsymbol{G}(\boldsymbol{q}) & 0 & 0 \end{bmatrix} \begin{bmatrix} \boldsymbol{0} \\ \boldsymbol{v} \\ \boldsymbol{\sigma} \\ \boldsymbol{\lambda} \end{bmatrix} + \begin{bmatrix} 0 \\ \boldsymbol{B}_\Omega(\boldsymbol{q}) \\ 0 \\ 0 \end{bmatrix} \boldsymbol{u}_\Omega, \tag{4.21}$$

where the so-called *descriptor* matrix $\mathcal{E} = \operatorname{diag}(\boldsymbol{I}, \boldsymbol{M}_o, \boldsymbol{C}, \boldsymbol{0})$ is constant, symmetric and rank deficient by at least 9 due to the 6 algebraic constraints and the singular mass matrix. If certain stiffnesses are assumed to tend to infinity (e.g., by describing a shear-rigid beam), the rank deficiency increases accordingly due to a singular compliance matrix $\boldsymbol{C}$, see Example 2.11 in Chapter 2 of this work for an explanatory example in the finite-dimensional setting. In short form one can rewrite (4.21) in the pH framework by [23, 161, 162][2] as

$$\begin{aligned} \mathcal{E}\partial_t \boldsymbol{x} &= \mathcal{J}(\boldsymbol{x})\boldsymbol{z}(\boldsymbol{x}) + \mathcal{B}_\Omega(\boldsymbol{x})\boldsymbol{u}_\Omega, \\ \boldsymbol{y}_\Omega &= \mathcal{B}_\Omega(\boldsymbol{x})^\top \boldsymbol{z}(\boldsymbol{x}), \end{aligned} \tag{4.22}$$

where the state vector $\boldsymbol{x} \in \mathbb{R}^{36}$ comprises the primary unknowns

$$\boldsymbol{x} = (\boldsymbol{q}, \boldsymbol{v}, \boldsymbol{\sigma}, \boldsymbol{\lambda}). \tag{4.23}$$

The other newly introduced quantities in (4.22) can be identified by comparison with (4.21). Moreover, $\mathcal{J}(\boldsymbol{x})$ is a differential operator matrix, termed *structure* operator matrix, which involves partial derivatives. Further, the costate function $\boldsymbol{z}$ has been introduced and assumes the linear form $\boldsymbol{z}(\boldsymbol{x}) = \mathcal{Q}\boldsymbol{x}$ with $\mathcal{Q} = \operatorname{diag}(\boldsymbol{0}, \boldsymbol{I}, \boldsymbol{I}, \boldsymbol{I})$. In (4.22), we have appended the distributed output relation, yielding $\boldsymbol{y}_\Omega = (\boldsymbol{v}_\varphi, \boldsymbol{\omega})$, i.e., the centerline velocity and the spatial angular velocity $\boldsymbol{\omega}$. By definition this distributed output is power-conjugated to the distributed input forces and torques $\boldsymbol{u}_\Omega = (\bar{\boldsymbol{n}}, \bar{\boldsymbol{m}})$.

Port-Hamiltonian structure. At this point, it remains to show that the above equations possess a pH structure. This requires that (i) the costate function $\boldsymbol{z}$ is properly linked to the underlying Hamiltonian of the system, and that (ii) the structure operator matrix $\mathcal{J}$ is formally skew-adjoint, i.e., $\mathcal{J}(\boldsymbol{x}) = -\mathcal{J}(\boldsymbol{x})^*$. These two conditions ensure that the pH system has an underlying Stokes–Dirac structure and consequently satisfies a power balance equation.

Condition (i), see [23, 161, 162], requires that

$$\mathcal{E}^\top \boldsymbol{z}(\boldsymbol{x}) = \delta_{\boldsymbol{x}} \mathcal{H}. \tag{4.24}$$

Therein, $\delta_{\boldsymbol{x}}\mathcal{H}$ is the variational derivative of a suitable Hamiltonian (2.72). See (2.73) for the definition of the variational derivative. With the above definitions of $\mathcal{E}$ and $\boldsymbol{z}(\boldsymbol{x})$ this is indeed the case for the Hamiltonian given by

$$\mathcal{H}(\boldsymbol{x}) = \int_\Omega h(\boldsymbol{x}) \,\mathrm{d}s = \frac{1}{2}\int_\Omega \boldsymbol{x}^\top \mathcal{Q}^\top \mathcal{E}\boldsymbol{x} \,\mathrm{d}s = \frac{1}{2}\int_\Omega \left(\boldsymbol{v}^\top \boldsymbol{M}_o \boldsymbol{v} + \boldsymbol{\sigma}^\top \boldsymbol{C}\boldsymbol{\sigma}\right) \,\mathrm{d}s, \tag{4.25}$$

[2] See also the adaptions in the context of infinite-dimensional systems in [C2, A2, A1]. These models can also be found in Chapters 3 and 6. A detailed definition of infinite-dimensional port-Hamiltonian descriptor systems is given in Definition 2.19 contained in Chapter 2 of this work.

which represents the total mechanical energy of the system, i.e., the sum of kinetic energy and the complementary energy stored in the beam due to deformation. Consequently, $\delta_{\boldsymbol{x}}\mathcal{H} = \partial_{\boldsymbol{x}} h = \mathcal{Q}^\top \mathcal{E}\boldsymbol{x}$ and (4.24) holds true since $\mathcal{Q}^\top\mathcal{E} = \mathcal{E}^\top\mathcal{Q}$. Note that the Hamiltonian does not depend on $\boldsymbol{q}$ and $\boldsymbol{\lambda}$, since these do not contribute to the energy of the system. These properties are reflected by the corresponding zero blocks in the matrices $\mathcal{Q}$ and $\mathcal{E}$, respectively.

Concerning condition (ii), the property of formal skew-adjointness of $\mathcal{J}$ in (4.21) can be regarded as the extension of skew-symmetry for matrices to differential matrix operators. Loosely speaking, this means that the computation of $(\boldsymbol{z}, \mathcal{J}\boldsymbol{z})_\Omega$ may only yield boundary terms after integration by parts. For details, see Definition 2.16 and the surrounding discussion in Section 2.4. For elements that do not involve spatial derivatives, such as $\boldsymbol{I}$ and $\boldsymbol{G}$, the proof is straightforward by checking the skew-symmetry. However, for the differential operators $\mathcal{J}_{\boldsymbol{\sigma}}$ and $\mathcal{J}_{\boldsymbol{v}}$ this requires some more attention. Eventually, the result

$$(\boldsymbol{z}, \mathcal{J}\boldsymbol{z})_\Omega = \left[\boldsymbol{v}_\varphi^\top \boldsymbol{n} + \boldsymbol{\omega}^\top \boldsymbol{m}\right]_{\partial\Omega} =: \boldsymbol{y}_{\partial\Omega}^\top \boldsymbol{u}_{\partial\Omega} \tag{4.26}$$

is obtained along the lines of Appendix 4.C. This product encodes the power flow through the boundary $\partial\Omega = \{0, L\}$ exerted by means of the outputs $\boldsymbol{y}_{\partial\Omega}$ and boundary inputs $\boldsymbol{u}_{\partial\Omega}$. The latter are given by the boundary values of the initial boundary value problem. For example, in the case of the pure Neumann boundary conditions with prescribed quantities $\square_{\mathrm{N}}$ on the Neumann boundary $\partial\Omega_{\mathrm{N}} = \{0, L\}$, one has

$$\boldsymbol{u}_{\partial\Omega} = \begin{bmatrix} -\boldsymbol{n}_{\mathrm{N},0}(t) \\ -\boldsymbol{m}_{\mathrm{N},0}(t) \\ \boldsymbol{n}_{\mathrm{N},L}(t) \\ \boldsymbol{m}_{\mathrm{N},L}(t) \end{bmatrix}, \qquad \boldsymbol{y}_{\partial\Omega} = \begin{bmatrix} \boldsymbol{v}_\varphi(0,t) \\ \boldsymbol{\omega}(0,t) \\ \boldsymbol{v}_\varphi(L,t) \\ \boldsymbol{\omega}(L,t) \end{bmatrix}. \tag{4.27}$$

Power balance equation. Since both conditions have been verified, the governing equations (4.22) have pH structure. As a consequence, an underlying power balance equation with respect to the Hamiltonian (4.25) is induced as

$$\dot{\mathcal{H}} = \int_\Omega \delta_{\boldsymbol{x}}\mathcal{H}^\top \dot{\boldsymbol{x}}\,\mathrm{d}s = \int_\Omega \boldsymbol{z}^\top \mathcal{E}\dot{\boldsymbol{x}}\,\mathrm{d}s = \int_\Omega \boldsymbol{z}^\top \left(\mathcal{J}\boldsymbol{z} + \mathcal{B}_\Omega \boldsymbol{u}_\Omega\right)\,\mathrm{d}s = \boldsymbol{y}_{\partial\Omega}^\top \boldsymbol{u}_{\partial\Omega} + \int_\Omega \boldsymbol{y}_\Omega^\top \boldsymbol{u}_\Omega\,\mathrm{d}s, \tag{4.28}$$

where we have used the chain rule, (4.22), (4.24) and (4.26) and omitted the state-dependence of the respective quantities. Note that the power balance (4.28) automatically ensures conservation of energy for closed systems (i.e., for $\boldsymbol{u}_\Omega = \boldsymbol{0}$, $\boldsymbol{u}_{\partial\Omega} = \boldsymbol{0}$) and demonstrates the property of passivity. This property lies at the core of pH systems and can be exploited when designing energy–momentum-consistent methods. Thus, when it comes to the numerical discretization, we aim to preserve the pH structure to retain this property in simulations.

Remark 4.2. *The underlying mathematical notion is that of a Stokes–Dirac structure, which defines so-called* flow *and* effort *variables on respective dual spaces. As pointed out for finite-dimensional systems of the same structure [23], the present framework is consistent with that geometric viewpoint on pH systems. In fact, we can define flows $\boldsymbol{f} = \mathcal{E}\dot{\boldsymbol{x}}$ and efforts $\boldsymbol{e} = \boldsymbol{z}(\boldsymbol{x}) = \mathcal{Q}\boldsymbol{x}$. Here, the Stokes–Dirac structure is modulated by the state, which can be seen from the state-dependence of the structure matrix operator $\mathcal{J}(\boldsymbol{x})$. This property traces back to the geometric nonlinearity of the problem at hand and is discussed in Chapter 2 of the present work by means of a finite dimensional model problem, cf. Example 2.3. An in-depth explanation of Dirac structures is omitted here for the sake of conciseness, but can be found in Section 2.2.* ♧

4.3.3. Weak form

The weak form of the problem can be derived in a straightforward manner from the differential form (4.21) and serves as the basis for the following FE discretization. Accordingly, premultiplying on both sides by appropriate test functions $(\boldsymbol{M}_o\delta\boldsymbol{v}, \delta\boldsymbol{q}, \delta\boldsymbol{\sigma}, \delta\boldsymbol{\lambda})$, integrating over the spatial domain Ω and applying integration by parts yields the detailed weak relations

$$\left(\rho A\delta\boldsymbol{v}_\varphi, \dot{\boldsymbol{\varphi}} - \boldsymbol{v}_\varphi\right)_\Omega = 0, \tag{4.29a}$$
$$\left(\boldsymbol{M}_\rho\delta\boldsymbol{v}_d, \dot{\boldsymbol{d}} - \boldsymbol{v}_d\right)_\Omega = 0, \tag{4.29b}$$
$$\left(\delta\boldsymbol{\varphi}, \rho A\dot{\boldsymbol{v}}_\varphi - \bar{\boldsymbol{n}}\right)_\Omega + \left(\delta\boldsymbol{\varphi}_{,s}, \boldsymbol{\Lambda}\boldsymbol{N}\right)_\Omega - \left[\delta\boldsymbol{\varphi}, \boldsymbol{n}_\mathrm{N}\right]_{\partial\Omega} = 0, \tag{4.29c}$$
$$\left(\delta\boldsymbol{d}, \boldsymbol{M}_\rho\dot{\boldsymbol{v}}_d + \boldsymbol{J}_{\boldsymbol{N}}\boldsymbol{N} + \boldsymbol{G}_d^\top\boldsymbol{\lambda} - \boldsymbol{T}\bar{\boldsymbol{m}}\right)_\Omega + \left(\mathcal{J}_{\boldsymbol{K}}\delta\boldsymbol{d}, \boldsymbol{M}\right)_\Omega - \left[\delta\boldsymbol{d}, \boldsymbol{T}\boldsymbol{m}_\mathrm{N}\right]_{\partial\Omega} = 0, \tag{4.29d}$$
$$\left(\delta\boldsymbol{N}, \boldsymbol{C}_N\dot{\boldsymbol{N}} - \boldsymbol{\Lambda}^\top\boldsymbol{v}_{\varphi,s} - \boldsymbol{J}_{\boldsymbol{N}}^\top\boldsymbol{v}_d\right)_\Omega = 0, \tag{4.29e}$$
$$\left(\delta\boldsymbol{M}, \boldsymbol{C}_M\dot{\boldsymbol{M}} - \mathcal{J}_{\boldsymbol{K}}\boldsymbol{v}_d\right)_\Omega = 0, \tag{4.29f}$$
$$\left(\delta\boldsymbol{\lambda}, \boldsymbol{G}_d\boldsymbol{v}_d\right)_\Omega = 0, \tag{4.29g}$$

for all test functions from appropriate spaces. This weak form can also be linked to a Hellinger–Reissner principle, as shown in Appendix 4.B.2.

Remark 4.3. *The weak form* (4.29) *is valid if the Dirichlet boundary conditions are considered in the space of admissible test functions. However, if the Dirichlet boundary conditions are enforced in a weak sense, the weak form must be slightly modified, e.g., by introducing additional Lagrange multipliers and accounting for the prescribed boundary values. In general, enforcing non-homogeneous mixed boundary conditions for pH systems requires additional care [45, 46, 217, 218].* ♧

Remark 4.4. *Notably the presented formulation also satisfies the fundamental balance of total angular momentum, which can be shown by means of the weak form* (4.29)*, as proven in Appendix 4.D.* ♧

4.3.4. Objectivity

Let us discuss how the presented formulation, with weak form (4.29), behaves under superimposed rigid body motions, or, for that matter equivalently, a change of observer. To this end, consider $\boldsymbol{c}(t) \in \mathbb{R}^3$ and $\boldsymbol{P}(t) \in SO(3)$ that prescribe superimposed finite translations and rotations of the beam. Thus, the kinematic quantities change as

$$\boldsymbol{\varphi}^\# = \boldsymbol{c} + \boldsymbol{P}\boldsymbol{\varphi}, \qquad \boldsymbol{d}_i^\# = \boldsymbol{P}\boldsymbol{d}_i, \qquad \boldsymbol{v}_\varphi^\# = \dot{\boldsymbol{c}} + \boldsymbol{P}\boldsymbol{v}_\varphi + \dot{\boldsymbol{P}}\boldsymbol{\varphi}, \qquad \boldsymbol{v}_{d,i}^\# = \boldsymbol{P}\boldsymbol{v}_{d,i} + \dot{\boldsymbol{P}}\boldsymbol{d}_i \tag{4.30}$$

for $i \in \{1, 2, 3\}$, Here, $\square^\#$ denotes a transformed quantity taking into account the superimposed rigid body motion. The external distributed loads transform as

$$\bar{\boldsymbol{n}}^\# = \boldsymbol{P}\bar{\boldsymbol{n}}, \qquad \bar{\boldsymbol{m}}^\# = \boldsymbol{P}\bar{\boldsymbol{m}}. \tag{4.31}$$

The material strains (4.3) remain invariant under that transformation, see also [33, p. 1781] and [193, p. 1689]. Correspondingly, it can be stated that

$$\boldsymbol{\Gamma}(\boldsymbol{d}^\#, \partial_s\boldsymbol{\varphi}^\#) = \boldsymbol{\Gamma}(\boldsymbol{d}, \partial_s\boldsymbol{\varphi}), \qquad \boldsymbol{K}(\boldsymbol{d}^\#, \partial_s\boldsymbol{d}^\#) = \boldsymbol{K}(\boldsymbol{d}, \partial_s\boldsymbol{d}). \tag{4.32}$$

Using $\dot{\boldsymbol{P}}^\top\boldsymbol{P} + \boldsymbol{P}^\top\dot{\boldsymbol{P}} = \boldsymbol{0}$, it can also be shown that the corresponding strain rates $\dot{\boldsymbol{\Gamma}}$ and $\dot{\boldsymbol{K}}$ are unaltered such that the compliance equations in time-differentiated form (4.18) are identically satisfied by transformed

quantities. This ensures the objectivity of the stress measures and their time-derivatives. Further, the orthonormality constraints on velocity level (4.19) are not affected by such superimposed rigid body motions. Lastly, pre-multiplying the kinematic relation (4.16) and the balance equations (4.17) with $\boldsymbol{P}$ and $\mathrm{diag}(\boldsymbol{P}, \boldsymbol{P}, \boldsymbol{P})$, respectively, yields again the same relations expressed in the transformed quantities.

This proof may alternatively be done by means of the weak form (4.29) with the appropriately transformed test functions. Consequently, the present mixed formulation for pH geometrically exact beams is objective. Notably, this property is not altered by the discretization methods proposed in the subsequent section, cf. Remark 4.5.

4.4. Structure-preserving discretization

4.4.1. Discretization in space

We pursue a structure-preserving discretization in space using a mixed FE method as for the 2D case in [A2], see also Section 3.4 of the present work. The pH system for the Cosserat rod dynamics (4.21) is readily available for spatial discretization via its weak form (4.29).

Discretization ansatz. We discretize the domain into n_e finite elements, i.e., $\Omega = \cup_{e=1}^{n_\mathrm{e}} \Omega^e$, according to general standard procedures [115]. Depending on the choice of ansatz functions this corresponds to n_n nodes on the FE grid. Displacement and velocity quantities $(\boldsymbol{q}, \boldsymbol{v})$ are approximated with $\mathscr{C}^0$-continuous, Lagrangian polynomial ansatz functions of order p, while stress type quantities $\boldsymbol{\sigma}$ use discontinuous Lagrangian polynomial ansatz functions of order $p-1$. The corresponding spaces are denoted

$$\begin{aligned}
\mathcal{V}_\mathrm{h} &= \left\{ \boldsymbol{q}_\mathrm{h} \in \mathscr{H}^1(\Omega, \mathbb{R}^{12}) \,\middle|\, \boldsymbol{q}_\mathrm{h}|_{\Omega^e} \in \mathscr{P}^p(\Omega^e, \mathbb{R}^{12}) \,\forall\, \Omega^e \in \Omega, \boldsymbol{q}_\mathrm{h}|_{\partial\Omega_\mathrm{D}} = \boldsymbol{q}_\mathrm{D} \right\}, \\
\mathcal{V}_\mathrm{h}^0 &= \left\{ \boldsymbol{q}_\mathrm{h} \in \mathscr{H}^1(\Omega, \mathbb{R}^{12}) \,\middle|\, \boldsymbol{q}_\mathrm{h}|_{\Omega^e} \in \mathscr{P}^p(\Omega^e, \mathbb{R}^{12}) \,\forall\, \Omega^e \in \Omega, \boldsymbol{q}_\mathrm{h}|_{\partial\Omega_\mathrm{D}} = \boldsymbol{0} \right\}, \\
\mathcal{S}_\mathrm{h} &= \left\{ \boldsymbol{\sigma}_\mathrm{h} \in \mathscr{L}^2(\Omega, \mathbb{R}^6) \,\middle|\, \boldsymbol{\sigma}_\mathrm{h}|_{\Omega^e} \in \mathscr{P}^{p-1}(\Omega^e, \mathbb{R}^6) \,\forall\, \Omega^e \in \Omega \right\},
\end{aligned} \tag{4.33}$$

for $p \in \{1, 2\}$, where $\square_\mathrm{h}$ denotes an approximation. Moreover, $\mathscr{H}^1$ denotes the Sobolev space of square-integrable functions with square-integrable first derivatives, $\mathscr{L}^2$ the space of square-integrable functions and $\mathscr{P}^p$ is the space of polynomial functions of order p. By this choice, we have $n_\mathrm{n} = n_\mathrm{e}\, p + 1$.

The Lagrange multipliers are evaluated collocation-wise, i.e., with discrete values at the nodes and zero elsewhere, their approximated space denoted as $\mathcal{L}_\mathrm{h}$. This can be formally realized via delta functions [13, Chapter 1.11]. Correspondingly, the orthonormality of the directors (4.19) is relaxed to nodal points of the FE mesh. This facilitates the use of Lagrange polynomials for $(\boldsymbol{q}, \boldsymbol{v})$ and is a common approach in the literature [31, 33, 193]. Alternatively, a weak enforcement can be employed, see [100, 235]. Concerning the interpolation between nodes, "*the lack of orthonormality of the director frame can be regarded as a discretization error, which diminishes if the number of elements is increased*"[67]. As employed later, an interpolation using quadratic ansatz functions yields practically indistinguishable interpolations compared to an $SE(3)$-finite element accounting for the correct manifold, see Figure 2 in [69].

The discrete weak formulation using a Bubnov–Galerkin approach is then stated as follows. Find $(\boldsymbol{q}_\mathrm{h}, \boldsymbol{v}_\mathrm{h}, \boldsymbol{\sigma}_\mathrm{h}, \boldsymbol{\lambda}_\mathrm{h}) \in \mathcal{V}_\mathrm{h} \times \mathcal{V}_\mathrm{h} \times \mathcal{S}_\mathrm{h} \times \mathcal{L}_\mathrm{h}$, such that (4.29) holds for all $(\delta\boldsymbol{q}_\mathrm{h}, \delta\boldsymbol{v}_\mathrm{h}, \delta\boldsymbol{\sigma}_\mathrm{h}, \delta\boldsymbol{\lambda}_\mathrm{h}) \in \mathcal{V}_\mathrm{h}^0 \times \mathcal{V}_\mathrm{h}^0 \times \mathcal{S}_\mathrm{h} \times \mathcal{L}_\mathrm{h}$. To this end, we formulate the approximative quantities by means of ansatz matrices $\boldsymbol{\Phi}, \boldsymbol{\Psi}, \boldsymbol{\Xi}$ as

$$\begin{aligned} \boldsymbol{q}_\mathrm{h}(s,t) &= \boldsymbol{\Phi}(s)\hat{\boldsymbol{q}}(t) \in \mathcal{V}_\mathrm{h}, \qquad & \boldsymbol{v}_\mathrm{h}(s,t) &= \boldsymbol{\Phi}(s)\hat{\boldsymbol{v}}(t) \in \mathcal{V}_\mathrm{h}, \\ \boldsymbol{\sigma}_\mathrm{h}(s,t) &= \boldsymbol{\Psi}(s)\hat{\boldsymbol{\sigma}}(t) \in \mathcal{S}_\mathrm{h}, \qquad & \boldsymbol{\lambda}_\mathrm{h}(s,t) &= \boldsymbol{\Xi}(s)\hat{\boldsymbol{\lambda}}(t) \in \mathcal{L}_\mathrm{h}, \end{aligned} \tag{4.34}$$

where $\hat{\boldsymbol{q}}, \hat{\boldsymbol{v}} \in \mathbb{R}^{12(n_\mathrm{e}p+1)}$, $\hat{\boldsymbol{\sigma}} \in \mathbb{R}^{6n_\mathrm{e}p}$ and $\hat{\boldsymbol{\lambda}} \in \mathbb{R}^{6(n_\mathrm{e}p+1)}$ contain the unknowns from all finite elements and the respective nodes. Moreover, for the approximation of the corresponding test function $\delta\square_\mathrm{h}$ consider the same approximation ansatz as for the function $\square_\mathrm{h}$. In this context, the above ansatz matrices contain the polynomial ansatz functions, e.g., $\boldsymbol{q}_\mathrm{h}(s,t) = \boldsymbol{\Phi}(s)\hat{\boldsymbol{q}}(t) = \sum_{i=1}^{n_\mathrm{n}} N_i(s)\hat{\boldsymbol{q}}_i(t)$. Therein, N_i are basis functions for $\mathscr{P}^p(\Omega)$. For further details see Appendix 3.B of the previous chapter dealing with the planar case. We further follow common FE procedures, see for instance [115], which also includes an assembly of the global system matrices and vectors accounting for the respective degrees of freedom. Additionally, we perform all computations on element level and consider the isoparametric concept to transform all calculations to a standard reference element with $\xi \in \hat{\Omega} = [-1, 1]$.

Finite-dimensional pH system. The discrete system dynamics are obtained by approximating the weak form (4.29) with the ansatz spaces (4.34). Taking into account the arbitrariness of the test function nodal values, we obtain the pH differential-algebraic equations (pH DAE)

$$\begin{bmatrix} \boldsymbol{I} & 0 & 0 & 0 \\ 0 & \hat{\boldsymbol{M}}_o & 0 & 0 \\ 0 & 0 & \hat{\boldsymbol{C}} & 0 \\ 0 & 0 & 0 & \boldsymbol{0} \end{bmatrix} \frac{\mathrm{d}}{\mathrm{d}t} \begin{bmatrix} \hat{\boldsymbol{q}} \\ \hat{\boldsymbol{v}} \\ \hat{\boldsymbol{\sigma}} \\ \hat{\boldsymbol{\lambda}} \end{bmatrix} = \begin{bmatrix} 0 & \boldsymbol{I} & 0 & 0 \\ -\boldsymbol{I} & 0 & -\hat{\boldsymbol{J}}_{\sigma v}(\hat{\boldsymbol{q}})^\top & -\hat{\boldsymbol{G}}(\hat{\boldsymbol{q}})^\top \\ 0 & \hat{\boldsymbol{J}}_{\sigma v}(\hat{\boldsymbol{q}}) & 0 & 0 \\ 0 & \hat{\boldsymbol{G}}(\hat{\boldsymbol{q}}) & 0 & 0 \end{bmatrix} \begin{bmatrix} \boldsymbol{0} \\ \hat{\boldsymbol{v}} \\ \hat{\boldsymbol{\sigma}} \\ \hat{\boldsymbol{\lambda}} \end{bmatrix} + \begin{bmatrix} 0 & 0 \\ \hat{\boldsymbol{B}}_\Omega & \hat{\boldsymbol{B}}_\partial \\ 0 & 0 \\ 0 & 0 \end{bmatrix} \begin{bmatrix} \hat{\boldsymbol{u}}_\Omega \\ \boldsymbol{u}_\partial \end{bmatrix}. \tag{4.35}$$

The discrete system matrices can be found in Appendix 4.E. Analogously to the infinite-dimensional version (4.22), we can recast the semi-discrete set of equations in a pH framework [23, 161, 162] given by

$$\begin{aligned} \boldsymbol{E}\frac{\mathrm{d}}{\mathrm{d}t}\hat{\boldsymbol{x}} &= \boldsymbol{J}(\hat{\boldsymbol{x}})\hat{\boldsymbol{z}}(\hat{\boldsymbol{x}}) + \boldsymbol{B}(\hat{\boldsymbol{x}})\hat{\boldsymbol{u}}, \\ \hat{\boldsymbol{y}} &= \boldsymbol{B}(\hat{\boldsymbol{x}})^\top \hat{\boldsymbol{z}}(\hat{\boldsymbol{x}}), \end{aligned} \tag{4.36}$$

where we have appended the discrete output equations for $\hat{\boldsymbol{y}} = (\hat{\boldsymbol{y}}_\Omega, \hat{\boldsymbol{y}}_\partial)$, containing both distributed nodal as well as boundary terms. These quantities have the physical interpretation of velocities, that are power-conjugated to the nodal distributed and boundary input forces and torques. See Appendix 4.E for more details and Section 2.3 for a detailed introduction to such a pH descriptor system formulation. Here, the finite-dimensional version of the state (4.23) contains the degrees of freedom of all finite elements and is given by

$$\hat{\boldsymbol{x}} = (\hat{\boldsymbol{q}}, \hat{\boldsymbol{v}}, \hat{\boldsymbol{\sigma}}, \hat{\boldsymbol{\lambda}}). \tag{4.37}$$

Inserting the ansatz (4.34) into (4.25) gives rise to the approximated Hamiltonian

$$\mathcal{H}(\boldsymbol{x}_\mathrm{h}) = \hat{\mathcal{H}}(\hat{\boldsymbol{x}}) = \frac{1}{2}\hat{\boldsymbol{v}}^\top \hat{\boldsymbol{M}}_o \hat{\boldsymbol{v}} + \frac{1}{2}\hat{\boldsymbol{\sigma}}^\top \hat{\boldsymbol{C}}\hat{\boldsymbol{\sigma}} = \frac{1}{2}\hat{\boldsymbol{x}}^\top \boldsymbol{Q}\boldsymbol{E}\hat{\boldsymbol{x}}, \tag{4.38}$$

where $\boldsymbol{Q} = \mathrm{diag}(\boldsymbol{0}, \boldsymbol{I}, \boldsymbol{I}, \boldsymbol{I})$, $\boldsymbol{E} = \mathrm{diag}(\boldsymbol{I}, \hat{\boldsymbol{M}}_o, \hat{\boldsymbol{C}}, \boldsymbol{0})$ and further system matrices can be found in Appendix 4.E.

Port-Hamiltonian structure and power balance. We can again check the pH structure of the equations at hand. Firstly, corresponding to condition (i) from the infinite-dimensional setting, it can be stated that

$$\boldsymbol{E}^\top \hat{\boldsymbol{z}}(\hat{\boldsymbol{x}}) = \nabla \hat{\mathcal{H}}(\hat{\boldsymbol{x}}) \tag{4.39}$$

holds true for the semi-discrete system because of the discrete Hamiltonian (4.38) and the definitions of $\boldsymbol{E}$ and $\hat{\boldsymbol{z}}(\hat{\boldsymbol{x}}) = \boldsymbol{Q}\hat{\boldsymbol{x}}$ in the pH DAE (4.35). Secondly, the formally skew-adjoint nature of the structure operator $\mathcal{J}$ has been retained as skew-symmetry of the structure matrix $\boldsymbol{J}(\hat{\boldsymbol{x}}) = -\boldsymbol{J}(\hat{\boldsymbol{x}})^\top$ in (4.35). Note that the state-dependence of $\boldsymbol{J}$ highlights the geometric nonlinearity of the problem at hand[3]. This corresponds to condition (ii) from the infinite-dimensional setting.

As already discussed, one core property of the pH formulation is that it satisfies a formalized power balance equation, see (4.28). Since (4.36) is a discrete pH DAE system, it satisfies the semi-discrete power balance equation

$$\frac{\mathrm{d}}{\mathrm{d}t}\hat{\mathcal{H}} = \nabla \hat{\mathcal{H}}(\hat{\boldsymbol{x}})^\top \frac{\mathrm{d}}{\mathrm{d}t}\hat{\boldsymbol{x}} = \hat{\boldsymbol{z}}(\hat{\boldsymbol{x}})^\top \boldsymbol{E}\frac{\mathrm{d}}{\mathrm{d}t}\hat{\boldsymbol{x}} = \hat{\boldsymbol{z}}(\hat{\boldsymbol{x}})^\top \left(\boldsymbol{J}(\hat{\boldsymbol{x}})\hat{\boldsymbol{z}}(\hat{\boldsymbol{x}}) + \boldsymbol{B}(\hat{\boldsymbol{x}})\hat{\boldsymbol{u}}\right) = \hat{\boldsymbol{y}}^\top \hat{\boldsymbol{u}}, \tag{4.40}$$

where we have made use of (4.36), (4.39) and the skew-symmetry of $\boldsymbol{J}(\hat{\boldsymbol{x}})$. The equation resembles a discrete version of (4.28), showcasing that the property of passivity and losslessness has been preserved within the discretization procedure.

Remark 4.5. *We have outlined how to prove the objectivity of the present beam formulation in Section 4.3.4. The same property is retained by the present space discretization and the proof is conducted in a completely analogous manner as before. To this end, keep in mind that spatial approximations are mere linear combinations of the nodal unknowns, e.g.,*

$$(\boldsymbol{\varphi}_\mathrm{h})^\# = \sum_{i=1}^{n_n} N_i(s)\hat{\boldsymbol{\varphi}}_i^\#(t), \tag{4.41}$$

such that discretization and superimposition of rigid body motions commute. Consequently, the objectivity is inherited from the pure displacement-based formulations [33, 193], see also numerical verifications in the cited references. ♧

4.4.2. Discretization in time

We further aim at a structure-preserving time discretization of the pH DAE (4.36). To this end, we apply the implicit mid-point rule. Let $\hat{\boldsymbol{x}}^n \approx \hat{\boldsymbol{x}}(t^n)$ at time instance t^n and consider an equidistant time-grid such that $\mathbb{T} = [0, t_\mathrm{end}] = \cup_{n=0}^{N}[t^n, t^{n+1}]$ with $N \geq 1$ time steps of constant size $h = t^{n+1} - t^n > 0$. The time-stepping scheme we propose reads

$$\begin{aligned} \boldsymbol{E}\left(\hat{\boldsymbol{x}}^{n+1} - \hat{\boldsymbol{x}}^n\right) &= h\,\boldsymbol{J}(\hat{\boldsymbol{x}}^{n+1/2})\hat{\boldsymbol{z}}(\hat{\boldsymbol{x}}^{n+1/2}) + h\,\boldsymbol{B}(\hat{\boldsymbol{x}}^{n+1/2})\hat{\boldsymbol{u}}^{n+1/2}, \\ \hat{\boldsymbol{y}}^{n+1/2} &= \boldsymbol{B}(\hat{\boldsymbol{x}}^{n+1/2})^\top \hat{\boldsymbol{z}}(\hat{\boldsymbol{x}}^{n+1/2}), \end{aligned} \tag{4.42}$$

for $n = 0, \ldots, N-1$, where the midpoint state $\hat{\boldsymbol{x}}^{n+1/2} := \frac{1}{2}(\hat{\boldsymbol{x}}^{n+1} + \hat{\boldsymbol{x}}^n)$ and $\hat{\boldsymbol{u}}^{n+1/2} = \hat{\boldsymbol{u}}(t^{n+1/2})$. Correspondingly, $\hat{\boldsymbol{y}}^{n+1/2} \approx \hat{\boldsymbol{y}}(t^{n+1/2})$. Additionally, the time-discrete costate vector $\hat{\boldsymbol{z}}(\hat{\boldsymbol{x}}^{n+1/2})$ verifies

$$\boldsymbol{E}^\top \hat{\boldsymbol{z}}(\hat{\boldsymbol{x}}^{n+1/2}) = \nabla \hat{\mathcal{H}}(\hat{\boldsymbol{x}}^{n+1/2}), \tag{4.43}$$

[3] This property is discussed in Chapter 2 of the present work by means of a model problem, cf. Example 2.3.

since this is a mere pointwise evaluation of (4.39).

The structure-preserving scheme is energy-consistent and second-order accurate. Let us demonstrate that an exact energy balance in discrete time is obtained. For at most quadratic Hamiltonians, like here (4.38), the midpoint-evaluated gradient satisfies the directionality property[4], which mimics the chain rule in the discrete time setting such that $\nabla\hat{\mathcal{H}}(\hat{\boldsymbol{x}}^{n+1/2})^\top\left(\hat{\boldsymbol{x}}^{n+1}-\hat{\boldsymbol{x}}^{n}\right)=\hat{\mathcal{H}}(\hat{\boldsymbol{x}}^{n+1})-\hat{\mathcal{H}}(\hat{\boldsymbol{x}}^{n})$, see also Remark 4.7. Exploiting this property we obtain

$$\begin{aligned}\hat{\mathcal{H}}(\hat{\boldsymbol{x}}^{n+1})-\hat{\mathcal{H}}(\hat{\boldsymbol{x}}^{n}) &= \nabla\hat{\mathcal{H}}(\hat{\boldsymbol{x}}^{n+1/2})^\top\left(\hat{\boldsymbol{x}}^{n+1}-\hat{\boldsymbol{x}}^{n}\right)\\ &= \hat{\boldsymbol{z}}(\hat{\boldsymbol{x}}^{n+1/2})^\top\boldsymbol{E}\left(\hat{\boldsymbol{x}}^{n+1}-\hat{\boldsymbol{x}}^{n}\right)\\ &= h\hat{\boldsymbol{z}}(\hat{\boldsymbol{x}}^{n+1/2})^\top\left(\boldsymbol{J}(\hat{\boldsymbol{x}}^{n+1/2})\hat{\boldsymbol{z}}(\hat{\boldsymbol{x}}^{n+1/2})+\boldsymbol{B}(\hat{\boldsymbol{x}}^{n+1/2})\hat{\boldsymbol{u}}^{n+1/2}\right)\\ &= h\,(\hat{\boldsymbol{y}}^{n+1/2})^\top\hat{\boldsymbol{u}}^{n+1/2},\end{aligned} \tag{4.44}$$

where we have used (4.42), (4.43) and the skew-symmetry of $\boldsymbol{J}$, analogously to the continuous-time derivation (4.40). This proves that the present time-stepping scheme exhibits passivity and losslessness (which includes energy-conservation in the case of vanishing inputs).

Remark 4.6. *The presented time discretization also respects the balance of total angular momentum, see Appendix 4.D.* ♧

Remark 4.7. *The above directionality condition can be traced back to the mean value theorem. In fact, given an at most quadratic polynomial function $f\in\mathscr{C}^1(\mathbb{R}^d,\mathbb{R})$, $f(\boldsymbol{b})-f(\boldsymbol{a})=\nabla f(\frac{\boldsymbol{a}+\boldsymbol{b}}{2})^\top(\boldsymbol{b}-\boldsymbol{a})$, for any $\boldsymbol{a},\boldsymbol{b}\in\mathbb{R}^d$. Likewise, this property extends to bilinear, vector-valued functions of two arguments $\boldsymbol{f}\in\mathscr{C}^1(\mathbb{R}^d\times\mathbb{R}^d,\mathbb{R}^l)$ such that $\boldsymbol{f}(\boldsymbol{b},\boldsymbol{d})-\boldsymbol{f}(\boldsymbol{a},\boldsymbol{c})=\boldsymbol{f}(\frac{\boldsymbol{a}+\boldsymbol{b}}{2},\boldsymbol{d}-\boldsymbol{c})+\boldsymbol{f}(\boldsymbol{b}-\boldsymbol{a},\frac{\boldsymbol{c}+\boldsymbol{d}}{2})$, for any $\boldsymbol{a},\boldsymbol{b},\boldsymbol{c},\boldsymbol{d}\in\mathbb{R}^d$.* ♧

4.4.3. Kinematic consistency in discrete time

This section is concerned with two aspects regarding the approximated kinematics of the proposed model. Firstly, the orthonormality constraint (4.12c) is satisfied by the proposed time integration approach despite using the velocity-level constraint (4.19). To show this, consider the first line of (4.35), which is discretized in time by means of (4.42) such that we obtain the discrete time kinematics for the directors

$$\hat{\boldsymbol{d}}_k^{n+1}-\hat{\boldsymbol{d}}_k^{n}=h\hat{\boldsymbol{v}}_{d,k}^{n+1/2}, \tag{4.45}$$

for each FE node k. Note that $\hat{\boldsymbol{d}}_k\in\mathbb{R}^9$ refers to all three director unknowns at node k. Furthermore, the fourth line of (4.35), which is discretized in time by means of (4.42), yields

$$\boldsymbol{G}_d(\hat{\boldsymbol{d}}_k^{n+1/2})\hat{\boldsymbol{v}}_{d,k}^{n+1/2}=\boldsymbol{0}, \tag{4.46}$$

for each node k, see further details in relations (4.120) and (4.121) in the Appendix. We can now make use of Remark 4.7, since the orthonormality constraints (4.2) are quadratic and (4.46) contains the constraint Jacobian $\boldsymbol{G}_d(\boldsymbol{d})=\mathrm{D}\boldsymbol{g}(\boldsymbol{d})$. Substituting (4.45) in (4.46) for the midpoint velocities, one thus obtains

$$\boldsymbol{0}=\mathrm{D}\boldsymbol{g}(\hat{\boldsymbol{d}}_k^{n+1/2})(\hat{\boldsymbol{d}}_k^{n+1}-\hat{\boldsymbol{d}}_k^{n})=\boldsymbol{g}(\hat{\boldsymbol{d}}_k^{n+1})-\boldsymbol{g}(\hat{\boldsymbol{d}}_k^{n}) \tag{4.47}$$

[4] This property can also be exploited for more general Hamiltonians when using discrete gradient methods [97, C2, C4]. This scenario is discussed for the case of geometrically exact strings in Chapter 6 of this work. More details on discrete gradients can be found in Chapter 5.

for all k. Eventually, given a consistent initial choice of orthonormal directors $(\hat{\boldsymbol{d}}_k)_0$ the constraints

$$\boldsymbol{g}(\hat{\boldsymbol{d}}_k^n) = \boldsymbol{0} \tag{4.48}$$

are exactly fulfilled for all k, $n \geq 1$. Thus, the orthonormality constraint is satisfied at each FE node in each discrete point in time. This is due to the structure-preserving midpoint time discretization of the velocity-level constraints (4.19) pertaining to the present pH model.

Consistent strain approximation. Further, we can show that the discrete strains calculated from the independent stresses via (4.10)

$$\boldsymbol{\Gamma}_{\mathrm{h}}^n := \boldsymbol{C}_N \boldsymbol{N}_{\mathrm{h}}^n + \boldsymbol{\Gamma}_0, \qquad \boldsymbol{K}_{\mathrm{h}}^n := \boldsymbol{C}_M \boldsymbol{M}_{\mathrm{h}}^n + \boldsymbol{K}_0 \tag{4.49}$$

are variationally consistent with the discrete strains computed in terms of the displacement quantities (4.4), i.e., $\boldsymbol{\Gamma}(\boldsymbol{\varphi}_{\mathrm{h}}^n, \boldsymbol{d}_{\mathrm{h}}^n)$ and $\boldsymbol{K}(\boldsymbol{d}_{\mathrm{h}}^n)$. Note our Remark 4.1 on the assumed reference strains $\boldsymbol{\Gamma}_0$, $\boldsymbol{K}_0$. This consistency ensures a physically valid approximation in each time instance despite the fact that the pH model is based on the evolution equations (4.18). Hereto, we evaluate (4.4) in the different time instances and use the findings from Remark 4.7 due to the bilinearity of the strain functions. This yields

$$\begin{aligned} \boldsymbol{\Gamma}(\boldsymbol{\varphi}_{\mathrm{h}}^{n+1}, \boldsymbol{d}_{\mathrm{h}}^{n+1}) - \boldsymbol{\Gamma}(\boldsymbol{\varphi}_{\mathrm{h}}^n, \boldsymbol{d}_{\mathrm{h}}^n) &= \boldsymbol{\Lambda}(\boldsymbol{d}_{\mathrm{h}}^{n+1/2})^\top \partial_s(\boldsymbol{\varphi}_{\mathrm{h}}^{n+1} - \boldsymbol{\varphi}_{\mathrm{h}}^n) + \boldsymbol{J}_{\boldsymbol{N}}(\partial_s \boldsymbol{\varphi}_{\mathrm{h}}^{n+1/2})^\top (\boldsymbol{d}_{\mathrm{h}}^{n+1} - \boldsymbol{d}_{\mathrm{h}}^n), \\ \boldsymbol{K}(\boldsymbol{d}_{\mathrm{h}}^{n+1}) - \boldsymbol{K}(\boldsymbol{d}_{\mathrm{h}}^n) &= \boldsymbol{L}(\partial_s \boldsymbol{d}_{\mathrm{h}}^{n+1/2})(\boldsymbol{d}_{\mathrm{h}}^{n+1} - \boldsymbol{d}_{\mathrm{h}}^n) - \boldsymbol{L}(\boldsymbol{d}_{\mathrm{h}}^{n+1/2}) \partial_s(\boldsymbol{d}_{\mathrm{h}}^{n+1} - \boldsymbol{d}_{\mathrm{h}}^n). \end{aligned} \tag{4.50}$$

On the other hand, consider the third line of (4.35), which is discretized in time by means of (4.42). The equivalent discrete space and time versions of the weak forms (4.29e) and (4.29f) are given by

$$\begin{aligned} \left(\delta \boldsymbol{N}_{\mathrm{h}}, \boldsymbol{\Gamma}_{\mathrm{h}}^{n+1} - \boldsymbol{\Gamma}_{\mathrm{h}}^n - h\boldsymbol{\Lambda}(\boldsymbol{d}_{\mathrm{h}}^{n+1/2})^\top \partial_s \boldsymbol{v}_{\varphi,\mathrm{h}}^{n+1/2} - h\boldsymbol{J}_{\boldsymbol{N}}(\boldsymbol{\varphi}_{\mathrm{h}}^{n+1/2})^\top \boldsymbol{v}_{d,\mathrm{h}}^{n+1/2}\right)_\Omega &= 0, \\ \left(\delta \boldsymbol{M}_{\mathrm{h}}, \boldsymbol{K}_{\mathrm{h}}^{n+1} - \boldsymbol{K}_{\mathrm{h}}^n - h\mathcal{J}_{\boldsymbol{K}}(\boldsymbol{d}_{\mathrm{h}}^{n+1/2}) \boldsymbol{v}_{d,\mathrm{h}}^{n+1/2}\right)_\Omega &= 0. \end{aligned} \tag{4.51}$$

We may now use $\boldsymbol{\varphi}_{\mathrm{h}}^{n+1} - \boldsymbol{\varphi}_{\mathrm{h}}^n = h\boldsymbol{v}_{\varphi,\mathrm{h}}^{n+1/2}$ and $\boldsymbol{d}_{\mathrm{h}}^{n+1} - \boldsymbol{d}_{\mathrm{h}}^n = h\boldsymbol{v}_{d,\mathrm{h}}^{n+1/2}$, which are equivalent to the time-discretized first line of (4.35), and account for the definition (4.13) of $\mathcal{J}_{\boldsymbol{K}}$. Eventually, taking into account (4.50), (4.51) yields

$$\begin{aligned} \left(\delta \boldsymbol{N}_{\mathrm{h}}, \boldsymbol{\Gamma}_{\mathrm{h}}^{n+1} - \boldsymbol{\Gamma}_{\mathrm{h}}^n - \left(\boldsymbol{\Gamma}(\boldsymbol{\varphi}_{\mathrm{h}}^{n+1}, \boldsymbol{d}_{\mathrm{h}}^{n+1}) - \boldsymbol{\Gamma}(\boldsymbol{\varphi}_{\mathrm{h}}^n, \boldsymbol{d}_{\mathrm{h}}^n)\right)\right)_\Omega &= 0, \\ \left(\delta \boldsymbol{M}_{\mathrm{h}}, \boldsymbol{K}_{\mathrm{h}}^{n+1} - \boldsymbol{K}_{\mathrm{h}}^n - \left(\boldsymbol{K}(\boldsymbol{d}_{\mathrm{h}}^{n+1}) - \boldsymbol{K}(\boldsymbol{d}_{\mathrm{h}}^n)\right)\right)_\Omega &= 0, \end{aligned} \tag{4.52}$$

for all $n \geq 0$. We now assume initial values for the stress variables $\boldsymbol{N}_{\mathrm{h}}^0$, $\boldsymbol{M}_{\mathrm{h}}^0$ that, through (4.49), induce consistent strain measures satisfying $\boldsymbol{\Gamma}_{\mathrm{h}}^0 = \boldsymbol{\Gamma}(\boldsymbol{\varphi}_{\mathrm{h}}^0, \boldsymbol{d}_{\mathrm{h}}^0)$ and $\boldsymbol{K}_{\mathrm{h}}^0 = \boldsymbol{K}(\boldsymbol{d}_{\mathrm{h}}^0)$. This yields the variational identities

$$\begin{aligned} \left(\delta \boldsymbol{N}_{\mathrm{h}}, \boldsymbol{\Gamma}_{\mathrm{h}}^0 - \boldsymbol{\Gamma}(\boldsymbol{\varphi}_{\mathrm{h}}^0, \boldsymbol{d}_{\mathrm{h}}^0)\right)_\Omega &= 0, \\ \left(\delta \boldsymbol{M}_{\mathrm{h}}, \boldsymbol{K}_{\mathrm{h}}^0 - \boldsymbol{K}(\boldsymbol{d}_{\mathrm{h}}^0)\right)_\Omega &= 0. \end{aligned} \tag{4.53}$$

Eventually, (4.52) yields the result

$$\begin{aligned} \left(\delta \boldsymbol{N}_{\mathrm{h}}, \boldsymbol{\Gamma}_{\mathrm{h}}^{n+1} - \boldsymbol{\Gamma}(\boldsymbol{\varphi}_{\mathrm{h}}^{n+1}, \boldsymbol{d}_{\mathrm{h}}^{n+1})\right)_\Omega &= 0, \\ \left(\delta \boldsymbol{M}_{\mathrm{h}}, \boldsymbol{K}_{\mathrm{h}}^{n+1} - \boldsymbol{K}(\boldsymbol{d}_{\mathrm{h}}^{n+1})\right)_\Omega &= 0, \end{aligned} \tag{4.54}$$

for all $n \geq 0$. Consequently, despite the original rate form of the underlying pH formulation, consistent values for $\boldsymbol{\Gamma}_{\mathrm{h}}^{n+1}$ and $\boldsymbol{K}_{\mathrm{h}}^{n+1}$ are recovered at discrete times t^{n+1}. By (4.49), this implies variationally consistent mixed stress quantities $\boldsymbol{N}_{\mathrm{h}}^{n+1}$ and $\boldsymbol{M}_{\mathrm{h}}^{n+1}$.

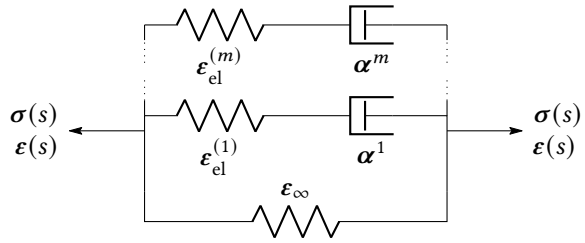

Figure 4.2.: Schematic rheological model for the generalized-Maxwell approach.

4.5. Extension of the model

In practical applications, such as soft robotics, viscoelastic material behavior and actuation via pneumatic chambers and tendons are highly relevant. To this end, we show in this section that the inclusion of such concepts into the pH formulation (4.21) is seamlessly possible. These extensions do not interfere with the discretization procedure from the previous chapter.

4.5.1. Extension to viscoelasticity

We target an extension to viscoelastic material behavior using the generalized-Maxwell model. It represents an *internal variable model* and has been discussed in, e.g., [75, 140, 236] in the context of Cosserat rods, or [A1] for geometrically exact strings (see also Chapter 6). While we apply this approach to each strain measure separately, some works only include damping for the bending behaviour [140].

The model consists of an elastic element and $m \geq 1$ viscous Maxwell elements in parallel, see the rheological model in Figure 4.2. It is also referred to as *generalized relaxation model*, see [204, Chapter 10]. In this context, each additional branch introduces new material parameters, allowing for a more precise modeling of the time-dependent material behavior compared to, for example, the common Kelvin-Voigt model [144]. For the sake of the deductions in this section, consider $\boldsymbol{\varepsilon} = (\boldsymbol{\Gamma}, \boldsymbol{K})$ as well as the definition of the stress quantities $\boldsymbol{\sigma}$ and the compliance matrix $\boldsymbol{C}$, see (4.20).

Due to the structure of the model, the stress quantities of all branches add up to the total stress,

$$\boldsymbol{\sigma} = \boldsymbol{\sigma}_\infty + \sum_{i=1}^{m} \boldsymbol{\sigma}_{\text{el}}^{(i)}, \tag{4.55}$$

where $\boldsymbol{\sigma}_\infty$ is the long-term elastic stress and $\boldsymbol{\sigma}_{\text{el}}^{(i)}$ are the individual stress contributions of each branch. Note that in each viscous branch the elastic stress is equal to the viscous stress in the Maxwell element $\boldsymbol{\sigma}_{\text{el}}^{(i)} = \boldsymbol{\sigma}_{\text{visc}}^{(i)}$. Moreover, the total strain is equal to the strain in each branch, i.e.,

$$\boldsymbol{\varepsilon}(\boldsymbol{\varphi}, \boldsymbol{d}) = \boldsymbol{\varepsilon}_\infty = \boldsymbol{\varepsilon}_{\text{el}}^{(i)} + \boldsymbol{\alpha}^{(i)}, \tag{4.56}$$

for each i, where $\boldsymbol{\alpha}^{(i)}$ is the viscous strain in the damper element of the respective branch and $\boldsymbol{\varepsilon}_\infty$ is the strain in the purely elastic branch. A common assumption is that the viscous stress

$$\boldsymbol{\sigma}_{\text{visc}}^{(i)} = \boldsymbol{V}^{(i)} \dot{\boldsymbol{\alpha}}^{(i)} \tag{4.57}$$

is linearly related to the viscous strain rate via a symmetric, positive semi-definite viscosity matrix $\boldsymbol{V}^{(i)}$.

To account for this linearly viscoelastic behavior in the pH model, we first introduce additional state variables $\boldsymbol{\sigma}_{\text{el}}^{(i)} = \boldsymbol{\sigma}_{\text{visc}}^{(i)}$ for each branch. Next, we include additional stress contributions in the balance of momentum (4.21) according to (4.55). Lastly, we account for evolution equations

$$\begin{aligned} \boldsymbol{C}_\infty \dot{\boldsymbol{\sigma}}_\infty &= \dot{\boldsymbol{\varepsilon}}(\boldsymbol{\varphi}, \boldsymbol{d}), \\ \boldsymbol{C}^{(i)} \dot{\boldsymbol{\sigma}}_{\text{el}}^{(i)} &= \dot{\boldsymbol{\varepsilon}}(\boldsymbol{\varphi}, \boldsymbol{d}) - \boldsymbol{V}^{(i)-1} \boldsymbol{\sigma}_{\text{el}}^{(i)}, \quad i = 1, \dots, m, \end{aligned} \tag{4.58}$$

for the long term elastic stress $\boldsymbol{\sigma}_\infty$ and for each individual elastic stress contribution $\boldsymbol{\sigma}_{\text{el}}^{(i)}$ in a compliance form based on the time derivative of the two equalities in (4.56). We have further accounted for the constitutive relation (4.57) as well as $\boldsymbol{C}_\infty \boldsymbol{\sigma}_\infty = \boldsymbol{\varepsilon}_\infty$ and $\boldsymbol{C}^{(i)} \boldsymbol{\sigma}_{\text{el}}^{(i)} = \boldsymbol{\varepsilon}_{\text{el}}^{(i)}$. Note that for consistency with a purely elastic beam model with elasticity matrices $\boldsymbol{C}_\Gamma$ and $\boldsymbol{C}_K$, see Equation (4.8), the elasticity matrices of all branches must add up to those matrices.

Remark 4.8. *A common approach [75, 144] is to assume diagonal viscosity matrices $\boldsymbol{V}^{(i)}$ based on the same structure as the elasticity matrices. To this end, one can introduce dynamic viscosities $\eta_G, \eta_E \geq 0$ for shear and torsion as well as dilatation and bending, respectively, such that*

$$\tau_G = \frac{\eta_G}{G}, \qquad \tau_E = \frac{\eta_E}{E} \tag{4.59}$$

are the corresponding characteristic relaxation times. Here, $E, G \geq 0$ denote Young's modulus and the shear modulus, respectively. This eventually gives rise to the viscosity matrices

$$\boldsymbol{V}^{(i)} = \begin{bmatrix} \boldsymbol{V}_\Gamma^{(i)} & \boldsymbol{0} \\ \boldsymbol{0} & \boldsymbol{V}_K^{(i)} \end{bmatrix} \quad \text{with} \quad \boldsymbol{V}_\Gamma^{(i)} = \begin{bmatrix} \tau_G^{(i)} & 0 & 0 \\ 0 & \tau_G^{(i)} & 0 \\ 0 & 0 & \tau_E^{(i)} \end{bmatrix} \boldsymbol{C}_\Gamma^{(i)}, \qquad \boldsymbol{V}_K^{(i)} = \begin{bmatrix} \tau_E^{(i)} & 0 & 0 \\ 0 & \tau_E^{(i)} & 0 \\ 0 & 0 & \tau_G^{(i)} \end{bmatrix} \boldsymbol{C}_K^{(i)}, \tag{4.60}$$

where $\boldsymbol{C}_\Gamma^{(i)}$ and $\boldsymbol{C}_K^{(i)}$ are elasticity matrices consistent with the compliance matrix $\boldsymbol{C}^{(i)}$ of the i-th viscous branch. ♧

Remark 4.9. *The Kelvin-Voigt dissipation model, as for instance used in [105, 144], is contained in the present framework if $m = 1$ dissipative Maxwell branch is considered. In this branch, the compliance of the elastic element has to be zero, such that it behaves rigidly.* ♧

Dissipative pH model The dissipative system can again be viewed from a pH perspective. To this end, we concatenate all stresses of the Maxwell branches in $\boldsymbol{\sigma}_{\text{vis}} = (\boldsymbol{\sigma}_{\text{el}}^{(1)}, \dots, \boldsymbol{\sigma}_{\text{el}}^{(m)})$ to define the state and costate of the new pH system as

$$\boldsymbol{x} = (\boldsymbol{\varphi}, \boldsymbol{v}, \boldsymbol{\sigma}_\infty, \boldsymbol{\sigma}_{\text{vis}}, \boldsymbol{\lambda}), \qquad \boldsymbol{z}(\boldsymbol{x}) = (\boldsymbol{0}, \boldsymbol{v}, \boldsymbol{\sigma}_\infty, \boldsymbol{\sigma}_{\text{vis}}, \boldsymbol{\lambda}). \tag{4.61}$$

together with the Hamiltonian

$$\mathcal{H}(\boldsymbol{x}) = \int_\Omega \left(\frac{1}{2} \boldsymbol{v}^\top \boldsymbol{M}_o \boldsymbol{v} + \frac{1}{2} \boldsymbol{\sigma}_\infty^\top \boldsymbol{C}_\infty \boldsymbol{\sigma}_\infty + \frac{1}{2} \boldsymbol{\sigma}_{\text{vis}}^\top \boldsymbol{C}_{\text{vis}} \boldsymbol{\sigma}_{\text{vis}} \right) \mathrm{d}s, \tag{4.62}$$

comprising the kinetic energy as of before together with all complementary strain energy terms pertaining to the elastic elements of the generalized-Maxwell model with $\boldsymbol{C}_{\text{vis}} = \operatorname{diag}(\boldsymbol{C}^{(1)}, \dots, \boldsymbol{C}^{(m)})$.

Similarly, we define $\boldsymbol{V}^{-1} = \operatorname{diag}((\boldsymbol{V}^{(1)})^{-1}, \dots, (\boldsymbol{V}^{(m)})^{-1})$, $\mathcal{J}_{\boldsymbol{v}}^{\text{vis}} = [\mathcal{J}_{\boldsymbol{v}} \dots \mathcal{J}_{\boldsymbol{v}}]$ and $\mathcal{J}_{\boldsymbol{\sigma}}^{\text{vis}} = \left[\mathcal{J}_{\boldsymbol{\sigma}}^\top \dots \mathcal{J}_{\boldsymbol{\sigma}}^\top\right]^\top$ with m copies of the respective quantity. Thus, we write the dynamics as

$$\begin{bmatrix} \boldsymbol{I} & 0 & 0 & 0 & 0 \\ 0 & \boldsymbol{M}_o & 0 & 0 & 0 \\ 0 & 0 & \boldsymbol{C}_\infty & 0 & 0 \\ 0 & 0 & 0 & \boldsymbol{C}_{\text{vis}} & 0 \\ 0 & 0 & 0 & 0 & \boldsymbol{0} \end{bmatrix} \partial_t \begin{bmatrix} \boldsymbol{q} \\ \boldsymbol{v} \\ \boldsymbol{\sigma}_\infty \\ \boldsymbol{\sigma}_{\text{vis}} \\ \boldsymbol{\lambda} \end{bmatrix} = \begin{bmatrix} 0 & \boldsymbol{I} & 0 & 0 & 0 \\ -\boldsymbol{I} & 0 & -\mathcal{J}_{\boldsymbol{v}} & -\mathcal{J}_{\boldsymbol{v}}^{\text{vis}} & -\boldsymbol{G}^\top \\ 0 & \mathcal{J}_{\boldsymbol{\sigma}} & 0 & 0 & 0 \\ 0 & \mathcal{J}_{\boldsymbol{\sigma}}^{\text{vis}} & 0 & -\boldsymbol{V}^{-1} & 0 \\ 0 & \boldsymbol{G} & 0 & 0 & 0 \end{bmatrix} \begin{bmatrix} \boldsymbol{0} \\ \boldsymbol{v} \\ \boldsymbol{\sigma}_\infty \\ \boldsymbol{\sigma}_{\text{vis}} \\ \boldsymbol{\lambda} \end{bmatrix} + \begin{bmatrix} 0 \\ \boldsymbol{B}_\Omega \\ 0 \\ 0 \\ 0 \end{bmatrix} \boldsymbol{u}_\Omega. \tag{4.63}$$

In short, this fits again into the pH framework [23, 161, 162]

$$\begin{aligned} \mathcal{E}\partial_t \boldsymbol{x} &= (\mathcal{J}(\boldsymbol{x}) - \mathcal{R})\boldsymbol{z}(\boldsymbol{x}) + \mathcal{B}_\Omega(\boldsymbol{x})\boldsymbol{u}_\Omega, \\ \boldsymbol{y}_\Omega &= \mathcal{B}_\Omega(\boldsymbol{x})^\top \boldsymbol{z}, \end{aligned} \tag{4.64}$$

where $\mathcal{R} = \operatorname{diag}(\boldsymbol{0}, \boldsymbol{0}, \boldsymbol{0}, \boldsymbol{V}^{-1}, \boldsymbol{0})$ is a constant, symmetric, positive semi-definite matrix[5]. The positive semi-definite property can be checked by means of the block-diagonal structure and $(\boldsymbol{V}^{(i)})^{-1}$ being symmetric and positive semi-definite, see Remark 4.8.

The power balance equation induced by this pH system extends the one by the purely elastic model (4.28) such that

$$\dot{\mathcal{H}} = \boldsymbol{y}_{\partial\Omega}^\top \boldsymbol{u}_{\partial\Omega} + \int_\Omega \boldsymbol{y}_\Omega^\top \boldsymbol{u}_\Omega \, \mathrm{d}s - P_R. \tag{4.65}$$

Here, we have introduced the dissipated power due to viscous deformations (also called *dissipation function* [204])

$$P_R = \int_\Omega \boldsymbol{z}^\top \mathcal{R} \boldsymbol{z} \, \mathrm{d}s = \int_\Omega (\boldsymbol{\sigma}_{\text{vis}})^\top \boldsymbol{V}^{-1} \boldsymbol{\sigma}_{\text{vis}} \, \mathrm{d}s = \int_\Omega \sum_{i=1}^{m} (\boldsymbol{\sigma}_{\text{el}}^{(i)})^\top (\boldsymbol{V}^{(i)})^{-1} \boldsymbol{\sigma}_{\text{el}}^{(i)} \, \mathrm{d}s \geq 0. \tag{4.66}$$

Consequently, the power balance equations (4.65) immediately leads to the dissipation inequality

$$\dot{\mathcal{H}} \leq \boldsymbol{y}_{\partial\Omega}^\top \boldsymbol{u}_{\partial\Omega} + \int_\Omega \boldsymbol{y}_\Omega^\top \boldsymbol{u}_\Omega \, \mathrm{d}s, \tag{4.67}$$

proving the passivity of the dissipative infinite-dimensional pH system.

Remark 4.10. *As shown in [A1] for geometrically exact strings, we can obtain the model* (4.63) *alternatively by power-preserving interconnection. In this context, all viscous Maxwell branches are interpreted as purely dissipative pH models and the elastic branch as its own model similar to* (4.21)*. The overall model is obtained by means of a gyrator interconnection of passive subsystems. Find more details in Sections 6.2.2 and 6.2.3.* ♧

4.5.2. Extension to pneumatic and tendon actuation

In the context of soft robotic manipulators, two state-of-the-art actuation approaches are given by elastic cables acting as so-called tendons [195, 220] and pneumatic chambers [70, 220]. Both can be included seamlessly in the present beam model in a unified way. We follow the approach from [70, 220], see also [3], and include additional stress contributions acting as distributed actuation terms[6].

[5] In general, this notion can be extended to a state-dependent, self-adjoint differential operator.

[6] Equivalently, one can account for these effects using the distributed forces and moments per unit length $(\bar{\boldsymbol{n}}, \bar{\boldsymbol{m}})$ combined with related Neumann boundary terms. This approach is however more tedious to implement in an FE framework.

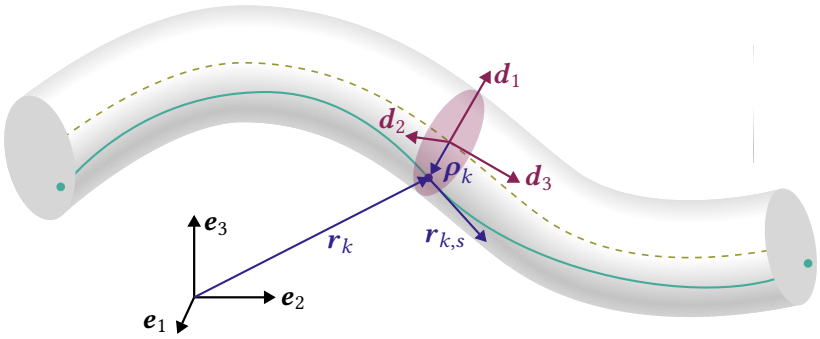

Figure 4.3.: Schematic depiction for the actuation of a Cosserat rod, where the k-th actuation element and related kinematic quantities are displayed.

Thus, we extend the equations of motion (4.21) by introducing additional terms as

$$\boldsymbol{N} \longrightarrow \boldsymbol{N} + \boldsymbol{\Lambda}(\boldsymbol{d})^\top \boldsymbol{n}_u, \qquad \boldsymbol{M} \longrightarrow \boldsymbol{M} + \boldsymbol{\Lambda}(\boldsymbol{d})^\top \boldsymbol{m}_u, \tag{4.68}$$

where $\boldsymbol{n}_u, \boldsymbol{m}_u \in \mathbb{R}^3$ are additional internal forces and moments emerging from input actuation. For both tendon and pressure chamber actuation they assume the form

$$\boldsymbol{n}_u = \sum_{k=1}^{N} \tau_k \boldsymbol{t}_k, \qquad \boldsymbol{m}_u = \sum_{k=1}^{N} \boldsymbol{\rho}_k \times \tau_k \boldsymbol{t}_k, \tag{4.69}$$

where k is the index of the actuation element, i.e., tendon or pressure chamber, and

$$\tau_k = \begin{cases} p_k(t) A_k \leq 0 & \text{for pressure actuation,} \\ T_k(t) \geq 0 & \text{for tendon actuation,} \end{cases} \tag{4.70}$$

the actuation force magnitude. Therein, p_k is the pressure and A_k is the cross section area of the pressurized chamber, while T_k is the tension force in a tendon. Both $p_k(t)$ and $T_k(t)$ are regarded as known input quantities, which will be related to a distributed forcing term. Moreover in (4.69), $\boldsymbol{t}_k$ is the corresponding unit direction vector and $\boldsymbol{\rho}_k(s,t) = \rho_k^\alpha \boldsymbol{d}_\alpha(s,t)$, for $\alpha = 1, 2$, describes the vector from the centerline of the beam to the line of centroids of the k-th actuation element. Here, ρ_k^α are material coordinates, which are fixed. Correspondingly, $\boldsymbol{r}_k = \boldsymbol{\varphi} + \boldsymbol{\rho}_k$. The only difference between the two actuation methods is that tendons induce traction in tangential direction of the tendons while pressure chambers induce traction in cross-section normal direction. This is realized via the unit direction vector $\boldsymbol{t}_k$ such that

$$\boldsymbol{t}_k = \begin{cases} \boldsymbol{d}_3 & \text{for pressure actuation,} \\ \dfrac{\boldsymbol{r}_{k,s}}{||\boldsymbol{r}_{k,s}||} & \text{for tendon actuation.} \end{cases} \tag{4.71}$$

For a schematic depiction for the case of tendon actuation see Figure 4.3. In the strong form (4.21), these terms result in additional distributed inputs of the form $\boldsymbol{B}_u(\boldsymbol{x})\boldsymbol{\tau}$, where $\boldsymbol{\tau} = (\tau_1, \ldots, \tau_N) \in \mathbb{R}^N$ are additional input quantities. To account for (4.17), (4.68) and (4.69), we introduce the distributed port matrix

$$\boldsymbol{B}_u(\boldsymbol{x}) = \begin{bmatrix} (\boldsymbol{t}_{k,s})_{k=1}^N \\ -(\boldsymbol{J}_N \boldsymbol{\Lambda}^\top \boldsymbol{t}_k + \mathcal{J}_M(\boldsymbol{\Lambda}^\top \tilde{\boldsymbol{\rho}}_k \boldsymbol{t}_k))_{k=1}^N \end{bmatrix} \in \mathbb{R}^{6 \times N}, \tag{4.72}$$

where each column of the matrix corresponds to the influence of one actuation element. Note that the state-dependence of the port matrix does not only emerge from the operators but also from the

Table 4.1.: Flying spaghetti: Physical and numerical parameters.

h	t_{end}	n_{e}	$\varepsilon_{\text{Newton}}$	L	ρA	$M_\rho^{11} = M_\rho^{22}$	$k_{\text{b1}} = k_{\text{b2}} = k_{\text{t}}$	$k_{\text{s1}} = k_{\text{s2}} = k_{\text{e}}$
0.1	15	10	10^{-11}	10	1	10	10^3	10^4

unit direction vector $\boldsymbol{t}_k$ introduced in (4.71). Likewise, this also leads to an additional input term in the differential form of the pH dynamics (4.22), eventually extended to

$$\mathcal{E}\partial_t \boldsymbol{x} = \mathcal{J}(\boldsymbol{x})\boldsymbol{z}(\boldsymbol{x}) + \mathcal{B}_\Omega(\boldsymbol{x})\boldsymbol{u}_\Omega + \boldsymbol{B}_{\boldsymbol{\tau}}(\boldsymbol{x})\boldsymbol{\tau}, \qquad \text{where} \qquad \boldsymbol{B}_{\boldsymbol{\tau}}(\boldsymbol{x}) = \begin{bmatrix} 0 \\ \boldsymbol{B}_u(\boldsymbol{x}) \\ 0 \\ 0 \end{bmatrix}. \tag{4.73}$$

Similarly, these additional contributions are accounted for in the weak form analogously to the internal forces and moments via additional terms $\left(\delta\boldsymbol{\varphi}_{,s}, \boldsymbol{n}_u\right)_\Omega$ and $\left(\mathcal{J}_{\boldsymbol{K}}\delta\boldsymbol{d}, \boldsymbol{\Lambda}^\top \boldsymbol{m}_u\right)_\Omega$ in (4.29c) and (4.29d), respectively.

4.6. Numerical examples

Let us apply the proposed framework to representative numerical examples. Newton's method is used to solve the nonlinear discrete time equations (4.42) in every time step with an absolute tolerance $\varepsilon_{\text{Newton}}$ on the norm of the residual. The spatial integrals are approximated by means of a three-point Gauss quadrature and for the polynomials ansatz functions we choose $p = 2$. The Dirichlet boundary conditions for the displacements and velocities are incorporated directly into the ansatz functions, see Remark 4.3, and no gravitational effects are considered. The computations have been performed using the finite element code `moofeKIT`[7], and the generated data are published in [124] and archived under [125]. The first example is used to assess the structure-preservation of the employed discretization approach. Additionally, good agreements with an analytical solution are shown. In the second benchmark, we find good agreement of our results with data reported in the literature and verify kinematic consistency properties according to Section 4.4.3. This example also deals with the viscoelastic extension from Section 4.5.1 and underlines the usability of the present framework for inextensible Kirchhoff beams. The third example studies the formulation in a quasistatic scenario showing that the present formulation matches an analytical solution and avoids locking. Lastly, we use our formulation to simulate the dynamic motion of a soft robotic arm actuated by means of pneumatic chambers, as introduced in Section 4.5.2.

4.6.1. Flying spaghetti

This first benchmark problem has been initially proposed in [208, 210] and taken up many times by, inter alia, [51, 106, 112, 155, 242, 245]. The main objective of this free flight problem is to verify the benefitial properties of the proposed beam formulation and compare the results with data from the literature. We adopt the parameters chosen in [106, 242][8], see Table 4.1. Initially at rest in an inclined

[7] `https://github.com/kit-ifm/moofeKIT`

[8] The validity of the parameters reported by Simo and co-workers have been questioned in [106, 112]. With the parameters employed here, the authors of [106, 242] could reproduce the results from the original works.

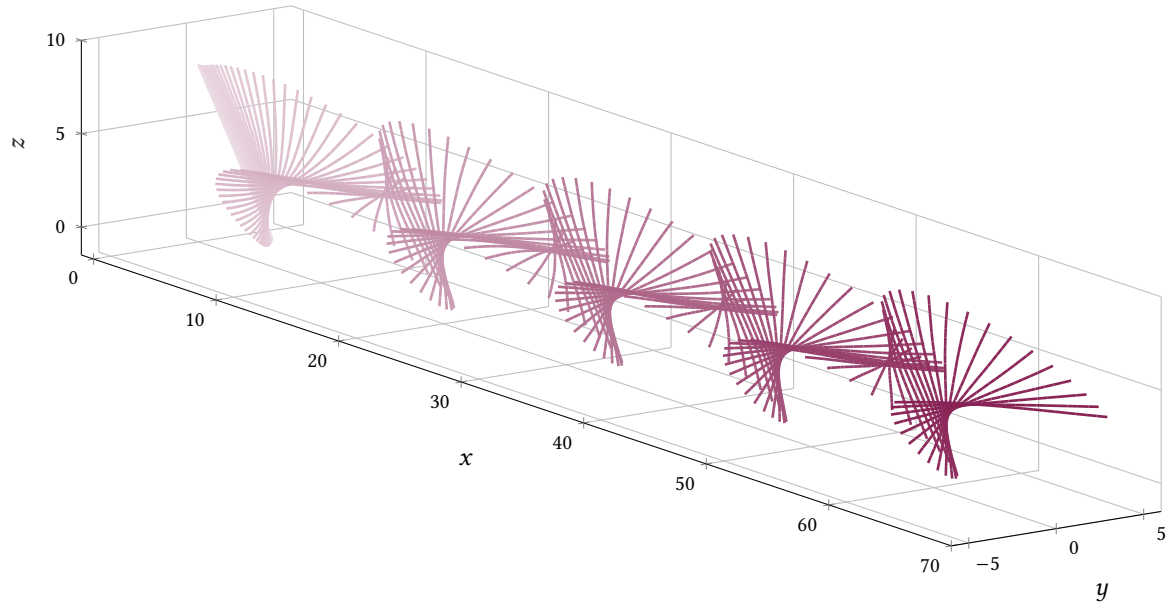

Figure 4.4.: Flying spaghetti: Snapshots of the *kayak-rowing* motion with azimuth and elevation perspective angles (55, 15) and the colormap for time t^n with ∈ $[0, 15]$.

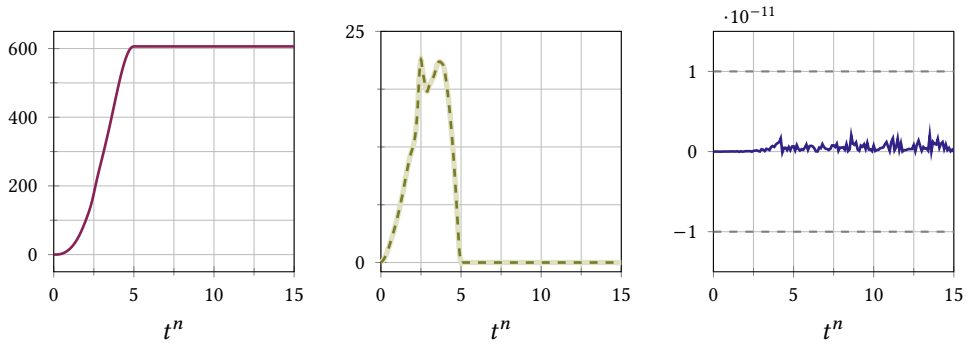

Figure 4.5.: Flying spaghetti: Total energy — $\hat{\mathcal{H}}(\boldsymbol{x}^n)$, input work — W_{ext}^n, total energy increments - - - $\hat{\mathcal{H}}(\hat{\boldsymbol{x}}^{n+1}) - \hat{\mathcal{H}}(\hat{\boldsymbol{x}}^n)$, and energy balance violation — ΔE^n.

configuration with $\boldsymbol{\varphi}_{\text{h}}(s = 0, t = 0) = (6, 0, 0)$ and $\boldsymbol{\varphi}_{\text{h}}(s = L, t = 0) = (0, 0, 8)$, the beam is subject to an external force and torque at $s = L$, both of which are applied for a short period of time, i.e., $\boldsymbol{n}(s = L, t) = \boldsymbol{\nu}(t)$ and $\boldsymbol{m}(s = L, t) = \boldsymbol{\mu}(t)$ with

$$\boldsymbol{\nu}(t) = f(t) \begin{bmatrix} \frac{1}{10} \\ 0 \\ 0 \end{bmatrix}, \quad \boldsymbol{\mu}(t) = f(t) \begin{bmatrix} 0 \\ 1 \\ \frac{1}{2} \end{bmatrix}, \quad f(t) = \begin{cases} 80t, & \text{for} \quad t \leq 2.5, \\ 400 - 80t, & \text{for} \quad 2.5 < t \leq 5, \\ 0, & \text{for} \quad t > 5. \end{cases} \tag{4.74}$$

At $t = 5$, the system is closed as both boundary inputs become zero and the beam continues with a free flight, where total energy, linear and angular momentum should be preserved. The resulting motion fits well to the depictions from [51, 106, 245], see snapshots in Figure 4.4. Moreover, the conservation of total energy[9] can be seen from Figure 4.5. In each time step, the work done by the external load $W_{\text{ext}}^n = h(\hat{\boldsymbol{u}}^{n+1/2})^\top \hat{\boldsymbol{y}}^{n+1/2}$ identically matches the total energy increase $\hat{\mathcal{H}}(\hat{\boldsymbol{x}}^{n+1}) - \hat{\mathcal{H}}(\hat{\boldsymbol{x}}^n)$ during the

[9] References [51, 242, 245], in which the originally reported parameters are used, report significantly larger energy plateaus but similar angular momentum levels.

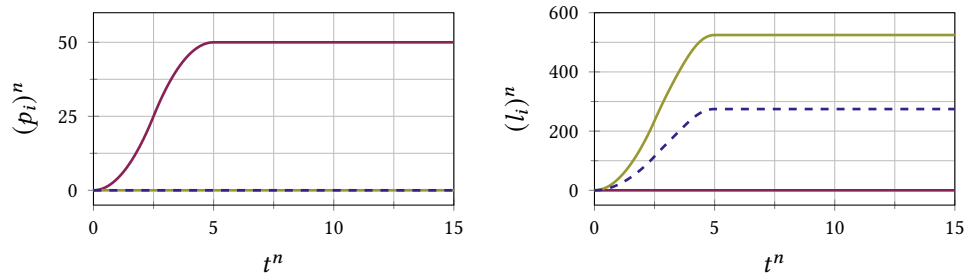

Figure 4.6.: Flying spaghetti: Total linear momentum components $(p_i)^n = \boldsymbol{p}(\hat{\boldsymbol{x}}^n)^\top \boldsymbol{e}_i$ and total angular momentum components $(l_i)^n = \boldsymbol{l}(\hat{\boldsymbol{x}}^n)^\top \boldsymbol{e}_i$, where $i \in \{1$ ——, 2 ——, 3 - - -$\}$.

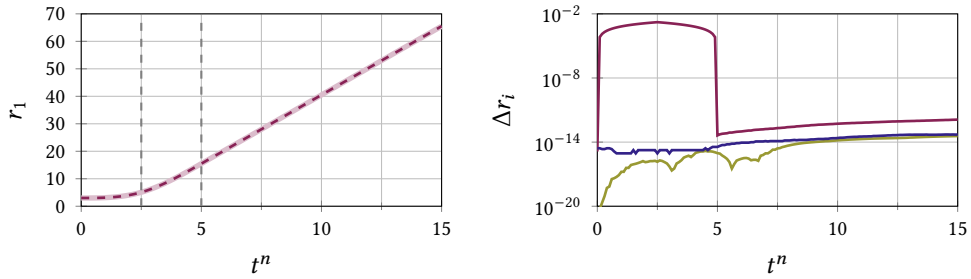

Figure 4.7.: Flying spaghetti: Analytical solution (——) and numerical solution (- - -) for 1-component of the center of mass as well as deviation Δr_i with $i \in \{1$ ——, 2 ——, 3 ——$\}$.

loading phase. Correspondingly, at all times, the energy balance violation $\Delta E^n := \hat{\mathcal{H}}(\hat{\boldsymbol{x}}^{n+1}) - \hat{\mathcal{H}}(\hat{\boldsymbol{x}}^n) - W^n_{\text{ext}}$ remains at the level of machine precision, confirming the discrete-time power balance (4.44). The conservation of total linear and angular momentum after the loading phase can be seen from Figure 4.6, confirming the results from Appendix 4.D. Further, the constant total linear momentum of $\boldsymbol{p} = (50, 0, 0)$ for $t \geq 5$, matches the analytical solution exactly within machine precision. Moreover, the load function (4.74), together with the chosen boundary conditions, allows for an analytical solution for the position of the center of mass of the beam during motion [112, 242], given by

$$\boldsymbol{r} = \begin{bmatrix} r_1(t) \\ 0 \\ 4 \end{bmatrix}, \qquad r_1(t) = \begin{cases} 3 + \frac{2}{15}t^3, & \text{for} \quad t \leq 2.5, \\ \frac{43}{6} - 5t + 2t^2 - \frac{2}{15}t^3, & \text{for} \quad 2.5 < t \leq 5, \\ -\frac{19}{2} + 5t, & \text{for} \quad t > 5. \end{cases} \tag{4.75}$$

This is closely matched by the simulated center of mass $\boldsymbol{r}_\text{h}(t) := \frac{1}{L}\int_\Omega \boldsymbol{\varphi}_\text{h}(s,t)\,\text{d}s$ obtained with our approach, see Figure 4.7. Some slight deviations $\Delta r_i := \boldsymbol{e}_i^\top \boldsymbol{r}_\text{h} - r_i$ are still present during the loading phase for the 1-component but after $t = 5$, all three curves are in the range of computer precision. Additionally, a convergence study is performed to investigate the temporal discretization accuracy for the centerline position and velocity at the free end with $s = 0$ with respect to the temporal discretization. The results in Figure 4.8 show that the relative error

$$e_{\square} = \frac{||\square_\text{h}(s=0,t=\bar{t}) - \square^\text{ref}(s=0,t=\bar{t})||}{||\square^\text{ref}(s=0,t=\bar{t})||}, \tag{4.76}$$

for $\square \in \{\boldsymbol{\varphi}, \boldsymbol{v}_\varphi\}$, obtained with our approach decreases with order two with increasing temporal resolution. This is in line with the expected behavior for the midpoint-type discretization. Here, the evaluation time is chosen as $\bar{t} = 5$. Moreover, $\square^\text{ref}$ is the finely discretized reference solution obtained with $h = 10^{-3}$ and $||\square||$ denotes the Euclidean norm. In this context, the Newton tolerance was reduced for all simulations to 10^{-8}.

Table 4.2.: Nonlinear oscillation of a cantilever: Physical and numerical parameters.

h	t_{end}	n_{e}	$\varepsilon_{\text{Newton}}$	L	ρ	A	$M_\rho^{11} = M_\rho^{22}$	$k_{\text{b1}} = k_{\text{b2}}$	k_{t}	$k_{\text{s1}} = k_{\text{s2}} = k_{\text{e}}$
10^{-3}	0.3	8	10^{-12}	1	2850	$\pi d^2/4$	ρI	EI	GI_T	∞

Another notable advantage of the time integration method, which is made possible by the pH formulation, is its remarkable stability and robustness. In theory, the time step size is not constrained by the stability of the integrator but only by the deterioration of the Newton method due to poor initial guesses at excessively large steps. In practice, the method must adequately resolve the loading function profile (4.74). Notably, choosing $h = 2.5$ poses no difficulty for the proposed method, while other works simulating this example typically report time step sizes of $h = 0.01$ or 0.02. However, in light of the preceding convergence analysis, the accuracy of the results with larger time step sizes should definitly be questioned.

4.6.2. Nonlinear oscillation of a cantilever

The example of an oscillating slender aluminum beam has been recently included in [105]. The beam has a circular cross-section with diameter $d = 4 \cdot 10^{-3}$ and we assume material parameters for Young's modulus $E = 7.2 \cdot 10^{10}$, Poisson ratio $\nu = 0.35$ and shear modulus $G = E/(2(1+\nu))$. This leads to cross-sectional moments of area $I_1 = I_2 = 1/2 I_T = \pi d^4/64$. Further details are comprised in Table 4.2. Note that this beam is relatively slender with a high slenderness ratio of $L/d = 250$. Conforming with [105], we thus assume an inextensible Kirchhoff beam and impose the related kinematic constraints of shear rigidity and inextensibility. To this end, we set $\boldsymbol{C}_N = \boldsymbol{0}$ in the compliance equation (4.18), thus ensuring $\dot{\boldsymbol{\Gamma}} = \boldsymbol{0}$. Moreover, note that we are able to choose a relatively large time step size of $h = 10^{-3}$ due to the robustness of the employed energy–momentum time integration (4.42) (see paragraph in the first example). Compared to the original setting in [105], where the largest possible time step size was $h = 4 \cdot 10^{-5}$, we obtain results even for $h = 5 \cdot 10^{-2}$. Initially at rest and positioned along the $\boldsymbol{e}_1$-direction, the beam is subject to an external force and torque at $s = L$, both of which are applied for a short period of time, i.e., $\boldsymbol{n}(s = L, t) = \boldsymbol{\nu}(t)$ and $\boldsymbol{m}(s = L, t) = \boldsymbol{\mu}(t)$ with

$$\boldsymbol{\nu}(t) = f(t) \begin{bmatrix} 0 \\ 1 \\ 1 \end{bmatrix} \quad \boldsymbol{\mu}(t) = f(t) \begin{bmatrix} 0.25 \\ 0 \\ 0 \end{bmatrix}, \quad f(t) = \begin{cases} \frac{1}{2}\left(1 - \cos\left(\frac{2\pi}{0.05} t\right)\right), & \text{for} \quad t \leq 0.05, \\ 0, & \text{for} \quad t > 0.05. \end{cases} \tag{4.77}$$

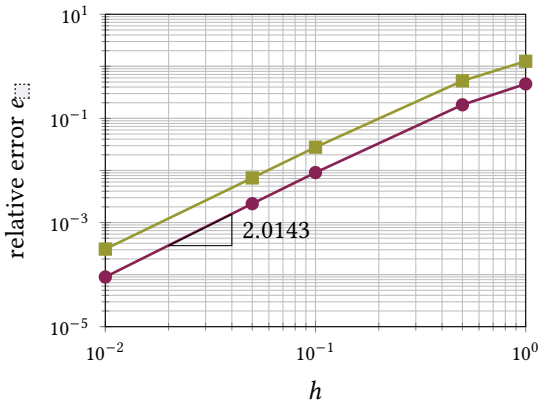

Figure 4.8.: Flying spaghetti: Convergence of the relative error for centerline position $e_{\boldsymbol{\varphi}}$ and velocity $e_{\boldsymbol{v}_\varphi}$ with varying time step size parameter.

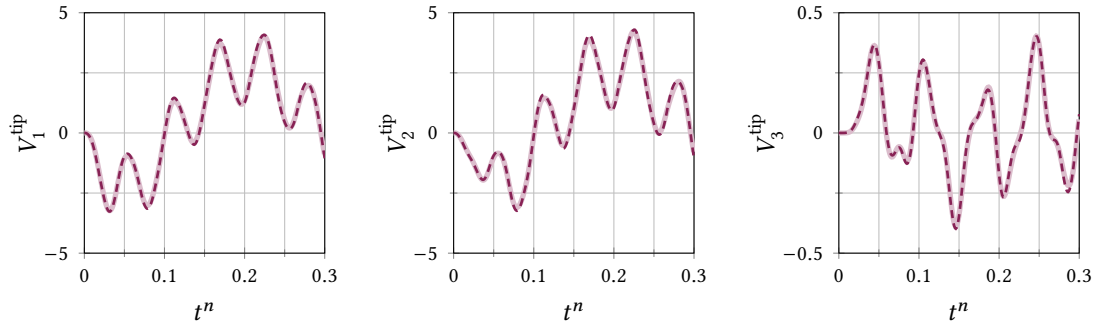

Figure 4.9.: Nonlinear oscillation of a cantilever: Tip velocities in cross-section frame V_i^{tip}. Results from our approach (- - -) and reference solution (——) [105] coincide. The sign flip and different order of components compared to the reference is due to a different director frame orientation.

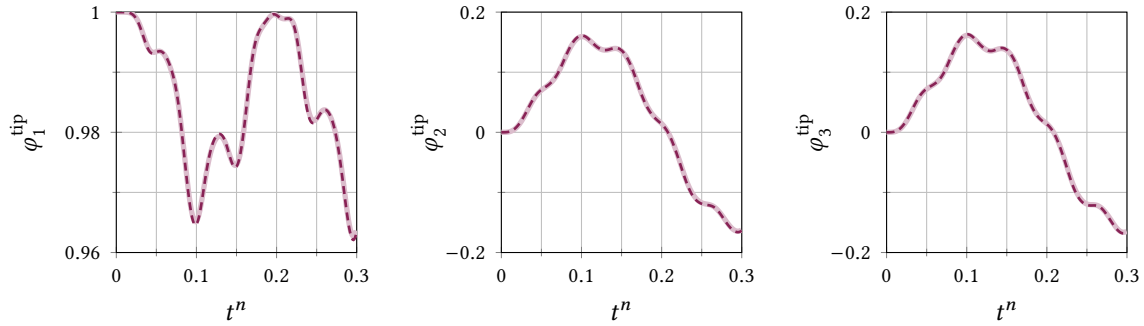

Figure 4.10.: Nonlinear oscillation of a cantilever: Tip positions in inertial frame φ_i^{tip}. Results from our approach (- - -) and reference solution (——) [105]. The sign flip and different order of components compared to the reference is due to a different director frame orientation.

We can observe good agreements of the material tip velocities $V_i^{\text{tip}} := \boldsymbol{e}_i^\top \boldsymbol{\Lambda}(\boldsymbol{d}_{\text{h}}(s = L, t = t^n))^\top \boldsymbol{v}_{\varphi,\text{h}}(s = L, t = t^n)$, see Figure 4.9, and spatial tip centerline positions $\varphi_i^{\text{tip}} := \boldsymbol{e}_i^\top \boldsymbol{\varphi}_{\text{h}}(s = L, t = t^n)$, see Figure 4.10, with the results from [105]. Furthermore, confirming (4.48), it can be verified that the orthonormality constraints (4.2) for the directors at the center FE node $(g_i)_{\text{h}} := g_i(\boldsymbol{d}_{\text{h}}(s = L/2, t = t^n))$ are numerically zero during the whole simulation, see Figure 4.11. These results are representative also for the other nodes. Additionally, also the kinematic accuracy can be verified. The dilatation and shear strain components derived from the mixed variables vanish identically. When computed from the displacements by means of (4.4), these strains are also variationally consistent with the imposed kinematic constraints (see the variational identity (4.54)). The curvature and torsion components are likewise approximated consistently. The results depicted in Figure 4.12 are expressed in terms of the $\mathscr{L}^2$-norms over the

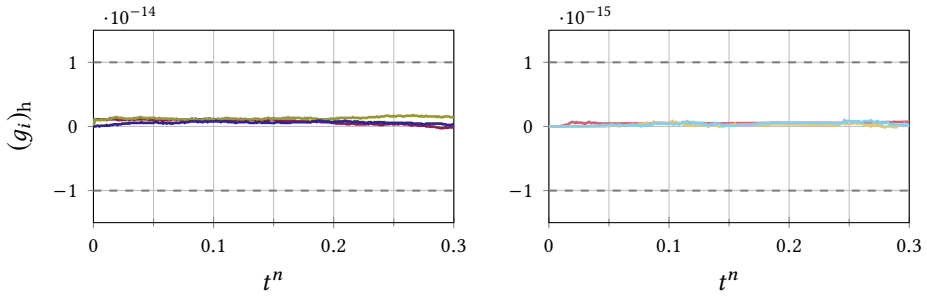

Figure 4.11.: Nonlinear oscillation of a cantilever: Orthonormality constraints $(g_i)_{\text{h}}$ with $i \in \{1$ ——, 2 ——, 3 ——, 4 ——, 5 ——, 6 ——$\}$.

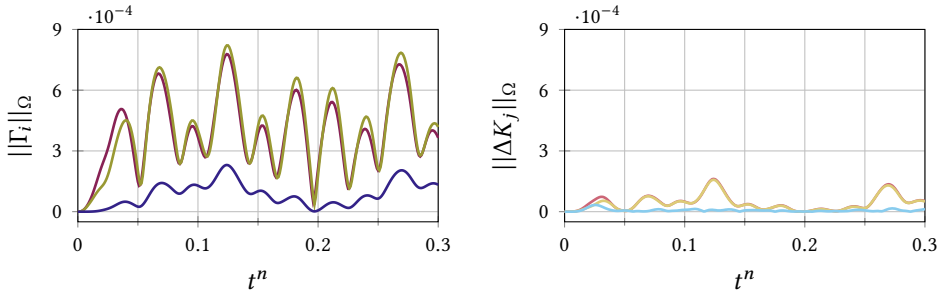

Figure 4.12.: Nonlinear oscillation of a cantilever: $\mathscr{L}^2$-norms of the shear and dilatation strain components computed from displacement quantities, i.e., $||\Gamma_i||_\Omega$ with $i \in \{1$ —, 2 —, 3 —$\}$. $\mathscr{L}^2$-norms of the drift between the curvature and torsion strain measures computed from the stress quantities and the ones computed from displacement quantities, denoted as$||\Delta K_j||_\Omega$ for $j \in \{$ 1 —, 2 —, 3 —$\}$.

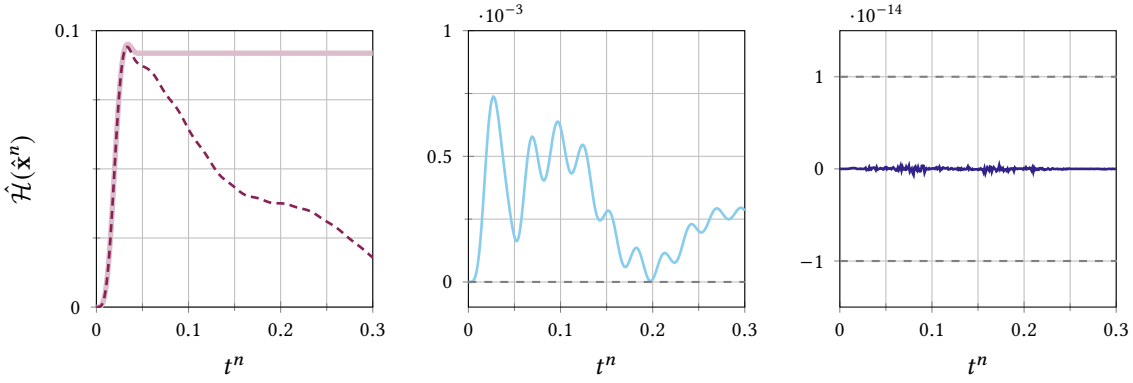

Figure 4.13.: Nonlinear oscillation of a cantilever: Total energy $\hat{\mathcal{H}}(\boldsymbol{x}^n)$ with dissipation ($\tau = 0.08$ - - -) and without dissipation ($\tau \to \infty$ —). Strictly positive dissipated energy per timestep $(\hat{P}_R)^n$ — and energy balance violation ΔE^n —.

spatial domain, i.e., $||\Gamma_i||_\Omega := (\int_0^L \Gamma_i(\boldsymbol{q}_\mathrm{h}^n, \partial_s \boldsymbol{q}_\mathrm{h}^n)^2 \,\mathrm{d}s)^{1/2}$ and $||\Delta K_j||_\Omega := (\int_0^L ((K_j)^n - K_j(\boldsymbol{q}_\mathrm{h}^n, \partial_s \boldsymbol{q}_\mathrm{h}^n))^2 \,\mathrm{d}s)^{1/2}$, respectively.

Lastly, we consider the viscoelastic generalized Maxwell model, introduced in Section 4.5.1, with $m = 1$ viscous branch and $\tau_E = \tau_G = \tau = 0.08$ as relaxation time. The stiffness parameters are split up consistently on both branches, with fractions of 1/4 in the purely elastic and 3/4 in the viscous branch. Note that for this simulation with viscous effects, we also keep the kinematic assumptions from above, such that only the bending and torsion modes are damped and $\boldsymbol{V}_\Gamma^{-1} = \boldsymbol{0}$. Correspondingly, Figure 4.13 extends the findings from the flying spaghetti problem, see Section 4.6.1, to verify the consistent discrete-time representation of the power balance equation. The total energy decreases over time and the dissipated energy $(\hat{P}_R)^n := h\hat{\boldsymbol{z}}(\hat{\boldsymbol{x}}^{n+1/2})^\top \boldsymbol{R}\hat{\boldsymbol{z}}(\hat{\boldsymbol{x}}^{n+1/2})$ is strictly positive. Thus, the subfigure on the right-hand side of Figure 4.13 shows that the violation of the discrete time energy balance (4.44) denoted as $\Delta E^n := \hat{\mathcal{H}}(\hat{\boldsymbol{x}}^{n+1}) - \hat{\mathcal{H}}(\hat{\boldsymbol{x}}^n) - W_\mathrm{ext}^n - \hat{D}(\hat{\boldsymbol{x}}^n)$ is numerically zero.

4.6.3. Quasistatic cantilever problem

This numerical experiment displays the usage of the presented formulation in a quasistatic use case and has been taken from [100, 104]. We show results for an initially straight and clamped beam with length $L = 2\pi$, whose initial configuration aligns with the $\boldsymbol{e}_1$-axis. Further parameters are shown in Table 4.3. We consider a load case with point force and moment at the free end at $s = L$ such that $\boldsymbol{n}(s = L, t) = \boldsymbol{\nu}(t)$ and $\boldsymbol{m}(s = L, t) = \boldsymbol{\mu}(t)$ with

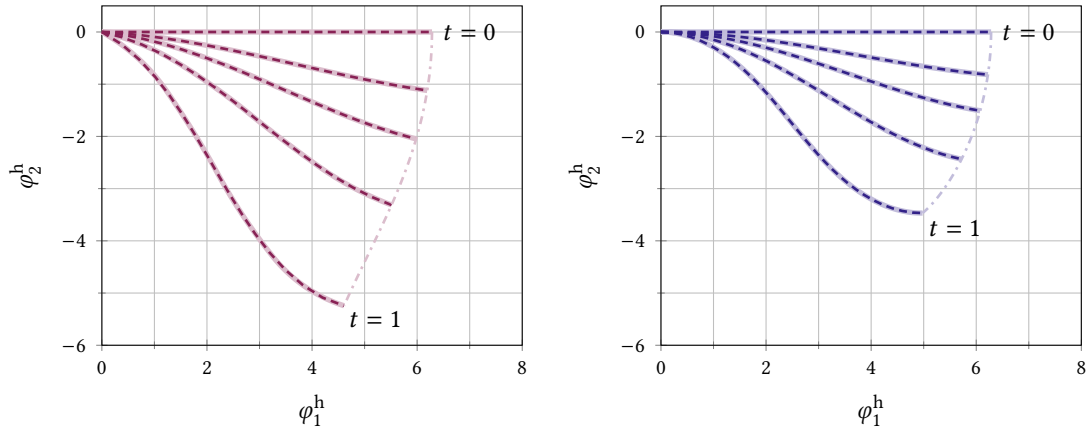

Figure 4.14.: Quasistatic cantilever problem: Centerline position $(\varphi_i)_{\mathrm{h}} = \boldsymbol{e}_i^{\top}\boldsymbol{\varphi}_{\mathrm{h}}$ for $t^n \in \{0, 0.1, 0.2, 0.4, 1\}$. Good agreement between our results (- - -, - - -) and the ones reported in [104] (——) for the unconstrained setting and the analytical solution (——) for the constrained setting. The tip centerline moves along the dash-dotted lines (-·-·-, -·-·-).

$$\boldsymbol{\nu}(t) = t \begin{bmatrix} 0 \\ -P \\ 0 \end{bmatrix}, \quad \boldsymbol{\mu}(t) = t \begin{bmatrix} 0 \\ 0 \\ 2.5P \end{bmatrix}, \qquad \text{where} \quad t \in [0, 1]. \tag{4.78}$$

Time t is regarded in this context as a load factor, see Section 3.5.2 in the previous chapter for further explanations. Correspondingly, the inertial parameters are set to zero to achieve quasistatic simulations, which only take place in the $\boldsymbol{e}_1$-$\boldsymbol{e}_2$-plane. We distinguish two scenarios, one shear-deformable and extensible ("unconstrained") and one shear-rigid and inextensible ("constrained"). In the latter one, we have set the related compliance parameters to zero to achieve an additional kinematic constraint, see Example 2.11 in Chapter 2 of this work for an explanatory example in the finite dimensional setting. In this case, the related stress quantities act as Lagrange multipliers. Eventually, an analytical solution based on the Euler's elastica can be given [100]. The resulting equilibria for both constrained and unconstrained settings are shown in Figure 4.14 and compared to reference results. These confirm not only the correct implementation but also the absence of locking effects.

4.6.4. Dynamic maneuver of a soft robotic arm

In this last example, we simulate a soft robotic arm, that is clamped at its bottom and is actuated with pneumatic chambers, see Section 4.5.2. The cantilever beam has a circular cross section with diameter $d = 0.03$ and we assume the material parameters corresponding to the silicone DragonSkin™ 30, i.e., Young's modulus $E = 6 \cdot 10^5$ and shear modulus $G = 2 \cdot 10^5$ [70]. This corresponds to a Poisson ratio of $\nu = 0.35$. Furthermore, we have cross-sectional moments of area $I_1 = I_2 = 1/2 I_T = \pi d^4/64$. Further details are comprised in Table 4.4. The beam is actuated by means of three pneumatic chambers with index $k \in \{1, 2, 3\}$, whose lines of centroids are parallel to the beam's centerline with a distance of $r_k = 6.5 \cdot 10^{-2}$, for all k. With respect to the global $\boldsymbol{e}_1$-axis these chambers are located initially at angles of $\alpha_k \in \{\frac{\pi}{6}, \frac{5\pi}{6}, \frac{9\pi}{6}\}$, yielding material coordinates in the cross-section frame $(\rho_k^1, \rho_k^2) = (r_k \cos\alpha_k, r_k \sin\alpha_k)$ for $k = 1, 2, 3$. We prescribe pneumatic forces

Table 4.3.: Quasistatic cantilever problem: Physical and numerical parameters.

h	t_{end}	n_{e}	$\varepsilon_{\mathrm{Newton}}$	L	ρA	$M_\rho^{11} = M_\rho^{22}$	$k_{\mathrm{b1}} = k_{\mathrm{b2}}$	k_{t}	$k_{\mathrm{s1}} = k_{\mathrm{s2}}$	k_{e}	P
10^{-2}	1	8	10^{-12}	2π	0	0	2	0.5	1	5	$10k_{\mathrm{b1}}/L^2$

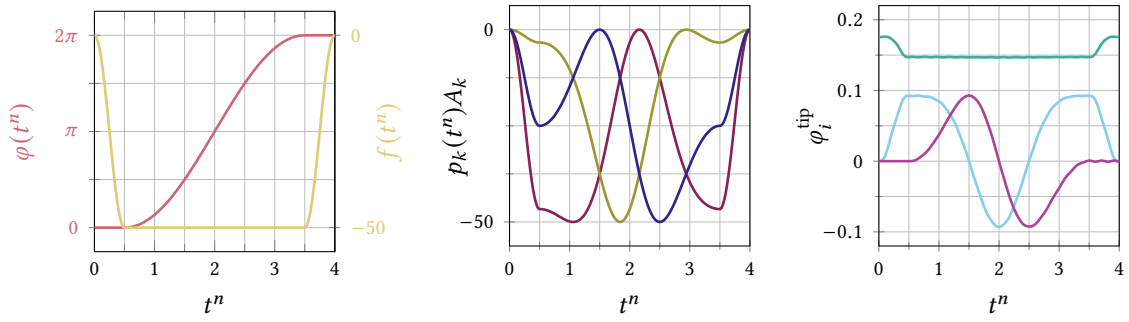

Figure 4.15.: Dynamic maneuver of a soft robotic arm: Phase angle function, amplitude function and corresponding pneumatic forces for $k \in \{1, 2, 3\}$. The tip position components $\varphi_i^{\text{tip}} = \boldsymbol{e}_i^\top \boldsymbol{\varphi}^{\text{tip}}$ with $i \in \{1, 2, 3\}$.

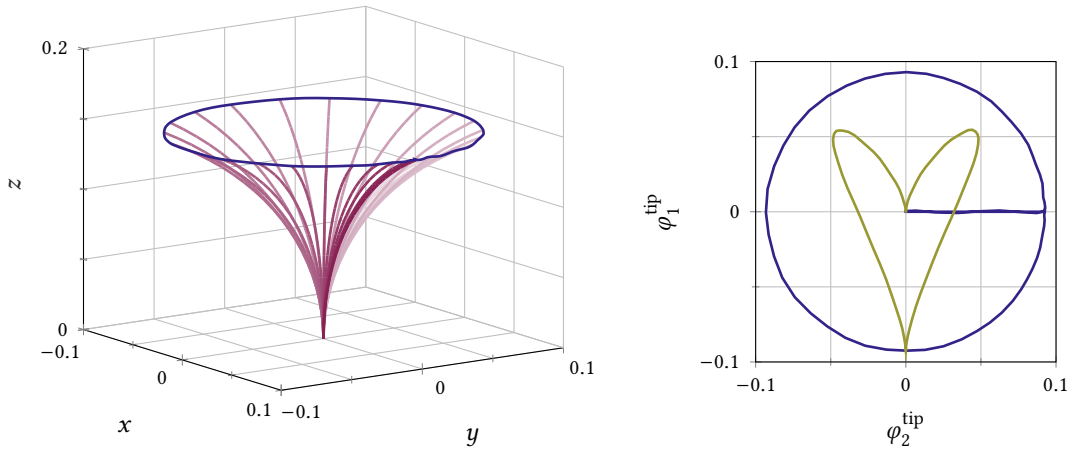

Figure 4.16.: Dynamic maneuver of a soft robotic arm: Snapshots of the centerline with azimuth and elevation perspective angles (55, 15) and the colormap for time t^n with $\in [0.5, 3.5]$. The tip position $\boldsymbol{\varphi}^{\text{tip}}$ follows a circular path (—). For the modified input functions (4.81) the tip follows a heart-shaped path (—).

$$p_k(t)A_k = \frac{1}{2} f(t)\left[1 + \cos(\varphi(t) - \alpha_k)\right] \tag{4.79}$$

with the time-dependent functions

$$f(t) = \begin{cases} \frac{1}{2} f_{\max}\left(1 - \cos\left(\frac{\pi t}{t_1}\right)\right), & 0 \le t \le t_1, \\ f_{\max}, & t_1 < t \le t_2, \\ \frac{1}{2} f_{\max}\left(1 + \cos\left(\pi \frac{t - t_2}{T - t_2}\right)\right), & t_2 < t \le T, \end{cases} \qquad \varphi(t) = \begin{cases} 0, & 0 \le t \le t_1, \\ \pi\left(1 - \cos\left(\pi \frac{t - t_1}{t_2 - t_1}\right)\right), & t_1 < t \le t_2, \\ 2\pi, & t_2 < t \le T, \end{cases} \tag{4.80}$$

that describe the amplitude and the phase angle, respectively. Therein, we set $f_{\max} = -50$, $t_1 = 0.5$, $t_2 = 3.5$ and $T = 4$. These functions are visualized in Figure 4.15. With a straight initial configuration along the $\boldsymbol{e}_3$-axis, the soft robotic arm first undergoes a bending motion in the $\boldsymbol{e}_1$-$\boldsymbol{e}_3$-plane until $t = t_1$. This is followed by a rotational motion, in which the tip position $\boldsymbol{\varphi}^{\text{tip}} := \boldsymbol{\varphi}_{\text{h}}(s = L, t = t^n)$ moves approximately on a constant height, see right depiction in Figure 4.16. At $t = t_2$ the arm has completed

Table 4.4.: Dynamic maneuver of a soft robotic arm: Physical and numerical parameters.

h	t_{end}	n_{e}	$\varepsilon_{\text{Newton}}$	L	ρ	A	$M_\rho^{11} = M_\rho^{22}$	$k_{\text{b1}} = k_{\text{b2}}$	k_{t}	$k_{\text{s1}} = k_{\text{s2}}$	k_{e}
0.05	4	10	10^{-11}	0.1755	1080	$\pi d^2/4$	ρI	EI	GI_T	GA	EA

one rotation and bends back until $t = t_{\text{end}}$. The snapshots shown in Figure 4.16 only track the circular motion phase for the sake of clarity. This approach can be further exploited to let the tip follow a more complex path in the $\boldsymbol{e}_1$-$\boldsymbol{e}_2$ plane, e.g., a heart-shaped one. To this end, for $\vartheta \in [0, 2\pi]$ a heart-shaped graph has the coordinates $x(\vartheta) = \sin^3(\vartheta)$ and $y(\vartheta) = \cos(\vartheta) - \cos(2\vartheta)$. The corresponding distance to the origin is given by $r(\vartheta) = \sqrt{x(\vartheta)^2 + y(\vartheta)^2}$ and can be normalized as $\tilde{r}(\vartheta) = r(\vartheta)/\max_{\vartheta\in[0,2\pi]} r(\vartheta)$. With $\vartheta = 2\pi\frac{t}{T}$ and $\tilde{\varphi}(\vartheta) = \operatorname{atan2}(y(\vartheta), x(\vartheta))$, we can eventually specify the amplitude and phase angle functions in (4.79) as

$$f(t) = f_{\max}\tilde{r}\left(2\pi\frac{t}{T}\right), \qquad \varphi(t) = \tilde{\varphi}\left(2\pi\frac{t}{T}\right). \tag{4.81}$$

The tip of the soft robotic arm then exhibits a heart shaped trajectory, see Figure 4.16. More complex deformation patterns can be achieved by including tendons and pneumatic chambers, whose line of centroids do not lie parallel to the centerline of the beam, or by dividing the beam into multiple segments with individual actuation input forces.

4.7. Conclusion and outlook

In this work, we have presented a mixed formulation and structure-preserving discretization procedure for the dynamics of spatial Cosserat rods. The proposed framework is objective, locking-free and enjoys many favorable properties due to its port-Hamiltonian structure. Through a compliance equation also shear-rigid and inextensible beam formulations can be seamlessly simulated within the present framework.

The employed pH formalism naturally leads to a structure-preserving mixed FE method. In this setting, the resulting pH differential-algebraic equations admit a particularly simple time-integration strategy based on pure midpoint approximations. The scheme is energy- and momentum-consistent, provides second-order accuracy and is remarkably robust. A further consequence is the accurate representation of crucial kinematic relations. Both the compliance equation and the orthonormality constraints have been differentiated with respect to time to reveal the pH structure. The proposed time integration scheme exactly integrates those relations.

For convenience, we have restricted ourselves to initially straight and stress-free beam problems with constant cross-section geometry and material parameters. An extension of the proposed framework to more general settings would merely impose more tedious algebra. While the presented formulation features the full geometrical nonlinearity, i.e., allowing for large displacements and rotations in three dimensions, we have always assumed linear constitutive relations. The present framework can be extended to general hyperelasticity along the lines of Chapter 6 of the present work, requiring the inclusion of a discrete gradient time integration approach, which goes well with the pH structure [91, C2, A3, C4]. Discrete gradient methods for pH DAEs are discussed in the following, see Chapter 5.

Control-oriented actuation mechanisms and viscoelastic material behavior have been included into the pH framework in a straightforward manner, making it ideally suited for interesting application fields [2, 62]. One future research direction would be the inclusion of our model into novel control strategies, like control by interconnection or energy shaping methods [50, 162, 171].

By employing a singularity-free director parametrization, the pitfalls of numerical methods for finite rotations have been circumvented. Despite its conceptual simplicity, the director formulation however does not reproduce the correct rotation inside the finite element, since the orthonormality condition on the directors is violated inside the element in general. In the future, projected unit quaternions [61, 101, 133, 235] could be used to obtain a manifold-consistent discrete pH formulation for Cosserat

rod dynamics, coming at the price of additional nonlinearities and configuration-dependent mass matrices.

Appendix to Chapter 4

4.A. Director velocities and virtual director displacements

This section introduces an important relation between virtual rotations and virtual director displacements. Additionally, convenient matrix identities are provided for later use.

The directors $\{\boldsymbol{d}_i\}_{i=1}^3$ introduced in Section 4.2.1 satisfy the orthogonality condition (4.2) to be a valid parametrization of finite rotations. Correspondingly, we have $\boldsymbol{d}_i = \boldsymbol{\Lambda}\boldsymbol{e}_i$ for each $i \in \{1, 2, 3\}$ such that the time derivative and the variation of a director is given by [100]

$$\delta\boldsymbol{d}_i = \delta\boldsymbol{\varphi} \times \boldsymbol{d}_i, \qquad \dot{\boldsymbol{d}}_i = \boldsymbol{\omega} \times \boldsymbol{d}_i, \tag{4.82}$$

where the spatial angular velocity $\boldsymbol{\omega}$ and the virtual rotation $\delta\boldsymbol{\varphi}$ are defined by means of their skew-symmetric matrices $\delta\tilde{\boldsymbol{\varphi}} = \delta\boldsymbol{\Lambda}\boldsymbol{\Lambda}^\top$ and $\tilde{\boldsymbol{\omega}} = \dot{\boldsymbol{\Lambda}}\boldsymbol{\Lambda}^\top$. To invert relation (4.82), we make use of Graßmann's identity (or also referred to as Lagrange's formula) for the vector triple product

$$\boldsymbol{a} \times (\boldsymbol{b} \times \boldsymbol{c}) = \boldsymbol{b}(\boldsymbol{a}^\top\boldsymbol{c}) - \boldsymbol{c}(\boldsymbol{a}^\top\boldsymbol{b}) \qquad \Leftrightarrow \qquad \tilde{\boldsymbol{a}}\tilde{\boldsymbol{b}} = \boldsymbol{b}\boldsymbol{a}^\top - (\boldsymbol{a}^\top\boldsymbol{b})\boldsymbol{I} \tag{4.83}$$

to show that $\boldsymbol{d}_i \times \delta\boldsymbol{d}_i = 2\delta\boldsymbol{\varphi}$, [28, 100]. Consequently, the virtual rotation $\delta\boldsymbol{\varphi}$ and angular velocity $\boldsymbol{\omega}$ can be expressed as

$$\delta\boldsymbol{\varphi} = \frac{1}{2}\boldsymbol{d}_i \times \delta\boldsymbol{d}_i = \frac{1}{2}\tilde{\boldsymbol{d}}_i\delta\boldsymbol{d}_i, \qquad \boldsymbol{\omega} = \frac{1}{2}\boldsymbol{d}_i \times \dot{\boldsymbol{d}}_i = \frac{1}{2}\tilde{\boldsymbol{d}}_i\dot{\boldsymbol{d}}_i. \tag{4.84}$$

These identities can be rewritten as

$$\delta\boldsymbol{\varphi} = \boldsymbol{T}(\boldsymbol{d})^\top\delta\boldsymbol{d}, \qquad \boldsymbol{\omega} = \boldsymbol{T}(\boldsymbol{d})^\top\dot{\boldsymbol{d}}, \tag{4.85}$$

where we made use of $\boldsymbol{d} = (\boldsymbol{d}_1, \boldsymbol{d}_2, \boldsymbol{d}_3) \in \mathbb{R}^9$ and the director-dependent matrix $\boldsymbol{T}(\boldsymbol{d}) \in \mathbb{R}^{9\times3}$ introduced in (4.14). This matrix moreover appears in the identities

$$\begin{aligned} &\boldsymbol{T}(\boldsymbol{d})^\top\boldsymbol{d} = \boldsymbol{0}, \qquad \boldsymbol{L}(\boldsymbol{d}_{,s})\boldsymbol{T}(\boldsymbol{d}) = \boldsymbol{L}(\boldsymbol{d})\boldsymbol{T}(\boldsymbol{d}_{,s}), \qquad \boldsymbol{T}(\boldsymbol{d})^\top\boldsymbol{T}(\boldsymbol{d}) = -\frac{1}{2}\boldsymbol{I}, \\ &\boldsymbol{G}_d(\boldsymbol{d})\boldsymbol{T}(\boldsymbol{d}) = \boldsymbol{0}, \qquad \boldsymbol{T}(\boldsymbol{d})^\top\boldsymbol{J}_{\boldsymbol{N}}(\boldsymbol{\varphi}_{,s}) = -\frac{1}{2}\tilde{\boldsymbol{\varphi}}_{,s}\boldsymbol{\Lambda}(\boldsymbol{d}), \end{aligned} \tag{4.86}$$

which will be used at a later stage. The matrices $\boldsymbol{\Lambda}$, $\boldsymbol{L}$, $\boldsymbol{J}_{\boldsymbol{N}}$ and $\boldsymbol{G}_d$, are defined in (4.1), (4.5) and (4.15), respectively.

4.B. Principle of virtual work

4.B.1. Displacement-based principle of virtual work

The partial differential equations governing the dynamics of the Cosserat rod can be derived from the principle of virtual work [33, 100], in which the equality

$$\delta W^{\mathrm{dyn}} + \delta W^{\mathrm{int}} + \delta W^{\mathrm{ext}} + \delta W^{\mathrm{c}} = 0 \tag{4.87}$$

holds for all admissible and arbitrary virtual displacements and where the four terms denote the virtual work contributions of dynamical, internal, external and constraint forces, respectively. The individual terms are discussed to obtain first the formulation (4.11), which can be found in standard literature [10, 209], and then the director-based formulation [33, 193], which we here formulated by means of operator matrices in (4.12).

Formulation in terms of virtual rotations Formulation (4.11) can be obtained by expressing the virtual work contributions in (4.87) in terms of virtual centerline displacements $\delta\boldsymbol{\varphi}$ and virtual rotation vectors $\delta\boldsymbol{\varphi}$, see relations in Appendix 4.A. The dynamical virtual work δW^{dyn} reads

$$\delta W^{\mathrm{dyn}} = \int_\Omega \left(\delta\boldsymbol{\varphi}^\top \rho A \ddot{\boldsymbol{\varphi}} + \delta\boldsymbol{\varphi}^\top (\boldsymbol{I}_\rho \dot{\boldsymbol{\omega}} + \boldsymbol{\omega} \times \boldsymbol{I}_\rho \boldsymbol{\omega})\right) \mathrm{d}s, \tag{4.88}$$

see [68]. The spatial inertia tensor $\boldsymbol{I}_\rho$ is related to its material counterpart $\boldsymbol{J}_\rho = M_\rho^{\alpha\alpha}\boldsymbol{I} - M_\rho^{\alpha\beta}\boldsymbol{e}_\alpha \otimes \boldsymbol{e}_\beta$ via $\boldsymbol{I}_\rho = \boldsymbol{\Lambda}\boldsymbol{J}_\rho\boldsymbol{\Lambda}^\top$. $M_\rho^{\alpha\beta}$ for $\alpha, \beta = 1, 2$ are the uniformly distributed second moments of mass of the cross section with respect to the director basis. The internal virtual work δW^{int} emanates from the variation of the elastic potential (4.8)

$$\delta W^{\mathrm{int}} = \delta \int_\Omega \check{W}(\boldsymbol{\Gamma}, \boldsymbol{K})\, \mathrm{d}s = \int_\Omega \left(\boldsymbol{N}^\top \delta\boldsymbol{\Gamma} + \boldsymbol{M}^\top \delta\boldsymbol{K}\right) \mathrm{d}s, \tag{4.89}$$

in which $\boldsymbol{N} = \partial_{\boldsymbol{\Gamma}}\check{W}$ and $\boldsymbol{M} = \partial_{\boldsymbol{K}}\check{W}$ are the dual quantities to the variation of the strain measures, see [33, 68], given by

$$\delta\boldsymbol{\Gamma} = \boldsymbol{\Lambda}^\top(\delta\boldsymbol{\varphi}_{,s} - \delta\boldsymbol{\varphi} \times \boldsymbol{\varphi}_{,s}) \qquad\qquad \delta\boldsymbol{K} = \boldsymbol{\Lambda}^\top \delta\boldsymbol{\varphi}_{,s}. \tag{4.90}$$

Substituting (4.90) into (4.89) and using (4.7), the internal virtual work takes the alternative form

$$\delta W^{\mathrm{int}} = \int_\Omega \left(\boldsymbol{n}^\top \left(\delta\boldsymbol{\varphi}_{,s} - \delta\boldsymbol{\varphi} \times \boldsymbol{\varphi}_{,s}\right) + \boldsymbol{m}^\top \delta\boldsymbol{\varphi}_{,s}\right) \mathrm{d}s. \tag{4.91}$$

The external virtual work due to distributed forces and torques as well as Neumann boundary terms can be written as

$$\delta W^{\mathrm{ext}} = -\int_\Omega \left(\delta\boldsymbol{\varphi}^\top \bar{\boldsymbol{n}} + \delta\boldsymbol{\varphi}^\top \bar{\boldsymbol{m}}\right) \mathrm{d}s - \left[\delta\boldsymbol{\varphi}^\top \boldsymbol{n}_{\mathrm{N}} + \delta\boldsymbol{\varphi}^\top \boldsymbol{m}_{\mathrm{N}}\right]_{\partial\Omega_{\mathrm{N}}}. \tag{4.92}$$

There are no constraints appearing in this formulation, hence $\delta W^{\mathrm{c}} = 0$. Eventually, one proceeds by collecting all terms connected to the virtual centerline displacements and virtual rotations in (4.87). After integration by parts and stating the arbitrariness of the virtual quantities one obtains the local balance equations (4.11) together with the corresponding Neumann boundary conditions.

Formulation in terms of directors Again, we begin with stating the terms appearing in the principle of virtual work (4.87). Accounting for the director-kinematics, the dynamical virtual work (4.88) has the alternative representation [33, 68]

$$\delta W^{\mathrm{dyn}} = \int_\Omega \left(\delta\boldsymbol{\varphi}^\top \rho A \ddot{\boldsymbol{\varphi}} + \delta\boldsymbol{d}_\alpha^\top M_\rho^{\alpha\beta} \ddot{\boldsymbol{d}}_\beta \right) \mathrm{d}s = \int_\Omega \left(\delta\boldsymbol{\varphi}^\top \rho A \ddot{\boldsymbol{\varphi}} + \delta\boldsymbol{d}^\top \boldsymbol{M}_\rho \ddot{\boldsymbol{d}} \right) \mathrm{d}s, \tag{4.93}$$

where we have used the director-related mass matrix $\boldsymbol{M}_\rho$, introduced in Section 4.2.3. For the internal virtual work (4.89), we can express the variation of the strain measures (4.90) alternatively as $\delta\boldsymbol{\Gamma} = (\delta\boldsymbol{d}_k^\top \boldsymbol{\varphi}_{,s} + \boldsymbol{d}_k^\top \delta\boldsymbol{\varphi}_{,s})\boldsymbol{e}_k$ and $\delta\boldsymbol{K} = \frac{1}{2}\varepsilon_{ijk}(\delta\boldsymbol{d}_k^\top \boldsymbol{d}_{j,s} + \boldsymbol{d}_k^\top \delta\boldsymbol{d}_{j,s})\boldsymbol{e}_i$, see definitions (4.3). This can be recast as

$$\delta\boldsymbol{\Gamma} = \boldsymbol{J}_{\boldsymbol{N}}(\boldsymbol{\varphi}_{,s})^\top \delta\boldsymbol{d} + \Lambda(\boldsymbol{d})^\top \delta\boldsymbol{\varphi}_{,s}, \qquad \delta\boldsymbol{K} = \boldsymbol{L}(\boldsymbol{d}_{,s})\delta\boldsymbol{d} - \boldsymbol{L}(\boldsymbol{d})\delta\boldsymbol{d}_{,s}, \tag{4.94}$$

conforming with (4.4). Substituting these variations of the strain measures into (4.90) and performing integration by parts yields

$$\delta W^{\mathrm{int}} = \int_\Omega \left(\delta\boldsymbol{d}^\top \boldsymbol{J}_{\boldsymbol{N}}(\boldsymbol{\varphi}_{,s})\boldsymbol{N} - \delta\boldsymbol{\varphi}^\top \partial_s(\Lambda(\boldsymbol{d})\boldsymbol{N}) + \delta\boldsymbol{d}^\top \mathcal{J}_{\boldsymbol{M}}(\boldsymbol{d})\boldsymbol{M} \right) \mathrm{d}s + \left[\delta\boldsymbol{\varphi}^\top \boldsymbol{n} + \delta\boldsymbol{d}^\top \boldsymbol{T}(\boldsymbol{d})\boldsymbol{m} \right]_{\partial\Omega}. \tag{4.95}$$

Here, we have made use of (4.7), (4.82), (4.85) and the relation $\boldsymbol{T}(\boldsymbol{d}) = -\boldsymbol{L}(\boldsymbol{d})^\top \Lambda(\boldsymbol{d})^\top$, which can be shown by using (4.83). Eventually, the matrix $\boldsymbol{J}_{\boldsymbol{N}}$ as defined in (4.5) and the matrix operator $\mathcal{J}_{\boldsymbol{M}}$ as defined in (4.13) could be identified. For the external virtual work (4.92), relation (4.85) is employed to obtain

$$\delta W^{\mathrm{ext}} = -\int_\Omega \left(\delta\boldsymbol{\varphi}^\top \bar{\boldsymbol{n}} + \delta\boldsymbol{d}^\top \boldsymbol{T}(\boldsymbol{d})\bar{\boldsymbol{m}} \right) \mathrm{d}s - \left[\delta\boldsymbol{\varphi}^\top \boldsymbol{n}_{\mathrm{N}} + \delta\boldsymbol{d}^\top \boldsymbol{T}(\boldsymbol{d})\boldsymbol{m}_{\mathrm{N}} \right]_{\partial\Omega_{\mathrm{N}}}. \tag{4.96}$$

And lastly, the virtual work done by the constraint forces related to the orthonormality conditions (4.2), is given by

$$\delta W^{\mathrm{c}} = \delta \int_\Omega \left(\boldsymbol{\lambda}^\top \boldsymbol{G}_d(\boldsymbol{d}) \right) \mathrm{d}s = \int_\Omega \left(\delta\boldsymbol{\lambda}^\top \boldsymbol{G}_d(\boldsymbol{d}) + \delta\boldsymbol{d}^\top \boldsymbol{G}_d(\boldsymbol{d})^\top \boldsymbol{\lambda} \right) \mathrm{d}s, \tag{4.97}$$

where the constraint Jacobian $\boldsymbol{G}_d = \mathrm{D}\boldsymbol{g}(\boldsymbol{d})$ is specified in (4.15). Eventually, one proceeds by collecting the different terms related to the virtual centerline displacements, virtual director displacements and virtual Lagrange multipliers. Subsequently, accounting for the arbitrariness of the virtual quantities yields the equations (4.12).

4.B.2. Hellinger–Reissner type principle of virtual work

The weak form of the pH formulation employed in this work (4.29) can be traced back to a Hellinger–Reissner type virtual work principle.Let us start by modifying the internal virtual work, which lies at the core of Hellinger–Reissner approaches. As shown in [104], the strain energy density function pertaining to a Hellinger–Reissner two-field principle is given by

$$W = W^{\mathrm{HR}}(\boldsymbol{\Gamma}, \boldsymbol{K}, \boldsymbol{N}, \boldsymbol{M}) = -W^\star(\boldsymbol{N}, \boldsymbol{M}) + \boldsymbol{N}^\top \boldsymbol{\Gamma} + \boldsymbol{M}^\top \boldsymbol{K} \tag{4.98}$$

where the strains are functions of the displacement quantities, see (4.3) and $W^\star$ is the complementary strain energy density (4.9) depending on independent stress quantities. Correspondingly, the virtual internal work appearing in the principle of virtual work (4.87) assumes the alternative form

$$\delta W^{\mathrm{int,HR}} = \delta \int_\Omega W^{\mathrm{HR}} \mathrm{d}s = \int_\Omega \left(\delta\boldsymbol{\Gamma}^\top \boldsymbol{N} + \delta\boldsymbol{K}^\top \boldsymbol{M} + \delta\boldsymbol{N}^\top (\boldsymbol{\Gamma} - \boldsymbol{C}_N \boldsymbol{N}) + \delta\boldsymbol{M}^\top (\boldsymbol{K} - \boldsymbol{C}_M \boldsymbol{M}) \right) \mathrm{d}s, \tag{4.99}$$

where we have substituted (4.10). In contrast to (4.89), the stress quantities are assumed to be independent from the displacement quantities. Correspondingly, the additional terms in (4.99) enforce the compliance relation (4.10) for compatibility. This expression is further rewritten similarly to (4.95) as

$$\delta W^{\text{int,HR}} = \int_\Omega \left(\delta \boldsymbol{\varphi}_{,s}^\top \boldsymbol{n} + \delta \boldsymbol{d}^\top \boldsymbol{J}_{\boldsymbol{N}} \boldsymbol{N} + \boldsymbol{M}^\top \mathcal{J}_{\boldsymbol{K}}(\boldsymbol{d}) \delta \boldsymbol{d} + \delta \boldsymbol{N}^\top (\boldsymbol{\Gamma} - \boldsymbol{C}_N \boldsymbol{N}) + \delta \boldsymbol{M}^\top (\boldsymbol{K} - \boldsymbol{C}_M \boldsymbol{M}) \right) \mathrm{d}s, \tag{4.100}$$

where the differential operator matrix $\mathcal{J}_{\boldsymbol{K}}$ is given in (4.13). Additionally, we can modify the virtual work of dynamical forces in the director formulation (4.93) to account for independent velocities (4.16) by mimicking the Hellinger–Reissner approach (4.99) as

$$\delta W^{\text{dyn,HR}} = \int_\Omega \left(\delta \boldsymbol{\varphi}^\top \rho A \dot{\boldsymbol{v}}_\varphi + \delta \boldsymbol{d}^\top \boldsymbol{M}_\rho \dot{\boldsymbol{v}}_d + \rho A \delta \boldsymbol{v}_\varphi^\top (\dot{\boldsymbol{\varphi}} - \boldsymbol{v}_\varphi) + (\boldsymbol{M}_\rho \delta \boldsymbol{v}_d)^\top (\dot{\boldsymbol{d}} - \boldsymbol{v}_d) \right) \mathrm{d}s, \tag{4.101}$$

where the kinematic relation (4.16) is enforced to ensure compatible independent velocities. Collecting the terms (4.96), (4.97), (4.100) and (4.101), and separating the terms corresponding to the different virtual quantities yields the weak form

$$\begin{aligned}
\left(\rho A \delta \boldsymbol{v}_\varphi, \dot{\boldsymbol{\varphi}} - \boldsymbol{v}_\varphi\right)_\Omega &= 0, && \text{(4.102a)}\\
\left(\boldsymbol{M}_\rho \delta \boldsymbol{v}_d, \dot{\boldsymbol{d}} - \boldsymbol{v}_d\right)_\Omega &= 0, && \text{(4.102b)}\\
\left(\delta \boldsymbol{\varphi}, \rho A \dot{\boldsymbol{v}}_\varphi - \bar{\boldsymbol{n}}\right)_\Omega + (\partial_s(\delta \boldsymbol{\varphi}), \boldsymbol{\Lambda} \boldsymbol{N})_\Omega - [\delta \boldsymbol{\varphi}, \boldsymbol{n}_{\mathrm{N}}]_{\partial\Omega} &= 0, && \text{(4.102c)}\\
\left(\delta \boldsymbol{d}, \boldsymbol{M}_\rho \dot{\boldsymbol{v}}_d + \boldsymbol{J}_{\boldsymbol{N}} \boldsymbol{N} + \boldsymbol{G}_d^\top \boldsymbol{\lambda} - \boldsymbol{T} \bar{\boldsymbol{m}}\right)_\Omega + (\mathcal{J}_{\boldsymbol{K}} \delta \boldsymbol{d}, \boldsymbol{M})_\Omega - [\delta \boldsymbol{d}, \boldsymbol{T} \boldsymbol{m}_{\mathrm{N}}]_{\partial\Omega} &= 0, && \text{(4.102d)}\\
\left(\delta \boldsymbol{N}, \boldsymbol{C}_N \boldsymbol{N} - \boldsymbol{\Lambda}^\top \boldsymbol{\varphi}_{,s}\right)_\Omega &= 0, && \text{(4.102e)}\\
\left(\delta \boldsymbol{M}, \boldsymbol{C}_M \boldsymbol{M} - \boldsymbol{L}(\boldsymbol{d}_{,s}) \boldsymbol{d}\right)_\Omega &= 0, && \text{(4.102f)}\\
\left(\delta \boldsymbol{\lambda}, \boldsymbol{g}(\boldsymbol{d})\right)_\Omega &= 0. && \text{(4.102g)}
\end{aligned}$$

which can be linked to the weak form (4.29) by replacing the last three relations with their time-differentiated version.

4.C. Proof: Formally skew-adjoint structure operator

Let us here verify that the structure operator $\mathcal{J}$ contained in the dynamics (4.22) is formally skew-adjoint. This is equivalent with showing that (4.26) holds true and the inner product $(\boldsymbol{z}, \boldsymbol{J}\boldsymbol{z})_\Omega$ only yields boundary terms. For elements of $\mathcal{J}$ that do not involve spatial derivatives, the formal skew-adjointness boils down to skew-symmetry and no integration by parts is required. The corresponding terms cancel each other out. To this end, it remains to show that

$$\left(\begin{bmatrix} \boldsymbol{v} \\ \boldsymbol{\sigma} \end{bmatrix}, \begin{bmatrix} 0 & -\mathcal{J}_{\boldsymbol{v}} \\ \mathcal{J}_{\boldsymbol{\sigma}} & 0 \end{bmatrix} \begin{bmatrix} \boldsymbol{v} \\ \boldsymbol{\sigma} \end{bmatrix} \right)_\Omega = (\boldsymbol{\sigma}, \mathcal{J}_{\boldsymbol{\sigma}} \boldsymbol{v})_\Omega - (\boldsymbol{v}, \mathcal{J}_{\boldsymbol{v}} \boldsymbol{\sigma})_\Omega = \left[\boldsymbol{v}_\varphi^\top \boldsymbol{n} + \boldsymbol{\omega}^\top \boldsymbol{m} \right]_{\partial\Omega}. \tag{4.103}$$

This is a representation of the abstract integration-by-parts formula (2.69) and eventually corresponds to $\mathcal{J}_{\boldsymbol{v}}^* = \mathcal{J}_{\boldsymbol{\sigma}}$. Condition (4.103) can be expressed more detailed as

$$\begin{aligned}
&\left(\begin{bmatrix} \boldsymbol{N} \\ \boldsymbol{M} \end{bmatrix}, \begin{bmatrix} \boldsymbol{\Lambda}(\boldsymbol{d})^\top \partial_s[\,\cdot\,] & \boldsymbol{J}_{\boldsymbol{N}}(\boldsymbol{\varphi}_{,s})^\top \\ \boldsymbol{0} & \mathcal{J}_{\boldsymbol{K}}(\boldsymbol{d}, \boldsymbol{d}_{,s}) \end{bmatrix} \begin{bmatrix} \boldsymbol{v}_\varphi \\ \boldsymbol{v}_d \end{bmatrix} \right)_\Omega \\
&\qquad - \left(\begin{bmatrix} \boldsymbol{v}_\varphi \\ \boldsymbol{v}_d \end{bmatrix}, \begin{bmatrix} -\partial_s(\boldsymbol{\Lambda}(\boldsymbol{d})[\,\cdot\,]) & \boldsymbol{0} \\ \boldsymbol{J}_{\boldsymbol{N}}(\boldsymbol{\varphi}_{,s}) & \mathcal{J}_{\boldsymbol{M}}(\boldsymbol{d}, \boldsymbol{d}_{,s}) \end{bmatrix} \begin{bmatrix} \boldsymbol{N} \\ \boldsymbol{M} \end{bmatrix} \right)_\Omega = \left[\boldsymbol{v}_\varphi^\top \boldsymbol{n} + \boldsymbol{\omega}^\top \boldsymbol{m} \right]_{\partial\Omega}.
\end{aligned} \tag{4.104}$$

Here, one can identify three terms. The first one vanishes due to skew-symmetry, i.e.,

$$\int_\Omega \left(\boldsymbol{N}^\top \boldsymbol{J}_{\boldsymbol{N}}(\boldsymbol{\varphi}_{,s})^\top \boldsymbol{v}_d - \boldsymbol{v}_d^\top \boldsymbol{J}_{\boldsymbol{N}}(\boldsymbol{\varphi}_{,s}) \boldsymbol{N} \right) \mathrm{d}s = 0. \tag{4.105}$$

The second term can be analyzed as

$$\int_\Omega \left(\boldsymbol{N}^\top \boldsymbol{\Lambda}(\boldsymbol{d})^\top \boldsymbol{v}_{\varphi,s} + \boldsymbol{v}_\varphi^\top \partial_s(\boldsymbol{\Lambda}(\boldsymbol{d})\boldsymbol{N}) \right) \mathrm{d}s = \int_\Omega \left(\boldsymbol{v}_\varphi^\top \boldsymbol{n}_{,s} + \boldsymbol{n}^\top \boldsymbol{v}_{\varphi,s} \right) \mathrm{d}s = \left[\boldsymbol{v}_\varphi^\top \boldsymbol{n} \right]_{\partial\Omega}, \tag{4.106}$$

which is equivalent to $(\partial_s(\boldsymbol{\Lambda}(\boldsymbol{d})\square))^* = -\boldsymbol{\Lambda}(\boldsymbol{d})^\top \partial_s \square$. The third and last term yields

$$\begin{aligned} &\int_\Omega \left(\boldsymbol{M}^\top \mathcal{J}_{\boldsymbol{K}} \boldsymbol{v}_d - \boldsymbol{v}_d^\top \mathcal{J}_{\boldsymbol{M}} \boldsymbol{M} \right) \mathrm{d}s \\ &\qquad = \int_\Omega \left(\boldsymbol{M}^\top \boldsymbol{L}(\boldsymbol{d}_{,s}) \boldsymbol{v}_d - \boldsymbol{M}^\top \boldsymbol{L}(\boldsymbol{d}) \boldsymbol{v}_{d,s} - \boldsymbol{v}_d^\top \boldsymbol{L}(\boldsymbol{d}_{,s})^\top \boldsymbol{M} - \boldsymbol{v}_d^\top \partial_s(\boldsymbol{L}(\boldsymbol{d})^\top \boldsymbol{M}) \right) \mathrm{d}s \\ &\qquad = \left[-\boldsymbol{v}_d^\top \boldsymbol{L}(\boldsymbol{d})^\top \boldsymbol{M} \right]_{\partial\Omega} = \left[-\boldsymbol{v}_d^\top \boldsymbol{L}(\boldsymbol{d})^\top \boldsymbol{\Lambda}(\boldsymbol{d})^\top \boldsymbol{m} \right]_{\partial\Omega} = \left[\boldsymbol{\omega}^\top \boldsymbol{m} \right]_{\partial\Omega} \end{aligned} \tag{4.107}$$

and shows that $\mathcal{J}_{\boldsymbol{M}}^* = \mathcal{J}_{\boldsymbol{K}}$. In the last equation, we have used (4.85) and the relation $\boldsymbol{T}(\boldsymbol{d}) = -\boldsymbol{L}(\boldsymbol{d})^\top \boldsymbol{\Lambda}(\boldsymbol{d})^\top$, which can be shown by using (4.83). Eventually, the claim (4.103) follows from adding up the last three relations and comparing them with (4.104).

4.D. Balance of total angular momentum

The fundamental balance of total angular momentum can be shown by choosing specific test functions in the weak form (4.29). In the present case, the total angular momentum [193] is given by

$$\boldsymbol{l}(\boldsymbol{q}, \boldsymbol{v}) = \int_\Omega \left(\boldsymbol{\varphi} \times \rho A \boldsymbol{v}_\varphi + \boldsymbol{d}_\alpha \times M_\rho^{\alpha\beta} \boldsymbol{v}_\beta \right) \mathrm{d}s = \int_\Omega \left(\tilde{\boldsymbol{\varphi}} \rho A \boldsymbol{v}_\varphi - 2\boldsymbol{T}(\boldsymbol{d})^\top \boldsymbol{M}_\rho \boldsymbol{v}_d \right) \mathrm{d}s, \tag{4.108}$$

where summation over $\alpha = 1, 2$ is implied and (4.14) has been used. To show the balance of total angular momentum, we assume pure Neumann boundary conditions such that we are allowed to choose the test functions

$$\begin{aligned} \delta\boldsymbol{\varphi} &= \boldsymbol{\xi} \times \boldsymbol{\varphi} = -\tilde{\boldsymbol{\varphi}}\boldsymbol{\xi}, \quad & \delta\boldsymbol{v}_\varphi &= \boldsymbol{\xi} \times \boldsymbol{v}_\varphi = -\tilde{\boldsymbol{v}}_\varphi \boldsymbol{\xi}, \\ \delta\boldsymbol{d}_i &= \boldsymbol{\xi} \times \boldsymbol{d}_i = -\tilde{\boldsymbol{d}}_i \boldsymbol{\xi}, \quad & \delta\boldsymbol{v}_i &= \boldsymbol{\xi} \times \boldsymbol{v}_i = -\tilde{\boldsymbol{v}}_i \boldsymbol{\xi}, \end{aligned} \tag{4.109}$$

in (4.29). With constant but arbitrary $\boldsymbol{\xi} \in \mathbb{R}^3$, this corresponds to a rigid body rotation. Using (4.14), we have

$$\delta\boldsymbol{d} = -2\boldsymbol{T}(\boldsymbol{d})\boldsymbol{\xi}, \qquad \delta\boldsymbol{v}_d = -2\boldsymbol{T}(\boldsymbol{v}_d)\boldsymbol{\xi}. \tag{4.110}$$

Next, we insert these test functions into (4.29a) - (4.29d). Adding up (4.29c) and (4.29d) and subtracting (4.29a) and (4.29b) yields after some algebraic manipulations

$$\dot{\boldsymbol{l}} = \int_\Omega (\boldsymbol{\varphi} \times \bar{\boldsymbol{n}} + \bar{\boldsymbol{m}}) \, \mathrm{d}s + \left[\boldsymbol{\varphi} \times \boldsymbol{n}_\mathrm{N} + \boldsymbol{m}_\mathrm{N} \right]_{\partial\Omega}, \tag{4.111}$$

Here, we have used the properties (4.86) and the arbitrariness of the constant $\boldsymbol{\xi}$. Equation (4.111) states that the rate of change of total angular momentum is equal to the sum of all external moments acting on the beam, both distributed and concentrated at the boundaries. In case of closed systems, the total angular momentum is a conserved quantity.

Remark 4.11. *Note that in a similar fashion one may show the balance of total linear momentum and of total energy. The latter has already been demonstrated in a more appealing way by means of the pH structure, see* (4.28). ♧

Discrete time angular momentum balance. It can be shown that the time stepping scheme (4.42) retains the balance equation for total angular momentum (4.111). In the bulk part of this work we have derived the time integration method (4.42) by means of a sequential space- and time approximation of the continuous weak form (4.29). In fact, the first four lines of (4.42) can be equivalently rewritten in a discrete weak form given by

$$\left(\rho A \delta \boldsymbol{v}_{\varphi,\mathrm{h}}, \boldsymbol{\varphi}_{\mathrm{h}}^{n+1} - \boldsymbol{\varphi}_{\mathrm{h}}^{n} - h\boldsymbol{v}_{\varphi,\mathrm{h}}^{n+1/2}\right)_{\Omega} = 0, \tag{4.112a}$$

$$\left(\boldsymbol{M}_{\rho}\delta \boldsymbol{v}_{d,\mathrm{h}}, \boldsymbol{d}_{\mathrm{h}}^{n+1} - \boldsymbol{d}_{\mathrm{h}}^{n} - h\boldsymbol{v}_{d,\mathrm{h}}^{n+1/2}\right)_{\Omega} = 0, \tag{4.112b}$$

$$\begin{aligned}\left(\delta\boldsymbol{\varphi}_{\mathrm{h}}, \rho A\boldsymbol{v}_{\varphi,\mathrm{h}}^{n+1} - \rho A\boldsymbol{v}_{\varphi,\mathrm{h}}^{n} - h\bar{\boldsymbol{n}}^{n+1/2}\right)_{\Omega} + \left(\partial_s(\delta\boldsymbol{\varphi}_{\mathrm{h}}), h\boldsymbol{\Lambda}(\boldsymbol{d}_{\mathrm{h}}^{n+1/2})\boldsymbol{N}_{\mathrm{h}}^{n+1/2}\right)_{\Omega} \\ - \left[\delta\boldsymbol{\varphi}_{\mathrm{h}}, h\boldsymbol{n}_{\mathrm{N}}^{n+1/2}\right]_{\partial\Omega} = 0,\end{aligned} \tag{4.112c}$$

$$\begin{aligned}&\left(\delta\boldsymbol{d}_{\mathrm{h}}, \boldsymbol{M}_{\rho}\boldsymbol{v}_{d,\mathrm{h}}^{n+1} - \boldsymbol{M}_{\rho}\boldsymbol{v}_{d,\mathrm{h}}^{n} + h\boldsymbol{J}_{\boldsymbol{N}}(\boldsymbol{\varphi}_{\mathrm{h}}^{n+1/2})\boldsymbol{N}_{\mathrm{h}}^{n+1/2} + hG_d(\boldsymbol{d}_{\mathrm{h}}^{n+1/2})^{\top}\boldsymbol{\lambda}_{\mathrm{h}}^{n+1/2}\right)_{\Omega} \\ &\quad - \left(\delta\boldsymbol{d}_{\mathrm{h}}, h\boldsymbol{T}(\boldsymbol{d}_{\mathrm{h}}^{n+1/2})\bar{\boldsymbol{m}}^{n+1/2}\right)_{\Omega} + \left(\mathcal{J}_K(\boldsymbol{d}_{\mathrm{h}}^{n+1/2})\delta\boldsymbol{d}_{\mathrm{h}}, h\boldsymbol{M}_{\mathrm{h}}^{n+1/2}\right)_{\Omega} \\ &\quad - \left[\delta\boldsymbol{d}_{\mathrm{h}}, h\boldsymbol{T}(\boldsymbol{d}_{\mathrm{h}}^{n+1/2})\boldsymbol{m}_{\mathrm{N}}^{n+1/2}\right]_{\partial\Omega} = 0.\end{aligned} \tag{4.112d}$$

Due to the bilinear form of the total angular momentum (4.108), we can apply the findings from Remark 4.7 to the difference from one time step to another, such that

$$\begin{aligned}\boldsymbol{l}(\boldsymbol{q}_{\mathrm{h}}^{n+1}, \boldsymbol{v}_{\mathrm{h}}^{n+1}) - \boldsymbol{l}(\boldsymbol{q}_{\mathrm{h}}^{n}, \boldsymbol{v}_{\mathrm{h}}^{n}) = \int_{\Omega} \Big(&\tilde{\boldsymbol{\varphi}}_{\mathrm{h}}^{n+1/2}\rho A(\boldsymbol{v}_{\varphi,\mathrm{h}}^{n+1} - \boldsymbol{v}_{\varphi,\mathrm{h}}^{n}) - 2\boldsymbol{T}(\boldsymbol{d}_{\mathrm{h}}^{n+1/2})^{\top}\boldsymbol{M}_{\rho}(\boldsymbol{v}_{d,\mathrm{h}}^{n+1} - \boldsymbol{v}_{d,\mathrm{h}}^{n}) \\ &+ (\tilde{\boldsymbol{\varphi}}_{\mathrm{h}}^{n+1} - \tilde{\boldsymbol{\varphi}}_{\mathrm{h}}^{n})\rho A\boldsymbol{v}_{\varphi,\mathrm{h}}^{n+1/2} - 2\boldsymbol{T}(\boldsymbol{d}_{\mathrm{h}}^{n+1} - \boldsymbol{d}_{\mathrm{h}}^{n})^{\top}\boldsymbol{M}_{\rho}\boldsymbol{v}_{d,\mathrm{h}}^{n+1/2}\Big)\,\mathrm{d}s.\end{aligned} \tag{4.113}$$

Similar to above, we choose test functions

$$\delta\boldsymbol{\varphi} = -\tilde{\boldsymbol{\varphi}}_{\mathrm{h}}^{n+1/2}\xi, \quad \delta\boldsymbol{v}_{\varphi} = -\tilde{\boldsymbol{v}}_{\varphi,\mathrm{h}}^{n+1/2}\xi, \quad \delta\boldsymbol{d} = -2\boldsymbol{T}(\boldsymbol{d}_{\mathrm{h}}^{n+1/2})\xi, \quad \delta\boldsymbol{v}_{d} = -2\boldsymbol{T}(\boldsymbol{v}_{d,\mathrm{h}}^{n+1/2})\xi \tag{4.114}$$

in the discrete-time weak forms (4.112a)-(4.112d). As in the continuous case, adding up (4.112c) and (4.112d) and subtracting (4.112a) and (4.112b) eventually yields for arbitrary ξ

$$\begin{aligned}&\boldsymbol{l}(\boldsymbol{q}_{\mathrm{h}}^{n+1}, \boldsymbol{v}_{\mathrm{h}}^{n+1}) - \boldsymbol{l}(\boldsymbol{q}_{\mathrm{h}}^{n}, \boldsymbol{v}_{\mathrm{h}}^{n}) = \\ &\qquad h\int_{\Omega}(\boldsymbol{\varphi}_{\mathrm{h}}^{n+1/2}\times\bar{\boldsymbol{n}}^{n+1/2} + \bar{\boldsymbol{m}}^{n+1/2})\,\mathrm{d}s + h\left[\boldsymbol{\varphi}_{\mathrm{h}}^{n+1/2}\times\boldsymbol{n}_{\mathrm{N}}^{n+1/2} + \boldsymbol{m}_{\mathrm{N}}^{n+1/2}\right]_{\partial\Omega},\end{aligned} \tag{4.115}$$

where we have also substituted (4.113). This calculation further involves the identities (4.86).

4.E. System matrices after discretization in space

Here, we display detailed definitions of the matrices contained in the pH system (4.35) after spatial discretization. Consistently with (4.34), we write the FE ansatz as

$$\begin{aligned}&\begin{bmatrix}\boldsymbol{\varphi}_{\mathrm{h}}(s,t)\\ \boldsymbol{d}_{\mathrm{h}}(s,t)\end{bmatrix} = \begin{bmatrix}\boldsymbol{\Phi}_{\varphi}(s) & 0\\ 0 & \boldsymbol{\Phi}_{d}(s)\end{bmatrix}\begin{bmatrix}\hat{\boldsymbol{\varphi}}(t)\\ \hat{\boldsymbol{d}}(t)\end{bmatrix}, \qquad \begin{bmatrix}\boldsymbol{v}_{\varphi,\mathrm{h}}(s,t)\\ \boldsymbol{v}_{d,\mathrm{h}}(s,t)\end{bmatrix} = \begin{bmatrix}\boldsymbol{\Phi}_{\varphi}(s) & 0\\ 0 & \boldsymbol{\Phi}_{d}(s)\end{bmatrix}\begin{bmatrix}\hat{\boldsymbol{v}}_{\varphi}(t)\\ \hat{\boldsymbol{v}}_{d}(t)\end{bmatrix},\\ &\begin{bmatrix}\boldsymbol{N}_{\mathrm{h}}(s,t)\\ \boldsymbol{M}_{\mathrm{h}}(s,t)\end{bmatrix} = \begin{bmatrix}\boldsymbol{\Psi}_{N}(s) & 0\\ 0 & \boldsymbol{\Psi}_{M}(s)\end{bmatrix}\begin{bmatrix}\hat{\boldsymbol{N}}(t)\\ \hat{\boldsymbol{M}}(t)\end{bmatrix}, \qquad \boldsymbol{\lambda}_{\mathrm{h}}(s,t) = \Xi(s)\hat{\boldsymbol{\lambda}}(t),\end{aligned} \tag{4.116}$$

together with the same ansatz for the respective test functions. Inserting these relations into the weak form (4.29) and accounting for arbitrary test functions yields the semi-discrete set of differential-algebraic equations

$$\begin{aligned}
\dot{\hat{\boldsymbol{\varphi}}} &= \hat{\boldsymbol{v}}_\varphi, \\
\dot{\hat{\boldsymbol{d}}} &= \hat{\boldsymbol{v}}_d, \\
\rho A \hat{\boldsymbol{M}}_\varphi \dot{\hat{\boldsymbol{v}}}_\varphi &= -\hat{\boldsymbol{G}}_{\varphi N}(\hat{\boldsymbol{q}})^\top \hat{\boldsymbol{N}} + \hat{\boldsymbol{M}}_\varphi \hat{\bar{\boldsymbol{n}}} + \hat{\boldsymbol{B}}_{\partial,n} \boldsymbol{n}_\mathrm{N}, \\
\hat{\boldsymbol{M}}_d \dot{\hat{\boldsymbol{v}}}_d &= -\hat{\boldsymbol{G}}_{dN}(\hat{\boldsymbol{q}})^\top \hat{\boldsymbol{N}} - \hat{\boldsymbol{G}}_{dM}(\hat{\boldsymbol{q}})^\top \hat{\boldsymbol{M}} - \hat{\boldsymbol{G}}_d(\hat{\boldsymbol{d}})^\top \hat{\boldsymbol{\lambda}} + \hat{\boldsymbol{B}}_{\Omega,m}(\hat{\boldsymbol{q}}) \hat{\bar{\boldsymbol{m}}} + \hat{\boldsymbol{B}}_{\partial,m}(\hat{\boldsymbol{q}}) \boldsymbol{m}_\mathrm{N}, \\
\hat{\boldsymbol{C}}_N \dot{\hat{\boldsymbol{N}}} &= \hat{\boldsymbol{G}}_{\varphi N}(\hat{\boldsymbol{q}}) \hat{\boldsymbol{v}}_\varphi + \hat{\boldsymbol{G}}_{dN}(\hat{\boldsymbol{q}}) \hat{\boldsymbol{v}}, \\
\hat{\boldsymbol{C}}_M \dot{\hat{\boldsymbol{M}}} &= \hat{\boldsymbol{G}}_{dM}(\hat{\boldsymbol{q}}) \hat{\boldsymbol{v}}_d, \\
\boldsymbol{0} &= \hat{\boldsymbol{G}}_d(\hat{\boldsymbol{d}}) \hat{\boldsymbol{v}}_d,
\end{aligned} \tag{4.117}$$

which are equivalent to the finite-dimensional pH system (4.35). To show this in depth, consider the abbreviations

$$\begin{aligned}
&\hat{\boldsymbol{M}}_o = \int_\Omega \boldsymbol{\Phi}^\top \boldsymbol{M}_o \boldsymbol{\Phi} \,\mathrm{d}s = \mathrm{diag}(\rho A \hat{\boldsymbol{M}}_\varphi, \hat{\boldsymbol{M}}_d), \quad \hat{\boldsymbol{C}} = \int_\Omega \boldsymbol{\Psi}^\top \boldsymbol{C} \boldsymbol{\Psi} \,\mathrm{d}s = \mathrm{diag}(\hat{\boldsymbol{C}}_N, \hat{\boldsymbol{C}}_M), \\
&\hat{\boldsymbol{G}}(\hat{\boldsymbol{q}}) = \begin{bmatrix} \boldsymbol{0} & \hat{\boldsymbol{G}}_d \end{bmatrix}, \quad \hat{\boldsymbol{J}}_{\sigma v}(\hat{\boldsymbol{q}}) = \begin{bmatrix} \hat{\boldsymbol{G}}_{\varphi N} & \hat{\boldsymbol{G}}_{dN} \\ \boldsymbol{0} & \hat{\boldsymbol{G}}_{dM} \end{bmatrix}, \quad \hat{\boldsymbol{B}}_\Omega(\hat{\boldsymbol{q}}) = \begin{bmatrix} \hat{\boldsymbol{M}}_\varphi & \boldsymbol{0} \\ \boldsymbol{0} & \hat{\boldsymbol{B}}_{\Omega,m} \end{bmatrix}, \quad \hat{\boldsymbol{B}}_\partial(\hat{\boldsymbol{q}}) = \begin{bmatrix} \hat{\boldsymbol{B}}_{\partial,n} & \boldsymbol{0} \\ \boldsymbol{0} & \hat{\boldsymbol{B}}_{\partial,m} \end{bmatrix}
\end{aligned} \tag{4.118}$$

with the mass and compliance matrices

$$\hat{\boldsymbol{M}}_\varphi = \int_\Omega \boldsymbol{\Phi}_\varphi^\top \boldsymbol{\Phi}_\varphi \,\mathrm{d}s, \quad \hat{\boldsymbol{M}}_d = \int_\Omega \boldsymbol{\Phi}_d^\top \boldsymbol{M}_\rho \boldsymbol{\Phi}_d \,\mathrm{d}s, \quad \hat{\boldsymbol{C}}_N = \int_\Omega \boldsymbol{\Psi}_N^\top \boldsymbol{C}_N \boldsymbol{\Psi}_N \,\mathrm{d}s, \quad \hat{\boldsymbol{C}}_M = \int_\Omega \boldsymbol{\Psi}_M^\top \boldsymbol{C}_M \boldsymbol{\Psi}_M \,\mathrm{d}s,$$

and discrete elements of the structure matrix

$$\begin{aligned}
\hat{\boldsymbol{G}}_{\varphi N}(\hat{\boldsymbol{q}}) &= \int_\Omega \boldsymbol{\Psi}_N^\top \boldsymbol{\Lambda}(\boldsymbol{d}_\mathrm{h})^\top \partial_s \boldsymbol{\Phi}_\varphi \,\mathrm{d}s, \\
\hat{\boldsymbol{G}}_{dN}(\hat{\boldsymbol{q}}) &= \int_\Omega \boldsymbol{\Psi}_N^\top \boldsymbol{J}_N(\partial_s \boldsymbol{\varphi}_\mathrm{h}) \boldsymbol{\Phi}_d \,\mathrm{d}s, \\
\hat{\boldsymbol{G}}_{dM}(\hat{\boldsymbol{q}}) &= \int_\Omega \boldsymbol{\Psi}_M^\top (\boldsymbol{L}(\partial_s \boldsymbol{d}_\mathrm{h}) \boldsymbol{\Phi}_d - \boldsymbol{L}(\boldsymbol{d}_\mathrm{h}) \partial_s \boldsymbol{\Phi}_d) \,\mathrm{d}s,
\end{aligned} \tag{4.119}$$

Concerning the treatment of the constraint equation, consider the approximation of (4.29g) using n_n delta functions $\bar{\delta}(s - s_i)$, cf. [103, Chapter 1.11], given by

$$\left(\delta\boldsymbol{\lambda}_\mathrm{h}, \boldsymbol{G}_d(\boldsymbol{d}_\mathrm{h}) \boldsymbol{v}_{d,\mathrm{h}}\right)_\Omega = \left(\sum_{i=1}^{n_\mathrm{n}} \bar{\delta}(s - s_i) \delta\boldsymbol{\lambda}_i, \boldsymbol{G}_d(\boldsymbol{d}_\mathrm{h}) \boldsymbol{v}_{d,\mathrm{h}} \right)_\Omega = \sum_{i=1}^{n_\mathrm{n}} \delta\boldsymbol{\lambda}_i^\top \boldsymbol{G}_d(\hat{\boldsymbol{d}}_i) \hat{\boldsymbol{v}}_{d,i} = 0. \tag{4.120}$$

Therein, $\delta\boldsymbol{\lambda}_i \in \mathbb{R}^6$ are the test functions corresponding to the Lagrange multipliers that enforce the orthonormality of the directors located at the FE node at $s = s_i$, comprised in $\hat{\boldsymbol{d}}_i$. The related director velocities are comprised in $\boldsymbol{v}_{d,i} \in \mathbb{R}^9$. The last identity in (4.120) has made use of the sifting property of dirac functions [103, Equation 1.159], i.e., $\left(f(s), \bar{\delta}(s - a)\right)_\Omega = f(a)$ for some $f : \Omega \to \mathbb{R}$ and $a \in \Omega$. Eventually, we may rewrite (4.120) in terms of the system vectors $\delta\hat{\boldsymbol{\lambda}}$ and $\hat{\boldsymbol{v}}_d$, such that

$$\delta\hat{\boldsymbol{\lambda}}^\top \hat{\boldsymbol{G}}_d(\hat{\boldsymbol{d}}) \hat{\boldsymbol{v}}_d = 0, \qquad \text{where} \quad \hat{\boldsymbol{G}}_d(\hat{\boldsymbol{d}}) = \begin{bmatrix} \boldsymbol{G}_d(\hat{\boldsymbol{d}}_1) & \boldsymbol{0} & & \boldsymbol{0} \\ \boldsymbol{0} & \boldsymbol{G}_d(\hat{\boldsymbol{d}}_2) & & \boldsymbol{0} \\ & & \ddots & \\ \boldsymbol{0} & \boldsymbol{0} & & \boldsymbol{G}_d(\hat{\boldsymbol{d}}_{n_\mathrm{n}}) \end{bmatrix} \tag{4.121}$$

has therefore full rank. Futhermore, the port matrices are defined as

$$\hat{\boldsymbol{B}}_{\Omega,m}(\hat{\boldsymbol{q}}) = \int_{\Omega} \boldsymbol{\Phi}_d^{\top} \boldsymbol{T}(\boldsymbol{d}_{\mathrm{h}}) \boldsymbol{\Phi}_{\varphi} \,\mathrm{d}s, \quad \hat{\boldsymbol{B}}_{\partial,n} = \boldsymbol{\Phi}_{\varphi}^{\top}|_{\partial\Omega_N}, \quad \hat{\boldsymbol{B}}_{\partial,m}(\hat{\boldsymbol{q}}) = (\boldsymbol{\Phi}_d^{\top} \boldsymbol{T}(\boldsymbol{d}_{\mathrm{h}}))|_{\partial\Omega_N}. \tag{4.122}$$

Consequently, the output relations in (4.36) can be written in a more detailed manner as

$$\hat{\boldsymbol{y}}_{\Omega} = \hat{\boldsymbol{B}}_{\Omega}^{\top} \hat{\boldsymbol{v}} = \begin{bmatrix} \hat{\boldsymbol{M}}_{\varphi} & \boldsymbol{0} \\ \boldsymbol{0} & \hat{\boldsymbol{B}}_{\Omega,m}^{\top} \end{bmatrix} \begin{bmatrix} \hat{\boldsymbol{v}}_{\varphi}(t) \\ \hat{\boldsymbol{v}}_d(t) \end{bmatrix} = \begin{bmatrix} \int_{\Omega} \boldsymbol{\Phi}_{\varphi}^{\top} \boldsymbol{v}_{\varphi,\mathrm{h}} \,\mathrm{d}s \\ \int_{\Omega} \boldsymbol{\Phi}_d^{\top} \boldsymbol{\omega}_{\mathrm{h}} \,\mathrm{d}s \end{bmatrix} \tag{4.123}$$

and

$$\hat{\boldsymbol{y}}_{\partial} = \hat{\boldsymbol{B}}_{\partial}^{\top} \hat{\boldsymbol{v}} = \begin{bmatrix} \hat{\boldsymbol{B}}_{\partial,n}^{\top} & \boldsymbol{0} \\ \boldsymbol{0} & \hat{\boldsymbol{B}}_{\partial,m}^{\top} \end{bmatrix} \begin{bmatrix} \hat{\boldsymbol{v}}_{\varphi}(t) \\ \hat{\boldsymbol{v}}_d(t) \end{bmatrix} = \begin{bmatrix} \boldsymbol{\Phi}_{\varphi}|_{\partial\Omega_N} \hat{\boldsymbol{v}}_{\varphi}(t) \\ (\boldsymbol{T}(\boldsymbol{d}_{\mathrm{h}})^{\top} \boldsymbol{\Phi}_d)|_{\partial\Omega_N} \hat{\boldsymbol{v}}_d(t) \end{bmatrix} = \begin{bmatrix} \boldsymbol{v}_{\varphi,\mathrm{h}} \\ \boldsymbol{\omega}_{\mathrm{h}} \end{bmatrix}_{\partial\Omega_N}. \tag{4.124}$$

While the discrete output can be regarded as the projection of the centerline velocity and angular velocity onto the FE nodes, the boundary output can be traced back to the simple evaluation of the approximated centerline velocity and angular velocity at the Neumann boundaries. Both results ensure that the discrete power balance equation (4.40) yields

$$\dot{\hat{H}} = \begin{bmatrix} \hat{\boldsymbol{y}}_{\Omega} \\ \hat{\boldsymbol{y}}_{\partial} \end{bmatrix}^{\top} \begin{bmatrix} \hat{\boldsymbol{u}}_{\Omega} \\ \boldsymbol{u}_{\partial} \end{bmatrix} = \int_{\Omega} (\bar{\boldsymbol{n}}^{\top} \boldsymbol{v}_{\varphi,\mathrm{h}} + \bar{\boldsymbol{m}}^{\top} \boldsymbol{\omega}_{\mathrm{h}}) \,\mathrm{d}s + \boldsymbol{u}_{\partial}^{\top} \hat{\boldsymbol{y}}_{\partial}, \tag{4.125}$$

which is the consistent approximation of the infinite-dimensional power balance (4.28), see also (4.26).

5. Discrete gradient methods for port-Hamiltonian differential-algebraic equations

This chapter is based on:*
Kinon PL, Morandin R, and Schulze P. "Discrete gradient methods for port-Hamiltonian differential-algebraic equations". In: *Applied Numerical Mathematics*, 223: 45–75, 2026. DOI: 10.1016/j.apnum.2025.12.006

Abstract: Discrete gradient methods are a powerful tool for the time discretization of dynamical systems, since they are structure-preserving regardless of the form of the total energy. In this work, we discuss the application of discrete gradient methods to the system class of nonlinear port-Hamiltonian differential-algebraic equations — as they emerge from the port- and energy-based modeling of physical systems in various domains. We introduce a novel numerical scheme tailored for semi-explicit differential-algebraic equations and further address more general settings using the concepts of discrete gradient pairs and Dirac–dissipative structures. Additionally, the behavior under system transformations is investigated and we demonstrate that under suitable assumptions port-Hamiltonian differential-algebraic equations admit a representation which consists of a parametrized port-Hamiltonian semi-explicit system and an unstructured equation. Finally, we present the application to multibody system dynamics and discuss numerical results to demonstrate the capabilities of our approach.

Keywords: Port-Hamiltonian systems • Differential-algebraic equations • Structure-preserving discretization • Time integration methods • Discrete gradients.

5.1. Introduction

Port-Hamiltonian (pH) systems have gained significant importance in various research areas, with a particular focus on the modeling, simulation, and control of dynamical systems [63, 224]. Port-Hamiltonian (pH) systems offer a valuable framework for analyzing complex problems, where the complexity may arise from multi-physical interactions, non-trivial domains, and various nonlinearities. One of the key advantages of the pH representation is its explicit description of power interfaces, known as ports, which facilitate power-preserving interconnections between submodules. Thus, this approach simplifies the modular composition of models, which often leads to the presence of algebraic constraints. Correspondingly, the governing equations at hand are *differential-algebraic equations* (DAEs), also known as *descriptor systems* in the context of control theory. If the system has in addition a pH structure, we speak of *port-Hamiltonian differential-algebraic equations* (pH DAEs). A definition for linear time-varying pH DAEs was provided in [23] and a full, nonlinear generalization has been provided in [161]. An important subclass consists of semi-explicit pH DAEs, see, e.g., [223, Equation 3.16], where local representations of implicit port-Hamiltonian DAEs are discussed. In [228, 229], the Hamiltonian

as a backbone of pH systems is replaced by Lagrangian subspaces or submanifolds to define generalized pH DAEs.

In general, discretizing a structured dynamical system, such as a pH system, can result in the loss of its continuous-time properties, potentially leading to numerical solutions that exhibit unphysical behavior (see, for example, [97, Chapter 1]). One way to circumvent this issue is by employing a structure-preserving time discretization scheme, as the system's properties are often embedded in the algebraic or geometric structure of the original continuous-time model. Examples of such systems include gradient [108], Hamiltonian [14], and, particularly relevant to this work, pH systems. Structure-preserving time discretization approaches for Hamiltonian systems have been widely studied, with [97] offering a general overview. Notably, the development of structure-preserving discretization methods has been driven by computational mechanics [35, 88, 90, B3, 207], where variational integrators [35, 142, 156] represent an important discretization approach within the group of symplectic methods [138]. An interesting approach is also given by time finite element methods [29, 30, 32, 65, 159]. Structure-preserving techniques for other system classes are for example explored in [120, 131, 172, 211].

Compared to those works, the structure-preserving time discretization of pH systems is still a relatively young field. When performing numerical integration of pH systems, it is essential to account for the energy exchange through the ports resulting in the presence of a power balance equation. The following developments have been made in recent years:

- In [127], the authors show that certain collocation methods can achieve an exact power balance at the discrete level, provided that the total energy function, the *Hamiltonian*, is a quadratic function of the state. This result is further extended to descriptor systems in [161].
- Structure-preserving discretization approaches based on Petrov–Galerkin projections have been proposed in [65, 84] and are closely connected to the aforementioned time finite element approaches. Although these methods can provide continuous solutions also between discrete points in time, and one can obtain arbitrarily high convergence rates, they require the numerical approximation of integrals in time. If the integrand is non-polynomial, one may not be able to integrate these formulas sufficiently accurately, which can lead to the loss of the desired convergence and conservation properties [29]. Moreover, this numerical quadrature imposes additional numerical costs for the emanating schemes.
- In several recent works, e.g. [17, 18, 164], the authors consider splitting schemes that separate the energy-conserving and dissipative parts of the dynamics. While this approach can achieve high order convergence and seems quite promising, to the best of our knowledge, it has been so far only applied to linear port-Hamiltonian systems with quadratic Hamiltonian.
- Another approach consists in dropping the requirement for an exact time-discrete power balance, while focusing on minimizing its violation, for example by refining adaptively the time grid of the discretization, see, e.g., [19].

Contrary to these approaches, the present work pursues a *discrete gradient* approach, which achieves exact time-discrete power balances also for non-quadratic Hamiltonians. Additionally, the implementation of such schemes is comparably simple and straightforward. While most of the known discrete gradient schemes are restricted to second order convergence rates, there are recent developments to obtain higher accuracy as well (see [66] and the references therein). Another notable work [197] deals with DAEs with a gradient structure and constant descriptor matrix.

Most of the approaches in the literature for pH systems [12, 55, 72, 80, 91, C4, 166], which achieve an exact power balance at the discrete level for general Hamiltonians, share the characteristic that they

focus on *pH ordinary-differential equations*, where the gradient of the Hamiltonian explicitly appears in the system equations. A challenge with applying methods like discrete gradient techniques to more general systems as introduced in [161] lies in the fact that the gradient of the Hamiltonian in general only appears implicitly in the system equations. The development of discrete gradient pairs [201] has recently addressed this issue.

In contrast to the works focusing on ordinary differential equations, we want to generalize the application field of discrete gradient methods to pH DAEs with possibly state-dependent descriptor matrices, as introduced in [161]. The primary contributions of this work are outlined in the following[1]:

C1) Discussion of discrete gradient pairs for general pH DAEs along with a corresponding time integration approach, see Section 5.4.1.

C2) Development of a tangible discrete gradient method for *semi-explicit* pH DAEs, see Section 5.4.2. This already covers many application problems.

C3) Introduction of discrete gradient methods for general pH DAEs, based on a different modeling approach which emphasizes the underlying Dirac structure, see Section 5.4.3.

The remainder of this work is structured as follows: Preliminary basics are recapitulated in Section 5.2, including the definition of pH DAEs and discrete gradients. In Section 5.3 we focus on a certain class of pH DAEs, namely semi-explicit pH DAEs. We then introduce new methods for the numerical integration of pH DAEs using discrete gradients in Section 5.4. Section 5.5 is entirely devoted to the application of our approaches to multibody systems, including numerical experiments. Conclusions and a brief outlook are given in Section 5.6.

Notation. We denote by $\mathbb{N}$ the positive natural numbers and by $\mathbb{N}_0$ the natural numbers including zero. With $\boldsymbol{I}_n \in \mathbb{R}^{n\times n}$ or simply $\boldsymbol{I}$ we denote the identity matrix and with 0 the zero matrix or vector. We mostly assume that the dimension should become clear from the context. For every matrix $\boldsymbol{A} \in \mathbb{R}^{n\times m}$ or vector $\boldsymbol{v} \in \mathbb{R}^n = \mathbb{R}^{n\times 1}$ we denote by $\boldsymbol{A}^\top \in \mathbb{R}^{m\times n}$ and $\boldsymbol{v}^\top \in \mathbb{R}^{1\times n}$ their corresponding transposes.

We denote by $\mathscr{C}(\mathscr{A}, \mathscr{B})$ the continuous functions between two topological spaces $\mathscr{A}$ and $\mathscr{B}$. For $k \in \mathbb{N}_0 \cup \{\infty\}$ we denote by $\mathscr{C}^k(\mathscr{X}_1, \mathscr{X}_2)$ the k-times continuously differentiable functions from $\mathscr{X}_1$ to $\mathscr{X}_2$, where typically $\mathscr{X}_1 \subseteq \mathbb{R}^n$ and $\mathscr{X}_2 \subseteq \mathbb{R}^m$ are open subsets for some $n, m \in \mathbb{N}$.

If $f \in \mathscr{C}^1(\mathscr{X}, \mathbb{R})$ with $\mathscr{X} \subseteq \mathbb{R}^n$ open, we denote by $\nabla f \in \mathscr{C}(\mathscr{X}, \mathbb{R}^n)$ the gradient of f, intended as a column vector function. If $\boldsymbol{F} \in \mathscr{C}^1(\mathscr{X}, \mathbb{R}^m)$ with $\mathscr{X} \subseteq \mathbb{R}^n$ open, we denote by $\mathrm{D}\boldsymbol{F} \in \mathscr{C}(\mathscr{X}, \mathbb{R}^{m\times n})$ the Jacobian of $\boldsymbol{F}$, intended as a matrix function whose rows transposed are the gradients of the entries of $\boldsymbol{F}$. Furthermore, given a partition $\boldsymbol{F} = (\boldsymbol{F}_1, \dots, \boldsymbol{F}_m)$ for the function and $\boldsymbol{x} = (\boldsymbol{x}_1, \dots, \boldsymbol{x}_r)$ of the state, with $\boldsymbol{x}_i = (\boldsymbol{x}_{i,1}, \dots, \boldsymbol{x}_{i,n_i}) \in \mathbb{R}^{n_i}$ for $i = 1, \dots, r$, we denote the corresponding partial gradients and partial Jacobians as

$$\nabla_{\boldsymbol{x}_i} f = \begin{bmatrix} \frac{\partial f}{\partial \boldsymbol{x}_{i,1}} \\ \vdots \\ \frac{\partial f}{\partial \boldsymbol{x}_{i,n_i}} \end{bmatrix}, \qquad \mathrm{D}_{\boldsymbol{x}_i} \boldsymbol{F} = \begin{bmatrix} \frac{\partial \boldsymbol{F}_1}{\partial \boldsymbol{x}_{i,1}} & \cdots & \frac{\partial \boldsymbol{F}_1}{\partial \boldsymbol{x}_{i,n_i}} \\ \vdots & \ddots & \vdots \\ \frac{\partial \boldsymbol{F}_m}{\partial \boldsymbol{x}_{i,1}} & \cdots & \frac{\partial \boldsymbol{F}_m}{\partial \boldsymbol{x}_{i,n_i}} \end{bmatrix},$$

[1] One further contribution of the original paper is the in-depth analysis of relations between the proposed methods and their behavior under coordinate transformations. The related parts are omitted here to match the overall focus of this thesis, but can be found in Section 5 of the original work [A3].

such that in particular

$$\nabla f = \begin{bmatrix} \nabla_{x_1} f \\ \vdots \\ \nabla_{x_r} f \end{bmatrix}, \qquad \mathrm{D}\boldsymbol{F} = \begin{bmatrix} \mathrm{D}_{x_1}\boldsymbol{F} & \cdots & \mathrm{D}_{x_r}\boldsymbol{F} \end{bmatrix}. \tag{5.1}$$

Additionally, the derivative with respect to time t deserves its own notation, which is $\dot{\boldsymbol{x}} \coloneqq \frac{\mathrm{d}\boldsymbol{x}}{\mathrm{d}t}$.

If $\boldsymbol{f} : \mathscr{X} \to \mathscr{Y}$ and $\boldsymbol{g} : \mathscr{Y} \to \mathscr{Z}$ are two maps, we denote as usual with $\boldsymbol{g} \circ \boldsymbol{f} : \mathscr{X} \to \mathscr{Z}$ their composition, i.e., $\boldsymbol{g} \circ \boldsymbol{f}(\boldsymbol{x}) = \boldsymbol{g}(\boldsymbol{f}(\boldsymbol{x}))$. When $\overline{\boldsymbol{g}} : \mathscr{Y} \times \mathscr{Y} \to \mathscr{Z}$, we sometimes abuse the notation and write $\overline{\boldsymbol{g}} \circ \boldsymbol{f} : \mathscr{X} \times \mathscr{X} \to \mathscr{Z}$ to denote the map $\overline{\boldsymbol{g}} \circ \boldsymbol{f}(\boldsymbol{x}, \boldsymbol{x}') = \overline{\boldsymbol{g}}(\boldsymbol{f}(\boldsymbol{x}), \boldsymbol{f}(\boldsymbol{x}'))$.

For every matrix function $\boldsymbol{A} \in \mathscr{C}(\mathscr{X}, \mathbb{R}^{m\times n})$, we denote by $\boldsymbol{A}^\top \in \mathscr{C}(\mathscr{X}, \mathbb{R}^{n\times m})$ its pointwise transpose $\boldsymbol{A}^\top(\boldsymbol{x}) = \boldsymbol{A}(\boldsymbol{x})^\top$. If furthermore $m = n$ and $\boldsymbol{A}$ is pointwise invertible, we usually denote by $\boldsymbol{A}^{-1} \in \mathscr{C}(\mathscr{X}, \mathbb{R}^{n\times n})$ its pointwise inverse $\boldsymbol{A}^{-1}(\boldsymbol{x}) = \boldsymbol{A}(\boldsymbol{x})^{-1}$, instead of the inverse map, unless otherwise specified. We also introduce the short notation $\boldsymbol{A}^{-\top}$ for $(\boldsymbol{A}^{-1})^\top = (\boldsymbol{A}^\top)^{-1}$. Given a subset $\mathscr{V} \subseteq \mathbb{R}^n$, we denote by $\operatorname{span}(\mathscr{V}) \subseteq \mathbb{R}^n$ the smallest linear subspace of $\mathbb{R}^n$ containing $\mathscr{V}$, and by

$$\mathscr{V}^\perp = \{\boldsymbol{v} \in \mathbb{R}^n \mid \boldsymbol{v} \perp \boldsymbol{w} \text{ for all } \boldsymbol{w} \in \mathscr{V}\}$$

its orthogonal complement. When $\mathscr{V}$ consists of only one vector $\boldsymbol{v} \in \mathbb{R}^n$, we simply write $\operatorname{span}(\boldsymbol{v})$ and $\boldsymbol{v}^\perp$ instead of $\operatorname{span}(\{\boldsymbol{v}\})$ and $\{\boldsymbol{v}\}^\perp$. Given a subset $\mathscr{X} \subseteq \mathbb{R}^{n_1} \times \mathbb{R}^{n_2}$, we usually denote by $\boldsymbol{\pi}_1 : \mathscr{X} \to \mathbb{R}^{n_1}$ and $\boldsymbol{\pi}_2 : \mathscr{X} \to \mathbb{R}^{n_2}$ the corresponding orthogonal projections, i.e., $\boldsymbol{\pi}_1(\boldsymbol{x}_1, \boldsymbol{x}_2) = \boldsymbol{x}_1$ and $\boldsymbol{\pi}_2(\boldsymbol{x}_1, \boldsymbol{x}_2) = \boldsymbol{x}_2$ for all $(\boldsymbol{x}_1, \boldsymbol{x}_2) \in \mathscr{X}$.

5.2. Preliminaries

In this section, we recall some preliminary concepts and definitions that will be useful in the remainder of this work.

5.2.1. Differential-algebraic equations

Differential-algebraic equations are systems of the form

$$\boldsymbol{F}\left(t, \boldsymbol{x}, \frac{\mathrm{d}\boldsymbol{x}}{\mathrm{d}t}, \ldots, \frac{\mathrm{d}^k\boldsymbol{x}}{\mathrm{d}t^k}\right) = \boldsymbol{0} \tag{5.2}$$

for some map[2] $\boldsymbol{F} : \mathscr{D}_{\boldsymbol{F}} \to \mathbb{R}^m$, where $t \in \mathbb{T} \subseteq \mathbb{R}$ denotes the time variable, $\boldsymbol{x} \in \mathscr{X} \subseteq \mathbb{R}^n$ the state, and $\mathscr{D}_{\boldsymbol{F}} \subseteq \mathbb{R}^{1+(k+1)n}$ is the domain of $\boldsymbol{F}$. Here n is the dimension of the state, m the number of equations, and k is the order of the DAE. Typically, the domain of $\boldsymbol{F}$ is of the form $\mathscr{D}_{\boldsymbol{F}} = \mathbb{T} \times \mathscr{X} \times \mathbb{R}^{kn}$, where $\mathbb{T} \subseteq \mathbb{R}$ is an open (possibly unbounded) interval and $\mathscr{X} \subseteq \mathbb{R}^n$ is an open subset, while the solutions of (5.2) are to be found in $\mathscr{C}^k(\mathbb{T}, \mathscr{X})$.

We are particularly interested in first order quasilinear DAEs, i.e., equations of the form

$$\boldsymbol{E}(t, \boldsymbol{x})\dot{\boldsymbol{x}} = \boldsymbol{f}(t, \boldsymbol{x}), \tag{5.3}$$

see, e.g., [181, 214], for some maps $\boldsymbol{E} : \mathscr{D}_{\boldsymbol{E}} \to \mathbb{R}^{m\times n}$ and $\boldsymbol{f} : \mathscr{D}_{\boldsymbol{f}} \to \mathbb{R}^m$, where $\mathscr{D}_{\boldsymbol{E}}, \mathscr{D}_{\boldsymbol{f}} \subseteq \mathbb{R}^{1+n}$. In particular, if we had $n = m$ and $\boldsymbol{E}$ were pointwise invertible, then (5.3) would be equivalent to

[2] The reader should not confuse the domain of the operators here with the notion of Dirac structures, cf. Chapter 2.

$\dot{\boldsymbol{x}} = \boldsymbol{E}(t,\boldsymbol{x})^{-1}\boldsymbol{f}(t,\boldsymbol{x})$, which is a system of first order ordinary differential equations (ODEs). However, when this property is not satisfied, the system might include algebraic constraints and be under- or overdetermined. This presents several challenges, both in the study of the existence and uniqueness of solutions and in the time discretization of the system [132]. In particular, dedicated numerical methods are often necessary.

Enriching a DAE with input and output variables $\boldsymbol{u} \in \mathbb{R}^p$ and $\boldsymbol{y} \in \mathbb{R}^q$ we obtain a *descriptor system*

$$\begin{aligned} \boldsymbol{E}(t,\boldsymbol{x})\dot{\boldsymbol{x}} &= \boldsymbol{f}(t,\boldsymbol{x},\boldsymbol{u}), \\ \boldsymbol{y} &= \boldsymbol{g}(t,\boldsymbol{x},\boldsymbol{u}), \end{aligned} \tag{5.4}$$

for some maps $\boldsymbol{E} : \mathscr{D}_{\boldsymbol{E}} \to \mathbb{R}^{m\times n}$, $\boldsymbol{f} : \mathscr{D}_{\boldsymbol{f}} \to \mathbb{R}^m$, and $\boldsymbol{g} : \mathscr{D}_{\boldsymbol{g}} \to \mathbb{R}^q$, where $\mathscr{D}_{\boldsymbol{E}} \subseteq \mathbb{R}^{1+n}$ and $\mathscr{D}_{\boldsymbol{f}}, \mathscr{D}_{\boldsymbol{g}} \subseteq \mathbb{R}^{1+n+p}$. In applications, the input $\boldsymbol{u}$ is typically a given fixed time-varying function, a state feedback, or an output feedback.

5.2.2. Port-Hamiltonian DAE systems

In this paper we focus on time-invariant port-Hamiltonian DAE (or *descriptor*) systems. We introduce first the concept of gradient pair, which will replace the gradient of the Hamiltonian in the equations.

Definition 5.1. *Let $\mathscr{X} \subseteq \mathbb{R}^n$ be an open set and let $\mathcal{H} \in \mathscr{C}^1(\mathscr{X},\mathbb{R})$, $\boldsymbol{E} \in \mathscr{C}(\mathscr{X},\mathbb{R}^{n\times n})$, and $\boldsymbol{z} \in \mathscr{C}(\mathscr{X},\mathbb{R}^n)$. We say that $(\boldsymbol{E},\boldsymbol{z})$ is a* gradient pair *for $\mathcal{H}$ if*

$$\boldsymbol{E}(\boldsymbol{x})^\top \boldsymbol{z}(\boldsymbol{x}) = \nabla\mathcal{H}(\boldsymbol{x}) \tag{5.5}$$

holds for all $\boldsymbol{x} \in \mathscr{X}$. ♤

Port-Hamiltonian descriptor systems are then defined as follows.

Definition 5.2 (see also [161])**.** *Consider a time interval $\mathbb{T} = [0, t_{\text{end}}]$ with $t_{\text{end}} > 0$ and an open state space $\mathscr{X} \subseteq \mathbb{R}^n$. A* time-invariant port-Hamiltonian descriptor system*, in short* pH DAE*, is a descriptor system of the form*

$$\begin{aligned} \boldsymbol{E}(\boldsymbol{x})\dot{\boldsymbol{x}} &= \big(\boldsymbol{J}(\boldsymbol{x}) - \boldsymbol{R}(\boldsymbol{x})\big)\boldsymbol{z}(\boldsymbol{x}) + \boldsymbol{B}(\boldsymbol{x})\boldsymbol{u}, \\ \boldsymbol{y} &= \boldsymbol{B}(\boldsymbol{x})^\top \boldsymbol{z}(\boldsymbol{x}), \end{aligned} \tag{5.6}$$

together with a Hamiltonian *$\mathcal{H} \in \mathscr{C}^1(\mathscr{X},\mathbb{R})$, where $\boldsymbol{E},\boldsymbol{J},\boldsymbol{R} \in \mathscr{C}(\mathscr{X},\mathbb{R}^{n\times n})$, $\boldsymbol{B} \in \mathscr{C}(\mathscr{X},\mathbb{R}^{n\times m})$, and $\boldsymbol{z} \in \mathscr{C}(\mathscr{X},\mathbb{R}^n)$ satisfy the properties $\boldsymbol{J}(\boldsymbol{x}) = -\boldsymbol{J}(\boldsymbol{x})^\top$, $\boldsymbol{R}(\boldsymbol{x}) = \boldsymbol{R}(\boldsymbol{x})^\top \succeq 0$ for all $\boldsymbol{x} \in \mathscr{X}$, and $(\boldsymbol{E},\boldsymbol{z})$ is a gradient pair for $\mathcal{H}$. Here $\boldsymbol{E},\boldsymbol{J},\boldsymbol{R}$ are called the* descriptor, structure*, and* dissipation *matrix functions, respectively, and $\boldsymbol{z}$ is called the* costate *function.* ♤

See also Section 2.3 for a detailed introduction to such a pH descriptor system formulations, with the equivalent Definition 2.7.

Remark 5.3. *In the context of the modeling of pH systems, the state variables $\boldsymbol{x}$ are also sometimes called* energy variables *(see, e.g., [223] and [224, Chapter 11]), since the Hamiltonian $\mathcal{H} : \boldsymbol{x} \mapsto \mathcal{H}(\boldsymbol{x})$ depends on them. Likewise, the* coenergy variables *$\boldsymbol{e}$ are given as the derivative of the Hamiltonian with respect to the energy variables, i.e., $\boldsymbol{e} = \nabla\mathcal{H}(\boldsymbol{x})$. While the energy variables can be interpreted as points on a differential manifold $\boldsymbol{x} \in \mathscr{X}$, the coenergy variables are elements of the cotangent bundle $\boldsymbol{e} \in T^*\mathscr{X}$. We have then a natural duality induced by the pair $(T\mathscr{X}, T^*\mathscr{X})$, which yields a power balance equation*

given as $\frac{\mathrm{d}}{\mathrm{d}t}\mathcal{H}(\boldsymbol{x}(t)) = \langle \dot{\boldsymbol{x}}, \boldsymbol{e}(\boldsymbol{x})\rangle = \langle \dot{\boldsymbol{x}}, \nabla\mathcal{H}(\boldsymbol{x})\rangle$. *This also corresponds to the duality between flow and effort variables.*

In the present case however, the coenergy variables $\boldsymbol{e}$ *do not directly correspond to the costate function* $\boldsymbol{x} \mapsto \boldsymbol{z}(\boldsymbol{x})$, *but to* $\boldsymbol{x} \mapsto \boldsymbol{e}(\boldsymbol{x}) = \boldsymbol{E}(\boldsymbol{x})^\top \boldsymbol{z}(\boldsymbol{x}) = \nabla\mathcal{H}(\boldsymbol{x})$ *instead. Furthermore, as we will see in more detail in Section 5.3, the presence of algebraic equations typically induces a partition on both the state and costate of the system, which decouples some of the variables from the energy. Thus, to avoid ambiguity, in the context of pH DAEs we refer to* $\boldsymbol{x}$ *as the state and to* $\boldsymbol{z}$ *as the costate, evading the energy/coenergy nomenclature altogether.* ♧

Remark 5.4. *In this work we formally consider only systems without a feedthrough term in the output equation. Nevertheless, our results can be easily adapted for systems with feedthrough, i.e., replacing the output equation with* $\boldsymbol{y} = \boldsymbol{C}(\boldsymbol{x})^\top \boldsymbol{z}(\boldsymbol{x}) + \boldsymbol{D}(\boldsymbol{x})\boldsymbol{u}$ *for some matrix functions* $\boldsymbol{C}, \boldsymbol{D}$ *and requiring some additional dissipative structure involving* $\boldsymbol{R}, \boldsymbol{B}, \boldsymbol{C}, \boldsymbol{D}$, *see, e.g., definitions in [161, 162].* ♧

Remark 5.5. *Although the system from Definition 5.2 could emerge from a change of variables of a pH ODE system, see Section 2.3, the presented framework additionally covers many more cases.* ♧

Note that in Definition 5.2 the input and output variables, usually taken as functions in $\mathscr{C}(\mathbb{T}, \mathbb{R}^m)$, have the same size. In fact, the product $\boldsymbol{y}^\top \boldsymbol{u}$ typically has the same physical dimension as power. In particular, one can easily verify (see, e.g., [161]) that every pH DAE of the form (5.6) satisfies the *power balance equation* (PBE)

$$\frac{\mathrm{d}}{\mathrm{d}t}\mathcal{H}\big(\boldsymbol{x}(t)\big) = -\boldsymbol{z}\big(\boldsymbol{x}(t)\big)^\top \boldsymbol{R}\big(\boldsymbol{x}(t)\big)\boldsymbol{z}\big(\boldsymbol{x}(t)\big) + \boldsymbol{y}(t)^\top \boldsymbol{u}(t) \tag{5.7}$$

and the dissipation inequality

$$\frac{\mathrm{d}}{\mathrm{d}t}\mathcal{H}\big(\boldsymbol{x}(t)\big) \leq \boldsymbol{y}(t)^\top \boldsymbol{u}(t), \tag{5.8}$$

along every solution $(\boldsymbol{x}, \boldsymbol{u}, \boldsymbol{y})$ of (5.6), for all $t \in \mathbb{T}$. Note that the PBE and the dissipation inequality can be reinterpreted in integral form as

$$\mathcal{H}\big(\boldsymbol{x}(t_1)\big) - \mathcal{H}\big(\boldsymbol{x}(t_0)\big) = \int_{t_0}^{t_1} \big(-\boldsymbol{z}(\boldsymbol{x}(t))^\top \boldsymbol{R}(\boldsymbol{x}(t))\boldsymbol{z}(\boldsymbol{x}(t)) + \boldsymbol{y}(t)^\top \boldsymbol{u}(t)\big)\mathrm{d}t \tag{5.9}$$

and

$$\mathcal{H}\big(\boldsymbol{x}(t_1)\big) - \mathcal{H}\big(\boldsymbol{x}(t_0)\big) \leq \int_{t_0}^{t_1} \boldsymbol{y}(t)^\top \boldsymbol{u}(t)\,\mathrm{d}t \tag{5.10}$$

respectively, for every $t_0, t_1 \in \mathbb{T},\ t_0 \leq t_1$.

Let us now briefly introduce another equivalent representation of pH DAEs, which will be used throughout this work. Similarly as introduced in [165], by defining a new variable $\boldsymbol{f} = \boldsymbol{z}(\boldsymbol{x})$ representing the costate, and adding the gradient-pair condition $\boldsymbol{E}(\boldsymbol{x})^\top \boldsymbol{f} = \nabla\mathcal{H}(\boldsymbol{x})$ explicitly to the pH DAE equations (5.6), we obtain an equivalent system defined as follows.

Definition 5.6 (Dirac–dissipative representation)**.** *Consider a pH DAE* (5.6), *then*

$$\begin{bmatrix} \nabla\mathcal{H}(\boldsymbol{x}) \\ 0 \\ \boldsymbol{y} \end{bmatrix} + \begin{bmatrix} 0 & -\boldsymbol{E}(\boldsymbol{x})^\top & 0 \\ \boldsymbol{E}(\boldsymbol{x}) & \boldsymbol{J}(\boldsymbol{x}) - \boldsymbol{R}(\boldsymbol{x}) & \boldsymbol{B}(\boldsymbol{x}) \\ 0 & -\boldsymbol{B}(\boldsymbol{x})^\top & 0 \end{bmatrix} \begin{bmatrix} -\dot{\boldsymbol{x}} \\ \boldsymbol{f} \\ \boldsymbol{u} \end{bmatrix} = \boldsymbol{0}, \tag{5.11a}$$

$$\boldsymbol{f} = \boldsymbol{z}(\boldsymbol{x}), \tag{5.11b}$$

is referred to as the Dirac–dissipative representation *(DDR) related to* (5.6). ♤

Note that we use a different letter to denote the costate as a variable, to avoid ambiguity with the costate function and its discrete approximations that will be introduced in the following sections. Moreover, it should be highlighted that the pH structure is entirely encoded in (5.11a). In fact, this equation corresponds to the intersection of the Dirac structure and the dissipative structure of the pH system, and has the form $\mathfrak{e} + (\mathfrak{J}(\boldsymbol{x}) - \mathfrak{R}(\boldsymbol{x}))\mathfrak{f} = \mathbf{0}$, where $\mathfrak{f} = (-\dot{\boldsymbol{x}}, \boldsymbol{f}, \boldsymbol{u})$ and $\mathfrak{e} = (\nabla\mathcal{H}(\boldsymbol{x}), \mathbf{0}, \boldsymbol{y})$ are the flow and effort vectors, and $\mathfrak{J} = -\mathfrak{J}^\top$ and $\mathfrak{R} = \mathfrak{R} \succeq 0$ hold pointwise, see [165] for further details. Furthermore, consult Section 2.2 of the present work for a more detailed explanation.

As we will discuss in Section 5.4.3, similarly as in [165], the Dirac–dissipative representation can be particularly useful for the structure-preserving discretization of pH DAEs. This can be deducted particularly due to its structure yielding the following result.

Theorem 5.7. *Every solution* $(\boldsymbol{x}, \boldsymbol{f}, \boldsymbol{u}, \boldsymbol{y})$ *of* (5.11a) *satisfies the PBE and dissipation inequality, since*

$$\frac{\mathrm{d}}{\mathrm{d}t}\mathcal{H}\big(\boldsymbol{x}(t)\big) - \boldsymbol{y}(t)^\top \boldsymbol{u}(t) = -\mathfrak{f}^\top \mathfrak{e} = \mathfrak{f}^\top \big(\mathfrak{J}(\boldsymbol{x}) - \mathfrak{R}(\boldsymbol{x})\big)\mathfrak{f} = -\mathfrak{f}^\top \mathfrak{R}(\boldsymbol{x})\mathfrak{f} = -\boldsymbol{f}^\top \boldsymbol{R}(\boldsymbol{x})\boldsymbol{f} \leq 0.$$

Remark 5.8. *The reader should not confuse the acronym* DDR *with the notion of* difference and differential representations*, which has been coined in, e.g., [167]. While both concepts are related to pH systems and both can be combined with discrete gradient methods, the works related to the difference and differential representation propose a hybrid approach combining discrete-time equations with differential equations. Contrarily, the DDR in the present work lives in continuous time and highlights the underlying geometric structure.* ♧

Since the PBE (5.7) and dissipation inequality (5.8) are fundamental properties satisfied by every pH system, there is much effort in the literature [65, 80, 84, C4, 127, 161, 201] in developing time-discretization schemes to preserve them on a discrete level. This is also the focus of this paper.

5.2.3. Discrete gradients

Discrete gradients are a popular tool for generating structure-preserving integration methods for dynamical systems [87, 97, 160]. A general definition is as follows.

Definition 5.9 (Discrete gradients [97])**.** *Given a function* $f \in \mathscr{C}^1(\mathscr{X}, \mathbb{R})$ *with* $\mathscr{X} \subseteq \mathbb{R}^n$ *open, a* discrete gradient *for* f *is any vector function* $\overline{\nabla} f \in \mathscr{C}(\mathscr{X} \times \mathscr{X}, \mathbb{R}^n)$ *that satisfies the properties*

(i) $\overline{\nabla} f(\boldsymbol{x}, \boldsymbol{x}')^\top (\boldsymbol{x}' - \boldsymbol{x}) = f(\boldsymbol{x}') - f(\boldsymbol{x})$ *for all* $\boldsymbol{x}, x' \in \mathscr{X}$*,*

(ii) $\overline{\nabla} f\,(\boldsymbol{x}, \boldsymbol{x}) = \nabla f\,(\boldsymbol{x})$ *for all* $x \in \mathscr{X}$*,*

where Property (i) is referred to as directionality property and Property (ii) as consistency condition. ♤

Especially the directionality property will be handy later on for the design of structure-preserving discretizations. The following definition provides an example for a discrete gradient, which can yield a symmetric method of second order accuracy, as it represents a second-order approximation to the exact gradients.

Definition 5.10 (Gonzalez discrete gradient [87])**.** *For a given function* $f \in \mathscr{C}^1(\mathscr{X}, \mathbb{R})$ *with* $\mathscr{X} \subseteq \mathbb{R}^n$ *convex open subset, its Gonzalez (or midpoint) discrete gradient* $\overline{\nabla} f \in \mathscr{C}(\mathscr{X} \times \mathscr{X}, \mathbb{R}^n)$ *is defined by*

$$\overline{\nabla} f(\boldsymbol{x}, \boldsymbol{x}') = \begin{cases} \nabla f\left(\frac{\boldsymbol{x}+\boldsymbol{x}'}{2}\right) + \dfrac{f(\boldsymbol{x}') - f(\boldsymbol{x}) - \nabla f\left(\frac{\boldsymbol{x}+\boldsymbol{x}'}{2}\right)^\top (\boldsymbol{x}' - \boldsymbol{x})}{||\boldsymbol{x}' - \boldsymbol{x}||^2}(\boldsymbol{x}' - \boldsymbol{x}) & \text{if } \boldsymbol{x}' \neq \boldsymbol{x}, \\ \nabla f\,(\boldsymbol{x}) & \text{otherwise.} \end{cases} \tag{5.12}$$

Notably, the Gonzalez discrete gradient is determined by the directionality condition together with its action on the orthogonal complement $(x' - x)^\perp$*, that is,* $\overline{\nabla} f(x, x')^\top z = \nabla f(\frac{x+x'}{2})^\top z$ *for all* $x, x' \in \mathscr{X}$ *and* $z \in (x' - x)^\perp$. ♤

Note that for the special case of polynomial functions with degree of at most two, the Gonzalez discrete gradient is equivalent to a midpoint evaluation of the analytical gradient. Next, the concept of discrete gradients may also be generalized to vector-valued functions.

Definition 5.11 (Discrete Jacobians [160, Definition 3.3])**.** *Given a vector-valued function* $F \in \mathscr{C}^1(\mathscr{X}, \mathbb{R}^m)$ *with* $\mathscr{X} \subseteq \mathbb{R}^n$ *open, a* discrete Jacobian *for* F *is any matrix function* $\overline{\mathrm{D}} F \in \mathscr{C}(\mathscr{X} \times \mathscr{X}, \mathbb{R}^{m \times n})$ *that satisfies the directionality and consistency properties*

(i) $\overline{\mathrm{D}} F(x, x')(x' - x) = F(x') - F(x)$,

(ii) $\overline{\mathrm{D}} F(x, x) = \mathrm{D} F(x)$,

for all $x, x' \in \mathscr{X}$. ♤

As pointed out in [160], a discrete Jacobian $\overline{\mathrm{D}} F$ may be equivalently characterized by the fact that all of its rows are discrete gradients of the corresponding component functions of F. In a similar notation as in (5.1), we write

$$\overline{\nabla} F = \begin{bmatrix} \overline{\nabla}_{x_1} F \\ \vdots \\ \overline{\nabla}_{x_r} F \end{bmatrix}, \qquad \overline{\mathrm{D}} F = \begin{bmatrix} \overline{\mathrm{D}}_{x_1} F & \cdots & \overline{\mathrm{D}}_{x_r} F \end{bmatrix}$$

for partial discrete derivatives and a partition $x = (x_1, \ldots, x_r)$ of the state. In particular, as long as $\mathscr{X} \subseteq \mathbb{R}^n$ is convex, we define the *Gonzalez discrete Jacobian* of a differentiable vector field $F \in \mathscr{C}^1(\mathscr{X}, \mathbb{R}^m)$ as

$$\overline{\mathrm{D}} F(x, x') = \begin{cases} \mathrm{D} F\left(\frac{x+x'}{2}\right) + \dfrac{F(x') - F(x) - \mathrm{D} F\left(\frac{x+x'}{2}\right)(x' - x)}{\|x' - x\|^2} (x' - x)^\top & \text{if } x' \neq x, \\ \mathrm{D} F(x) & \text{otherwise,} \end{cases}$$

which is again determined by the directionality condition together with $\overline{\mathrm{D}} F(x, x') w = \mathrm{D} F(\frac{x+x'}{2}) w$ for all $x, x' \in \mathscr{X}$ and $w \in (x' - x)^\perp$.

Remark 5.12. *For the construction of classical discrete gradients or discrete Jacobians, some assumptions on the state space* $\mathscr{X}$*, like its convexity, are usually necessary. However, in general the existence of discrete gradients is actually independent from the structure of* $\mathscr{X}$*. For example, replacing* $\nabla f(\frac{x+x'}{2})$ *by* $\nabla f(x)$ *or* $\nabla f(x')$ *in* (5.12) *yields a discrete gradient regardless of the structure of* $\mathscr{X}$*, although its usefulness for discretization is unclear.* ♧

Let us focus again on discrete gradients and observe the following property.

Lemma 5.13. *Let* $f \in \mathscr{C}^1(\mathscr{X}, \mathbb{R})$ *with* $\mathscr{X} = \mathscr{X}_1 \times \mathscr{X}_2$*, where* $\mathscr{X}_1 \subseteq \mathbb{R}^{n_1}$ *and* $\mathscr{X}_2 \subseteq \mathbb{R}^{n_2}$ *are open and* $\mathscr{X}_2$ *is convex, let us partition* $x = (x_1, x_2) \in \mathbb{R}^{n_1} \times \mathbb{R}^{n_2}$*, and suppose that* $\nabla_{x_2} f = 0$ *holds everywhere in* $\mathscr{X}$*. Then there is* $f_1 \in \mathscr{C}^1(\mathscr{X}_1, \mathbb{R})$ *such that* $f_1(x_1) = f(x_1, x_2)$ *and* $\nabla f_1(x_1) = \nabla_{x_1} f(x_1, x_2)$ *for every* $(x_1, x_2) \in \mathscr{X}$*, or in short* $f_1 \circ \pi_1 = f$ *and* $\nabla f_1 \circ \pi_1 = \nabla_{x_1} f$*. Let now* $\overline{\nabla} f_1$ *be a discrete gradient for* f_1 *and* $\overline{\nabla} f = (\overline{\nabla} f_1 \circ \pi_1, 0) : \mathscr{X} \times \mathscr{X} \to \mathbb{R}^{n_1} \times \mathbb{R}^{n_2}$*, i.e.,*

$$\overline{\nabla} f(x, x') = \begin{bmatrix} \overline{\nabla} f_1(x_1, x_1') \\ 0 \end{bmatrix}$$

for every $x = (x_1, x_2)$*,* $x' = (x_1', x_2') \in \mathscr{X}$*. Then* $\overline{\nabla} f$ *is a discrete gradient for* f.

Proof. The interested reader is referred to Appendix A of [A3] for some detailed lines showing that there is $f_1 \in \mathscr{C}^1(\mathscr{X}_1, \mathbb{R})$ such that $f_1(\boldsymbol{x}_1) = f(\boldsymbol{x}_1, \boldsymbol{x}_2)$ and $\nabla f_1(\boldsymbol{x}_1) = \nabla_{\boldsymbol{x}_1} f(\boldsymbol{x}_1, \boldsymbol{x}_2)$ for every $(\boldsymbol{x}_1, \boldsymbol{x}_2) \in \mathscr{X}$. We now show that $\overline{\nabla} f$ is a discrete gradient for f. In fact, for every $\boldsymbol{x} = (\boldsymbol{x}_1, \boldsymbol{x}_2), \boldsymbol{x}' = (\boldsymbol{x}_1', \boldsymbol{x}_2') \in \mathscr{X}$ it holds that

$$\overline{\nabla} f(\boldsymbol{x}, \boldsymbol{x}) = \begin{bmatrix} \overline{\nabla} f_1(\boldsymbol{x}_1, \boldsymbol{x}_1) \\ \boldsymbol{0} \end{bmatrix} = \begin{bmatrix} \nabla f_1(\boldsymbol{x}_1) \\ \boldsymbol{0} \end{bmatrix} = \begin{bmatrix} \nabla_{\boldsymbol{x}_1} f(\boldsymbol{x}) \\ \nabla_{\boldsymbol{x}_2} f(\boldsymbol{x}) \end{bmatrix} = \nabla f(\boldsymbol{x})$$

and

$$\begin{aligned} \overline{\nabla} f(\boldsymbol{x}, \boldsymbol{x}')^\top (\boldsymbol{x}' - \boldsymbol{x}) = \begin{bmatrix} \overline{\nabla} f_1(\boldsymbol{x}_1, \boldsymbol{x}_1') \\ \boldsymbol{0} \end{bmatrix}^\top \begin{bmatrix} \boldsymbol{x}_1' - \boldsymbol{x}_1 \\ \boldsymbol{x}_2' - \boldsymbol{x}_2 \end{bmatrix} &= \overline{\nabla} f_1(\boldsymbol{x}_1, \boldsymbol{x}_1')^\top (\boldsymbol{x}_1' - \boldsymbol{x}_1) \\ &= f_1(\boldsymbol{x}_1') - f_1(\boldsymbol{x}_1) = f(\boldsymbol{x}') - f(\boldsymbol{x}), \end{aligned}$$

which concludes the proof. □

Remark 5.14. *The previous lemma is still true when replacing the assumption that $\mathscr{X}$ has the form $\mathscr{X}_1 \times \mathscr{X}_2$ with convex $\mathscr{X}_2$ by some weaker assumptions. Moreover, assuming the convexity of a state space is in practice not restrictive. Since discrete gradients and other consistent approximations are used for time discretization, it can be usually assumed that they will only be evaluated for arbitrarily close $\boldsymbol{x}, \boldsymbol{x}' \in \mathscr{X}$, up to reducing the time step accordingly. Find further details in [A3], cf. Remarks 6 and 7 therein.* ♧

Discrete gradients have been applied successfully to the time discretization of pH ODEs [55, 80, C4]. Here, we want to tackle pH DAEs as described in Definition 5.2. This brings with it the striking challenge that the gradient of the Hamiltonian, which is supposed to be approximated with a discrete gradient, appears only implicitly within the relation (5.5) and is not directly part of the DAEs (5.6), which govern the dynamics of the system. Particularly for singular descriptor matrices, this leads to a non-invertible relation to the costate function. In this context the recent work [201] proposed the notion of *discrete gradient pairs*, which we regard to be helpful throughout the present work.

Definition 5.15 (Discrete gradient pair [201])**.** *Let $(\boldsymbol{E}, \boldsymbol{z})$ be a gradient pair for $\mathcal{H}$. We call $(\overline{\boldsymbol{E}}, \overline{\boldsymbol{z}}) \in \mathscr{C}(\mathscr{X} \times \mathscr{X}, \mathbb{R}^{n \times n}) \times \mathscr{C}(\mathscr{X} \times \mathscr{X}, \mathbb{R}^n)$ a* discrete gradient pair *for $(\mathcal{H}, \boldsymbol{E}, \boldsymbol{z})$ if the conditions*

(i) $\overline{\boldsymbol{z}}(\boldsymbol{x}, \boldsymbol{x}')^\top \overline{\boldsymbol{E}}(\boldsymbol{x}, \boldsymbol{x}')(\boldsymbol{x}' - \boldsymbol{x}) = \mathcal{H}(\boldsymbol{x}') - \mathcal{H}(\boldsymbol{x})$,

(ii) $\overline{\boldsymbol{E}}(\boldsymbol{x}, \boldsymbol{x}) = \boldsymbol{E}(\boldsymbol{x})$, *and*

(iii) $\overline{\boldsymbol{z}}(\boldsymbol{x}, \boldsymbol{x}) = \boldsymbol{z}(\boldsymbol{x})$,

are satisfied for all $\boldsymbol{x}', \boldsymbol{x} \in \mathscr{X}$. ♤

These conditions essentially yield that $\overline{\boldsymbol{E}}^\top \overline{\boldsymbol{z}}$ is a discrete gradient, see Definition 5.9. Property (i) can be interpreted as the directionality condition, while Properties (ii) and (iii) ensure the consistency condition for this specific discrete gradient. As it has become obvious from the previous definitions in this section, the property of *consistency* is rather crucial. We therefore make the following statement.

Definition 5.16. *Given two functions $\boldsymbol{F} \in \mathscr{C}(\mathscr{X}, \mathbb{R}^n)$ and $\overline{\boldsymbol{F}} \in \mathscr{C}(\mathscr{X} \times \mathscr{X}, \mathbb{R}^n)$, we call $\overline{\boldsymbol{F}}$ a* consistent approximation or discretization of $\boldsymbol{F}$ *if $\overline{\boldsymbol{F}}(\boldsymbol{x}, \boldsymbol{x}) = \boldsymbol{F}(\boldsymbol{x})$ for all $\boldsymbol{x} \in \mathscr{X}$.* ♤

Having discussed basic notions of pH DAEs and discrete gradients, we stress that a special class of pH DAEs is pivotal in this work, see the upcoming section.

5.3. Semi-explicit port-Hamiltonian DAE systems

We now specify that the pH DAEs under investigation are semi-explicit. This subclass already covers many applications and will be the starting point pivotal for derivations of corresponding time integration methods. We start by introducing the related concept of semi-explicit gradient pairs.

Definition 5.17. *Let $(\boldsymbol{E}, z)$ be a gradient pair for $\mathcal{H}$. We say that $(\boldsymbol{E}, z)$ is a* semi-explicit gradient pair *if $\mathscr{X} = \mathscr{X}_1 \times \mathscr{X}_2$ with $\mathscr{X}_1 \subseteq \mathbb{R}^{n_1}$ and $\mathscr{X}_2 \subseteq \mathbb{R}^{n_2}$ open and $\mathscr{X}_2$ convex , and $\boldsymbol{E} = \operatorname{diag}(\boldsymbol{E}_{11}, \boldsymbol{0})$ for some pointwise invertible matrix function $\boldsymbol{E}_{11} \in \mathscr{C}(\mathscr{X}, \mathbb{R}^{n_1 \times n_1})$.* ♤

Semi-explicit gradient pairs satisfy the following property.

Lemma 5.18. *Let $(\boldsymbol{E}, z)$ be a semi-explicit gradient pair for $\mathcal{H}$. Then there exists $\mathcal{H}_1 \in \mathscr{C}^1(\mathscr{X}_1, \mathbb{R})$ such that $\mathcal{H}_1 \circ \boldsymbol{\pi}_1 = \mathcal{H}$ and $\nabla \mathcal{H}_1 \circ \boldsymbol{\pi}_1 = \nabla_{\boldsymbol{x}_1} \mathcal{H}$, i.e.,*

$$\mathcal{H}_1(\boldsymbol{x}_1) = \mathcal{H}(\boldsymbol{x}_1, \boldsymbol{x}_2), \qquad \nabla \mathcal{H}_1(\boldsymbol{x}_1) = \nabla_{\boldsymbol{x}_1} \mathcal{H}(\boldsymbol{x}_1, \boldsymbol{x}_2) \tag{5.13}$$

for all $\boldsymbol{x}_1 \in \mathscr{X}_1,\ \boldsymbol{x}_2 \in \mathscr{X}_2$. In particular, the gradient-pair property (5.5) *is determined by*

$$\nabla \mathcal{H}_1(\boldsymbol{x}_1) = \boldsymbol{E}_{11}(\boldsymbol{x}_1, \boldsymbol{x}_2)^\top z_1(\boldsymbol{x}_1, \boldsymbol{x}_2), \tag{5.14}$$

for all $\boldsymbol{x}_1 \in \mathscr{X}_1,\ \boldsymbol{x}_2 \in \mathscr{X}_2$, where $z = (z_1, z_2)$ is the corresponding partition of z.

Proof. Due to the structure of $\boldsymbol{E}$, the gradient-pair property (5.5) can be written as $\nabla_{\boldsymbol{x}_1} \mathcal{H} = \boldsymbol{E}_{11}^\top z_1$ and $\nabla_{\boldsymbol{x}_2} \mathcal{H} = \boldsymbol{0}$. The latter equation implies with Lemma 5.13 that there exists $\mathcal{H}_1 \in \mathscr{C}^1(\mathscr{X}_1, \mathbb{R})$ satisfying (5.13), while the former is immediately reinterpreted as (5.14). □

By abuse of terminology, we will also refer to $\mathcal{H}_1$ as *Hamiltonian* in the remainder of this work, while ensuring that it is clear from the context whether we refer to $\mathcal{H}\colon \mathscr{X} \to \mathbb{R}$ or to $\mathcal{H}_1\colon \mathscr{X}_1 \to \mathbb{R}$.

Definition 5.19. *Consider a state space $\mathscr{X} = \mathscr{X}_1 \times \mathscr{X}_2 \subseteq \mathbb{R}^n$ with $\mathscr{X}_1 \subseteq \mathbb{R}^{n_1}$ open and $\mathscr{X}_2 \subseteq \mathbb{R}^{n_2}$ open convex, and let us partition the state $\boldsymbol{x} = (\boldsymbol{x}_1, \boldsymbol{x}_2) \in \mathscr{X}$ accordingly. A* semi-explicit pH DAE *is a port-Hamiltonian descriptor system in the sense of Definition 5.2 with $\boldsymbol{E} = \operatorname{diag}(\boldsymbol{E}_{11}, \boldsymbol{0})$, where $\boldsymbol{E}_{11} \in \mathscr{C}(\mathscr{X}, \mathbb{R}^{n_1 \times n_1})$ is pointwise invertible. In particular it admits the form*

$$\begin{aligned} \begin{bmatrix} \boldsymbol{E}_{11}(\boldsymbol{x}) & 0 \\ 0 & 0 \end{bmatrix} \begin{bmatrix} \dot{\boldsymbol{x}}_1 \\ \dot{\boldsymbol{x}}_2 \end{bmatrix} &= (\boldsymbol{J}(\boldsymbol{x}) - \boldsymbol{R}(\boldsymbol{x})) \begin{bmatrix} z_1(\boldsymbol{x}) \\ z_2(\boldsymbol{x}) \end{bmatrix} + \boldsymbol{B}(\boldsymbol{x})\boldsymbol{u}, \\ \boldsymbol{y} &= \boldsymbol{B}(\boldsymbol{x})^\top \begin{bmatrix} z_1(\boldsymbol{x}) \\ z_2(\boldsymbol{x}) \end{bmatrix}, \end{aligned} \tag{5.15}$$

together with a Hamiltonian $\mathcal{H}_1 \in \mathscr{C}^1(\mathscr{X}_1, \mathbb{R})$ that satisfies the gradient-pair property (5.14) *and conforms with Lemma 5.18. Since only the time-derivative of $\boldsymbol{x}_1$ appears in* (5.15)*, $\boldsymbol{x}_1$ is termed* differential *state and $\boldsymbol{x}_2$ is called* algebraic *state. Conforming with Lemma 5.18, the algebraic state does not contribute to the Hamiltonian of the system.* ♤

Note that systems of the form (5.15) have also been considered in [165], where the application of partitioned Runge-Kutta schemes for their time discretization was considered. We now illustrate Lemma 5.18 and Definition 5.19 by exploring some examples[3].

[3] Readers with an interest in electrical systems may additionally consult the original work [A3], which also contains the example of a synchronous machine.

Example 5.20. *Consider the simple linear semi-explicit pH DAE of differential index 1 with* $\boldsymbol{x} = (x_1, x_2)$ *governed by*

$$\begin{bmatrix} 1 & 0 \\ 0 & 0 \end{bmatrix} \begin{bmatrix} \dot{x}_1 \\ \dot{x}_2 \end{bmatrix} = \begin{bmatrix} 0 & 1 \\ -1 & -1 \end{bmatrix} \begin{bmatrix} x_1 \\ x_2 \end{bmatrix}, \tag{5.16}$$

together with its Hamiltonian $\mathcal{H}_1(x_1) = \frac{1}{2}x_1^2$. *Conforming with Definition 5.19,* x_1 *is the differential state,* x_2 *is the algebraic state, and the Hamiltonian only depends on* x_1. *Moreover, the gradient-pair property* (5.14) *is satisfied with* $E_{11} = 1$ *and* $z_1(x_1, x_2) = x_1$. ◇

Example 5.21 (Constrained input-output pH systems in classical form)**.** *The above framework naturally includes all systems which are covered by the standard notion of pH systems in* constrained input-output representation *(see, e.g., [63, Equation 2.154] or [223, Equation 4.44]) described by local coordinates* $\tilde{\boldsymbol{x}}$ *satisfying*

$$\begin{aligned} \dot{\tilde{\boldsymbol{x}}} &= \left(\widetilde{\boldsymbol{J}}(\tilde{\boldsymbol{x}}) - \widetilde{\boldsymbol{R}}(\tilde{\boldsymbol{x}})\right) \nabla\widetilde{\mathcal{H}}(\tilde{\boldsymbol{x}}) + \boldsymbol{g}(\tilde{\boldsymbol{x}})\boldsymbol{u} + \boldsymbol{b}(\tilde{\boldsymbol{x}})\boldsymbol{\lambda}, \\ \boldsymbol{y} &= \boldsymbol{g}(\tilde{\boldsymbol{x}})^\top \nabla\widetilde{\mathcal{H}}(\tilde{\boldsymbol{x}}), \\ \boldsymbol{0} &= \boldsymbol{b}(\tilde{\boldsymbol{x}})^\top \nabla\widetilde{\mathcal{H}}(\tilde{\boldsymbol{x}}), \end{aligned}$$

with $\boldsymbol{x} = (\boldsymbol{x}_1, \boldsymbol{x}_2) = (\tilde{\boldsymbol{x}}, \boldsymbol{\lambda})$, $\mathcal{H}_1(\boldsymbol{x}_1) = \widetilde{\mathcal{H}}(\tilde{\boldsymbol{x}})$, $\boldsymbol{E}_{11} = \boldsymbol{I}$, $\boldsymbol{z}_1 = \nabla\widetilde{\mathcal{H}}(\tilde{\boldsymbol{x}})$, $\boldsymbol{z}_2 = \boldsymbol{\lambda}$, $\boldsymbol{B}(\boldsymbol{x})^\top = [\boldsymbol{g}(\tilde{\boldsymbol{x}})^\top, \boldsymbol{0}]$ *and*

$$\boldsymbol{J}(\boldsymbol{x}) - \boldsymbol{R}(\boldsymbol{x}) = \begin{bmatrix} \widetilde{\boldsymbol{J}}(\tilde{\boldsymbol{x}}) - \widetilde{\boldsymbol{R}}(\tilde{\boldsymbol{x}}) & \boldsymbol{b}(\tilde{\boldsymbol{x}}) \\ -\boldsymbol{b}(\tilde{\boldsymbol{x}})^\top & \boldsymbol{0} \end{bmatrix}.$$

Note that the Lagrange multipliers $\boldsymbol{x}_2 = \boldsymbol{\lambda}$ *are here algebraic state variables.* ◇

Example 5.22 (Nonlinear multibody systems)**.** *It can be shown that the governing equations for nonlinear multibody systems fit well into the above framework of semi-explicit pH DAEs, see for example [B6]. The equations of motion are given as*

$$\begin{bmatrix} \boldsymbol{I} & 0 & 0 \\ 0 & \boldsymbol{M} & 0 \\ 0 & 0 & \boldsymbol{0} \end{bmatrix} \begin{bmatrix} \dot{\boldsymbol{q}} \\ \dot{\boldsymbol{v}} \\ \dot{\boldsymbol{\lambda}} \end{bmatrix} = \left(\begin{bmatrix} 0 & \boldsymbol{I} & 0 \\ -\boldsymbol{I} & -\boldsymbol{R}_{\mathrm{R}}(\boldsymbol{q}) & -\mathrm{D}\boldsymbol{g}(\boldsymbol{q})^\top \\ 0 & \mathrm{D}\boldsymbol{g}(\boldsymbol{q}) & 0 \end{bmatrix} \right) \begin{bmatrix} \nabla V(\boldsymbol{q}) \\ \boldsymbol{v} \\ \boldsymbol{\lambda} \end{bmatrix} + \begin{bmatrix} 0 \\ \boldsymbol{I} \\ 0 \end{bmatrix} \boldsymbol{u},$$

$$\boldsymbol{y} = \begin{bmatrix} 0 & \boldsymbol{I} & 0 \end{bmatrix} \begin{bmatrix} \nabla V(\boldsymbol{q}) \\ \boldsymbol{v} \\ \boldsymbol{\lambda} \end{bmatrix}.$$

The Hamiltonian

$$\mathcal{H}(\boldsymbol{x}) = \frac{1}{2}\boldsymbol{v}^\top \boldsymbol{M}\boldsymbol{v} + V(\boldsymbol{q}) = T(\boldsymbol{v}) + V(\boldsymbol{q})$$

denotes the total energy. Verifying that $\boldsymbol{E}^\top \boldsymbol{z}(\boldsymbol{x}) = \nabla\mathcal{H}(\boldsymbol{x})$ *holds true is straightforward. In this example, the Lagrange multipliers* $\boldsymbol{\lambda}$ *appear as algebraic states, that do not appear in the Hamiltonian. For more details, especially concerning an introduction of the unknowns, see Section 5.5.1. A related formulation can also be found in Example 2.8 in Chapter 2 of the present work.* ◇

In the upcoming section we focus on the discretization of pH DAEs — as discussed both in Definition 5.2 and Definition 5.19.

5.4. Structure-preserving discretization in time

We start by discussing integration methods for general pH DAEs of the form (5.6) in Section 5.4.1. Here the concept of discrete gradient pairs will be of central importance. We continue with the discretization

of semi-explicit pH DAEs of the form (5.15) in Section 5.4.2, yielding a tangible time stepping method. Then, in Section 5.4.3 we discuss an alternative approach, based on the Dirac–dissipative representation associated to the pH DAE, that does not require the semi-explicit structure. Lastly, in Section 5.4.4 we investigate how the three different approaches are connected, when a semi-explicit representation is available.

5.4.1. Discrete gradient-pair methods for general port-Hamiltonian DAEs

Consider a pH DAE of the form (5.6) and a temporal grid $0 = t^0 < t^1 < \ldots < t^N = t_{\text{end}}$ with N time intervals of constant time step size $h = t^{n+1} - t^n$ for $n = 0, \ldots, N-1$. We consider uniform time grids for the sake of brevity and propose the scheme

$$\begin{aligned} \overline{E}(x^n, x^{n+1})(x^{n+1} - x^n) &= h\left(\overline{J}(x^n, x^{n+1}) - \overline{R}(x^n, x^{n+1})\right)\overline{z}(x^n, x^{n+1}) + h\,\overline{B}(x^n, x^{n+1})u^{n,n+1}, \\ y^{n,n+1} &= \overline{B}(x^n, x^{n+1})^\top \overline{z}(x^n, x^{n+1}). \end{aligned} \tag{5.17}$$

for $n = 0, \ldots, N-1$. In (5.17), we define discrete approximations of the state $x^n \approx x(t^n)$ assuming that also $x^n \in \mathscr{X}$ for sufficiently small time steps. The matrices $\overline{E}, \overline{J}, \overline{R}, \overline{B}$ are arbitrary consistent approximations of the matrix functions (see Definition 5.16), still satisfying $\overline{J} = -\overline{J}^\top$ and $\overline{R} = \overline{R}^\top \succeq 0$ pointwise. Moreover, $u^{n,n+1}$ is not necessarily the evaluation of the (possibly discontinuous) input function at t^n, but at some point within the time interval of interest or an average value of it. Correspondingly, the discrete-time output $y^{n,n+1}$ is an approximation for $y(t)$ for the whole time step interval.

Most importantly, we require that $(\overline{E}, \overline{z})$ is a discrete gradient pair for $(\mathcal{H}, E, z)$ in the sense of Definition 5.15. Finding such a discrete gradient pair is not trivial, but we will provide a construction for the case of semi-explicit pH DAEs in Section 5.4.2.1. This already covers a wide range of applications. For self-containedness of this work, we show that the usage of discrete gradient pairs yields an energy-consistent time integration.

Theorem 5.23. *Scheme* (5.17) *induces a discrete-time PBE given by*

$$\begin{aligned} \mathcal{H}(x^{n+1}) - \mathcal{H}(x^n) &= -h\overline{z}(x^n, x^{n+1})^\top \overline{R}(x^n, x^{n+1})\overline{z}(x^n, x^{n+1}) + h(y^{n,n+1})^\top u^{n,n+1} \\ &\leq h(y^{n,n+1})^\top u^{n,n+1}, \end{aligned} \tag{5.18}$$

mimicking the time-continuous power balance (5.7).

Proof. Combining the directionality condition (i) of the discrete gradient pair with (5.17) one obtains

$$\begin{aligned} \mathcal{H}(x^{n+1}) - \mathcal{H}(x^n) &= \overline{z}(x^n, x^{n+1})^\top \overline{E}(x^n, x^{n+1})(x^{n+1} - x^n) \\ &= h\overline{z}(x^n, x^{n+1})^\top \left(\overline{J}(x^n, x^{n+1}) - \overline{R}(x^n, x^{n+1})\right)\overline{z}(x^n, x^{n+1}) \\ &\quad + h\overline{z}(x^n, x^{n+1})^\top \overline{B}(x^n, x^{n+1})u^{n,n+1} \\ &= -h\overline{z}(x^n, x^{n+1})^\top \overline{R}(x^n, x^{n+1})\overline{z}(x^n, x^{n+1}) + h(y^{n,n+1})^\top u^{n,n+1} \\ &\leq h(y^{n,n+1})^\top u^{n,n+1}, \end{aligned}$$

which is the desired result. □

5.4.2. Discrete gradient methods for semi-explicit port-Hamiltonian DAEs

In the following we consider the special case of a semi-explicit pH DAE of the form (5.15) for which we present a concrete time discretization scheme. The scheme itself is outlined in Section 5.4.2.1 whereas a corresponding convergence analysis is presented in Section 5.4.2.2.

5.4.2.1. Time discretization scheme for semi-explicit pH DAEs

For a semi-explicit pH DAE of the form (5.15), the partitioning of the state and the block matrix structure allow for a straightforward approach using discrete gradients, which leads to a concrete time stepping method outlined in the following. Particularly, the semi-explicit gradient-pair property (5.14) allows for a direct approximation of z_1 in terms of the Hamiltonian $\mathcal{H}_1$. Essentially, the proposed method can be written just like equations (5.17), which have to be completed by the additional constraint

$$\overline{E}_{11}(x^n, x^{n+1})^\top \overline{z}_1(x^n, x^{n+1}) = \overline{\nabla}\mathcal{H}_1(x^n, x^{n+1}). \tag{5.19}$$

We now choose $\overline{\nabla}\mathcal{H}_1 \in \mathscr{C}(\mathscr{X}_1 \times \mathscr{X}_1, \mathbb{R}^{n_1})$ to be a discrete gradient of $\mathcal{H}_1$ and $\overline{E}_{11} \in \mathscr{C}(\mathscr{X} \times \mathscr{X}, \mathbb{R}^{n_1 \times n_1})$ to be a consistent discretization of E_{11}. This allows to determine uniquely $\overline{z}_1$ as a function of x^n, x^{n+1}, as long $\overline{E}_{11}$ is ensured to be invertible within our search scope.

This is for example the case if we choose the midpoint approximation $\overline{E}_{11}(x, x') \coloneqq E_{11}(\frac{x+x'}{2})$, since E_{11} is invertible in the convex space $\mathscr{X}$. More in general, any consistent approximation $\overline{E}_{11}$ will be invertible for sufficiently close x^n, x^{n+1}.

While there is in general no guarantee that a discrete matrix function is pointwise invertible[4], we expect to achieve this condition up to refining the time grid sufficiently. For the sake of simplicity, we introduce the following assumption.

Assumption 5.24. *$\overline{E}_{11}$ is pointwise invertible on $\mathscr{X} \times \mathscr{X}$.*

Furthermore, since $\overline{z} = (\overline{z}_1, \overline{z}_2)$ is not given as part of a gradient pair anymore, we will choose $\overline{z}_2$ as a consistent discretization of the time-continuous function z_2. In a more detailed fashion, also highlighting the partitioned state, we rewrite (5.17) and (5.19) combined as

$$\begin{bmatrix} \overline{E}_{11}(x^n, x^{n+1}) & 0 \\ 0 & 0 \end{bmatrix} \begin{bmatrix} x_1^{n+1} - x_1^n \\ x_2^{n+1} - x_2^n \end{bmatrix} = h\big(\overline{J}(x^n, x^{n+1}) - \overline{R}(x^n, x^{n+1})\big) \begin{bmatrix} z_1^{n,n+1} \\ \overline{z}_2(x^n, x^{n+1}) \end{bmatrix} + h\overline{B}(x^n, x^{n+1}) u^{n,n+1}, \tag{5.20a}$$

$$y^{n,n+1} = \overline{B}(x^n, x^{n+1})^\top \begin{bmatrix} z_1^{n,n+1} \\ \overline{z}_2(x^n, x^{n+1}) \end{bmatrix}, \tag{5.20b}$$

$$\overline{E}_{11}(x^n, x^{n+1})^\top z_1^{n,n+1} = \overline{\nabla}\mathcal{H}_1(x_1^n, x_1^{n+1}), \tag{5.20c}$$

which can be solved for the unknowns $(x_1^{n+1}, x_2^{n+1}, z_1^{n,n+1}, y^{n,n+1})$ in each time step (assuming that a solution exists). Note that $z_1^{n,n+1}$, which here replaces the uniquely determined function $\overline{z}_1$, is considered as an unknown of the time-discrete system, whereas $\overline{z}_2$ is a consistent discretization of z_2. This scheme extends the discrete gradient method from [C2, C4] to semi-explicit pH DAE systems with the specific structure of the descriptor matrix E.

Let us illustrate the proposed method by an example and show that it preserves the power balance equation in discrete time.

[4] The reader can find a counterexample in Example 9 in the appendix of the original work [A3].

Example 5.25. *We consider again the running example system from Example 5.20. Its discretization* (5.20) *is given by*

$$\begin{bmatrix} 1 & 0 \\ 0 & 0 \end{bmatrix} \begin{bmatrix} x_1^{n+1} - x_1^n \\ x_2^{n+1} - x_2^n \end{bmatrix} = h \begin{bmatrix} 0 & 1 \\ -1 & -1 \end{bmatrix} \begin{bmatrix} z_1^{n,n+1} \\ \bar{z}_2(\boldsymbol{x}^n, \boldsymbol{x}^{n+1}) \end{bmatrix}.$$
$$z_1^{n,n+1} = \overline{\nabla}\mathcal{H}_1(x_1^n, x_1^{n+1}) = \frac{1}{2}(x_1^n + x_1^{n+1}),$$

where we chose the Gonzalez discrete gradient for the latter relation, which corresponds to (5.20c)*. While* $z_1^{n,n+1}$ *is an unknown of the system,* $\bar{z}_2(\boldsymbol{x}^n, \boldsymbol{x}^{n+1})$ *still requires a consistent discretization of* $z_2(\boldsymbol{x}) = x_2$*. Sensible choices like*

$$\bar{z}_2(\boldsymbol{x}^n, \boldsymbol{x}^{n+1}) = x_2^n, \qquad \bar{z}_2(\boldsymbol{x}^n, \boldsymbol{x}^{n+1}) = x_2^{n+1} \qquad \text{or} \qquad \bar{z}_2(\boldsymbol{x}^n, \boldsymbol{x}^{n+1}) = \frac{1}{2}(x_2^n + x_2^{n+1})$$

complete the set of equations. ◊

Theorem 5.26. *Scheme* (5.20) *yields an energy-consistent approximation of the time-continuous power balance* (5.7) *given by*

$$\begin{aligned} \mathcal{H}(\boldsymbol{x}^{n+1}) - \mathcal{H}(\boldsymbol{x}^n) &= -h \begin{bmatrix} z_1^{n,n+1} \\ \overline{z}_2(\boldsymbol{x}^n, \boldsymbol{x}^{n+1}) \end{bmatrix}^\top \overline{\boldsymbol{R}}(\boldsymbol{x}^n, \boldsymbol{x}^{n+1}) \begin{bmatrix} z_1^{n,n+1} \\ \overline{z}_2(\boldsymbol{x}^n, \boldsymbol{x}^{n+1}) \end{bmatrix} + h(\boldsymbol{y}^{n,n+1})^\top \boldsymbol{u}^{n,n+1} \\ &\leq h(\boldsymbol{y}^{n,n+1})^\top \boldsymbol{u}^{n,n+1}. \end{aligned} \tag{5.21}$$

Proof. Combining the directionality property of the discrete gradient $\overline{\nabla}\mathcal{H}_1$ with (5.20) one obtains

$$\begin{aligned} \mathcal{H}(\boldsymbol{x}^{n+1}) - \mathcal{H}(\boldsymbol{x}^n) &= \mathcal{H}_1(x_1^{n+1}) - \mathcal{H}_1(x_1^n) = \overline{\nabla}\mathcal{H}_1(\boldsymbol{x}^n, \boldsymbol{x}^{n+1})^\top (\boldsymbol{x}^{n+1} - \boldsymbol{x}^n) \\ &= (z_1^{n,n+1})^\top \overline{\boldsymbol{E}}_{11}(\boldsymbol{x}^n, \boldsymbol{x}^{n+1})(x_1^{n+1} - x_1^n) = \begin{bmatrix} z_1^{n,n+1} \\ \overline{z}_2(\boldsymbol{x}^n, \boldsymbol{x}^{n+1}) \end{bmatrix}^\top \overline{\boldsymbol{E}}(\boldsymbol{x}^n, \boldsymbol{x}^{n+1})(\boldsymbol{x}^{n+1} - \boldsymbol{x}^n) \\ &= h \begin{bmatrix} z_1^{n,n+1} \\ \overline{z}_2(\boldsymbol{x}^n, \boldsymbol{x}^{n+1}) \end{bmatrix}^\top \left(\overline{\boldsymbol{J}}(\boldsymbol{x}^n, \boldsymbol{x}^{n+1}) - \overline{\boldsymbol{R}}(\boldsymbol{x}^n, \boldsymbol{x}^{n+1})\right) \begin{bmatrix} z_1^{n,n+1} \\ \overline{z}_2(\boldsymbol{x}^n, \boldsymbol{x}^{n+1}) \end{bmatrix} \\ &\qquad + h \begin{bmatrix} z_1^{n,n+1} \\ \overline{z}_2(\boldsymbol{x}^n, \boldsymbol{x}^{n+1}) \end{bmatrix}^\top \overline{\boldsymbol{B}}(\boldsymbol{x}^n, \boldsymbol{x}^{n+1}) \boldsymbol{u}^{n,n+1} \\ &= -h \begin{bmatrix} z_1^{n,n+1} \\ \overline{z}_2(\boldsymbol{x}^n, \boldsymbol{x}^{n+1}) \end{bmatrix}^\top \overline{\boldsymbol{R}}(\boldsymbol{x}^n, \boldsymbol{x}^{n+1}) \begin{bmatrix} z_1^{n,n+1} \\ \overline{z}_2(\boldsymbol{x}^n, \boldsymbol{x}^{n+1}) \end{bmatrix} + h(\boldsymbol{y}^{n,n+1})^\top \boldsymbol{u}^{n,n+1} \\ &\leq h(\boldsymbol{y}^{n,n+1})^\top \boldsymbol{u}^{n,n+1}, \end{aligned}$$

which is the desired result. □

The semi-explicit discrete gradient method introduced in this section can of course be applied to constrained input-output pH systems as introduced in Example 5.21, always achieving the desired exact PBE. While there is in general no guarantee that the algebraic constraints are satisfied exactly by the discrete solution, specific implementation choices may allow to meet additional requirements stemming from the particular application problem. This is shown for the example of nonlinear multibody systems in Section 5.5.2.

5.4.2.2. Convergence analysis for semi-explicit pH DAEs

To further motivate the proposed method, let us show that, under some additional assumptions on the structure of the system, second order convergence can be achieved. Following a similar idea as for the Dirac–dissipative representation, let us introduce the costate variables $\boldsymbol{f}_1 \in \mathbb{R}^{n_1}$ and the corresponding gradient-pair equation $\boldsymbol{E}_{11}(\boldsymbol{x})^\top \boldsymbol{f}_1 = \nabla \mathcal{H}_1(\boldsymbol{x}_1)$. We can then rewrite (5.15) as a semi-explicit DAE of the form

$$\dot{\boldsymbol{x}}_1 = \boldsymbol{F}(\boldsymbol{x}_1, \boldsymbol{u}, \boldsymbol{f}_1, \boldsymbol{x}_2), \tag{5.22a}$$
$$\boldsymbol{0} = \boldsymbol{G}_1(\boldsymbol{x}_1, \boldsymbol{u}, \boldsymbol{f}_1, \boldsymbol{x}_2), \tag{5.22b}$$
$$\boldsymbol{0} = \boldsymbol{G}_2(\boldsymbol{x}_1, \boldsymbol{f}_1, \boldsymbol{x}_2), \tag{5.22c}$$
$$\boldsymbol{0} = \boldsymbol{G}_3(\boldsymbol{x}_1, \boldsymbol{f}_1, \boldsymbol{x}_2, \boldsymbol{y}), \tag{5.22d}$$

where

$$\begin{aligned}
\boldsymbol{F}(\boldsymbol{x}_1, \boldsymbol{u}, \boldsymbol{f}_1, \boldsymbol{x}_2) &\coloneqq \boldsymbol{E}_{11}(\boldsymbol{x})^{-1} \big(\big(\boldsymbol{J}_{11}(\boldsymbol{x}_1, \boldsymbol{x}_2) - \boldsymbol{R}_{11}(\boldsymbol{x}_1, \boldsymbol{x}_2)\big)\boldsymbol{f}_1 \\
&\qquad + \big(\boldsymbol{J}_{12}(\boldsymbol{x}_1, \boldsymbol{x}_2) - \boldsymbol{R}_{12}(\boldsymbol{x}_1, \boldsymbol{x}_2)\big)\boldsymbol{z}_2(\boldsymbol{x}_1, \boldsymbol{x}_2) + \boldsymbol{B}_1(\boldsymbol{x}_1, \boldsymbol{x}_2)\boldsymbol{u}\big), \\
\boldsymbol{G}_1(\boldsymbol{x}_1, \boldsymbol{u}, \boldsymbol{f}_1, \boldsymbol{x}_2) &\coloneqq \big(\boldsymbol{J}_{21}(\boldsymbol{x}_1, \boldsymbol{x}_2) - \boldsymbol{R}_{21}(\boldsymbol{x}_1, \boldsymbol{x}_2)\big)\boldsymbol{f}_1 + \big(\boldsymbol{J}_{22}(\boldsymbol{x}_1, \boldsymbol{x}_2) - \boldsymbol{R}_{22}(\boldsymbol{x}_1, \boldsymbol{x}_2)\big)\boldsymbol{z}_2(\boldsymbol{x}_1, \boldsymbol{x}_2) + \boldsymbol{B}_2(\boldsymbol{x}_1, \boldsymbol{x}_2)\boldsymbol{u}, \\
\boldsymbol{G}_2(\boldsymbol{x}_1, \boldsymbol{f}_1, \boldsymbol{x}_2) &\coloneqq \boldsymbol{E}_{11}(\boldsymbol{x}_1, \boldsymbol{x}_2)^\top \boldsymbol{f}_1 - \nabla \mathcal{H}_1(\boldsymbol{x}_1), \\
\boldsymbol{G}_3(\boldsymbol{x}_1, \boldsymbol{f}_1, \boldsymbol{x}_2, \boldsymbol{y}) &\coloneqq \boldsymbol{y} - \boldsymbol{B}_1(\boldsymbol{x}_1, \boldsymbol{x}_2)^\top \boldsymbol{f}_1 - \boldsymbol{B}_2(\boldsymbol{x}_1, \boldsymbol{x}_2)^\top \boldsymbol{z}_2(\boldsymbol{x}_1, \boldsymbol{x}_2).
\end{aligned}$$

Suppose now that this augmented DAE has differentiation index 1, i.e., that $\boldsymbol{G}_1$ is continuously differentiable and its partial Jacobian $\mathrm{D}_{\boldsymbol{x}_2}\boldsymbol{G}_1$ is pointwise invertible. Then there exists $\mathcal{R} \in \mathscr{C}^1(\mathbb{R}^{n_1}, \mathbb{R}^{n_2})$ such that every solution of the augmented DAE satisfies $\boldsymbol{x}_2 = \mathcal{R}(\boldsymbol{x}_1)$, due to the implicit function theorem. In particular, every solution also satisfies

$$\dot{\boldsymbol{x}}_1 = \widetilde{\boldsymbol{F}}\big(\boldsymbol{x}_1, \nabla \mathcal{H}_1(\boldsymbol{x}_1), \boldsymbol{u}\big) \coloneqq \boldsymbol{F}\Big(\boldsymbol{x}_1, \boldsymbol{u}, \boldsymbol{E}_{11}\big(\boldsymbol{x}_1, \mathcal{R}(\boldsymbol{x}_1)\big)^{-\top} \nabla \mathcal{H}_1(\boldsymbol{x}_1), \mathcal{R}(\boldsymbol{x}_1)\Big), \tag{5.23}$$

which is an ODE in the variable $\boldsymbol{x}_1$.

Let us now consider the discrete system (5.20) obtained using a discrete gradient $\overline{\nabla}\mathcal{H}_1$ and the consistent discretizations stemming from midpoint evaluations, which we write as

$$\begin{aligned}
\boldsymbol{x}_1^{n+1} - \boldsymbol{x}_1^n &= h\boldsymbol{F}\Big(\boldsymbol{x}_1^{n+1/2}, \boldsymbol{u}^{n,n+1}, \boldsymbol{z}_1^{n,n+1}, \boldsymbol{x}_2^{n+1/2}\Big), \\
\boldsymbol{0} &= \begin{bmatrix} \boldsymbol{G}_1\Big(\boldsymbol{x}_1^{n+1/2}, \boldsymbol{u}^{n,n+1}, \boldsymbol{z}_1^{n,n+1}, \boldsymbol{x}_2^{n+1/2}\Big) \\ \boldsymbol{G}_2\Big(\boldsymbol{x}_1^{n+1/2}, \boldsymbol{z}_1^{n,n+1}, \boldsymbol{x}_2^{n+1/2}\Big) \\ \boldsymbol{G}_3\Big(\boldsymbol{x}_1^{n+1/2}, \boldsymbol{z}_1^{n,n+1}, \boldsymbol{x}_2^{n+1/2}, \boldsymbol{y}^{n,n+1}\Big) \end{bmatrix},
\end{aligned}$$

where $\boldsymbol{x}_1^{n+1/2} = \frac{1}{2}(\boldsymbol{x}_1^n + \boldsymbol{x}_1^{n+1})$ and $\boldsymbol{x}_2^{n+1/2} = \frac{1}{2}(\boldsymbol{x}_2^n + \boldsymbol{x}_2^{n+1})$. In particular, the discrete solutions also satisfy $\boldsymbol{x}_2^{n+1/2} = \mathcal{R}(\boldsymbol{x}_1^{n+1/2})$ for all $n \geq 0$, for the same map $\mathcal{R}$, and therefore

$$\begin{aligned}
\boldsymbol{x}_1^{n+1} - \boldsymbol{x}_1^n &= h\boldsymbol{F}\Big(\boldsymbol{x}_1^{n+1/2}, \boldsymbol{u}^{n,n+1}, \boldsymbol{E}_{11}\big(\boldsymbol{x}_1^{n+1/2}, \mathcal{R}(\boldsymbol{x}_1^{n+1/2})\big)^{-\top} \overline{\nabla}\mathcal{H}_1(\boldsymbol{x}_1^n, \boldsymbol{x}_1^{n+1}), \mathcal{R}(\boldsymbol{x}_1^{n+1/2})\Big) \\
&= h\widetilde{\boldsymbol{F}}\big(\boldsymbol{x}_1^{n+1/2}, \overline{\nabla}\mathcal{H}_1(\boldsymbol{x}^n, \boldsymbol{x}^{n+1}), \boldsymbol{u}^{n,n+1}\big).
\end{aligned}$$

In particular, applying a discrete gradient to a semi-explicit pH DAE using midpoint evaluations yields the same discrete sequence for $\boldsymbol{x}_1$ as if we applied the same discrete gradient and midpoint evaluations

to the ODE (5.23). Thus, the convergence error for the differential state x_1 will also be the same. In the case of the Gonzalez discrete gradient, this ensures second convergence order for x_1 [66, 160]. Then, proceeding analogously as in the second part of the proof of [132, Theorem 5.16], one can deduce that x_2 also converges with order 2. We summarize this discussion in the following statement.

Proposition 5.27. *Consider a semi-explicit pH DAE of the form* (5.15)*, to which the discretization scheme* (5.20) *obtained using the Gonzalez discrete gradient and midpoint evaluations is applied. If the augmented DAE* (5.22) *has differentiation index 1, then the method has convergence order 2.* ♡

More in general, the convergence of the method both depends on the differentiation index of the DAE and on the choice of discrete gradient and consistent discretizations. In the numerical example that we present in Section 5.5, which is a semi-explicit pH DAE with differentiation index 2, this same method appears to have convergence order 2 for the differential variables, but only convergence order 1 for the algebraic variable. We postpone further analysis to future works.

5.4.3. Discrete gradient methods applied to the Dirac–dissipative representation

We will now discuss an alternative structure-preserving discretization method, which requires neither a semi-explicit form nor a discrete gradient pair, based on the Dirac–dissipative representation, that can also be linked to previous works for ODE systems [C2, C4]. Given a DDR of a pH DAE (5.11), the DDR-method governs time-stepping via

$$\begin{bmatrix} \overline{\nabla}\mathcal{H}(x^n, x^{n+1}) \\ 0 \\ y^{n,n+1} \end{bmatrix} + \begin{bmatrix} 0 & -\overline{E}(x^n, x^{n+1})^\top & 0 \\ \overline{E}(x^n, x^{n+1}) & \overline{J}(x^n, x^{n+1}) - \overline{R}(x^n, x^{n+1}) & \overline{B}(x^n, x^{n+1}) \\ 0 & -\overline{B}(x^n, x^{n+1})^\top & 0 \end{bmatrix} \begin{bmatrix} -\frac{1}{h}(x^{n+1} - x^n) \\ f^{n,n+1} \\ u^{n,n+1} \end{bmatrix} = 0. \tag{5.24}$$

or written out

$$\begin{aligned} \overline{E}(x^n, x^{n+1})(x^{n+1} - x^n) &= h\big(\overline{J}(x^n, x^{n+1}) - \overline{R}(x^n, x^{n+1})\big) f^{n,n+1} + h\overline{B}(x^n, x^{n+1}) u^{n,n+1}, \\ y^{n,n+1} &= \overline{B}(x^n, x^{n+1})^\top f^{n,n+1}, \end{aligned} \tag{5.25a}$$

as well as

$$\overline{E}(x^n, x^{n+1})^\top f^{n,n+1} = \overline{\nabla}\mathcal{H}(x^n, x^{n+1}). \tag{5.25b}$$

Therein, $f^{n,n+1}$ are discrete-time approximations of the costate quantities. Additionally, we have borrowed definitions from Section 5.4.1 concerning the discrete state and matrices.

It is in general unclear whether these equations can be solved simultaneously for the unknowns $(x^{n+1}, f^{n,n+1}, y^{n,n+1})$ in each time step. While for pointwise invertible $\overline{E}$ one can at least recover $f^{n,n+1}$ as a function of x^{n+1}, and rewrite the discrete system only in terms of x^n and x^{n+1}, for an arbitrary, non-invertible $\overline{E}$ further analysis is required. In particular, (5.25a) could be underdetermined even if the original DAE was regular, thus it might be necessary to introduce additional constraints. We show this with an example.

Example 5.28. *Consider the regular linear semi-explicit pH DAE from Example 5.20 with Hamiltonian* $\mathcal{H}(x) = \frac{1}{2}x_1^2$*, where we can identify*

$$E = \begin{bmatrix} 1 & 0 \\ 0 & 0 \end{bmatrix}, \quad J = \begin{bmatrix} 0 & 1 \\ -1 & 0 \end{bmatrix}, \quad R = \begin{bmatrix} 0 & 0 \\ 0 & 1 \end{bmatrix}, \quad B = \begin{bmatrix} 0 \\ 0 \end{bmatrix}, \quad \nabla\mathcal{H}(x) = \begin{bmatrix} x_1 \\ 0 \end{bmatrix}.$$

The system's DDR (5.11) *reads*

$$\begin{bmatrix} x_1 \\ 0 \\ 0 \\ 0 \end{bmatrix} + \begin{bmatrix} 0 & 0 & -1 & 0 \\ 0 & 0 & 0 & 0 \\ 1 & 0 & 0 & 1 \\ 0 & 0 & -1 & -1 \end{bmatrix} \begin{bmatrix} -\dot{x}_1 \\ -\dot{x}_2 \\ f_1 \\ f_2 \end{bmatrix} = 0 \tag{5.26}$$

with $\boldsymbol{f} = \boldsymbol{z}(\boldsymbol{x})$. *Discretizing* (5.26) *with the Gonzalez discrete gradient and discarding the trivial parts of the equation yields*

$$f_1^{n,n+1} = -f_2^{n,n+1} = \frac{x_1^n + x_1^{n+1}}{2}, \qquad x_1^{n+1} = x_1^n - h\frac{x_1^n + x_1^{n+1}}{2}, \tag{5.27}$$

which is equivalent to reducing (5.16) *to* $\dot{x}_1 = -x_1$ *and solving this subsystem with the implicit midpoint method. However,* x_2 *remains undetermined, since the DDR-method discarded the connection between* f_2 *and* x_2.

One possible solution is to use our original knowledge from (5.16) *and define* $x_2^{n+1} = -x_1^{n+1}$, *conforming with the algebraic condition* $x_1 + x_2 = 0$. *Another possibility would be to observe that* $(f_1, f_2) = \boldsymbol{z}(\boldsymbol{x}) = (x_1, x_2)$ *and define* $x_2^{n+1} = f_2^{n,n+1} = -\frac{1}{2}(x_1^n + x_1^{n+1})$. *Note that both these ideas are based on a priori knowledge of the equation structure*[5]. ◇

Let us emphasize that the choice of additional constraints does not affect the power balance equation, which remains satisfied by (5.25a) and (5.25b). We also refer to [165, Example 7.4.1] where analogous deductions are made in the context of Galerkin projection schemes.

In the case where $\boldsymbol{E}$ is singular, the question arises whether there exists a discrete gradient of $\mathcal{H}$, which ensures that $\overline{\nabla}\mathcal{H}(\boldsymbol{x}, \boldsymbol{x}')$ is in the column space of $\overline{\boldsymbol{E}}(\boldsymbol{x}, \boldsymbol{x}')^\top$, i.e.,

$$\overline{\nabla}\mathcal{H}(\boldsymbol{x}, \boldsymbol{x}') \in \operatorname{colsp}(\overline{\boldsymbol{E}}(\boldsymbol{x}, \boldsymbol{x}')^\top), \tag{5.28}$$

for all $\boldsymbol{x}, \boldsymbol{x}' \in \mathbb{R}^n$. This ensures that (5.25b) can be solved for $\boldsymbol{f}^{n,n+1}$, although not necessarily uniquely. Further details and a corresponding counterexample can be found in Appendix C of [A3]. Let us now focus on the connections between the discrete methods introduced in this section.

5.4.4. Relations between the presented methods in the semi-explicit setting

In this subsection, it is demonstrated that the semi-explicit discrete gradient method from Section 5.4.2 is equivalent to special cases of the discrete gradient-pair approach from Section 5.4.1 and of the DDR approach from Section 5.4.3.

First, we observe that scheme (5.20) for semi-explicit pH DAEs of the form (5.15) corresponds to an underlying discrete gradient pair, see Definition 5.15. This is stated in the following theorem and corollary.

Theorem 5.29. *Let* $(\boldsymbol{E}, \boldsymbol{z})$ *be a semi-explicit gradient pair for* $\mathcal{H}$ *in the sense of Definition 5.17 and let* $\boldsymbol{z} = (\boldsymbol{z}_1, \boldsymbol{z}_2)$ *be split correspondingly. Furthermore, let* $\overline{\boldsymbol{E}}_{11} \in \mathscr{C}(\mathscr{X} \times \mathscr{X}, \mathbb{R}^{n_1 \times n_1})$ *and* $\overline{\boldsymbol{z}}_2 \in \mathscr{C}(\mathscr{X} \times \mathscr{X}, \mathbb{R}^{n_2})$

[5] Another solution to this issue is discussed in Example 6 of the original work [A3].

be consistent discretizations of E_{11} and z_2, respectively, suppose that $\overline{E}_{11}$ satisfies Assumption 5.24, and let $\overline{\nabla}\mathcal{H}_1$ be a discrete gradient for $\mathcal{H}_1 \in \mathscr{C}^1(\mathscr{X}_1, \mathbb{R})$. Then $(\overline{E}, \overline{z})$ with

$$\overline{E} = \begin{bmatrix} \overline{E}_{11} & 0 \\ 0 & 0 \end{bmatrix}, \qquad \overline{z} = \begin{bmatrix} \overline{E}_{11}^{-\top}(\overline{\nabla}\mathcal{H}_1 \circ \boldsymbol{\pi}_1) \\ \overline{z}_2 \end{bmatrix} \tag{5.29}$$

is a discrete gradient pair for $(\mathcal{H}, \boldsymbol{E}, z)$.

Proof. Property (ii) in Definition 5.15 is part of our hypotheses. We proceed to show that Properties (i) and (iii) are also valid. In fact, it holds that

$$\overline{z}(x, x) = \begin{bmatrix} \overline{E}_{11}(x, x)^{-\top}\overline{\nabla}\mathcal{H}_1(x_1, x_1) \\ \overline{z}_2(x, x) \end{bmatrix} = \begin{bmatrix} E_{11}(x)^{-\top}\nabla\mathcal{H}_1(x_1) \\ z_2(x) \end{bmatrix} = \begin{bmatrix} z_1(x) \\ z_2(x) \end{bmatrix} = z(x)$$

and

$$\begin{aligned} \overline{z}(x, x')^\top \overline{E}(x, x')(x' - x) &= \overline{z}_1(x, x')^\top \overline{E}_{11}(x, x')(x'_1 - x_1) = \\ &= \overline{\nabla}\mathcal{H}_1(x_1, x'_1)^\top (x'_1 - x_1) = \mathcal{H}_1(x'_1) - \mathcal{H}_1(x_1) = \mathcal{H}(x') - \mathcal{H}(x), \end{aligned}$$

for all $x = (x_1, x_2), x' = (x'_1, x'_2) \in \mathscr{X}$. □

Corollary 5.30. *Consider a semi-explicit pH DAE of the form* (5.15)*, let $\overline{\nabla}\mathcal{H}_1$, $\overline{E}_{11}$, $\overline{z}_2$, $\overline{E}$, and $\overline{z}$ be defined as in Theorem 5.29, and let us fix consistent discretizations for $\boldsymbol{J}$, $\boldsymbol{R}$, and $\boldsymbol{B}$. Then the semi-explicit discrete gradient method applied with $\overline{\nabla}\mathcal{H}_1$ governed by* (5.20) *and the discrete gradient pair method* (5.17) *applied with $(\overline{E}, \overline{z})$ yield the same solution.*

Proof. The claim immediately follows by construction, since

$$\overline{z}(x^n, x^{n+1}) = \begin{bmatrix} \overline{E}_{11}(x^n, x^{n+1})^{-\top}\overline{\nabla}\mathcal{H}_1(x_1^n, x_1^{n+1}) \\ \overline{z}_2(x^n, x^{n+1}) \end{bmatrix} = \begin{bmatrix} z_1^{n,n+1} \\ \overline{z}_2(x^n, x^{n+1}) \end{bmatrix}$$

holds true. □

We will now see that the discrete gradient method applied to semi-explicit pH DAEs can be equivalently reinterpreted as a specific DDR-method.

Theorem 5.31. *Under the same assumptions as in Theorem 5.29, the semi-explicit discrete gradient method* (5.20) *yields the same one-step method as the DDR-method* (5.24) *with the completing constraint $f_2^{n,n+1} = \overline{z}_2(x^n, x^{n+1})$.*

Proof. Due to the structure of the system, the DDR-method (5.24) applied to (5.15) yields the one-step method

$$\begin{bmatrix} \overline{\nabla}\mathcal{H}_1(x_1^n, x_1^{n+1}) \\ 0 \\ 0 \\ 0 \\ y^{n,n+1} \end{bmatrix} + \begin{bmatrix} 0 & 0 & -\overline{E}_{11}^\top & 0 & 0 \\ 0 & 0 & 0 & 0 & 0 \\ \overline{E}_{11} & 0 & \overline{J}_{11} - \overline{R}_{11} & \overline{J}_{12} - \overline{R}_{12} & \overline{B}_1 \\ 0 & 0 & \overline{J}_{21} - \overline{R}_{21} & \overline{J}_{22} - \overline{R}_{22} & \overline{B}_2 \\ 0 & 0 & -\overline{B}_1^\top & -\overline{B}_2^\top & 0 \end{bmatrix} \begin{bmatrix} -\frac{1}{h}(x_1^{n+1} - x_1^n) \\ -\frac{1}{h}(x_2^{n+1} - x_2^n) \\ f_1^{n,n+1} \\ f_2^{n,n+1} \\ u^{n,n+1} \end{bmatrix} = 0, \tag{5.30}$$

where the arguments (x^n, x^{n+1}) have been omitted for simplicity. In particular, the first equation of (5.30) yields

$$\overline{E}_{11}(x^n, x^{n+1})^\top f_1^{n,n+1} = \overline{\nabla}\mathcal{H}_1(x^n, x^{n+1}),$$

thus it is equivalent to the equation (5.20c), up to replacing $f_1^{n,n+1}$ with $z_1^{n,n+1}$. Then, since the second equation of (5.30) is trivial, we can remove it. Finally, by replacing $f_2^{n,n+1}$ with $\overline{z}_2(x^n, x^{n+1})$ due to the stated constraint, we get exactly (5.20). □

In summary, Corollary 5.30 and Theorem 5.31 demonstrate that the concrete time discretization scheme for semi-explicit pH DAEs provided in Section 5.4.2 may be regarded as a special case of the discrete gradient-pair approach from Section 5.4.1 and of the DDR method discussed in Section 5.4.3.

By employing system transformations, one can further investigate when it is possible to reformulate general pH DAEs as semi-explicit pH DAEs. This is done in Section 5 of the original work [A3] and is omitted here to match the overall focus of this thesis. We subsequently highlight the applicability of our proposed approach to a mechanical problem class.

5.5. Application to multibody system dynamics

Let us consider the example of nonlinear and constrained multibody systems (see Example 5.22). We discuss the modeling as a semi-explicit pH DAE in Section 5.5.1, showcase the application of a discrete gradient method in Section 5.5.2 and present a numerical experiment in Section 5.5.3.

5.5.1. Modeling multibody systems as semi-explicit port-Hamiltonian DAEs

The class of nonlinear multibody systems with redundant coordinates $q \in \mathscr{C}(\mathbb{T}, \mathscr{Q})$ fits well into the semi-explicit framework (5.15). More details on the derivations of the following equations may be found for example in the textbook [110, Chapter 1]. The configuration space $\mathscr{Q}$ is typically a differential manifold, but it can also be regarded as an open subset of $\mathbb{R}^d$ up to switching to local coordinates, where the dimension d of $\mathscr{Q}$ determines the number of coordinates. Correspondingly, admissible velocities $v = \dot{q}$ are elements of the tangent space $T_q\mathscr{Q}$ defined through the presence of holonomic constraints $g \in \mathscr{C}^1(\mathscr{Q}, \mathbb{R}^m)$, and can be reinterpreted in local coordinates as vectors in $\mathbb{R}^d$. Since

$$g\big(q(t)\big) = 0 \tag{5.31}$$

gives rise to the kinematic (i.e. velocity level) constraints (sometimes in the MBS community referred to as *hidden constraints*), admissible velocities need to satisfy

$$\mathrm{D}g\big(q(t)\big)v(t) = 0. \tag{5.32}$$

These constraints are enforced by means of Lagrange multipliers $\lambda \in \mathscr{C}(\mathbb{T}, \mathbb{R}^m)$, which now represent the purely algebraic states, i.e., $x_2 = \lambda$. Correspondingly, with $x_1 = (q, v)$ one defines the non-quadratic Hamiltonian as

$$\mathcal{H}(x) = \mathcal{H}_1(x_1) = \frac{1}{2}v^\top M v + V(q), \tag{5.33}$$

where the first term represents the kinetic energy with the symmetric and positive-definite mass matrix $M \in \mathbb{R}^{d\times d}$ and $V \in \mathscr{C}(\mathscr{Q}, \mathbb{R})$ denotes an arbitrary potential energy. The emanating potential forces are derived by taking the partial derivative with respect to the coordinates, i.e., $F_\mathrm{p} = \nabla V(q)$.

Additionally, we consider velocity-dependent viscous dissipation governed by the Rayleigh dissipation function $G(\boldsymbol{q},\boldsymbol{v}) = \frac{1}{2}\boldsymbol{v}^\top \boldsymbol{R}_\mathrm{R}(\boldsymbol{q})\boldsymbol{v}$, where $\boldsymbol{R}_\mathrm{R}(\boldsymbol{q}) \in \mathscr{C}(\mathscr{Q}, \mathbb{R}^{d\times d})$ is a symmetric and positive semi-definite dissipation matrix. The non-potential forces appearing in the balance of linear momentum are obtained through differentiation, i.e., $\boldsymbol{F}_\mathrm{np}(\boldsymbol{q},\boldsymbol{v}) = -\nabla_{\boldsymbol{v}} G(\boldsymbol{q},\boldsymbol{v}) = -\boldsymbol{R}_\mathrm{R}(\boldsymbol{q})\boldsymbol{v}$. This eventually yields the equations of motion as index-2 DAEs given by

$$\dot{\boldsymbol{q}} = \boldsymbol{v}, \tag{5.34a}$$

$$\boldsymbol{M}\dot{\boldsymbol{v}} = -\nabla V(\boldsymbol{q}) - \boldsymbol{R}_\mathrm{R}(\boldsymbol{q})\boldsymbol{v} - \mathrm{D}\boldsymbol{g}(\boldsymbol{q})^\top \boldsymbol{\lambda} + \boldsymbol{u}, \tag{5.34b}$$

$$\boldsymbol{0} = \mathrm{D}\boldsymbol{g}(\boldsymbol{q})\boldsymbol{v}, \tag{5.34c}$$

where $\boldsymbol{u}$ represents external input loads. These equations can be brought into the semi-explicit pH DAE representation (5.15) by rewriting them as

$$\begin{bmatrix} \boldsymbol{I} & 0 & 0 \\ 0 & \boldsymbol{M} & 0 \\ 0 & 0 & \boldsymbol{0} \end{bmatrix} \begin{bmatrix} \dot{\boldsymbol{q}} \\ \dot{\boldsymbol{v}} \\ \dot{\boldsymbol{\lambda}} \end{bmatrix} = \left(\begin{bmatrix} 0 & \boldsymbol{I} & 0 \\ -\boldsymbol{I} & -\boldsymbol{R}_\mathrm{R}(\boldsymbol{q}) & -\mathrm{D}\boldsymbol{g}(\boldsymbol{q})^\top \\ 0 & \mathrm{D}\boldsymbol{g}(\boldsymbol{q}) & 0 \end{bmatrix} \right) \begin{bmatrix} \nabla V(\boldsymbol{q}) \\ \boldsymbol{v} \\ \boldsymbol{\lambda} \end{bmatrix} + \begin{bmatrix} 0 \\ \boldsymbol{I} \\ 0 \end{bmatrix} \boldsymbol{u}, \tag{5.35a}$$

$$\boldsymbol{y} = \begin{bmatrix} 0 & \boldsymbol{I} & 0 \end{bmatrix} \begin{bmatrix} \nabla V(\boldsymbol{q}) \\ \boldsymbol{v} \\ \boldsymbol{\lambda} \end{bmatrix}. \tag{5.35b}$$

The verification that $\boldsymbol{E}^\top \boldsymbol{z}(\boldsymbol{x}) = \nabla \mathcal{H}(\boldsymbol{x})$ holds true is straightforward. Moreover, the system output collocated with the input forces coincides with the velocity, i.e., $\boldsymbol{y} = \boldsymbol{v}$.

Note that the pH formulation of the multibody system dynamics is characterized by explicitly accounting for the hidden velocity constraints (5.32) instead of the constraints on position level (5.31). Care has to be taken when it comes to the numerical discretization in order to avoid the violation of the constraints on position level during simulations (*drift-off*).

A related formulation can also be found in Example 2.8 in Chapter 2 of the present work. Notably, the formulation considered here can be seen as a special case of more general pH multibody models, as discussed in [B6, Section 3].

5.5.2. Structure-preserving time integration of multibody systems

For the time discretization of (5.35a), we propose the application of the semi-explicit discrete gradient method (5.20) with additional specifications, leading to the discrete time mapping

$$\begin{bmatrix} \boldsymbol{I} & 0 & 0 \\ 0 & \boldsymbol{M} & 0 \\ 0 & 0 & \boldsymbol{0} \end{bmatrix} \begin{bmatrix} \boldsymbol{q}^{n+1} - \boldsymbol{q}^n \\ \boldsymbol{v}^{n+1} - \boldsymbol{v}^n \\ \boldsymbol{\lambda}^{n+1} - \boldsymbol{\lambda}^n \end{bmatrix} = h \begin{bmatrix} 0 & \boldsymbol{I} & 0 \\ -\boldsymbol{I} & -\boldsymbol{R}_\mathrm{R}(\boldsymbol{q}^{n+1/2}) & -\overline{\mathrm{D}}\boldsymbol{g}(\boldsymbol{q}^n, \boldsymbol{q}^{n+1})^\top \\ 0 & \overline{\mathrm{D}}\boldsymbol{g}(\boldsymbol{q}^n, \boldsymbol{q}^{n+1}) & 0 \end{bmatrix} \begin{bmatrix} \boldsymbol{z}_{1,\boldsymbol{q}}^{n,n+1} \\ \boldsymbol{z}_{1,\boldsymbol{v}}^{n,n+1} \\ \boldsymbol{\lambda}^{n,n+1} \end{bmatrix} + h \begin{bmatrix} 0 \\ \boldsymbol{I} \\ 0 \end{bmatrix} \boldsymbol{u}^{n,n+1}, \tag{5.36a}$$

$$\begin{bmatrix} \boldsymbol{z}_{1,\boldsymbol{q}}^{n,n+1} \\ \boldsymbol{z}_{1,\boldsymbol{v}}^{n,n+1} \end{bmatrix} = \begin{bmatrix} \boldsymbol{I} & 0 \\ 0 & \boldsymbol{M} \end{bmatrix}^{-\top} \overline{\nabla} \mathcal{H}_1(\boldsymbol{x}_1^n, \boldsymbol{x}_1^{n+1}), \tag{5.36b}$$

$$\boldsymbol{y}^{n,n+1} = \boldsymbol{z}_{1,\boldsymbol{v}}^{n,n+1}, \tag{5.36c}$$

where $\boldsymbol{q}^{n+1/2} = \frac{1}{2}(\boldsymbol{q}^n + \boldsymbol{q}^{n+1})$ is the midpoint evaluation of the coordinates, and $\overline{\mathrm{D}}\boldsymbol{g}$ is a discrete Jacobian for $\boldsymbol{g}$. Here we discretized the Rayleigh dissipation term using the implicit midpoint rule, but we emphasize that any other consistent approximation which preserves the positive semi-definiteness of $\boldsymbol{R}_\mathrm{R}$ would be suitable as well. For the multipliers we make the choice $\boldsymbol{\lambda}^{n,n+1} := \boldsymbol{\lambda}^{n+1}$ such that no appropriate initialization for $\boldsymbol{\lambda}^0$ is required.

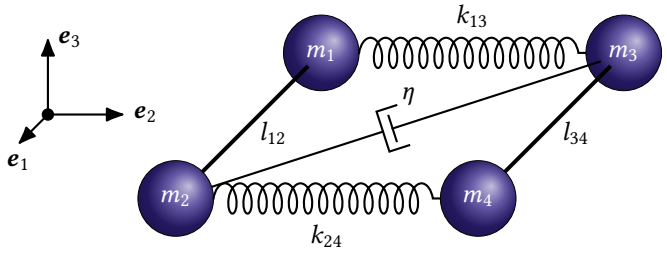

Figure 5.1.: Four-particle system.

As already mentioned, one might wonder about the drift-off effect. Since we approximate $\mathrm{D}\boldsymbol{g}$ with a discrete Jacobian, combining the first and third row of (5.36a) yields

$$\boldsymbol{g}(\boldsymbol{q}^{n+1}) - \boldsymbol{g}(\boldsymbol{q}^n) = \overline{\mathrm{D}}\boldsymbol{g}(\boldsymbol{q}^n, \boldsymbol{q}^{n+1})(\boldsymbol{q}^{n+1} - \boldsymbol{q}^n) = h\overline{\mathrm{D}}\boldsymbol{g}(\boldsymbol{q}^n, \boldsymbol{q}^{n+1})\boldsymbol{z}_{1,\boldsymbol{v}}^{n,n+1} = \boldsymbol{0}, \tag{5.37}$$

and therefore the drift-off vanishes, as long as the initial condition satisfies $\boldsymbol{g}(\boldsymbol{q}^0) = \boldsymbol{0}$. Thus, this scheme not only yields energy consistency in terms of Theorem 5.26, but also prevents the drift-off effect.

Remark 5.32. *The choice of using a discrete Jacobian to approximate* $\mathrm{D}\boldsymbol{g}$ *in general only guarantees that the velocity constraint* (5.32) *itself is satisfied approximately. For an energy-consistent multibody system integrator, which captures constraints both on position and on velocity level exactly, the interested reader is referred to [B3, Section 5].* ♧

Remark 5.33. *For lossless systems, one might be additionally interested in preserving momentum maps, like the angular momentum. This can be achieved by using* G-equivariant *discrete gradients, see [87, Section 3.7].* ♧

5.5.3. Numerical example

Let us now focus on a specific problem from the literature to highlight the applicability of our approach and discuss its performance.

5.5.3.1. Problem description

The four-particle system depicted in Figure 5.1 has been adapted from the literature [90, B3] and extended to include dissipation. The configuration of the system is characterized by the coordinate vector $\boldsymbol{q} = (\boldsymbol{q}_1, \boldsymbol{q}_2, \boldsymbol{q}_3, \boldsymbol{q}_4) \in \mathbb{R}^{12}$ comprising the Cartesian coordinates of four masses m_i, $i = 1, ..., 4$ in three dimensions. Two nonlinear springs give rise to the potential function

$$V(\boldsymbol{q}) = \frac{1}{2}k_{13}\left(\|\boldsymbol{q}_3 - \boldsymbol{q}_1\|^2 - 1\right)^2 + \frac{1}{2}k_{24}\left(\|\boldsymbol{q}_4 - \boldsymbol{q}_2\|^2 - 1\right)^2, \tag{5.38}$$

with the spring stiffness parameters k_{13} and k_{24}. The mass matrix is block diagonal, i.e., $\boldsymbol{M} = \mathrm{diag}\{m_1\boldsymbol{I}, m_2\boldsymbol{I}, m_3\boldsymbol{I}, m_4\boldsymbol{I}\}$. Additionally, we consider configuration-dependent viscous dissipation in terms of the Rayleigh dissipation function

$$G(\boldsymbol{q}, \boldsymbol{v}) = \frac{1}{2}\eta(\boldsymbol{q})v_{\mathrm{rel}}^2, \qquad v_{\mathrm{rel}} = \|\boldsymbol{v}_3 - \boldsymbol{v}_2\|, \tag{5.39}$$

Table 5.1.: Four-particle system: Simulation parameters.

h	t_{end}	$\varepsilon_{\text{Newton}}$	$\{k_{13}, k_{24}\}$	m_i	η_0	α
0.01	10	10^{-10}	$\{50, 500\}$	$\{1, 3, 2.3, 1.7\}$	1	0.5

where $\eta(\boldsymbol{q}) = \eta_0(1 + \alpha q_{\text{rel}}^2) \geq 0$ is the dynamic viscosity parameter and $q_{\text{rel}} = \|\boldsymbol{q}_3 - \boldsymbol{q}_2\|$. We have also introduced $\eta_0 > 0$ and $\alpha > 0$ as constant parameters. This leads to the dissipation matrix

$$\boldsymbol{R}_{\text{R}}(\boldsymbol{q}) = \eta(\boldsymbol{q}) \begin{bmatrix} 0 & 0 & 0 & 0 \\ 0 & \boldsymbol{I} & -\boldsymbol{I} & 0 \\ 0 & -\boldsymbol{I} & \boldsymbol{I} & 0 \\ 0 & 0 & 0 & 0 \end{bmatrix}. \tag{5.40}$$

There are two rigid bars connecting two masses, respectively, leading to the constraints on position level given by

$$g_1(\boldsymbol{q}) = \frac{1}{2}\left(\|\boldsymbol{q}_2 - \boldsymbol{q}_1\|^2 - 1\right) = 0, \qquad g_2(\boldsymbol{q}) = \frac{1}{2}\left(\|\boldsymbol{q}_4 - \boldsymbol{q}_3\|^2 - 1\right) = 0. \tag{5.41}$$

In the numerical simulations the initial conditions

$$\begin{aligned} \boldsymbol{q}_1^0 &= \begin{bmatrix} 0 & 0 & 0 \end{bmatrix}^\top, \ \boldsymbol{q}_2^0 = \begin{bmatrix} 1 & 0 & 0 \end{bmatrix}^\top, \ \boldsymbol{q}_3^0 = \begin{bmatrix} 0 & 1 & 0 \end{bmatrix}^\top, \ \boldsymbol{q}_4^0 = \begin{bmatrix} 1 & 1 & 0 \end{bmatrix}^\top, \\ \boldsymbol{v}_1^0 &= \begin{bmatrix} 0 & 0 & 0 \end{bmatrix}^\top, \ \boldsymbol{v}_2^0 = \begin{bmatrix} 0 & 0 & 0 \end{bmatrix}^\top, \ \boldsymbol{v}_3^0 = \begin{bmatrix} 0 & 0 & 0 \end{bmatrix}^\top, \ \boldsymbol{v}_4^0 = \begin{bmatrix} 0 & 0 & \frac{20}{17} \end{bmatrix}^\top, \end{aligned} \tag{5.42}$$

have been chosen consistently with the constraints (5.41) and their velocity level counterparts induced by (5.32).

5.5.3.2. Methods

The simulations have been conducted using our discrete gradient scheme for semi-explicit systems (5.20). Results obtained with this scheme are labeled “DG” . The equations have been solved in each time step using Newton’s method with a tolerance of $\varepsilon_{\text{Newton}}$. For the discrete gradients and Jacobians, we use the Gonzalez discrete gradient (5.12). Since the constraints (5.41) are quadratic, the application of the Gonzalez discrete Jacobian boils down to a midpoint evaluation. In this example we assume zero inputs.

The integration methods as well as the definition of the system have been implemented in the openly available Python package `pydykit`, which can be found at `https://github.com/pydykit/pydykit` and is archived under [F2]. The generated data along with the source code for the simulations are openly available for verification purposes in the repository `https://github.com/plkinon/phdae_discrete_gradients` and are archived at [126].

5.5.3.3. Results & Discussion

We simulate the four-particle system using the parameters comprised in Table 5.1. On the left part of Figure 5.2 one can observe the discrete evolution of the Hamiltonian in time. The exact representation of the power balance in discrete time (see (5.36) and Theorem 5.26) is demonstrated in the central part

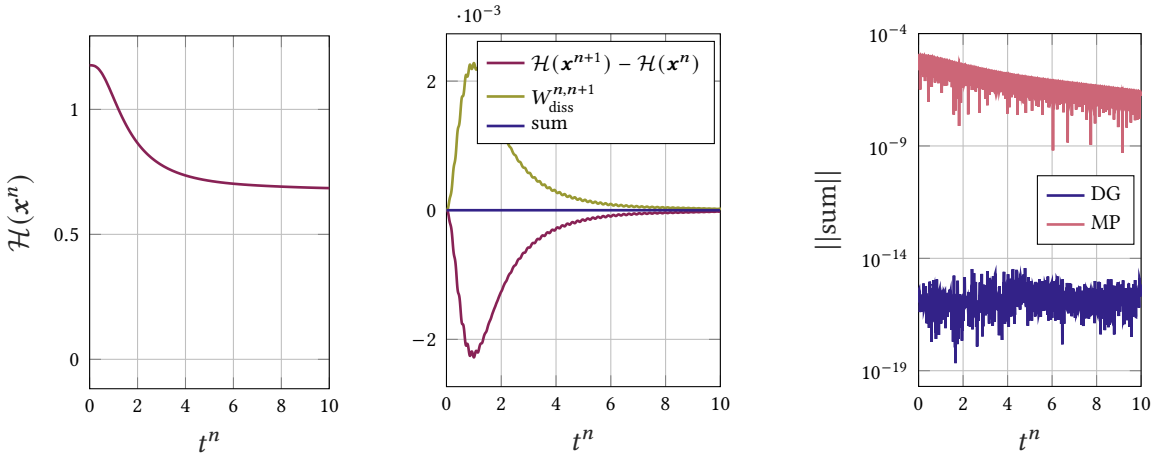

Figure 5.2.: Four-particle system: Hamiltonian evolution (left), discrete-time increments (center) and comparison with midpoint approach (right). "DG"denotes our approach and "MP"is the midpoint scheme.

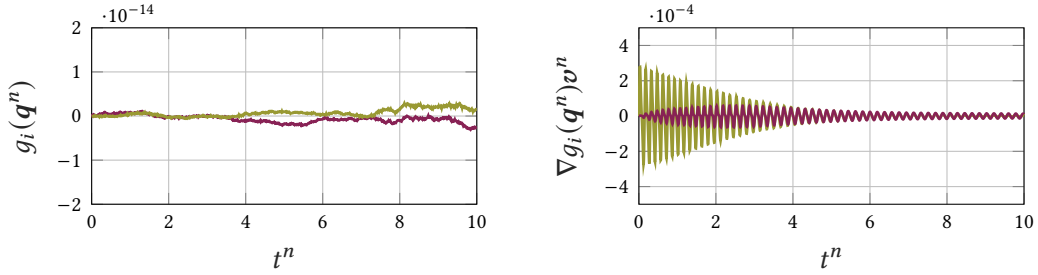

Figure 5.3.: Four-particle system: Constraints on position level (left) and on velocity level (right); — $i = 1$, — $i = 2$.

of Figure 5.2, since the Hamiltonian increments are always less or equal to zero and the dissipated work in each time step

$$W_{\text{diss}}^{n,n+1} := h \begin{bmatrix} z_1^{n,n+1} \\ \overline{z}_2(x^n, x^{n+1}) \end{bmatrix}^\top \overline{R}(x^n, x^{n+1}) \begin{bmatrix} z_1^{n,n+1} \\ \overline{z}_2(x^n, x^{n+1}) \end{bmatrix} = h z_{1,v}^{n,n+1\top} R_{\text{R}}(q^{n+1/2}) z_{1,v}^{n,n+1} \geq 0 \tag{5.43}$$

is equally large. The sum of the two terms is numerically zero. For comparison, a pure midpoint-based scheme (labeled "MP") does not achieve energy-consistency, as depicted on the right part of Figure 5.2.

On the left side of Figure 5.3 one can observe that the scheme under investigation does not suffer from drift-off, i.e., it accurately captures the constraints on position level (5.41), as expected from (5.37). On the right side of the same figure, the kinematic constraint is shown to have order of magnitude of 10^{-4} for each discrete point in time, due to the intermediate approximation of (5.32), as discussed in Remark 5.32. Next, we switch off viscous dissipation by setting $\eta_0 = 0$ in the dissipation law. The discrete-time energy conservation in the non-dissipative case is verified in Figure 5.4.

We have also performed a numerical convergence analysis (see Figure 5.5, left side) using the relative error measure

$$e_x = \frac{||x_{\text{ref}} - x||}{||x_{\text{ref}}||},$$

where $x \in \{q_4^n, v_4^n, \lambda_1^{n,n+1}\}$ are the solutions evaluated at $t^n = 0.1$ for different time step sizes and methods. The respective reference solution x_{ref} was obtained using our DG method with $h = 10^{-4}$. The scheme exhibits second order accuracy for the differential unknowns of position and velocity and approximately a first order convergence behavior in the Lagrange multiplier. It should be noted that the order of convergence can be affected by the discretization method used for the equation coefficients. The compared midpoint scheme MP yields similar convergence results.

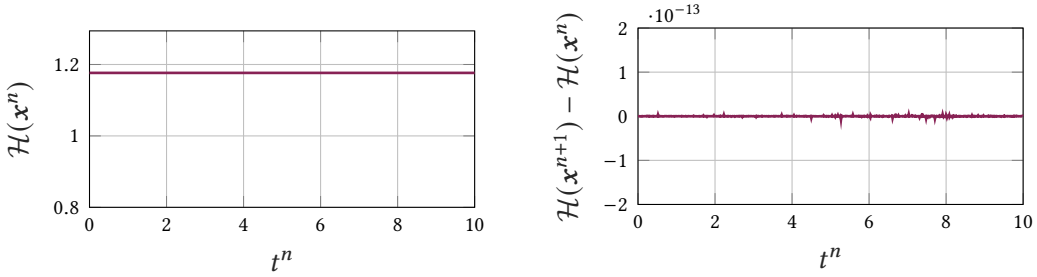

Figure 5.4.: Four-particle system: Hamiltonian evolution (left) and discrete-time increments (right) without dissipation, i.e., $\eta_0 = 0$.

Lastly, we investigated the numerical robustness of the proposed DG scheme compared to the MP scheme when choosing larger time step sizes. Both methods did not converge with time step sizes of 0.4 or larger. However, our DG method provided physically meaningful results up until $h = 0.25$, showing a qualitatively similar behavior as with the previous simulation (see Figure 5.5, right side). Contrarily to that, MP exhibits occasional total energy increase, thus violating the dissipativity of the system. This is in accordance with literature showing that discrete gradient methods are relatively robust compared to the midpoint rule in the nonlinear regime [89, B3].

5.6. Conclusion and outlook

In this work, we introduced discrete gradient methods for port-Hamiltonian differential-algebraic equations (pH DAEs), addressing the challenges associated with state-dependent and non-invertible descriptor matrices. We developed a promising time integration method for semi-explicit systems, discussed more general pH DAEs, and explored a method based on an alternative representation of pH DAEs. Additionally, we outlined conditions for constructing discrete gradient pairs for general pH DAEs, analyzed state transformations and the equivalence of different methods. In particular we proved that, under appropriate regularity assumptions, every pH DAE can be reinterpreted as the combination of a parametrized semi-explicit pH DAE and an unstructured DAE on the time-varying parameter. Lastly, we applied the proposed framework to the important application case of nonlinear multibody system dynamics, providing convincing simulation results.

Future research could focus on refining the conditions needed to apply discrete gradients to general pH DAEs, improving the numerical efficiency and accuracy. It will be of major interest to apply our

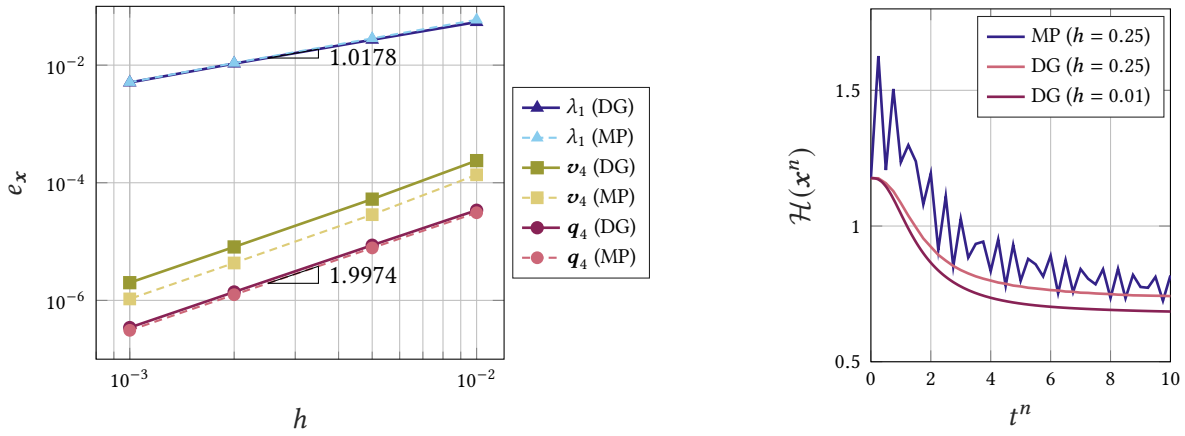

Figure 5.5.: Four-particle system: h-convergence (left) and robustness comparison with larger h (right).

framework to large-scale and multiphysics systems, as their modeling is seamlessly possible in the pH framework. Moreover, a rigorous convergence analysis of the time discretization schemes presented in this paper should be pursued in the future.

6. Generalized Maxwell viscoelasticity for geometrically exact strings: Nonlinear port-Hamiltonian formulation and structure-preserving discretization

This chapter is based on:*
Kinon PL, Thoma T, Betsch P, and Kotyczka P. "Generalized Maxwell viscoelasticity for geometrically exact strings: Nonlinear port-Hamiltonian formulation and structure-preserving discretization". In: *IFAC-PapersOnLine*, 58(6): 101–106, 2024. DOI: 10.1016/j.ifacol.2024.08.264

Abstract: This contribution proposes a nonlinear and dissipative infinite-dimensional port-Hamiltonian (pH) model for the dynamics of geometrically exact strings. The mechanical model provides a description of large deformations including finite elastic and inelastic strains in a generalized Maxwell model. It is shown that the overall system results from a power-preserving interconnection of pH subsystems. By using a structure-preserving mixed finite element approach, a finite-dimensional pH model is derived. Eventually, midpoint discrete gradients are employed to deduce an energy-consistent time-stepping method, which inherits discrete-time dissipativity for the irreversible system. An example simulation illustrates the numerical properties of the present approach.

Keywords: Nonlinear port-Hamiltonian systems • Generalized Maxwell model • Structure-preserving discretization • Mixed finite elements • Discrete gradients.

6.1. Introduction

The class of port-Hamiltonian (pH) systems has become increasingly important across multiple research fields dealing with modeling and control of complex dynamical systems, see e.g. [63]. A major benefit of the pH representation is the explicit formulation of power interfaces, so-called ports, which allows for an intrinsically energy-consistent interconnection, thus facilitating the modular composition of subsystems. Since many technical systems are modeled by partial differential equations, the theory of infinite-dimensional pH systems has been extended in recent years, see [183] for a review. Among various physical disciplines, pH formulations have also been proposed for mechanics.

The structural elements of strings are particularly interesting and are widely used in control and modeling of multibody systems [C2, 215]. Strings can be found in a large variety of systems such as cranes, cable robots or satellite systems. Accordingly, they are interconnected with their environment, which can be described beneficially in the pH framework. So far, works on geometrically exact strings have been restricted to purely elastic materials: linear elasticity in [218] and nonlinear elasticity in [C2]. However, modeling inelastic processes plays a crucial role for the realistic simulation of mechanical

systems [204]. Many works from structural and multibody dynamics deal with the Kelvin-Voigt model (e.g. [144]), which is not able to reproduce the relaxation test. Recently, more advanced models (such as the generalized Maxwell model) are investigated [22].

In this contribution, we make use of an infinite-dimensional, nonlinear and dissipative pH model related to [161, 247]. We thus extend the existing description of geometrically exact strings to viscoelasticity, introduce the (distributed) generalized Maxwell model to the pH context and explore the model's advantages concerning pH interconnection. With respect to the numerical discretization, the mixed finite element method has been employed to establish an approximate model under preservation of the pH structure, see [54], retaining the ports with their causality on the discrete level. Lastly, we propose an energy-consistent time discretization extending the one in [C4]. It is based on the midpoint discrete gradient due to [87] and can be related to the *discrete gradient pairs* by [201]. The resulting scheme inherits the dissipativity property of the underlying continuous model.

6.2. Infinite-dimensional model

In this section, we derive a model for geometrically exact strings, with a new extension to viscoelastic material using a generalized Maxwell model. After briefly recalling the purely hyperelastic model from [C2], we present a pH formulation of the parallel connection of distributed viscoelastic branches according to the generalized Maxwell model. Eventually, a power-preserving interconnection of both systems yields the final model.

6.2.1. Purely hyperelastic model

We consider a one-dimensional undeformed (material) string configuration $\Omega_0 \subset \mathbb{R}^d$ of length $L > 0$ and its current (spatial) configuration $\Omega_t \subset \mathbb{R}^d$, where $d \in \{1, 2, 3\}$ is the spatial dimension. Correspondingly, the position vector $\boldsymbol{r} : \Omega \times \mathbb{T} \to \Omega_t$ is introduced, depending on the material arc-length coordinate $s \in \Omega = [0, L]$ and on time $t \in \mathbb{T} = [0, t_{\text{end}}]$, where $t_{\text{end}} > 0$. See Figure 6.1 for an illustration. The balance of linear momentum

$$\rho A \ddot{\boldsymbol{r}}(s,t) = \partial_s \boldsymbol{n}(s,t) + \boldsymbol{b} + \boldsymbol{f}(s,t) \tag{6.1}$$

includes the constant mass density $\rho \in \mathbb{R}_{\geq 0}$, cross-section area $A \in \mathbb{R}_{\geq 0}$, constant body forces per unit length $\boldsymbol{b} \in \mathbb{R}^d$, and distributed input forces per unit length $\boldsymbol{f} \in \mathbb{R}^d$. For more details, the reader is referred to [10]. Further kinematic assumptions for arriving at the balance of linear momentum (6.1) are well summarized in [218]. The temporal partial derivative of a any function $\square$ is denoted $\dot{\square} := \partial_t \square$. Moreover, the contact force $\boldsymbol{n}(s,t) : \Omega \times \mathbb{T} \to \mathbb{R}^d$ has tangential direction, i.e.,

$$\boldsymbol{n}(s,t) = S(s,t) \partial_s \boldsymbol{r}(s,t), \tag{6.2}$$

where the stress-type quantity $S : \Omega \times \mathbb{T} \to \mathbb{R}$ has been introduced. More details on that regard are contained in Appendix 6.C.1 or in [C2]. We now drop both spatial and temporal arguments for the sake of brevity and only use them where the explicit mention is helpful. In similarity to (6.2), we assume that the distributed input forces are restricted to purely tangential contributions

$$\boldsymbol{f} = 2\partial_s \left(\frac{1}{2} S_u \partial_s \boldsymbol{r} \right) \tag{6.3}$$

with $S_u(s,t)$ the stress-type input. For the kinematic description we consider the scalar strain measure

$$C = \partial_s \boldsymbol{r}^\top \partial_s \boldsymbol{r}, \tag{6.4}$$

where $C = 1$ corresponds to a state without elongation. This quantity can be interpreted in analogy to the right Cauchy–Green strain tensor from elasticity [C2]. Accordingly, the conjugated stress quantity (in analogy to the second Piola–Kirchhoff stress tensor) can be obtained via (6.6). More details on that regard are contained in Appendix 6.C.1 or in [C2]. For the nonlinear elastic constitutive modeling with finite strains, a non-quadratic strain energy density function

$$W(C) = \frac{EA}{4}(C - \ln(C) - 1), \tag{6.5}$$

with $E > 0$, the constant axial stiffness parameter, is considered and is bounded from below by $W(1) = 0$. See Appendix 6.C.1 or [C2] for a model with linear stress-strain relation due to St. Venant–Kirchhoff. The axial stress is derived via differentiation as

$$S := 2\frac{\mathrm{d}W}{\mathrm{d}C} = 2W'(C). \tag{6.6}$$

The total energy of a geometrically exact string is described in terms of the state vector

$$\boldsymbol{x}_1 = (\boldsymbol{r}, \boldsymbol{v}, C) \in \mathbb{R}^{2d+1} \tag{6.7}$$

by its Hamiltonian (2.72), which in the present case is given by

$$\mathcal{H}_1(\boldsymbol{x}_1) = \int_0^L \left(\frac{\rho A}{2} \boldsymbol{v}^\top \boldsymbol{v} + W(C) - \boldsymbol{r}^\top \boldsymbol{b} \right) \mathrm{d}s. \tag{6.8}$$

It represents the sum of kinetic energy and potential energy. Correspondingly, the variational derivatives yield

$$\delta_{\boldsymbol{x}_1} \mathcal{H}_1 = (-\boldsymbol{b}, \rho A \boldsymbol{v}, W'(C)) \in \mathbb{R}^{2d+1}. \tag{6.9}$$

See (2.73) for the definition of the variational derivative.

Taking the balance of linear momentum (6.1), the kinematic relation $\dot{\boldsymbol{r}} = \boldsymbol{v}$, and the strain rate derived from (6.4), the state differential equations represent an infinite-dimensional version of the formulation by [161]

$$\begin{aligned} \mathcal{E}_1 \partial_t \boldsymbol{x}_1 &= \mathcal{J}_1(\boldsymbol{x}_1) \boldsymbol{z}_1(\boldsymbol{x}_1) + \mathcal{B}_\Omega(\boldsymbol{x}_1) u_1 \,, \qquad \text{where} \qquad \mathcal{E}_1^\top \boldsymbol{z}_1(\boldsymbol{x}_1) = \delta_{\boldsymbol{x}_1} \mathcal{H}_1 \,, \\ y_1 &= \mathcal{B}_\Omega^*(\boldsymbol{x}_1) \boldsymbol{z}_1(\boldsymbol{x}_1) \,, \end{aligned} \tag{6.10}$$

see also [247] for a recent linear operator-theoretic approach. A detailed definition of infinite-dimensional port-Hamiltonian descriptor systems is given in Definition 2.19 contained in Chapter 2 of this work. Note that (6.10) is specified by $\mathcal{E}_1 = \operatorname{diag}(\boldsymbol{I}, \rho A \boldsymbol{I}, 1)$, $\boldsymbol{z}_1(\boldsymbol{x}_1) = (-\boldsymbol{b}, \boldsymbol{v}, \frac{1}{2}S)$, the formally skew-adjoint ($\mathcal{J}_1 = -\mathcal{J}_1^*$) matrix differential operator

$$\mathcal{J}_1(\boldsymbol{x}_1) = \begin{bmatrix} 0 & \boldsymbol{I} & 0 \\ -\boldsymbol{I} & 0 & 2\partial_s(\square \partial_s \boldsymbol{r}) \\ 0 & 2\partial_s \boldsymbol{r}^\top \partial_s \square & 0 \end{bmatrix}, \tag{6.11}$$

which has a similar state-dependent structure as the one in [48] for von Kármán beams, and

$$\mathcal{B}_\Omega(\boldsymbol{x}_1) = \begin{bmatrix} 0 \\ 2\partial_s(\square \partial_s \boldsymbol{r}) \\ 0 \end{bmatrix}, \quad \mathcal{B}_\Omega^*(\boldsymbol{x}_1) = \begin{bmatrix} 0 & -2\partial_s \boldsymbol{r}^\top \partial_s \square & 0 \end{bmatrix}. \tag{6.12}$$

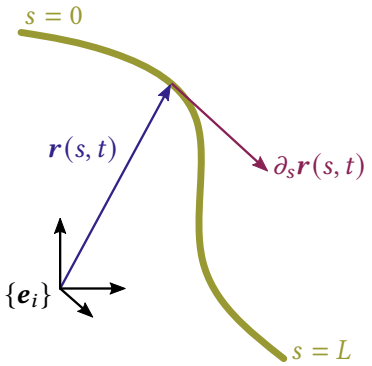

Figure 6.1.: Spatial string configuration. Reproduced with permission from [A1].

See [C2] for details without the distributed port, and the Appendices of this chapter for two related formulations. In Appendix 6.A the description of inextensible strings yielding partial DAEs is covered and Appendix 6.B proposes a representation in an extended state space, with a "standard" canonical differential operator, known from systems of two conservation laws. Additionally, the reader may consult Section 2.4, in which the geometrically exact string model serves as a running example.

Lastly, the power balance is shown as

$$\begin{aligned}\dot{\mathcal{H}}_1 = \left(\delta_{\boldsymbol{x}_1}\mathcal{H}_1, \partial_t \boldsymbol{x}_1\right)_\Omega = \left(z_1(\boldsymbol{x}_1), \mathcal{E}_1 \partial_t \boldsymbol{x}_1\right)_\Omega &= \left(z_1(\boldsymbol{x}_1), \mathcal{J}_1 z_1(\boldsymbol{x}_1)\right)_\Omega + \left(z_1(\boldsymbol{x}_1), \mathcal{B}_\Omega u_1\right)_\Omega, \\ &= \boldsymbol{u}_\partial^\top \boldsymbol{y}_\partial + (u_1, y_1)_\Omega\end{aligned} \tag{6.13}$$

in order to complete the pH system representation. Therein, we have used integration by parts along with (6.10) and (6.12). Furthermore, the boundary port $(\boldsymbol{u}_\partial, \boldsymbol{y}_\partial)$ has been defined due to pure Neumann boundary conditions (BCs) with

$$\boldsymbol{u}_\partial(t) = \begin{bmatrix} -\boldsymbol{n}_{\mathrm{N},0}(t) \\ \boldsymbol{n}_{\mathrm{N},L}(t) \end{bmatrix}, \quad \boldsymbol{y}_\partial(t) = \begin{bmatrix} \boldsymbol{v}(0,t) \\ \boldsymbol{v}(L,t) \end{bmatrix}, \tag{6.14}$$

where $\boldsymbol{n}_{\mathrm{N},0}(t)$ and $\boldsymbol{n}_{\mathrm{N},L}(t)$ are prescribed values for the total contact force $\boldsymbol{n}_{\mathrm{tot}} = S_{\mathrm{tot}} \partial_s \boldsymbol{r}$, with $S_{\mathrm{tot}} := S + S_u$, at the respective boundary points. The collocated distributed input-output pair in (6.13) is $(u_1, y_1) = (\frac{1}{2} S_u, -\dot{C})$, which have the dimension of a stress and strain-rate, respectively.

6.2.2. Distributed generalized Maxwell viscoelasticity

We now introduce viscoelastic material behavior. Particularly, we assume an *internal variable model*: the generalized Maxwell model with the rheological model from Figure 6.2, which consists of an elastic element and m viscous Maxwell elements in parallel. It is also referred to as *generalized relaxation model*, see [204, Chapter 10]. In this context, each additional branch introduces new material parameters, allowing for a more precise modeling of the time-dependent material behavior. Due to the model's structure, the total strain in each branch is equal to the overall total strain C_{tot}. Correspondingly, C_{tot} is also the strain in the purely elastic branch, which corresponds to the undamped string model with strain C from (6.4).

In each viscous branch, the elastic strain C_i^{el} and the inelastic strain α_i must add to the total strain $C_{\mathrm{tot}}(s)$,

$$C_i^{\mathrm{el}}(s) + \alpha_i(s) = C_{\mathrm{tot}}(s), \quad i = 1, \ldots, m, \tag{6.15}$$

or, in terms of the strain rates,

$$\dot{C}_i^{\mathrm{el}}(s) + \dot{\alpha}_i(s) = \dot{C}_{\mathrm{tot}}(s), \quad i = 1, \dots, m. \tag{6.16}$$

The parallel interconnection implies the addition of the stresses of each viscoelastic branch as

$$S_{\mathrm{v}}(s) = \sum_{i=1}^{m} S_i(s), \tag{6.17}$$

which adds with the stress in the purely elastic branch to $S_{\mathrm{tot}}(s) = S_{\mathrm{v}}(s) + S(s)$. Moreover, at each (distributed) dashpot element, inelastic strains and stresses are related by the constitutive relation

$$\dot{\alpha}_i(s) = \frac{1}{\eta_i A} S_i(s), \tag{6.18}$$

where $\eta_i > 0$ is the dynamic viscosity assigned to this branch. The stresses (which are equal in a branch), are obtained similar to (6.6) from a constitutive relation defined by $S_i := 2\tilde{W}_i'(C_i^{\mathrm{el}})$. Choosing a suitable hyperelastic energy density $\tilde{W}_i(C_i^{\mathrm{el}})$ as in (6.5), a stiffness parameter E_i is assigned to every elastic element[1]. The dissipation functional (see [204]) for the generalized Maxwell model is defined here as

$$P_R := \int_0^L \sum_{i=1}^{m} \frac{1}{2\eta_i A} S_i^2(s)\, \mathrm{d}s. \tag{6.19}$$

With the total energy

$$\mathcal{H}_2(\boldsymbol{x}_2) = \int_0^L \sum_{i=1}^{m} \tilde{W}_i(C_i^{\mathrm{el}})\, \mathrm{d}s, \quad \boldsymbol{x}_2 = (C_1^{\mathrm{el}}, \dots, C_m^{\mathrm{el}}) \in \mathbb{R}^m, \tag{6.20}$$

and the variational derivatives

$$\delta_{\boldsymbol{x}_2} \mathcal{H}_2 = (\tilde{W}_1'(C_1^{\mathrm{el}}), \dots, \tilde{W}_m'(C_m^{\mathrm{el}})) \tag{6.21}$$

the above equations can be combined to obtain the dynamics of the m viscoelastic Maxwell branches in purely dissipative pH form[2]

$$\begin{aligned} &\partial_t \boldsymbol{x}_2 = -\mathcal{R}_2 \boldsymbol{z}_2(\boldsymbol{x}_2) + \mathbf{1}\dot{C}_{\mathrm{tot}}, \qquad \text{where} \qquad \boldsymbol{z}_2(\boldsymbol{x}_2) = \delta_{\boldsymbol{x}_2} \mathcal{H}_2 \\ &\frac{1}{2} S_{\mathrm{v}} = \mathbf{1}^\top \boldsymbol{z}_2(\boldsymbol{x}_2), \end{aligned} \tag{6.22}$$

with $\boldsymbol{z}_2(\boldsymbol{x}_2) = (\frac{1}{2}S_1, \dots, \frac{1}{2}S_m)$, $\mathcal{R}_2 = \mathrm{diag}(\frac{2}{\eta_1 A}, \dots, \frac{2}{\eta_m A})$, $\mathbf{1} = (1, \dots, 1)$ and the distributed input-output pair $(u_2, y_2) = (\dot{C}_{\mathrm{tot}}, \frac{1}{2}S_{\mathrm{v}})$. Eventually, the dissipation inequality

$$\dot{\mathcal{H}}_2 = -P_R + (u_2, y_2)_\Omega \leq (u_2, y_2)_\Omega \tag{6.23}$$

is induced, using (6.19) as well as $P_R = (\boldsymbol{z}_2(\boldsymbol{x}_2), \mathcal{R}_2 \boldsymbol{z}_2(\boldsymbol{x}_2))_\Omega$.[3]

[1] To obtain consistency with a purely elastic string model with axial stiffness $\overline{EA}$, it is required that $EA + \sum_i^m E_i A = \overline{EA}$.

[2] A more standard approach in computational viscoelasticity defines the state via the inelastic strains α_i and would yield a slightly different pH model.

[3] With initial conditions $\boldsymbol{x}_2(0)$ and the distributed input $\dot{C}_{\mathrm{tot}}(s)$ acting on the complete domain Ω, no additional BCs need to be specified. This is in accordance with (6.23), which comes without boundary terms. This is clear from the $\mathcal{R}_2$ being constant.

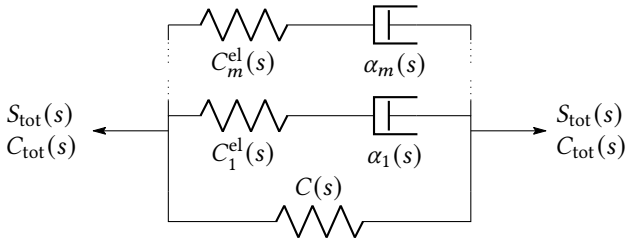

Figure 6.2.: Generalized Maxwell model. Reproduced with permission from [A1].

6.2.3. Interconnection and viscoelastic string model

According to the aforementioned model (see Figure 6.2), we interconnect the purely elastic model and the m viscoelastic Maxwell branches via the conditions $S_u = S_{\mathrm{v}}$, $\dot{C} = \dot{C}_{\mathrm{tot}}$, i.e., the total stress of the viscoelastic elements acts as distributed stress input to the purely elastic string, while kinematic continuity of the strains is given. In terms of the above-defined (u_1, y_1) and (u_2, y_2), this reads

$$\begin{bmatrix} u_1 \\ u_2 \end{bmatrix} = \begin{bmatrix} 0 & 1 \\ -1 & 0 \end{bmatrix} \begin{bmatrix} y_1 \\ y_2 \end{bmatrix}, \tag{6.24}$$

i.e., a standard power-preserving (gyrator) interconnection of two passive systems.

Theorem 6.1. *By combining the pH models* (6.10), (6.22) *with* (6.24), *the boundary controlled pH model of the geometrically exact string with generalized Maxwell viscoelasticity and imposed Neumann BCs is given by*

$$\mathcal{E}\partial_t \boldsymbol{x} = (\mathcal{J}(\boldsymbol{x}) - \mathcal{R})\boldsymbol{z}(\boldsymbol{x}), \qquad \mathcal{E}^\top \boldsymbol{z}(\boldsymbol{x}) = \delta_{\boldsymbol{x}} \mathcal{H}(\boldsymbol{x}), \tag{6.25}$$

with $\mathcal{E} = \mathrm{diag}(\mathcal{E}_1, \boldsymbol{I})$, *states* $\boldsymbol{x}_1 = (\boldsymbol{x}_1, \boldsymbol{x}_2) \in \mathbb{R}^{2d+1+m}$, *costates* $\boldsymbol{z}(\boldsymbol{x}) = (\boldsymbol{z}_1(\boldsymbol{x}_1), \boldsymbol{z}_2(\boldsymbol{x}_2)) \in \mathbb{R}^{2d+1+m}$ *and boundary port* $(\boldsymbol{u}_\partial, \boldsymbol{y}_\partial)$ *according to* (6.14), *as well as consistent initial conditions. The formally skew-adjoint system operator and the dissipation matrix are*

$$\mathcal{J}(\boldsymbol{x}) = \begin{bmatrix} 0 & \boldsymbol{I} & 0 & \cdots & 0 \\ -\boldsymbol{I} & 0 & 2\partial_s(\square\, \partial_s \boldsymbol{r}) & \cdots & 2\partial_s(\square\, \partial_s \boldsymbol{r}) \\ 0 & 2\partial_s \boldsymbol{r}^\top \partial_s \square & 0 & & 0 \\ & \vdots & & & \\ 0 & 2\partial_s \boldsymbol{r}^\top \partial_s \square & 0 & & 0 \end{bmatrix}. \tag{6.26}$$

and $\mathcal{R} = \mathrm{diag}(\boldsymbol{0}, \mathcal{R}_2)$. *The Hamiltonian is the sum of* (6.8) *and* (6.20),

$$\mathcal{H}(\boldsymbol{x}) = \mathcal{H}_1(\boldsymbol{x}_1) + \mathcal{H}_2(\boldsymbol{x}_2), \tag{6.27}$$

and satisfies the power balance

$$\dot{\mathcal{H}} = \boldsymbol{u}_\partial^\top \boldsymbol{y}_\partial - P_R \leq \boldsymbol{u}_\partial^\top \boldsymbol{y}_\partial, \tag{6.28}$$

with the non-negative dissipation functional, being identical with (6.19) *taking part in* (6.23), *such that*

$$P_R = (\boldsymbol{z}(\boldsymbol{x}), \mathcal{R}\boldsymbol{z}(\boldsymbol{x}))_\Omega \geq 0. \tag{6.29}$$

Proof. The form of the operators follows from direct substitution. The pH structure, with formal skew-adjointness of $\mathcal{J}$, see Definition 2.16, is a direct consequence of the power-conserving interconnection, just as the power balance, which follows from adding (6.13) and (6.23). □

6.3. Structure-preserving discretization

6.3.1. Discretization in space

A mixed finite element approach yields a semi-discrete state space model that fits again into the pH framework. To this end, the weak form pertaining to (6.25) is deduced using standard procedures as

$$(\delta \boldsymbol{b}, \dot{\boldsymbol{r}} - \boldsymbol{v})_\Omega = 0, \tag{6.30a}$$

$$(\delta \boldsymbol{v}, \rho A \dot{\boldsymbol{v}} - \boldsymbol{b})_\Omega + (\partial_s(\delta \boldsymbol{v}), S_{\mathrm{tot}} \partial_s \boldsymbol{r})_\Omega - \left[\delta \boldsymbol{v}^\top \boldsymbol{n}_{\mathrm{N}}\right]_{\partial\Omega} = 0, \tag{6.30b}$$

$$\left(\delta S, \dot{C} - 2\partial_s \boldsymbol{r}^\top \partial_s \boldsymbol{v}\right)_\Omega = 0, \tag{6.30c}$$

$$\left(\delta S_i, \dot{C}_i^{\mathrm{el}} - 2\partial_s \boldsymbol{r}^\top \partial_s \boldsymbol{v} + \frac{1}{\eta_i A} S_i\right)_\Omega = 0, \tag{6.30d}$$

for arbitrary test functions $\delta\boldsymbol{b}, \delta\boldsymbol{v}, \delta S$ and δS_i from appropriate spaces and $i = 1, \ldots, m$. Note that constitutive weak forms corresponding to $\mathcal{E}^\top \boldsymbol{z}(\boldsymbol{x}) = \delta_{\boldsymbol{x}} \mathcal{H}(\boldsymbol{x})$ given by

$$(\delta C, S - 2W'(C))_\Omega = 0, \tag{6.30e}$$

$$\left(\delta C_i^{\mathrm{el}}, S_i - 2\tilde{W}_i'(C_i^{\mathrm{el}})\right)_\Omega = 0, \tag{6.30f}$$

for $i = 1, \ldots, m$ with appropriate δC, δC_i^{el}, are appended to close the set of equations.

Now, the string domain is divided into n_{el} finite elements and we approximate $\boldsymbol{r}$,$\boldsymbol{v}$,$\boldsymbol{b}$ via C^0-continuous, linear Lagrangian shape functions and C, S, C_i^{el}, S_i via elementwise constant, discontinuous ansatz functions. The procedure is analogous to the ones outlined in Chapters 3 and 4. The reader can find more details on that regard in Appendix 6.C.2 or in [C2]. Considering a Bubnov Galerkin approach, the corresponding test functions are restricted to the same ansatz spaces. This yields

$$\tfrac{\mathrm{d}}{\mathrm{d}t}\hat{\boldsymbol{r}} = \hat{\boldsymbol{v}}, \tag{6.31a}$$

$$\boldsymbol{M}_\rho \tfrac{\mathrm{d}}{\mathrm{d}t}\hat{\boldsymbol{v}} = \boldsymbol{M}\hat{\boldsymbol{b}} - \boldsymbol{K}(\hat{\boldsymbol{r}})\hat{\boldsymbol{S}} - \sum_{i=1}^{m} \boldsymbol{K}(\hat{\boldsymbol{r}})\hat{\boldsymbol{S}}_i + \boldsymbol{B}_\partial \hat{\boldsymbol{u}}_\partial, \tag{6.31b}$$

$$\boldsymbol{M}_S \tfrac{\mathrm{d}}{\mathrm{d}t}\hat{\boldsymbol{C}} = 2\boldsymbol{K}(\hat{\boldsymbol{r}})^\top \hat{\boldsymbol{v}}, \tag{6.31c}$$

$$\boldsymbol{M}_S \tfrac{\mathrm{d}}{\mathrm{d}t}\hat{\boldsymbol{C}}_i^{\mathrm{el}} = 2\boldsymbol{K}(\hat{\boldsymbol{r}})^\top \hat{\boldsymbol{v}} - \frac{1}{\eta_i A}\boldsymbol{M}_S \hat{\boldsymbol{S}}_i, \tag{6.31d}$$

$$\boldsymbol{M}_S \frac{1}{2}\hat{\boldsymbol{S}} = \nabla \hat{W}(\hat{\boldsymbol{C}}), \tag{6.31e}$$

$$\boldsymbol{M}_S \frac{1}{2}\hat{\boldsymbol{S}}_i = \nabla \hat{\tilde{W}}_i(\hat{\boldsymbol{C}}_i^{\mathrm{el}}), \tag{6.31f}$$

for $i = 1, \ldots, m$, as semi-discrete equations of motion where $\hat{\square}$ indicates nodal values. More details on the formal expressions of the corresponding matrices and vectors are given in (6.62) in Appendix 6.C.2. There, also the derivation of the discrete constitutive equations (6.31e) and (6.31f) is outlined in more detail. These relations can be used to express the unknowns for the stress resultants in terms of unknowns for the strains, e.g., $\hat{\boldsymbol{S}} = \hat{\boldsymbol{S}}(\hat{\boldsymbol{C}})$. The discrete version of the Hamiltonian

$$\hat{\mathcal{H}}(\hat{\boldsymbol{x}}) = \frac{1}{2}\hat{\boldsymbol{v}}^\top \boldsymbol{M}_\rho \hat{\boldsymbol{v}} - \hat{\boldsymbol{r}}^\top \boldsymbol{M}\hat{\boldsymbol{b}} + \hat{W}(\hat{\boldsymbol{C}}) + \sum_{i=1}^{m} \hat{\tilde{W}}_i(\hat{\boldsymbol{C}}_i^{\mathrm{el}}) \tag{6.32}$$

with the states of the finite-dimensional model

$$\hat{\boldsymbol{x}} = (\hat{\boldsymbol{r}}, \hat{\boldsymbol{v}}, \hat{\boldsymbol{C}}, \hat{\boldsymbol{C}}_1^{\mathrm{el}}, \ldots, \hat{\boldsymbol{C}}_m^{\mathrm{el}}) \tag{6.33}$$

results from approximating (6.20) using the above ansatz functions. The discrete Hamiltonian $\hat{\mathcal{H}}$ gives rise to the partial derivatives

$$\nabla_{\hat{\boldsymbol{r}}}\hat{\mathcal{H}} = -\boldsymbol{M}\hat{\boldsymbol{b}}, \qquad \nabla_{\hat{\boldsymbol{v}}}\hat{\mathcal{H}} = \boldsymbol{M}_\rho\hat{\boldsymbol{v}}, \qquad \nabla_{\hat{\boldsymbol{C}}}\hat{\mathcal{H}} = \nabla\hat{W}(\hat{\boldsymbol{C}}), \qquad \nabla_{\hat{\boldsymbol{C}}_i^{\mathrm{el}}}\hat{\mathcal{H}} = \nabla\hat{\tilde{W}}_i(\hat{\boldsymbol{C}}_i^{\mathrm{el}}). \tag{6.34}$$

We are now able to rewrite equations (6.31) as finite-dimensional pH system. Similar to (6.25), we obtain

$$\begin{aligned} \boldsymbol{E}\tfrac{\mathrm{d}}{\mathrm{d}t}\hat{\boldsymbol{x}} &= \big(\boldsymbol{J}(\hat{\boldsymbol{x}}) - \boldsymbol{R}\big)\hat{\boldsymbol{z}}(\hat{\boldsymbol{x}}) + \boldsymbol{B}\hat{\boldsymbol{u}}, \\ \hat{\boldsymbol{y}} &= \boldsymbol{B}^\top\hat{\boldsymbol{z}}(\hat{\boldsymbol{x}}), \end{aligned} \qquad \text{and} \qquad \boldsymbol{E}^\top\hat{\boldsymbol{z}}(\hat{\boldsymbol{x}}) = \nabla\hat{\mathcal{H}}(\hat{\boldsymbol{x}}), \tag{6.35}$$

in which $\boldsymbol{J}(\hat{\boldsymbol{x}})^\top = -\boldsymbol{J}(\hat{\boldsymbol{x}})$ for all $\hat{\boldsymbol{x}}$, and $\boldsymbol{R} = \boldsymbol{R}^\top \succeq 0$. This formulations fits into Definition 2.7 of pH descriptor systems. Consult Section 2.3 for a more detailed discussion. In particular, for the present problem we have

$$\boldsymbol{J}(\hat{\boldsymbol{x}}) = \begin{bmatrix} 0 & \boldsymbol{I} & 0 & & 0 \\ -\boldsymbol{I} & 0 & -2\boldsymbol{K}(\hat{\boldsymbol{x}}) & \cdots & -2\boldsymbol{K}(\hat{\boldsymbol{x}}) \\ 0 & 2\boldsymbol{K}(\hat{\boldsymbol{x}})^\top & 0 & & 0 \\ & \vdots & & & \\ 0 & 2\boldsymbol{K}(\hat{\boldsymbol{x}})^\top & 0 & & 0 \end{bmatrix} \qquad \begin{aligned} \hat{\boldsymbol{z}}(\hat{\boldsymbol{x}}) &= (-\boldsymbol{M}\hat{\boldsymbol{b}}, \hat{\boldsymbol{v}}, \tfrac{1}{2}\hat{\boldsymbol{S}}, \tfrac{1}{2}\hat{\boldsymbol{S}}_1, \ldots, \tfrac{1}{2}\hat{\boldsymbol{S}}_m), \\ \boldsymbol{R} &= \operatorname{diag}(\boldsymbol{0}, \boldsymbol{0}, \boldsymbol{0}, \frac{2}{\eta_1 A}\boldsymbol{M}_S, \ldots, \frac{2}{\eta_m A}\boldsymbol{M}_S), \\ \boldsymbol{E} &= \operatorname{diag}(\boldsymbol{I}, \boldsymbol{M}_\rho, \boldsymbol{M}_S, \boldsymbol{M}_S, \ldots, \boldsymbol{M}_S), \\ \boldsymbol{B}\hat{\boldsymbol{u}} &= \boldsymbol{B}_\partial\hat{\boldsymbol{u}}_\partial. \end{aligned} \tag{6.36}$$

Note that $\boldsymbol{E}^\top = \boldsymbol{E}$. In analogy to (6.19) and (6.29), the non-negative dissipated power is

$$\hat{P}_R = \hat{\boldsymbol{z}}^\top\boldsymbol{R}\hat{\boldsymbol{z}} = \sum_{i=1}^{m} \frac{1}{2\eta_i A}\hat{\boldsymbol{S}}_i^\top\boldsymbol{M}_S\hat{\boldsymbol{S}}_i \geq 0. \tag{6.37}$$

Correspondingly, the discrete power balance

$$\frac{\mathrm{d}}{\mathrm{d}t}\hat{\mathcal{H}}(\hat{\boldsymbol{x}}) = \nabla\hat{\mathcal{H}}(\hat{\boldsymbol{x}})^\top\frac{\mathrm{d}}{\mathrm{d}t}\hat{\boldsymbol{x}} = \hat{\boldsymbol{z}}^\top\boldsymbol{E}\frac{\mathrm{d}}{\mathrm{d}t}\hat{\boldsymbol{x}} = -\hat{\boldsymbol{z}}^\top\boldsymbol{R}\hat{\boldsymbol{z}} + \hat{\boldsymbol{u}}^\top\hat{\boldsymbol{y}} \leq \hat{\boldsymbol{u}}^\top\hat{\boldsymbol{y}} \tag{6.38}$$

expresses the passivity and dissipativity of the finite-dimensional model, which includes energy conservation for vanishing inputs and $\boldsymbol{R} = \boldsymbol{0}$.

6.3.2. Discretization in time

Now, a suitable time discretization is applied to obtain a structure-preserving scheme, which extends the one in [C4]. Consider a pH system of the general form (6.35) and let $\hat{\boldsymbol{x}}^n \approx \hat{\boldsymbol{x}}(t^n)$ at time $t^n = nh$ with constant time step sizes $h = t^{n+1} - t^n$. We propose an implicit one-step scheme given by

$$\begin{aligned} \boldsymbol{E}\left(\hat{\boldsymbol{x}}^{n+1} - \hat{\boldsymbol{x}}^n\right) &= h(\bar{\boldsymbol{J}} - \boldsymbol{R})\bar{\boldsymbol{z}} + h\,\boldsymbol{B}\bar{\boldsymbol{u}}, \\ \bar{\boldsymbol{y}} &= \boldsymbol{B}^\top\bar{\boldsymbol{z}}, \end{aligned} \tag{6.39}$$

and

$$\boldsymbol{E}^\top\bar{\boldsymbol{z}} = \overline{\nabla}\hat{\mathcal{H}}(\hat{\boldsymbol{x}}^n, \hat{\boldsymbol{x}}^{n+1}), \tag{6.40}$$

where the solution via Newton's method is required in each time step. $\overline{\nabla}\hat{\mathcal{H}}(\hat{\boldsymbol{x}}^n, \hat{\boldsymbol{x}}^{n+1})$ is a midpoint discrete gradient in the sense of [87]. It is a second order perturbation to the midpoint evaluation of the analytical gradient and satisfies directionality and consistency, i.e.,

$$\overline{\nabla}\hat{\mathcal{H}}(\hat{\boldsymbol{x}}^n, \hat{\boldsymbol{x}}^{n+1})^\top \left(\hat{\boldsymbol{x}}^{n+1} - \hat{\boldsymbol{x}}^n\right) = \hat{\mathcal{H}}(\hat{\boldsymbol{x}}^{n+1}) - \hat{\mathcal{H}}(\hat{\boldsymbol{x}}^n), \tag{6.41}$$

$$\overline{\nabla}\hat{\mathcal{H}}(\hat{\boldsymbol{x}}^n, \hat{\boldsymbol{x}}^n) = \nabla\hat{\mathcal{H}}(\hat{\boldsymbol{x}}^n), \tag{6.42}$$

for arbitrary $\hat{\boldsymbol{x}}^n, \hat{\boldsymbol{x}}^{n+1}$. Further explanations on discrete gradient methods can be found in Chapter 5. For the system at hand, the discrete gradient can be designed analogously to [C2], see also Appendix 6.C.3. Using (6.41) and performing similar manipulations as in (6.38) we obtain the discrete-time power balance

$$\hat{\mathcal{H}}(\hat{\boldsymbol{x}}^{n+1}) - \hat{\mathcal{H}}(\hat{\boldsymbol{x}}^n) = h\,\bar{\boldsymbol{u}}^\top\bar{\boldsymbol{y}} - h\bar{D} \leq h\,\bar{\boldsymbol{u}}^\top\bar{\boldsymbol{y}}, \tag{6.43}$$

with the non-negative discrete-time dissipation function

$$\bar{P}_R = \bar{\boldsymbol{z}}^\top \boldsymbol{R}\bar{\boldsymbol{z}} \geq 0, \tag{6.44}$$

showing that the proposed integrator exhibits discrete-time passivity and dissipativity (including energy-conservation for $\bar{\boldsymbol{u}} = \boldsymbol{0}$, $\boldsymbol{R} = \boldsymbol{0}$). Discrete gradient methods are known for desirable robustness and stability properties.

Remark 6.2. *These properties hold regardless of the specific choices for the matrix- and vector-evaluations. As in [C4], we choose* $\bar{\boldsymbol{J}} = \boldsymbol{J}(\hat{\boldsymbol{x}}^{n+1/2})$ *based on* $\hat{\boldsymbol{x}}^{n+1/2} = \frac{1}{2}(\hat{\boldsymbol{x}}^{n+1} + \hat{\boldsymbol{x}}^n)$*, as well as* $\bar{\boldsymbol{u}} = \hat{\boldsymbol{u}}(t^{n+1/2})$ *such that* $\bar{\boldsymbol{y}} \approx \hat{\boldsymbol{y}}(t^{n+1/2})$*, to obtain a symmetric method.* ♧

Remark 6.3. *Our method falls into the definition of a* discrete gradient pair *[201, Section on 4] with*

$$\bar{\boldsymbol{E}} = \boldsymbol{E}, \qquad \bar{\boldsymbol{z}}(\hat{\boldsymbol{x}}^n, \hat{\boldsymbol{x}}^{n+1}) = \boldsymbol{E}^{-\top}\overline{\nabla}\hat{\mathcal{H}}(\hat{\boldsymbol{x}}^n, \hat{\boldsymbol{x}}^{n+1}), \tag{6.45}$$

satisfying the three conditions in [201]. This follows directly from the definition as well as (6.41) *and* (6.42)*. Despite using the midpoint discrete gradient, the proposed method differs from the* midpoint discrete gradient pair *in [201].* ♧

Additionally to the energetic consistency of the proposed scheme, also the kinematic relation (6.4) is exactly captured by the present method, i.e., $C_\mathrm{h}^n = (\partial_s \boldsymbol{r}_\mathrm{h}^n)^\top \partial_s \boldsymbol{r}_\mathrm{h}^n$ for all n. This requires starting with consistent initial conditions satisfying $C_\mathrm{h}^0 = (\partial_s \boldsymbol{r}_\mathrm{h}^0)^\top \partial_s \boldsymbol{r}_\mathrm{h}^0$.

6.4. Numerical example

We investigate the planar motion of a string made of rubber-like material ($E = 18400$, $\rho = 920$) with circular cross section (radius $r = 0.0186$). Without loss of generality, we consider the common *Zener model* (the one-dimensional *standard solid*, see [204]), which is the generalized Maxwell model with $m = 1$. For further parameters see Table 6.1.

It is discretized in space with $n_\mathrm{el} = 10$ finite elements and numerical quadrature of the integrals considered two Gauss points per element. Further parameters are shown in Table 6.1. Specifying the reference configuration Ω_0 by

$$\boldsymbol{r}_0(s) = s\begin{bmatrix}0\\-1\end{bmatrix}, \quad \boldsymbol{v}_0(s) = \boldsymbol{0}, \quad C_0(s) = 1, \tag{6.46}$$

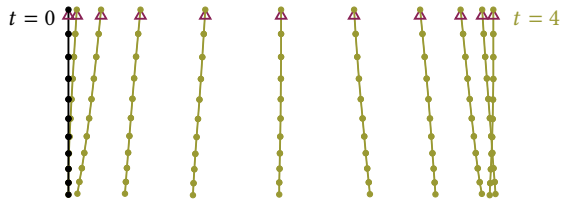

Figure 6.3.: Planar motion of a string: Initial configuration and snapshots. Reproduced with permission from [A1].

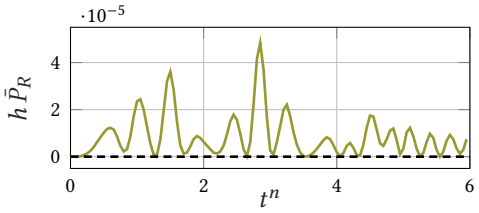

Figure 6.4.: Planar motion of a string: Discrete dissipated work $h\bar{P}_R$. Reproduced with permission from [A1].

we compute the static equilibrium in this vertical position determined by gravity $\boldsymbol{b} = -9.81\rho A\boldsymbol{e}_2$. To this end, the creeping process is simulated for a period of 10 s, where inertial forces are neglected. From this approximate steady state (marked in black in Figure 6.3), we perform the dynamics simulation, where Newton's method was used with a residual tolerance of $\varepsilon_{\text{Newton}} = 10^{-10}$. The finite element code `moofeKIT` has been used, see [78].

Considering mixed BCs[4]

$$\begin{aligned} &r_2(s=0,t) = 0, \quad v_2(s=0,t) = 0, \quad \forall t \\ &\boldsymbol{n}_{\text{N},0}(t) = \rho A \begin{bmatrix} 1 \\ 0 \end{bmatrix} \sin\left(\pi \frac{t}{2}\right), \qquad t \in [0,4], \end{aligned} \tag{6.47}$$

the homogeneous Dirichlet BCs are given by fixing the vertical component of the upper end of the string, and the non-homogeneous Neumann BC force acts at the upper end ($s = 0$) of the string during a loading phase in horizontal direction. Due to a free lower end, we consider homogeneous Neumann conditions at $s = L$. After $t = 4$, the system is closed. Snapshots of the motion are displayed in Figure 6.3 for $t \in \{0, 0.4, \ldots 3.6, 4\}$.

The dissipated work in each time step can be seen in Figure 6.4 and verifies (6.44). During the loading phase, the power-transmission through the boundaries can be observed in Figure 6.5. After the loading phase, our discrete gradient method (labeled "DG") captures the dissipativity down to a level of machine precision. Using the well-known implicit midpoint rule (labeled "MP") is not as accurate due to the nonlinear material (6.5). The difference between MP and DG is even more distinct for examples, which induce more elongation, see [C2].

[4] Here, homogeneous Dirichlet BCs are enforced directly into the ansatz functions. In general, enforcing non-homogeneous mixed BCs for pH systems requires further approaches, see [46].

Table 6.1.: Planar motion of a string: Simulation parameters. Reproduced with permission from [A1].

L	EA, E_1A	ρA	$\eta_1 A$	h	$\mathbb{T}$
1	10	1	0.4	$5 \cdot 10^{-2}$	$[0, 6]$

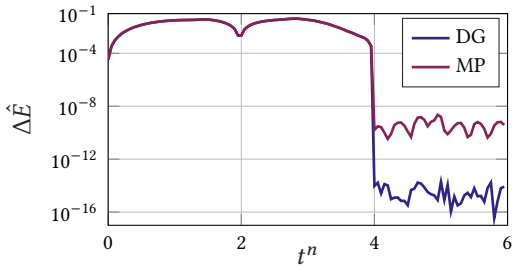

Figure 6.5.: Planar motion of a string: Discrete increments $\Delta\hat{E} := |\hat{\mathcal{H}}(\hat{\boldsymbol{x}}^{n+1}) - \hat{\mathcal{H}}(\hat{\boldsymbol{x}}^n) + h\bar{P}_R|$. Reproduced with permission from [A1].

6.5. Conclusion and outlook

In this work, we have proposed a new approach for the simulation of hyperelastic and viscously damped strings, which additionally enjoys a port-Hamiltonian structure. The infinite-dimensional model is nonlinear and dissipative and features boundary input/output ports. It could be shown that dissipation in the sense of a generalized Maxwell model can be provided via power-preserving pH connection of two subsystems. Subsequently, we have demonstrated advantageous properties of both spatial and temporal discretization techniques, which are structure-preserving: a mixed finite element approach in space, yielding a finite-dimensional pH state space model, and a discrete-gradient-based integrator in time, inheriting the passivity of the original system. Eventually, the behavior of the model could be showcased in an example simulation, demonstrating also the advantages with respect to a standard time discretization. Future research directions may investigate the usage of this model for control design as well as model order reduction.

Appendix to Chapter 6

6.A. Port-Hamiltonian PDAE case

By demanding the inextensibility constraint $C = 1$ for rigid strings or by time-differentiation $\partial_s \boldsymbol{r}^\top \partial_s \boldsymbol{v} = 0$, one obtains similarly the pH differential-algebraic equations (6.25) with Lagrange multipliers $\xi \in \mathbb{R}$. They represent the reaction stress enforcing inextensibility and take part in $\boldsymbol{z} = (-\boldsymbol{b}, \boldsymbol{v}, 1/2\xi)$. Moreover, $\mathcal{E} = \operatorname{diag}(\boldsymbol{I}, \rho A \boldsymbol{I}, 0)$ is singular, $\mathcal{R} = 0$ and $\delta_C \mathcal{H} = 0$. This model is equivalent to the one presented in [218] and can also be understood in the context of velocity-stress formulations, see Chapter 4 for a related formulation for the 3D geometrically exact beam. Consult Example 2.11 in the preliminary chapter of the present work to find a similar model of a finite-dimensional model problem.

6.B. Canonical case

An alternative pH representation for hyperelastic, geometrically exact strings can be obtained by choosing the states $\boldsymbol{x} = (\boldsymbol{p}, \boldsymbol{q}, \boldsymbol{r}) := (\rho A\dot{\boldsymbol{r}}, \partial_s \boldsymbol{r}, \boldsymbol{r})$ defining the Hamiltonian

$$\mathcal{H}(\boldsymbol{x}) = \int_\Omega \left(U(\boldsymbol{q}) - \boldsymbol{r}^\top \boldsymbol{b} + \frac{1}{2\rho A} \boldsymbol{p}^\top \boldsymbol{p} \right) \mathrm{d}s \tag{6.48}$$

with the stored energy density $U(\boldsymbol{q}) = W(\tilde{C}(\boldsymbol{q}))$, where $\tilde{C}(\boldsymbol{q}) = \boldsymbol{q}^\top \boldsymbol{q}$ is an expression of the kinematic relation (6.4) in terms of the state $\boldsymbol{q}$. The efforts are obtained as

$$\delta_{\boldsymbol{p}} \mathcal{H} = (\rho A)^{-1} \boldsymbol{p}, \quad \delta_{\boldsymbol{q}} \mathcal{H} = \nabla U(\boldsymbol{q}) =: \boldsymbol{n}(\boldsymbol{q}), \quad \delta_{\boldsymbol{r}} \mathcal{H} = -\boldsymbol{b}. \tag{6.49}$$

The second relation can be verified by chain rule

$$\nabla U(\boldsymbol{q}) = W'(C) \nabla \tilde{C}(\boldsymbol{q}) = S \partial_s \boldsymbol{r}. \tag{6.50}$$

Eventually, the state differential equations[5] are given by $\dot{\boldsymbol{x}} = \mathcal{J} \delta_{\boldsymbol{x}} \mathcal{H}$ with the formally skew-adjoint operator

$$\mathcal{J} = \begin{bmatrix} 0 & \partial_s \square & -\boldsymbol{I} \\ \partial_s \square & 0 & 0 \\ \boldsymbol{I} & 0 & 0 \end{bmatrix}. \tag{6.51}$$

6.C. Technical details

This section contains selected parts of [C2], which can be helpful to understand the background of Chapter 6, or the underlying work [A1]. In [C2] the nonlinear port-Hamiltonian model for geometrically exact strings with hyperelastic constitutive relations is proposed for the first time. It thus enhances the previous work [218] with respect to material nonlinearities and uses strain and stress measures inspired from nonlinear continuum mechanics. This formulation further requires a discrete gradient time discretization in order to achieve an energy-consistent discretization in time, which inherits the passivity property of the underlying continuous model. Details related to the structure-preserving discretization are provided here as well.

6.C.1. Details on the constitutive modeling

This subsection reproduces and slightly adapts [C2, Section 2.2]. As shown in [215] a stored energy density function for strings with hyperelastic material is given by

$$W_\nu(\nu) = \frac{EA}{4}(\nu^2 - 2\ln(\nu) - 1), \tag{6.52}$$

where the stretch $\nu = ||\partial_s \boldsymbol{r}|| = \sqrt{C}$ is used and EA denotes the constant axial stiffness. The energy density describes the stored energy per unit length due to elastic deformation. Consequently, the tension follows directly by differentiation, i.e.,

$$N(\nu) = W_\nu'(\nu). \tag{6.53}$$

[5] This model should also be deducible using an approach extending the work by [178] to nonquadratic Hamiltonians.

In the present work, however, the strain quantity (6.4) shall be used. Stating $W(C) = W_v(\tilde{v}(C))$, where $\tilde{v}(C) = \sqrt{C}$ is the stretch expressed in terms of the strain measure C, we obtain

$$W(C) = \frac{EA}{4}(C - 2\ln(\sqrt{C}) - 1) = \frac{EA}{4}(C - \ln(C) - 1). \tag{6.54}$$

This yields the stress

$$S = 2W'(C) = \frac{EA}{2}(1 - C^{-1}) = \frac{EA}{2C}(C - 1). \tag{6.55}$$

It is moreover crucial to find a relation between the tension N that appears in the general expression of the contact force [10, Equation 2.10b]

$$\boldsymbol{n}(s,t) = N(s,t)\frac{\partial_s \boldsymbol{r}(s,t)}{||\partial_s \boldsymbol{r}(s,t)||}, \tag{6.56}$$

and the corresponding stress S. To this end, relation (6.56) can be rewritten such that

$$\boldsymbol{n} = N(v)\frac{\partial_s \boldsymbol{r}}{||\partial_s \boldsymbol{r}||} = W_v'(v)\frac{\partial_s \boldsymbol{r}}{\sqrt{C}} = W'(C)\tilde{C}'(v)\frac{1}{\sqrt{C}}\partial_s \boldsymbol{r} = S\partial_s \boldsymbol{r}, \tag{6.57}$$

where $\tilde{C}(v) = v^2$ is the strain expressed in terms of the stretch v.

Remark 6.4 (Linear elasticity)**.** *The choice of a strain energy density function*

$$W = \breve{W}(C) = \frac{1}{2}EA(\sqrt{C} - 1)^2 = \frac{1}{2}EA\varepsilon^2, \tag{6.58}$$

with $\varepsilon := \sqrt{\partial_s \boldsymbol{r}^\top \partial_s \boldsymbol{r}} - 1 = \sqrt{C} - 1$, corresponds to the previous work [218]. Hence, the linear elastic case is covered by the present approach. ♧

Remark 6.5 (St. Venant–Kirchhoff material)**.** *A suitable representation of a linear stress-strain relation in the case of finite displacements (i.e., St. Venant–Kirchhoff material) is given by*

$$W = \tilde{W}(C) = \frac{1}{8}EA(C - 1)^2 \tag{6.59}$$

and thus the stress reads

$$S = 2\tilde{W}'(C) = \frac{1}{2}EA(C - 1). \tag{6.60}$$

The stored energy density function (6.59) *can be deduced by applying the 1D string kinematic assumptions to the 3D material law of St. Venant–Kirchhoff.* ♧

6.C.2. Details on the structure-preserving discretization in space

For the discretization in space we divide the string domain into n_{el} finite elements with respective domain Ω_e such that $\Omega = \cup_{e=1}^{n_{el}} \Omega_e$. Correspondingly, local ansatz functions are chosen and the isoparametric concept applies. In particular, we choose C^0-continuous, linear Lagrangian shape functions $\boldsymbol{\Phi}$ and elementwise constant, discontinuous ansatz functions $\boldsymbol{\Psi}$ such that the approximations are given by

$$\begin{aligned}
\boldsymbol{r}_\mathrm{h}(s,t) &= \boldsymbol{\Phi}(s)\hat{\boldsymbol{r}}(t), & \delta\boldsymbol{b}_\mathrm{h}(s) &= \boldsymbol{\Phi}(s)\delta\hat{\boldsymbol{b}}, & (C_i^\mathrm{el})_\mathrm{h}(s) &= \boldsymbol{\Psi}(s)\hat{\boldsymbol{C}}_i^\mathrm{el},\\
\boldsymbol{v}_\mathrm{h}(s,t) &= \boldsymbol{\Phi}(s)\hat{\boldsymbol{v}}(t), & \delta\boldsymbol{v}_\mathrm{h}(s) &= \boldsymbol{\Phi}(s)\delta\hat{\boldsymbol{v}}, & \delta(C_i^\mathrm{el})_\mathrm{h}(s) &= \boldsymbol{\Psi}(s)\delta\hat{\boldsymbol{C}}_i^\mathrm{el},\\
C_\mathrm{h}(s,t) &= \boldsymbol{\Psi}(s)\hat{\boldsymbol{C}}(t), & \delta C_\mathrm{h}(s) &= \boldsymbol{\Psi}(s)\delta\hat{\boldsymbol{C}}, & (S_i)_\mathrm{h}(s) &= \boldsymbol{\Psi}(s)\hat{\boldsymbol{S}}_i,\\
S_\mathrm{h}(s,t) &= \boldsymbol{\Psi}(s)\hat{\boldsymbol{S}}(t), & \delta S_\mathrm{h}(s) &= \boldsymbol{\Psi}(s)\delta\hat{\boldsymbol{S}}, & (\delta S_i)_\mathrm{h}(s) &= \boldsymbol{\Psi}(s)\delta\hat{\boldsymbol{S}}_i,
\end{aligned} \tag{6.61}$$

where $\hat{(\,)}$ are arrays containing the nodal vectors of the respective quantity. Inserting the approximations (6.61) into the weak form (6.30) yields the semi-discrete equations of motion (6.31) with the matrices

$$\boldsymbol{M}_\rho = \int_0^L \boldsymbol{\Phi}^\top \rho A \boldsymbol{\Phi}\, \mathrm{d}s, \quad \boldsymbol{M}_S = \int_0^L \boldsymbol{\Psi}^\top \boldsymbol{\Psi}\, \mathrm{d}s, \quad \boldsymbol{M} = \int_0^L \boldsymbol{\Phi}^\top \boldsymbol{\Phi}\, \mathrm{d}s, \quad \boldsymbol{K}(\hat{\boldsymbol{r}}) = \int_0^L \boldsymbol{\Phi}_{,s}^\top \boldsymbol{\Phi}_{,s} \hat{\boldsymbol{r}} \boldsymbol{\Psi}\, \mathrm{d}s. \tag{6.62}$$

The derivation of the discrete constitutive equations (6.31e) and (6.31f) requires some further explanations. To this end, consider the discrete Hamiltonian (6.32), where

$$\hat{W}(\hat{\boldsymbol{C}}) = \int_0^L W(C_\mathrm{h})\, \mathrm{d}s. \tag{6.63}$$

The derivative with respect to the discrete strain values makes use of the chain rule and reads

$$\nabla \hat{W}(\hat{\boldsymbol{C}}) = \int_0^L \boldsymbol{\Psi}^\top W'(C_\mathrm{h})\, \mathrm{d}s. \tag{6.64}$$

On the other hand, the discretization of the weak constitutive relation (6.30e) yields

$$\boldsymbol{M}_S \hat{\boldsymbol{S}} = \int_0^L \boldsymbol{\Psi}^\top 2W'(C_\mathrm{h})\, \mathrm{d}s. \tag{6.65}$$

By comparing the last two relations we obtain (6.31e), which can be interpreted as discrete version of the constitutive relation (6.6). The same procedure applies to the derivation of (6.31f).

6.C.3. Details on the structure-preserving discretization in time

The discrete gradient appearing in (6.40) needs to be specified in more detail. In particular, in view of the partial derivatives (6.34) and (6.64) we choose

$$\overline{\nabla} \hat{\mathcal{H}}(\hat{\boldsymbol{x}}^n, \hat{\boldsymbol{x}}^{n+1}) = \begin{bmatrix} \bar{\nabla}_{\hat{\boldsymbol{r}}} \hat{\mathcal{H}} \\ \bar{\nabla}_{\hat{\boldsymbol{v}}} \hat{\mathcal{H}} \\ \bar{\nabla}_{\hat{\boldsymbol{C}}} \hat{\mathcal{H}} \\ \bar{\nabla}_{\hat{\boldsymbol{C}}_i^\mathrm{el}} \hat{\mathcal{H}} \end{bmatrix} = \begin{bmatrix} -\boldsymbol{M}\hat{\boldsymbol{b}} \\ \boldsymbol{M}_\rho \hat{\boldsymbol{v}}^{n+1/2} \\ \int_0^L \boldsymbol{\Psi}^\top \frac{W(C_\mathrm{h}^{n+1}) - W(C_\mathrm{h}^n)}{C_\mathrm{h}^{n+1} - C_\mathrm{h}^n}\, \mathrm{d}s \\ \int_0^L \boldsymbol{\Psi}^\top \frac{\tilde{W}_i(C_\mathrm{h}^{n+1}) - \tilde{W}_i(C_\mathrm{h}^n)}{(C_i^\mathrm{el})_\mathrm{h}^{n+1} - (C_i^\mathrm{el})_\mathrm{h}^n}\, \mathrm{d}s \end{bmatrix}, \tag{6.66}$$

for the discrete gradient of the Hamiltonian, where the classical Greenspan's formula [93] has been applied. In the limit $C_\mathrm{h}^{n+1} \to C_\mathrm{h}^n$, the mid-point evaluation of the standard derivative is used. The design of this discrete gradient is completely analogous to the purely elastic case, see [C2]. It can be easily checked by a straightforward calculation that (6.66) does indeed satisfy the directionality property (6.41).

7. Conclusion

7.1. Summary

This thesis develops a unified, fully nonlinear port-Hamiltonian (pH) modeling framework for highly flexible slender structures, grounded in geometrically exact theories. To support their representation as constrained infinite-dimensional dynamical systems, a pH framework of sufficient generality is adopted (cf. **C 1**, Chapter 2). Within this setting, novel coordinate-based pH formulations are derived for geometrically exact planar beams, spatial beams, and strings. These formulations employ independent mixed field variables given by strains, stresses, or both, thereby enabling a flexible and systematic description of the underlying mechanics. Notably, the straightforward imposition of additional kinematic constraints is achieved through a compliance equation in time-differentiated form (cf. **C 2**–**C 4**, Chapters 3, 4 and 6). Moreover, the modeling framework is designed to accommodate hyperelastic and viscoelastic material behavior, as well as actuation mechanisms relevant in soft robotics (cf. **C 5**, Chapters 4 and 6).

Building on this modeling foundation, structure-preserving discretization techniques in space and time are developed, leveraging the unifying structure of the pH formalism. In particular, objective mixed FE methods are designed to retain the pH structure at the semi-discrete level, thereby naturally preventing locking (cf. **C 6**, Chapters 3, 4 and 6). With regard to the temporal discretization, midpoint-based integration schemes are proposed for systems with quadratic Hamiltonian (cf. **C 7**, Chapters 3 and 4), whereas discrete gradient methods are derived for general nonlinear pH ODE and DAE systems with non-quadratic Hamiltonian (cf. **C 8**, Chapters 5 and 6). Notably, these time integration schemes yield exact discrete-time representations of the power balance equation.

Together, these contributions demonstrate how the pH structure can be exploited to achieve energy-consistent simulations of geometrically and materially nonlinear slender structures in the context of flexible multibody dynamics. Hence, the identified research gaps and the emanating research aims, see Section 1.2, are fully addressed.

It is worth emphasizing that the proposed time integration methods are not tied to the specific mechanical models considered in this thesis but apply to the general classes of pH systems. This highlights a central advantage of the employed pH framework: any physical system formulated in this structure can directly benefit from the derived structure-preserving integration schemes. Conversely, the proposed pH models may also be discretized using alternative numerical methods developed for pH systems, underscoring the extensibility of the presented approach.

7.2. Outlook

The research presented in this thesis is subject to limitations, which have been discussed in Chapter 1 as well as in the individual chapters presenting the research papers (cf. Chapters 3 to 6). These limitations are primarily imposed by restricted temporal resources. Importantly, many of these limitations are

chosen deliberately to keep the modeling and analysis tractable and do not compromise the conceptual generality of the proposed pH formulations. Addressing them would primarily require additional modeling effort. This section outlines several promising avenues for future research that naturally build upon the results of this thesis.

A first natural extension concerns the treatment of finite rotations within the spatial geometrically exact beam models. While director-based formulations were used due to their favorable properties, future work could investigate manifold-consistent formulations based on (projected) unit quaternions [61, 101, 104, 133, 235]. In particular, quaternion-based formulations introduce state-dependent mass matrices and gyroscopic terms in the pH structure, which would require a careful reassessment of structure-preserving spatial and temporal discretization techniques. Understanding how these additional complexities affect energetic consistency at the discrete level remains an open and interesting question.

Another promising direction is the systematic exploitation of the interconnection properties of pH systems for modeling complex flexible multibody systems. While this thesis has focused on individual flexible elements, future work could address the modular interconnection of multiple pH subsystems — including flexible bodies, rigid bodies, joints, and actuators — to form more realistic multibody assemblies. Furthermore, there is still room for exploration of the pH modeling of rigid bodies [25, 77, 147, 153]. Moreover, the power-preserving interconnection paradigm may provide new insight into classical modeling notions such as ideal joints and kinematic pairs. A first step in this direction is taken in [B6], which introduces a director formulation for rigid bodies and investigates their consistent pH interconnection. The extension to flexible multibody systems, including the models developed in this thesis, is expected to apply directly.

Moreover, extending the modeling and discretization techniques developed in this thesis to geometrically exact shells [36, 185] or advanced FE formulations for continua [176, 206] would broaden the applicability of pH-based simulation methods even further. Particularly relevant application areas include nearly incompressible materials and dielectric elastomers, which have already attracted attention within the pH community [98, 191].

Another aspect deserving further attention is the treatment of boundary conditions. In this thesis, Dirichlet boundary conditions were implicitly enforced through the choice of function spaces. In practical applications, however, time-dependent boundary conditions are frequently required. While constrained formulations using Lagrange multipliers within the pH framework are well established [45, 218], explicit approaches based on boundary decomposition methods [46, 60, 217] have not been fully explored in the context of geometrically exact beams and flexible multibody systems. Incorporating such techniques could significantly improve computational efficiency, especially when combined with linearly implicit time integration schemes [47, 219].

Regarding the spatial discretization, this thesis exclusively employed Bubnov–Galerkin formulations, where test and trial functions are approximated with the same ansatz functions, which proved essential for preserving the pH structure at the discrete level. It would be worthwhile to investigate whether Petrov–Galerkin formulations can retain the same structure-preserving property. This could be especially relevant for formulations of spatial geometrically exact beams with redundant coordinates and minimal velocities [69, 102]. Moreover, questions related to alternative constraint treatments arise, e.g., using formulations based on Lagrangian subspaces [24, 25, 228]. Exploring whether the systems considered in this thesis can be reformulated in such settings, and how structure-preserving discretization can be achieved therein, remains a challenging research direction.

With regard to time integration, the discrete gradient methods developed in this thesis provide a robust foundation for energy-consistent simulation of nonlinear pH ODE and DAE systems. Nevertheless, there is considerable potential for extending pH-focused discrete gradient-schemes toward higher-order

accurate schemes while maintaining structure preservation [66, 168]. Alternatively, Galerkin-based time discretizations [8, 49, 65, 84, 159] represent an interesting option. A particularly challenging topic is the application of both families of methods to fully implicit pH DAEs.

Beyond these extensions, several emerging research directions appear particularly promising. Partitioned pH formulations [47, 219], in which kinematic relations are decoupled from the evolution of energy variables, may offer additional flexibility for both modeling and discretization. In the same spirit, linearly implicit structure-preserving time integrators — based on dual Störmer–Verlet schemes [96] — represent an attractive option. While first contributions in this direction exist [47, 219], their ability to robustly handle constraints and constraint drift requires further investigation.

Related to the developments presented here, a pH formulation for planar geometrically exact beams was published in [146], which employs spatial stress measures instead of material ones. While conceptually complementary, that work focuses on control design rather than structure-preserving discretization, as further developed in [145]. In this context it can be noted that the pH framework naturally lends itself to control-oriented extensions such as control by interconnection [171] or energy shaping [50]. Also worthwhile investigating is the emerging field of energy-optimal control for pH systems [74, 199, 200], which offers interesting opportunities to exploit the energetic structure of pH models for performance optimization. All in all, investigating how such control strategies can be systematically applied to the structure-preserving formulations developed in this thesis represents a promising avenue for future research.

Concluding statement. In total, this thesis contributes to the development of coherent pH foundations for the modeling and structure-preserving simulation of highly flexible slender structures and flexible multibody systems. Beyond the scope of this thesis, further questions arise, but the presented results suggest that the pH framework offers a unifying perspective that links modeling and discretization with physical principles. It is hoped that the concepts and methods developed in this work support future research, both in further refining the theoretical foundations and in addressing more complex and application-driven problems in flexible multibody dynamics.

Declaration of authorship

The initials of P. L. Kinon (PLK), P. Betsch (PB), S. R. Eugster (SRE), P. Kotyczka (PK), T. Thoma (TT), R. Morandin (RM) and P. Schulze (PS) are used below to mark the contributions of the respective author to the publications. To this end, the CRediT author taxonomy[1] is considered.

Multibody System Dynamics
https://doi.org/10.1007/s11044-025-10087-9

RESEARCH

Energy-momentum-consistent simulation of planar geometrically exact beams in a port-Hamiltonian framework

Philipp L. Kinon[1,2] · Peter Betsch[1] · Simon R. Eugster[2]

Received: 18 March 2025 / Accepted: 22 May 2025

Abstract
We propose a new, port-Hamiltonian formulation for the highly nonlinear dynamics of planar geometrically exact beams, which are amenable to arbitrary large deformations and rotations. A structure-preserving spatial and temporal discretization procedure - using mixed finite elements and second-order time-stepping methods - is proposed. It is observed that the present approach is objective, locking-free and provides an exact discrete representation of the energy and angular momentum balance. By comparing the approach to a classical displacement-based scheme from the literature it is shown that the port-Hamiltonian formulation paves new ways for the design of energy-momentum schemes in computational mechanics. Numerical examples underline the applicability to flexible multibody systems and beneficial numerical performance.

Keywords Planar Simo-Reissner beam · Port-Hamiltonian systems · Flexible multibody systems · Structure-preserving discretization · Mixed finite elements · Locking

1 Introduction

Highly flexible slender structures, such as beams, strings, rods, or shells, are ubiquitous in complex natural and technical systems. Typically, they function as sub-modules within larger flexible multibody systems, which may also include rigid components or joints [1, 2]. The dynamic behavior of such systems can be highly complex due to nonlinear geometry and intricate material properties. Accurately simulating these systems is crucial, particularly for long-term behavior, where numerical dissipation or energetic inconsistencies can lead to unphysical results.

A central approach to describing large deformations in thin, highly flexible structures is the use of geometrically exact beam (GEB) models, also known as Simo-Reissner beams [3, 4] or special Cosserat rods [5]. These highly popular models [6–12] accurately capture large displacements and rotations without relying on linear approximations and remain a

✉ P.L. Kinon
philipp.kinon@kit.edu

[1] Institute of Mechanics, Karlsruhe Institute of Technology (KIT), Otto-Ammann-Platz 9, 76131 Karlsruhe, Germany

[2] Department of Mechanical Engineering, Eindhoven University of Technology (TUe), 5600 MB Eindhoven, The Netherlands

Published online: 16 June 2025

Springer

Citation:
Kinon PL, Betsch P, and Eugster SR. "Energy-momentum-consistent simulation of planar geometrically exact beams in a port-Hamiltonian framework". In: *Multibody System Dynamics*, 2025. DOI: 10.1007/s11044-025-10087-9

Declaration:
Conceptualization & methodology: PLK, PB • software, investigation, visualization & data curation: PLK • validation & formal analysis: PLK, PB, SRE • writing — original draft preparation: PLK • writing — review and editing: PLK, PB, SRE • resources, supervision: PB, SRE • project administration & funding acquisition: PB.

Computer Methods in Applied Mechanics and Engineering 458 (2026) 118966

Contents lists available at ScienceDirect

Comput. Methods Appl. Mech. Engrg.

journal homepage: www.elsevier.com/locate/cma

Mixed formulation and structure-preserving discretization of Cosserat rod dynamics in a port-Hamiltonian framework

Philipp L. Kinon [a,b,*], Simon R. Eugster [a], Peter Betsch [a]

[a] Karlsruhe Institute of Technology (KIT), Germany
[b] Eindhoven University of Technology (TU/e), The Netherlands

ARTICLE INFO

Keywords:
Simo–Reissner beam
Kirchhoff beam
Port-Hamiltonian systems
Differential-algebraic equations
Structure-preserving discretization
Mixed finite elements

ABSTRACT

An energy-based modeling framework for the nonlinear dynamics of spatial Cosserat rods undergoing large displacements and rotations is proposed. The mixed formulation features independent displacement, velocity and stress variables and is further objective and locking-free. Finite rotations are represented using a director formulation that avoids singularities and yields a constant mass matrix. This results in an infinite-dimensional nonlinear port-Hamiltonian (PH) system governed by partial differential-algebraic equations with a quadratic energy functional. Using a time-differentiated compliance form of the stress-strain relation allows for the imposition of kinematic constraints, such as inextensibility or shear-rigidity. A structure-preserving finite element discretization leads to a finite-dimensional system with PH structure, thus facilitating the design of an energy–momentum consistent integration scheme. Dissipative material behavior (via the generalized Maxwell model) and non-standard actuation approaches (via pneumatic chambers or tendons) integrate naturally into the framework. As illustrated by selected numerical examples, the present framework establishes a new approach to energy–momentum consistent formulations in computational mechanics involving finite rotations.

1. Introduction

Flexible multibody systems consisting of rigid bodies and flexible components [1] have a plethora of applications, as for example in the fields of soft robotics [2] or cable dynamics [3]. These systems are inherently complex, driven by geometric nonlinearities and intricate material behavior, thus requiring accurate and robust simulation methods [4].

To this end, the present work provides a novel modeling framework for the dynamics of Cosserat rods [5], which are a cornerstone in modelling the nonlinear dynamics of thin, flexible structures. Herein, the governing equations are recast as a *port-Hamiltonian* (PH) system [6]. This approach inherently provides a mixed formulation in terms of independent displacement, velocity and stress variables and facilitates the *structure-preserving* discretization in space and time.

Cosserat rods. Cosserat rods are also referred to as Simo–Reissner beams [7,8] or geometrically exact beams [9,10].[3] These models have become highly influential [6–20], as they avoid linear or higher order approximations. Lately, these models appear also more frequently in soft robotics [21–24].

The complexity of this model is mostly due to its geometric nonlinearity originating from finite rotations, whose parametrization can be approached in various ways [1]. Possible options to parameterize the rotational degrees of freedom include, but are not

* Corresponding author at: Karlsruhe Institute of Technology (KIT), Germany.
E-mail address: philipp.kinon@kit.edu (P.L. Kinon).
[3] Throughout this work we use the terms *Cosserat rod* and *beam* interchangeably.

https://doi.org/10.1016/j.cma.2026.118966
Received 22 December 2025; Received in revised form 27 February 2026; Accepted 1 April 2026
Available online 6 May 2026

Citation:
Kinon PL, Eugster SR, and Betsch P. "Mixed formulation and structure-preserving discretization of Cosserat rod dynamics in a port-Hamiltonian framework". In: *Computer Methods in Applied Mechanics and Engineering*, 458: 118966, 2026. DOI: 10.1016/j.cma.2026.118966

Declaration:
Conceptualization: PLK, PB • methodology: PLK, SRE, PB • software, investigation, visualization & data curation: PLK • validation: PLK, SRE, PB • formal analysis: PLK, SRE, PB • resources: SRE, PB • writing — original draft preparation: PLK • writing — review and editing: SRE, PB • supervision: SRE, PB • project administration: PB • funding acquisition: PLK, PB.

[1] Cf. https://www.elsevier.com/researcher/author/policies-and-guidelines/credit-author-statement.

Appl. Numer. Math. 223 (2026) 45–75

Contents lists available at ScienceDirect

Applied Numerical Mathematics

journal homepage: www.elsevier.com/locate/apnum

Research Paper

Discrete gradient methods for port-Hamiltonian differential-algebraic equations

Philipp L. Kinon [a,b], Riccardo Morandin [c,*], Philipp Schulze [d,e]

[a] Institute of Mechanics, Karlsruhe Institute of Technology (KIT), Otto-Ammann-Platz 9, Karlsruhe, 76131, Germany
[b] Department of Mechanical Engineering, Eindhoven University of Technology (TU/e), Eindhoven, 5600MB, The Netherlands
[c] Faculty of Mathematics, OvGU Magdeburg, Universitätsplatz 2, Magdeburg, 39106, Germany
[d] Institute of Mathematics, Technische Universität Berlin, Str. des 17. Juni 136, Berlin, 10587, Germany
[e] Institute of Mathematics, University of Potsdam, Potsdam, 14476, Germany

ARTICLE INFO

2020 MSC:
34A09
65L80
65P10
70H35
93C10

Keywords:
Port-Hamiltonian systems
Differential-algebraic equations
Structure-preserving discretization
Time integration methods
Discrete gradients

ABSTRACT

Discrete gradient methods are a powerful tool for the time discretization of dynamical systems, since they are structure-preserving regardless of the form of the total energy. In this work, we discuss the application of discrete gradient methods to the system class of nonlinear port-Hamiltonian differential-algebraic equations – as they emerge from the port- and energy-based modeling of physical systems in various domains. We introduce a novel numerical scheme tailored for semi-explicit differential-algebraic equations and further address more general settings using the concepts of discrete gradient pairs and Dirac-dissipative structures. Additionally, the behavior under system transformations is investigated and we demonstrate that under suitable assumptions port-Hamiltonian differential-algebraic equations admit a representation which consists of a parametrized port-Hamiltonian semi-explicit system and an unstructured equation. Finally, we present the application to multibody system dynamics and discuss numerical results to demonstrate the capabilities of our approach.

1. Introduction

Port-Hamiltonian (pH) systems have gained significant importance in various research areas, with a particular focus on the modeling, simulation, and control of dynamical systems [1,2]. pH systems offer a valuable framework for analyzing complex problems, where the complexity may arise from multi-physical interactions, non-trivial domains, and various nonlinearities. One of the key advantages of the pH representation is its explicit description of power interfaces, known as ports, which facilitates power-preserving interconnections between submodules. Thus, this approach simplifies the modular composition of models, which often leads to the presence of algebraic constraints. Correspondingly, the governing equations at hand are *differential-algebraic equations* (DAEs), also known as *descriptor systems* in the context of control theory. If the system has in addition a pH structure, we speak of *port-Hamiltonian differential-algebraic equations* (pHDAEs). A definition for linear time-varying pHDAEs was provided in [1] and a full, nonlinear generalization has been provided in [4]. An important subclass consists of semi-explicit pHDAEs, see e.g. [5, Eq. 3.16], where local representations of implicit port-Hamiltonian DAEs are discussed. In [6,7], the Hamiltonian as a backbone of pH systems is replaced by Lagrangian subspaces or submanifolds to define generalized pHDAEs.

* Corresponding author.
E-mail addresses: philipp.kinon@kit.edu (P.L. Kinon), riccardo.morandin@ovgu.de (R. Morandin), pschulze@math.tu-berlin.de (P. Schulze).

https://doi.org/10.1016/j.apnum.2025.12.006
Received 3 June 2025; Received in revised form 19 December 2025; Accepted 23 December 2025
Available online 27 December 2025
0168-9274/© 2025 The Author(s). Published by Elsevier B.V. on behalf of IMACS. This is an open access article under the CC BY license (http://creativecommons.org/licenses/by/4.0/).

Citation:
Kinon PL, Morandin R, and Schulze P. "Discrete gradient methods for port-Hamiltonian differential-algebraic equations". In: *Applied Numerical Mathematics*, 223: 45–75, 2026. DOI: 10.1016/j.apnum.2025.12.006

Declaration:
Conceptualization, methodology, validation, formal analysis, writing — original draft preparation, writing — review and editing: PLK, RM, PS • software, investigation, visualization & data curation: PLK.

Available online at www.sciencedirect.com

ScienceDirect

IFAC PapersOnLine 58-6 (2024) 101–106

IFAC Papers Online CONFERENCE PAPER ARCHIVE

Generalized Maxwell viscoelasticity for geometrically exact strings: Nonlinear port-Hamiltonian formulation and structure-preserving discretization

P. L. Kinon * T. Thoma ** P. Betsch * P. Kotyczka **

* Institute of Mechanics, Karlsruhe Institute of Technology (KIT), Otto-Ammann-Platz 9, 76131 Karlsruhe, Germany (email: {philipp.kinon, peter.betsch}@kit.edu)
** TUM School of Engineering and Design, Technical University of Munich (TUM), Boltzmannstr. 15, 85748 Garching, Germany (email: {tobias.thoma, kotyczka}@tum.de)

Abstract: This contribution proposes a nonlinear and dissipative infinite-dimensional port-Hamiltonian (PH) model for the dynamics of geometrically exact strings. The mechanical model provides a description of large deformations including finite elastic and inelastic strains in a generalized Maxwell model. It is shown that the overall system results from a power-preserving interconnection of PH subsystems. By using a structure-preserving mixed finite element approach, a finite-dimensional PH model is derived. Eventually, midpoint discrete derivatives are employed to deduce an energy-consistent time-stepping method, which inherits discrete-time dissipativity for the irreversible system. An example simulation illustrates the numerical properties of the present approach.

Copyright © 2024 The Authors. This is an open access article under the CC BY-NC-ND license (https://creativecommons.org/licenses/by-nc-nd/4.0/).

Keywords: Nonlinear port-Hamiltonian systems, generalized Maxwell model, structure-preserving discretization, mixed finite elements, discrete gradients.

1. INTRODUCTION

The class of port-Hamiltonian (PH) systems has become increasingly important across multiple research fields dealing with modeling and control of complex dynamical systems, see e.g. Duindam et al. (2009). A major benefit of the PH representation is the explicit formulation of power interfaces, so-called ports, which allows for an intrinsically energy-consistent interconnection, thus facilitating the modular composition of subsystems. Since many technical systems are modeled by partial differential equations, the theory of infinite-dimensional PH systems has been extended in recent years, see Rashad et al. (2020) for a review. Among various physical disciplines, PH formulations have also been proposed for mechanics.

The structural elements of strings are particularly interesting and are widely used in control and modeling of multibody systems (cf. Strässle and Betsch (2022); Kinon et al. (2022a)). Strings can be found in a large variety of systems such as cranes, cable robots or satellite systems. Accordingly, they are interconnected with their environment, which can be described beneficially in the PH framework. So far, works on geometrically exact strings have been restricted to purely elastic materials: linear elasticity in Thoma and Kotyczka (2022) and nonlinear elasticity in Kinon et al. (2022a). However, modeling inelastic processes plays a crucial role for the realistic simulation of mechanical systems, see Simo and Hughes (2006). Many works from structural and multibody dynamics deal with the Kelvin-Voigt model (e.g. Linn et al. (2013)), which is not able to reproduce the relaxation test. Recently, more advanced models (such as the generalized Maxwell model) are investigated, see e.g. Bauchau and Nemani (2021).

In this contribution we make use of an infinite-dimensional, nonlinear and dissipative PH model related to Mehrmann and Morandin (2019); Mehrmann and Zwart (2024). We thus extend the existing description of geometrically exact strings to viscoelasticity, introduce the (distributed) generalized Maxwell model to the PH context and explore the model's advantages concerning PH interconnection. With respect to the numerical discretization, the mixed finite element method has been employed to establish an approximate model under preservation of the PH structure, see Cardoso-Ribeiro et al. (2021), retaining the ports with their causality on the discrete level. Lastly, we propose an energy-consistent time discretization extending the one in Kinon et al. (2022b). It is based on the midpoint discrete gradient due to Gonzalez (1996) and can be related to the *discrete-gradient pairs* by Schulze (2023). The resulting scheme inherits the dissipativity property of the underlying continuous model.

2. INFINITE-DIMENSIONAL MODEL

In this section, we derive a model for geometrically exact strings, with a new extension to viscoelastic material using

* The financial support by the DFG (German Research Foundation) – project number 388118188 – is gratefully acknowledged.

10.1016/j.ifacol.2024.08.264

Citation:
Kinon PL, Thoma T, Betsch P, and Kotyczka P. "Generalized Maxwell viscoelasticity for geometrically exact strings: Nonlinear port-Hamiltonian formulation and structure-preserving discretization". In: *IFAC-PapersOnLine*, 58(6): 101–106, 2024. DOI: 10.1016/j.ifacol.2024.08.264

Declaration:
Conceptualization: PLK, PB • methodology, validation & formal analysis: PLK, TT, PB, PK • investigation: PLK • software, visualization & data curation: PLK • writing — original draft preparation: PLK • writing — review and editing: PLK, TT, PB, PK • resources, supervision, project administration & funding acquisition: PB, PK.

Declaration of data availability:
Chapters 3 to 6 and the related articles contain numerical experiments. In order to enhance accessibility and reproducibility within the scientific community [64], the generated data and/or source code have been made openly available. References are included in the respective sections.

Declaration of AI-assisted tools:
During the preparation of this work, the author used generative artificial intelligence (AI) tools solely to review grammar, spelling, and stylistic clarity. After using these tools, the author carefully reviewed and edited the content as necessary and takes full responsibility for the content of this publication.

Publications and talks

Peer-reviewed publications in this thesis

[A1] **Kinon PL**, Thoma T, Betsch P, and Kotyczka P. "Generalized Maxwell viscoelasticity for geometrically exact strings: Nonlinear port-Hamiltonian formulation and structure-preserving discretization". In: *IFAC-PapersOnLine*, 58(6): 101–106, 2024. DOI: 10.1016/j.ifacol.2024.08.264.

[A2] **Kinon PL**, Betsch P, and Eugster SR. "Energy-momentum-consistent simulation of planar geometrically exact beams in a port-Hamiltonian framework". In: *Multibody System Dynamics*, 2025. DOI: 10.1007/s11044-025-10087-9.

[A3] **Kinon PL**, Morandin R, and Schulze P. "Discrete gradient methods for port-Hamiltonian differential-algebraic equations". In: *Applied Numerical Mathematics*, 223: 45–75, 2026. DOI: 10.1016/j.apnum.2025.12.006.

[A4] **Kinon PL**, Eugster SR, and Betsch P. "Mixed formulation and structure-preserving discretization of Cosserat rod dynamics in a port-Hamiltonian framework". In: *Computer Methods in Applied Mechanics and Engineering*, 458: 118966, 2026. DOI: 10.1016/j.cma.2026.118966.

Further peer-reviewed publications

[B1] Bauer JK, **Kinon PL**, Hund J, Latussek L, Meyer N, and Böhlke T. "Mechkit: A continuum mechanics toolkit in Python". In: *Journal of Open Source Software*, 7(78): 4389, 2022. DOI: 10.21105/joss.04389.

[B2] **Kinon PL**, Betsch P, and Schneider S. "The GGL variational principle for constrained mechanical systems". In: *Multibody System Dynamics*, 57(3): 211–236, 2023. DOI: 10.1007/s11044-023-09889-6.

[B3] **Kinon PL**, Betsch P, and Schneider S. "Structure-preserving integrators based on a new variational principle for constrained mechanical systems". In: *Nonlinear Dynamics*, 111: 14231–14261, 2023. DOI: 10.1007/s11071-023-08522-7.

[B4] **Kinon PL** and Betsch P. "Conserving integration of multibody systems with singular and non-constant mass matrix including quaternion-based rigid body dynamics". In: *Multibody System Dynamics*, 63(1): 303–340, 2025. DOI: 10.1007/s11044-024-10001-9.

[B5] Bauer JK, Krauß C, Blarr J, **Kinon PL**, Kärger L, and Böhlke T. "Evaluation of a decomposition-based interpolation method for fourth-order fiber-orientation tensors: An eigensystem approach". In: *Mathematics and Mechanics of Solids*, 30(3): 641–678, 2025. DOI: 10.1177/10812865241241002.

[B6] Latussek L, **Kinon PL**, and Betsch P. "Port-Hamiltonian multibody dynamics: Lagrangian formulation, consistent interconnection, structure-preserving simulation and index-reduction". In: *Multibody System Dynamics (under review)*, 2026. DOI: 10.48550/arXiv.2603.12841.

Non peer-reviewed publications

[C1] **Kinon PL** and Betsch P. "The GGL variational principle for constrained mechanical systems". In: *Proceedings of the 10th ECCOMAS Thematic Conference on Multibody Dynamics*. Budapest, Hungary, 2021, pp. 197–211. DOI: 10.3311/ECCOMASMBD2021-125.

[C2] **Kinon PL**, Thoma T, Betsch P, and Kotyczka P. "Port-Hamiltonian formulation and structure-preserving discretization of hyperelastic strings". In: *Proceedings of the 11th ECCOMAS Thematic Conference on Multibody Dynamics*. Lisbon, Portugal, 2023, pp. 1–10. DOI: 10.48550/arXiv.2304.10957.

[C3] **Kinon PL** and Betsch P. "Energy-consistent integration of mechanical systems based on Livens principle". In: *Proceedings of the 11th ECCOMAS Thematic Conference on Multibody Dynamics*. Lisbon, Portugal, 2023. DOI: 10.48550/arXiv.2312.02825.

[C4] **Kinon PL**, Thoma T, Betsch P, and Kotyczka P. "Discrete nonlinear elastodynamics in a port-Hamiltonian framework". In: *PAMM*, 23(3): e202300144, 2023. DOI: 10.1002/pamm.202300144.

[C5] **Kinon PL** and Betsch P. "Structure-preserving integrators for constrained mechanical systems in the framework of the GGL principle". In: *PAMM*, 22(1): e202200006, 2023. DOI: 10.1002/pamm.202200006.

Conference talks

[D1] **Kinon PL** and Betsch P. *The GGL variational principle for constrained mechanical systems*. 10th ECCOMAS Thematic Conference on Multibody Dynamics. Budapest, Hungary (virtual congress), Dec. 12–15, 2021.

[D2] **Kinon PL** and Betsch P. *Structure-preserving integrators for constrained mechanical systems in the framework of the GGL principle*. 92nd Annual Meeting of the International Association of Applied Mathematics and Mechanics. Aachen, Germany, Aug. 15–19, 2022.

[D3] **Kinon PL**, Thoma T, Betsch P, and Kotyczka P. *Modeling and simulation of geometrically exact strings in a nonlinear port-Hamiltonian framework*. 3rd Workshop of the Doctoral College "Port-Hamiltonian Systems: Modelling, Numerics and Control". Wuppertal, Germany, Mar. 28–30, 2023.

[D4] **Kinon PL**, Thoma T, Betsch P, and Kotyczka P. *Nonlinear elastodynamics in the context of port-Hamiltonian modeling: Formulation and structure-preserving discretization*. 93rd Annual Meeting of the International Association of Applied Mathematics and Mechanics. Dresden, Germany, May 30–June 2, 2023.

[D5] **Kinon PL** and Betsch P. *Energy-consistent integration of mechanical systems based on Livens principle*. 11th ECCOMAS Thematic Conference on Multibody Dynamics. Lisbon, Portugal, July 24–28, 2023.

[D6] **Kinon PL** and Betsch P. *Structure-preserving time discretization of multibody systems with singular inertia matrix*. 94th Annual Meeting of the International Association of Applied Mathematics and Mechanics. Magdeburg, Germany, Mar. 18–22, 2024.

[D7] **Kinon PL**, Thoma T, Betsch P, and Kotyczka P. *Generalized Maxwell viscoelasticity for geometrically exact strings: Nonlinear port-Hamiltonian formulation and structure-preserving discretization.* 8th IFAC Workshop on Lagrangian and Hamiltonian Methods for Nonlinear Control — LHMNC 2024. Besançon, France, June 10–12, 2024.

[D8] **Kinon PL**, Morandin R, and Schulze P. *Discrete gradient methods for semi-explicit port-Hamiltonian DAEs.* 6th Workshop of the Doctoral College "Port-Hamiltonian Systems: Modelling, Numerics and Control". Twente, The Netherlands, Oct. 16–18, 2024.

[D9] **Kinon PL**, Betsch P, and Eugster SR. *Geometrically exact planar beam dynamics: Port-Hamiltonian modeling and structure-preserving discretization.* 95th Annual Meeting of the International Association of Applied Mathematics and Mechanics. Poznań, Poland, Apr. 7–11, 2025.

[D10] **Kinon PL**, Betsch P, and Eugster SR. *Port-Hamiltonian formulation and structure-preserving discretization of geometrically exact beams.* 12th ECCOMAS Thematic Conference on Multibody Dynamics. Innsbruck, Austria, July 13–18, 2025.

[D11] **Kinon PL**, Eugster SR, and Betsch P. *Structure-preserving discretization of Cosserat rod dynamics in a mixed DAE-framework.* 96th Annual Meeting of the International Association of Applied Mathematics and Mechanics. Stuttgart, Germany, Apr. 7–11, 2026.

Poster contributions

[E1] **Kinon PL**. *Novel geometric integrators for multibody systems.* 94th Annual Meeting of the International Association of Applied Mathematics and Mechanics. Magdeburg, Germany, Mar. 18–22, 2024.

[E2] **Kinon PL**. *Energy-momentum-consistent simulation of planar geometrically exact beams as PHS.* Port-Hamiltonian Systems 2025 – Spring School on Theory and Applications of Port-Hamiltonian Systems. Frauenchiemsee, Germany, Mar. 23–28, 2025.

[E3] **Kinon PL**. *Structure-preserving methods for port-Hamiltonian flexible multibody systems.* 95th Annual Meeting of the International Association of Applied Mathematics and Mechanics. Poznań, Poland, Apr. 7–11, 2025.

[E4] **Kinon PL**. *Port-Hamiltonian Cosserat rod dynamics.* 96th Annual Meeting of the International Association of Applied Mathematics and Mechanics. Stuttgart, Germany, Apr. 7–11, 2026.

Open-source code

[F1] **Kinon PL** and Bauer JK. *metis: Computing constrained dynamical systems, v1.1.1.* Zenodo. 2024. DOI: 10.5281/zenodo.11917636.

[F2] **Kinon PL** and Bauer JK. *pydykit: A Python-based dynamics simulation toolkit, v0.0.6.* Zenodo. 2025. DOI: 10.5281/zenodo.14849865.

List of acronyms

BC	boundary condition
DAE	differential-algebraic equation
DDR	Dirac–dissipative representation
EM	energy–momentum
FE	finite element
GEB	geometrically exact beam
IBVP	initial boundary value problem
ODE	ordinary differential equation
PBE	power balance equation
PDAE	partial differential-algebraic equation
PDE	partial differential equation
pH	port-Hamiltonian

List of figures

List of tables

Bibliography

[1] Albersmeyer J and Diehl M. "The lifted Newton method and its application in optimization". In: *SIAM Journal on Optimization*, 20(3): 1655–1684, 2010. DOI: 10.1137/080724885 (cf. p. 5).

[2] Albu-Schäffer A, Eiberger O, Grebenstein M, Haddadin S, Ott C, Wimbock T, Wolf S, and Hirzinger G. "Soft robotics". In: *IEEE Robotics & Automation Magazine*, 15(3): 20–30, 2008. DOI: 10.1109/MRA.2008.927979 (cf. pp. 2, 6, 63, 91).

[3] Alessi C, Agabiti C, Caradonna D, Laschi C, Renda F, and Falotico E. *Rod models in continuum and soft robot control: a review*. Preprint. 2024. arXiv: 2407.05886v1 [cs.RO] (cf. pp. 3, 64, 65, 81).

[4] Altmann R, Mehrmann V, and Unger B. "Port-Hamiltonian formulations of poroelastic network models". In: *Mathematical and Computer Modelling of Dynamical Systems*, 27(1): 429–452, 2021. DOI: 10.1080/13873954.2021.1975137 (cf. p. 3).

[5] Altmann R and Schulze P. "A port-Hamiltonian formulation of the Navier–Stokes equations for reactive flows". In: *Systems & Control Letters*, 100: 51–55, 2017. DOI: 10.1016/j.sysconle.2016.12.005 (cf. p. 3).

[6] Altmann R and Schulze P. "A novel energy-based modeling framework". In: *Mathematics of Control, Signals, and Systems*, 37(2): 395–414, 2025. DOI: 10.1007/s00498-024-00405-5 (cf. p. 4).

[7] Altmann R, Cortes Garcia I, Paakkunainen E, Schulze P, and Schöps S. "Energy-based modeling for field–circuit coupling". In: *Applied Mathematical Modelling*, 155: 116688, 2026. DOI: 10.1016/j.apm.2025.116688 (cf. pp. 3, 4).

[8] Altmann R and Herzog R. "Continuous Galerkin schemes for semiexplicit differential-algebraic equations". In: *IMA Journal of Numerical Analysis*, 42(3): 2214–2237, 2022. DOI: 10.1093/imanum/drab037 (cf. pp. 5, 143).

[9] Altmann R, Karsai A, and Schulze P. *Structure-preserving discretization and model reduction for energy-based models*. Preprint. 2025. arXiv: 2507.21552v1 [math.NA] (cf. p. 5).

[10] Antman SS. *Nonlinear Problems of Elasticity*. 2nd ed. New York: Springer, 2005. DOI: 10.1007/0-387-27649-1 (cf. pp. 2, 6, 8, 13, 28, 29, 35, 39, 63, 69, 93, 128, 139).

[11] Aoues S, Cardoso-Ribeiro FL, Matignon D, and Alazard D. "Modeling and control of a rotating flexible spacecraft: a port-Hamiltonian approach". In: *IEEE Transactions on Control Systems Technology*, 27(1): 355–362, 2019. DOI: 10.1109/TCST.2017.2771244 (cf. pp. 4, 6).

[12] Aoues S, Loreto M di, Eberard D, and Marquis-Favre W. "Hamiltonian systems discrete-time approximation: Losslessness, passivity and composability". In: *Systems & Control Letters*, 110: 9–14, 2017. DOI: 10.1016/j.sysconle.2017.10.003 (cf. pp. 5, 7, 102).

[13] Arfken GB, Weber HJ, and Harris FE. *Mathematical methods for physicists: a comprehensive guide*. 7th ed. Amsterdam ; Boston: Elsevier, 2013 (cf. p. 74).

[14] Arnold VI. *Mathematical Methods of Classical Mechanics*. 2nd ed. New York: Springer, 1989 (cf. p. 102).

[15] Artola M, Wynn A, and Palacios R. “Modal-based nonlinear model predictive control for 3-D very flexible structures”. In: *IEEE Transactions on Automatic Control*, 67(5): 2145–2160, 2022. DOI: 10.1109/TAC.2021.3071326 (cf. pp. 4, 6, 64, 65).

[16] Ayala EP, Wu Y, Rabenorosoa K, and Le Gorrec Y. “Energy-based modeling and control of a piezotube actuated optical fiber”. In: *IEEE/ASME Transactions on Mechatronics*, 28(1): 385–395, 2023. DOI: 10.1109/TMECH.2022.3199566 (cf. pp. 4, 6, 64, 65).

[17] Bartel A, Diab M, Frommer A, and Günther M. *Operator splitting for semi-explicit differential-algebraic equations and port-Hamiltonian DAEs*. Preprint. 2023. arXiv: 2308.16736v1 [math.DS] (cf. pp. 5, 102).

[18] Bartel A, Diab M, Frommer A, Günther M, and Marheineke N. “Splitting techniques for DAEs with port-Hamiltonian applications”. In: *Applied Numerical Mathematics*, 214: 28–53, 2025. DOI: 10.1016/j.apnum.2025.03.004 (cf. pp. 5, 102).

[19] Bartel A and Schaller M. “Goal-oriented time adaptivity for port-Hamiltonian systems”. In: *Journal of Computational and Applied Mathematics*, 461: 116450, 2025. DOI: 10.1016/j.cam.2024.116450 (cf. p. 102).

[20] Bauchau OA. *Flexible Multibody Dynamics*. Dordrecht: Springer, 2011. DOI: 10.1007/978-94-007-0335-3 (cf. pp. 2, 35, 63, 64).

[21] Bauchau OA and Han S. “Interpolation of rotation and motion”. In: *Multibody System Dynamics*, 31(3): 339–370, 2014. DOI: 10.1007/s11044-013-9365-8 (cf. p. 64).

[22] Bauchau OA and Nemani N. “Modeling viscoelastic behavior in flexible multibody systems”. In: *Multibody System Dynamics*, 51(2): 159–194, 2021. DOI: 10.1007/s11044-020-09767-5 (cf. p. 128).

[23] Beattie C, Mehrmann V, Xu H, and Zwart H. “Linear port-Hamiltonian descriptor systems”. In: *Mathematics of Control, Signals, and Systems*, 30: 17, 2018. DOI: 10.1007/s00498-018-0223-3 (cf. pp. 4, 8, 21, 37, 47, 65, 71, 72, 75, 81, 101).

[24] Bendimerad-Hohl A, Haine G, Lefèvre L, and Matignon D. “Stokes-Lagrange and Stokes-Dirac representations of N-dimensional port-Hamiltonian systems for modeling and control”. In: *Communications in Analysis and Mechanics*, 17(2): 474–519, 2025. DOI: 10.3934/cam.2025020 (cf. pp. 4, 142).

[25] Berger T, Hochdahl R, Reis T, and Seifried R. “Port-Hamiltonian modeling of rigid multibody systems”. In: *Nonlinear Dynamics*, 113: 32037–32058, 2025. DOI: 10.1007/s11071-025-11776-y (cf. pp. 4, 142).

[26] Berzeri M, Campanelli M, and Shabana AA. “Definition of the elastic forces in the finite-element absolute nodal coordinate formulation and the floating frame of reference formulation”. In: *Multibody System Dynamics*, 5(1): 21–54, 2001. DOI: 10.1023/A:1026465001946 (cf. p. 56).

[27] Betsch P, Menzel A, and Stein E. “On the parametrization of finite rotations in computational mechanics”. In: *Computer Methods in Applied Mechanics and Engineering*, 155(3-4): 273–305, 1998. DOI: 10.1016/S0045-7825(97)00158-8 (cf. p. 64).

[28] Betsch P and Sänger N. “On the consistent formulation of torques in a rotationless framework for multibody dynamics”. In: *Computers & Structures*, 127: 29–38, 2013. DOI: 10.1016/j.compstruc.2012.10.005 (cf. p. 92).

[29] Betsch P and Steinmann P. “Conservation properties of a time FE method. Part I: time-stepping schemes for N-body problems”. In: *International Journal for Numerical Methods in Engineering*, 49(5): 599–638, 2000. DOI: 10.1002/1097-0207(20001020)49:5<599::AID-NME960>3.0.CO;2-9 (cf. pp. 5, 102).

[30] Betsch P and Steinmann P. "Conservation properties of a time FE method — part II: Time-stepping schemes for non-linear elastodynamics". In: *International Journal for Numerical Methods in Engineering*, 50(8): 1931–1955, 2001. DOI: 10.1002/nme.103 (cf. pp. 5, 102).

[31] Betsch P and Steinmann P. "A DAE approach to flexible multibody dynamics". In: *Multibody System Dynamics*, 8(3): 365–389, 2002. DOI: 10.1023/A:1020934000786 (cf. pp. 3, 64, 74).

[32] Betsch P and Steinmann P. "Conservation properties of a time FE method — part III: Mechanical systems with holonomic constraints". In: *International Journal for Numerical Methods in Engineering*, 53(10): 2271–2304, 2002. DOI: 10.1002/nme.347 (cf. pp. 5, 102).

[33] Betsch P and Steinmann P. "Frame-indifferent beam finite elements based upon the geometrically exact beam theory". In: *International Journal for Numerical Methods in Engineering*, 54(12): 1775–1788, 2002. DOI: 10.1002/nme.487 (cf. pp. 3, 5, 6, 9, 10, 64, 65, 67, 73, 74, 76, 93, 94).

[34] Betsch P and Steinmann P. "Constrained dynamics of geometrically exact beams". In: *Computational Mechanics*, 31(1-2): 49–59, 2003. DOI: 10.1007/s00466-002-0392-1 (cf. pp. 3, 5, 35, 64).

[35] Betsch P, ed. *Structure-preserving Integrators in Nonlinear Structural Dynamics and Flexible Multibody Dynamics*. Cham: Springer, 2016. DOI: 10.1007/978-3-319-31879-0 (cf. pp. 4, 5, 102).

[36] Betsch P and Janz A. "An energy-momentum consistent method for transient simulations with mixed finite elements developed in the framework of geometrically exact shells". In: *International Journal for Numerical Methods in Engineering*, 108(5): 423–455, 2016. DOI: 10.1002/nme.5217 (cf. pp. 4, 5, 15, 25, 26, 142).

[37] Betsch P, Janz A, and Hesch C. "A mixed variational framework for the design of energy-momentum schemes inspired by the structure of polyconvex stored energy functions". In: *Computer Methods in Applied Mechanics and Engineering*, 335: 660–696, 2018. DOI: 10.1016/j.cma.2018.01.013 (cf. pp. 4, 5).

[38] Bobenko AI and Suris YB. "Discrete time Lagrangian mechanics on Lie groups, with an application to the Lagrange top". In: *Communications in Mathematical Physics*, 204(1): 147–188, 1999. DOI: 10.1007/s002200050642 (cf. p. 5).

[39] Boffi D, Brezzi F, and Fortin M. *Mixed Finite Element Methods and Applications*. Berlin, Heidelberg: Springer, 2013. DOI: 10.1007/978-3-642-36519-5 (cf. p. 5).

[40] Bruckmann T and Pott A, eds. *Cable-Driven Parallel Robots*. Berlin, Heidelberg: Springer, 2013. DOI: 10.1007/978-3-642-31988-4 (cf. p. 2).

[41] Brugnoli A. "A port-Hamiltonian formulation of flexible structures. Modelling and structure-preserving finite element discretization". PhD thesis. Université de Toulouse, ISAE-SUPAERO, 2020 (cf. pp. 3, 6, 13, 28–33, 36, 42, 65).

[42] Brugnoli A, Alazard D, Pommier-Budinger V, and Matignon D. "Port-Hamiltonian formulation and symplectic discretization of plate models — part I: Mindlin model for thick plates". In: *Applied Mathematical Modelling*, 75: 940–960, 2019. DOI: 10.1016/j.apm.2019.04.035 (cf. pp. 4, 6, 36, 42, 64).

[43] Brugnoli A, Alazard D, Pommier-Budinger V, and Matignon D. "Port-Hamiltonian formulation and symplectic discretization of plate models — Part II: Kirchhoff model for thin plates". In: *Applied Mathematical Modelling*, 75: 961–981, 2019. DOI: 10.1016/j.apm.2019.04.036 (cf. pp. 4, 6, 36, 64).

[44] Brugnoli A, Alazard D, Pommier-Budinger V, and Matignon D. "Port-Hamiltonian flexible multibody dynamics". In: *Multibody System Dynamics*, 51(3): 343–375, 2021. DOI: 10.1007/s11044-020-09758-6 (cf. pp. 4–6, 9, 27, 36, 41, 42, 64).

[45] Brugnoli A, Cardoso-Ribeiro FL, Haine G, and Kotyczka P. "Partitioned finite element method for structured discretization with mixed boundary conditions". In: *IFAC-PapersOnLine*, 53(2): 7557–7562, 2020. DOI: 10.1016/j.ifacol.2020.12.1351 (cf. pp. 43, 73, 142).

[46] Brugnoli A, Haine G, and Matignon D. "Explicit structure-preserving discretization of port-Hamiltonian systems with mixed boundary control". In: *IFAC-PapersOnLine*, 55(30): 418–423, 2022. DOI: 10.1016/j.ifacol.2022.11.089 (cf. pp. 43, 73, 136, 142).

[47] Brugnoli A, Matignon D, and Morlier J. "A linearly-implicit energy-momentum preserving scheme for geometrically nonlinear mechanics based on non-canonical Hamiltonian formulations". In: *Nonlinear Dynamics*, 113: 27539–27566, 2025. DOI: 10.1007/s11071-025-11601-6 (cf. pp. 4, 26, 36, 142, 143).

[48] Brugnoli A, Rashad R, Califano F, Stramigioli S, and Matignon D. "Mixed finite elements for port-Hamiltonian models of von Kármán beams". In: *IFAC-PapersOnLine*, 54(19): 186–191, 2021. DOI: 10.1016/j.ifacol.2021.11.076 (cf. pp. 4–6, 9, 36, 64, 65, 129).

[49] Buchfink P, Glas S, and Zwart H. "Energy-stable port-Hamiltonian systems". In: *Applied Mathematics Letters*, 173: 109784, 2026. DOI: 10.1016/j.aml.2025.109784 (cf. pp. 4, 143).

[50] Caasenbrood B, Pogromsky A, and Nijmeijer H. "Energy-shaping controllers for soft robot manipulators through port-Hamiltonian Cosserat models". In: *SN Computer Science*, 3(6): 494, 2022. DOI: 10.1007/s42979-022-01373-w (cf. pp. 36, 64, 91, 143).

[51] Cammarata A, Greco L, Castello D, and Cuomo M. "An implicit time integrator for Cosserat rods based on the spherical Bézier interpolation". In: *Computer Methods in Applied Mechanics and Engineering*, 445: 118195, 2025. DOI: 10.1016/j.cma.2025.118195 (cf. pp. 83, 84).

[52] Campanelli M, Berzeri M, and Shabana AA. "Performance of the incremental and non-incremental finite element formulations in flexible multibody problems". In: *Journal of Mechanical Design*, 122(4): 498–507, 2000. DOI: 10.1115/1.1289636 (cf. p. 54).

[53] Cardona A and Géradin M. "A beam finite element non-linear theory with finite rotations". In: *International Journal for Numerical Methods in Engineering*, 26(11): 2403–2438, 1988. DOI: 10.1002/nme.1620261105 (cf. pp. 3, 35).

[54] Cardoso-Ribeiro FL, Matignon D, and Lefèvre L. "A partitioned finite element method for power-preserving discretization of open systems of conservation laws". In: *IMA Journal of Mathematical Control and Information*, 38(2): 493–533, 2021. DOI: 10.1093/imamci/dnaa038 (cf. pp. 5, 36, 64, 128).

[55] Celledoni E and Høiseth EH. *Energy-preserving and passivity-consistent numerical discretization of port-hamiltonian systems*. Preprint. 2017. arXiv: 1706.08621v1 [math.NA] (cf. pp. 5, 7, 102, 109).

[56] Celledoni E, Marthinsen H, and Owren B. "An introduction to Lie group integrators – basics, new developments and applications". In: *Journal of Computational Physics*, 257: 1040–1061, 2014. DOI: 10.1016/j.jcp.2012.12.031 (cf. p. 5).

[57] Češarek P, Saje M, and Zupan D. "Kinematically exact curved and twisted strain-based beam". In: *International Journal of Solids and Structures*, 49(13): 1802–1817, 2012. DOI: 10.1016/j.ijsolstr.2012.03.033 (cf. pp. 5, 6, 65).

[58] Courant TJ. "Dirac manifolds". In: *Transactions of the American Mathematical Society*, 319(2): 631–661, 1990. DOI: 10.1090/S0002-9947-1990-0998124-1 (cf. pp. 3, 17).

[59] Crisfield MA and Jelenić G. "Objectivity of strain measures in the geometrically exact three-dimensional beam theory and its finite-element implementation". In: *Proceedings: Mathematical, Physical and Engineering Sciences*, 455(1983): 1125–1147, 1999 (cf. pp. 3, 35, 64).

[60] De Jong S, Brugnoli A, Rashad R, Zhang Y, and Stramigioli S. "A domain decomposition strategy for natural imposition of mixed boundary conditions in port-Hamiltonian systems". In: *Applied Mathematical Modelling*, 156: 116775, 2026. DOI: 10.1016/j.apm.2026.116775 (cf. p. 142).

[61] Debeurre M, Grolet A, and Thomas O. "Quaternion-based finite-element computation of nonlinear modes and frequency responses of geometrically exact beam structures in three dimensions". In: *Multibody System Dynamics*, 63(4): 557–594, 2025. DOI: 10.1007/s11044-024-09999-9 (cf. pp. 3, 64, 91, 142).

[62] Dörlich V, Linn J, and Diebels S. "Flexible beam-like structures — Experimental investigation and modeling of cables". In: *Advances in Mechanics of Materials and Structural Analysis*. Ed. by Altenbach H, Jablonski F, Müller WH, Naumenko K, and Schneider P. Cham: Springer, 2018, pp. 27–46. DOI: 10.1007/978-3-319-70563-7_2 (cf. pp. 63, 91).

[63] Duindam V, Macchelli A, Stramigioli S, and Bruyninckx H. *Modeling and Control of Complex Physical Systems: The Port-Hamiltonian Approach*. Berlin, Heidelberg: Springer, 2009. DOI: 10.1007/978-3-642-03196-0 (cf. pp. 3, 13, 17, 27, 35, 42, 63, 64, 101, 111, 127).

[64] Ebel H, Van Delden J, Lüddecke T, Borse A, Gulakala R, Stoffel M, Yadav M, Stender M, Schindler L, De Payrebrune KM, Raff M, Remy CD, Röder B, Raj R, Rentschler T, Tismer A, Riedelbauch S, and Eberhard P. "Data publishing in mechanics and dynamics: challenges, guidelines, and examples from engineering design". In: *Data-Centric Engineering*, 6: e23, 2025. DOI: 10.1017/dce.2025.13 (cf. p. 146).

[65] Egger H, Habrich O, and Shashkov V. "On the energy stable approximation of Hamiltonian and gradient systems". In: *Computational Methods in Applied Mathematics*, 21(2): 335–349, 2021. DOI: 10.1515/cmam-2020-0025 (cf. pp. 5, 102, 107, 143).

[66] Eidnes S. "Order theory for discrete gradient methods". In: *BIT Numerical Mathematics*, 62(4): 1207–1255, 2022. DOI: 10.1007/s10543-022-00909-z (cf. pp. 5, 102, 116, 143).

[67] Eugster S, Hesch C, Betsch P, and Glocker C. "Director-based beam finite elements relying on the geometrically exact beam theory formulated in skew coordinates". In: *International Journal for Numerical Methods in Engineering*, 97(2): 111–129, 2014. DOI: 10.1002/nme.4586 (cf. pp. 3, 35, 64, 74).

[68] Eugster SR and Harsch J. "A variational formulation of classical nonlinear beam theories". In: *Developments and Novel Approaches in Nonlinear Solid Body Mechanics*. Ed. by Abali BE and Giorgio I. Cham: Springer, 2020, pp. 95–121. DOI: 10.1007/978-3-030-50460-1_9 (cf. pp. 93, 94).

[69] Eugster SR and Harsch J. "A family of total Lagrangian Petrov–Galerkin Cosserat rod finite element formulations". In: *GAMM-Mitteilungen*, 46(2): e202300008, 2023. DOI: 10.1002/gamm.202300008 (cf. pp. 3, 64, 74, 142).

[70] Eugster SR, Harsch J, Bartholdt M, Herrmann M, Wiese M, and Capobianco G. "Soft pneumatic actuator model based on a pressure-dependent spatial nonlinear rod theory". In: *IEEE Robotics and Automation Letters*, 7(2): 2471–2478, 2022. DOI: 10.1109/LRA.2022.3144788 (cf. pp. 3, 9, 64, 65, 81, 89).

[71] Evans LC. *Partial Differential Equations*. 2nd ed. Providence, Rhode Island: American Mathematical Society, 2010 (cf. p. 30).

[72] Falaize A and Hélie T. "Passive guaranteed simulation of analog audio circuits: a port-Hamiltonian approach". In: *Applied Sciences*, 6(10): 273, 2016. DOI: 10.3390/app6100273 (cf. pp. 5, 7, 102).

[73] Fan W. "An efficient recursive rotational-coordinate-based formulation of a planar Euler–Bernoulli beam". In: *Multibody System Dynamics*, 52(2): 211–227, 2021. DOI: 10.1007/s11044-021-09783-z (cf. p. 56).

[74] Faulwasser T, Maschke B, Philipp F, Schaller M, and Worthmann K. "Optimal control of port-Hamiltonian descriptor systems with minimal energy supply". In: *SIAM Journal on Control and Optimization*, 60(4): 2132–2158, 2022. DOI: 10.1137/21M1427723 (cf. p. 143).

[75] Ferri G, Ignesti D, and Marino E. "An efficient displacement-based isogeometric formulation for geometrically exact viscoelastic beams". In: *Computer Methods in Applied Mechanics and Engineering*, 417: 116413, 2023. DOI: 10.1016/j.cma.2023.116413 (cf. pp. 3, 9, 58, 65, 79, 80).

[76] Fiaz S, Zonetti D, Ortega R, Scherpen J, and van der Schaft AJ. "A port-Hamiltonian approach to power network modeling and analysis". In: *European Journal of Control*, 19(6): 477–485, 2013. DOI: 10.1016/j.ejcon.2013.09.002 (cf. p. 3).

[77] Forni P, Jeltsema D, and Lopes GA. "Port-Hamiltonian formulation of rigid-body attitude control". In: *IFAC-PapersOnLine*, 48(13): 164–169, 2015. DOI: 10.1016/j.ifacol.2015.10.233 (cf. p. 142).

[78] Franke M, Zähringer F, Hille M, Kinon PL, and Reiff P. *MoofeKIT: MATLAB object-oriented finite element KIT, v1.0.2*. Zenodo. 2023. DOI: 10.5281/zenodo.10416814 (cf. p. 136).

[79] Franke M, Zähringer F, Hille M, Kinon PL, and Reiff P. *MoofeKIT: MATLAB object-oriented finite element KIT, v1.0.3*. Zenodo. 2025. DOI: 10.5281/zenodo.15044922 (cf. p. 53).

[80] Frommer A, Günther M, Liljegren-Sailer B, and Marheineke N. *Operator splitting for port-Hamiltonian systems*. Preprint. 2023. arXiv: 2304.01766v1 [math.NA] (cf. pp. 7, 102, 107, 109).

[81] Gams M, Planinc I, and Saje M. "Energy conserving time integration scheme for geometrically exact beam". In: *Computer Methods in Applied Mechanics and Engineering*, 196(17-20): 2117–2129, 2007. DOI: 10.1016/j.cma.2006.10.012 (cf. p. 53).

[82] Géradin M and Cardona A. *Flexible Multibody Dynamics: A Finite Element Approach*. Chichester: Wiley, 2001 (cf. p. 2).

[83] Gerstmayr J, Sugiyama H, and Mikkola A. "Review on the absolute nodal coordinate formulation for large deformation analysis of multibody systems". In: *Journal of Computational and Nonlinear Dynamics*, 8(3): 031016, 2013. DOI: 10.1115/1.4023487 (cf. p. 2).

[84] Giesselmann J, Karsai A, and Tscherpel T. "Energy-consistent Petrov-Galerkin time discretization of port-Hamiltonian systems". In: *The SMAI Journal of computational mathematics*, 11: 335–367, 2025. DOI: 10.5802/smai-jcm.127 (cf. pp. 5, 65, 102, 107, 143).

[85] Goldstein H, Poole C, and Safko J. *Classical Mechanics*. 3rd ed. San Francisco, Munich: Addison Wesley, 2002 (cf. p. 15).

[86] Golo G, van der Schaft AJ, and Stramigioli S. "Hamiltonian formulation of planar beams". In: *IFAC Proceedings Volumes*, 36(2): 147–152, 2003. DOI: 10.1016/S1474-6670(17)38882-1 (cf. pp. 4, 36).

[87] Gonzalez O. "Time integration and discrete Hamiltonian systems". In: *Journal of Nonlinear Science*, 6(5): 449–467, 1996. DOI: 10.1007/BF02440162 (cf. pp. 7, 10, 48, 107, 121, 128, 135).

[88] Gonzalez O. “Exact energy and momentum conserving algorithms for general models in nonlinear elasticity”. In: *Computer Methods in Applied Mechanics and Engineering*, 190(13-14): 1763–1783, 2000. DOI: 10.1016/s0045-7825(00)00189-4 (cf. pp. 5, 102).

[89] Gonzalez O and Simo J. “On the stability of symplectic and energy-momentum algorithms for non-linear Hamiltonian systems with symmetry”. In: *Computer Methods in Applied Mechanics and Engineering*, 134(3-4): 197–222, 1996. DOI: 10.1016/0045-7825(96)01009-2 (cf. p. 124).

[90] Gonzalez O. “Mechanical systems subject to holonomic constraints: Differential–algebraic formulations and conservative integration”. In: *Physica D: Nonlinear Phenomena*, 132(1-2): 165–174, 1999. DOI: 10.1016/S0167-2789(99)00054-8 (cf. pp. 5, 102, 121).

[91] Gören-Sümer L and Yalçın Y. “Gradient based discrete-time modeling and control of Hamiltonian systems”. In: *IFAC Proceedings Volumes*, 41(2): 212–217, 2008. DOI: 10.3182/20080706-5-kr-1001.00036 (cf. pp. 5, 7, 65, 91, 102).

[92] Greco L, Castello D, and Cuomo M. “An objective and accurate G^1-conforming mixed Bézier FE-formulation for Kirchhoff–Love rods”. In: *Mathematics and Mechanics of Solids*, 29(4): 645–685, 2024. DOI: 10.1177/10812865231204972 (cf. pp. 5, 65).

[93] Greenspan D. “Conservative numerical methods for $\ddot{x} = f(x)$”. In: *Journal of Computational Physics*, 56(1): 28–41, 1984. DOI: 10.1016/0021-9991(84)90081-0 (cf. p. 140).

[94] Gruttmann F, Sauer R, and Wagner W. “Theory and numerics of three-dimensional beams with elastoplastic material behaviour”. In: *International Journal for Numerical Methods in Engineering*, 48(12): 1675–1702, 2000. DOI: 10.1002/1097-0207(20000830)48:12<1675::AID-NME957>3.0.CO;2-6 (cf. pp. 3, 64).

[95] Guan Q, Dai B, Cheng HH, and Hughes J. “Lattice structure musculoskeletal robots: Harnessing programmable geometric topology and anisotropy”. In: *Science Advances*, 11(29): eadu9856, 2025. DOI: 10.1126/sciadv.adu9856 (cf. p. 2).

[96] Hairer E, Lubich C, and Wanner G. “Geometric numerical integration illustrated by the Störmer–Verlet method”. In: *Acta Numerica*, 12: 399–450, 2003. DOI: 10.1017/s0962492902000144 (cf. p. 143).

[97] Hairer E, Lubich C, and Wanner G. *Geometric Numerical Integration*. Berlin, Heidelberg: Springer, 2006. DOI: 10.1007/3-540-30666-8 (cf. pp. 4, 5, 10, 48, 63, 64, 77, 102, 107).

[98] Hammoud A, Liu N, Le Gorrec Y, Civet Y, and Perriard Y. “Energy-based modeling and robust position control of a dielectric elastomer cardiac assist device”. In: *IFAC-PapersOnLine*, 58(6): 25–30, 2024. DOI: 10.1016/j.ifacol.2024.08.251 (cf. p. 142).

[99] Hante S, Tumiotto D, and Arnold M. “A Lie group variational integration approach to the full discretization of a constrained geometrically exact Cosserat beam model”. In: *Multibody System Dynamics*, 54(1): 97–123, 2022. DOI: 10.1007/s11044-021-09807-8 (cf. pp. 54, 55).

[100] Harsch J, Capobianco G, and Eugster SR. “Finite element formulations for constrained spatial nonlinear beam theories”. In: *Mathematics and Mechanics of Solids*, 26(12): 1838–1863, 2021. DOI: 10.1177/10812865211000790 (cf. pp. 74, 88, 89, 92, 93).

[101] Harsch J and Eugster SR. “Nonunit quaternion parametrization of a Petrov–Galerkin Cosserat rod finite element”. In: *PAMM*, 23(4): e202300172, 2023. DOI: 10.1002/pamm.202300172 (cf. pp. 64, 91, 142).

[102] Harsch J, Sailer S, and Eugster SR. “A total Lagrangian, objective and intrinsically locking-free Petrov–Galerkin $SE(3)$ Cosserat rod finite element formulation”. In: *International Journal for Numerical Methods in Engineering*, 124(13): 2965–2994, 2023. DOI: 10.1002/nme.7236 (cf. pp. 3, 35, 142).

[103] Hartmann WM. *Signals, sound, and sensation*. Woodbury, N.Y: American Institute of Physics, 1997 (cf. p. 98).

[104] Herrmann M, Castello D, Breuling J, Garcia IC, Greco L, and Eugster SR. *A mixed Petrov-Galerkin Cosserat rod finite element formulation*. Preprint. 2026. arXiv: 2507.01552v3 [math.NA] (cf. pp. 3, 5, 6, 9, 26, 64, 65, 88, 89, 94, 142).

[105] Herrmann M and Kotyczka P. "Relative-kinematic formulation of geometrically exact beam dynamics based on Lie group variational integrators". In: *Computer Methods in Applied Mechanics and Engineering*, 432: 117367, 2024. DOI: 10.1016/j.cma.2024.117367 (cf. pp. 3, 5, 35, 64, 80, 86, 87).

[106] Hesse H and Palacios R. "Consistent structural linearisation in flexible-body dynamics with large rigid-body motion". In: *Computers & Structures*, 110–111: 1–14, 2012. DOI: 10.1016/j.compstruc.2012.05.011 (cf. pp. 83, 84).

[107] Hille M, Betsch P, and Franke M. *Port-Hamiltonian formulation and structure-preserving discretization of finite elasticity based on a mixed Hu-Washizu-type formulation*. Preprint. 2025. DOI: 10.2139/ssrn.5551747 (cf. p. 4).

[108] Hirsch MW and Smale S. *Differential Equations, Dynamical Systems, and Linear Algebra*. New York: Academic Press, 1974 (cf. p. 102).

[109] Hodges DH. "A mixed variational formulation based on exact intrinsic equations for dynamics of moving beams". In: *International Journal of Solids and Structures*, 26(11): 1253–1273, 1990. DOI: 10.1016/0020-7683(90)90060-9 (cf. p. 64).

[110] Holm DD, Schmah T, and Stoica C. *Geometric Mechanics and Symmetry: From Finite to Infinite Dimensions*. Oxford: Oxford University Press, 2009. DOI: 10.1093/oso/9780199212903.001.0001 (cf. pp. 23, 119).

[111] Holzapfel GA. *Nonlinear Solid Mechanics: A Continuum Approach for Engineering*. Chichester: Wiley, 2000 (cf. pp. 16, 25).

[112] Hsiao KM, Lin JY, and Lin WY. "A consistent co-rotational finite element formulation for geometrically nonlinear dynamic analysis of 3-D beams". In: *Computer Methods in Applied Mechanics and Engineering*, 169(1-2): 1–18, 1999. DOI: 10.1016/S0045-7825(98)00152-2 (cf. pp. 83, 85).

[113] Hsiao KM and Jang JY. "Dynamic analysis of planar flexible mechanisms by co-rotational formulation". In: *Computer Methods in Applied Mechanics and Engineering*, 87(1): 1–14, 1991. DOI: 10.1016/0045-7825(91)90143-T (cf. p. 53).

[114] Huang D and Leyendecker S. "An electromechanically coupled beam model for dielectric elastomer actuators". In: *Computational Mechanics*, 69(3): 805–824, 2022 (cf. pp. 3, 58, 64).

[115] Hughes TJR. *The Finite Element Method: Linear Static and Dynamic Finite Element Analysis*. Mineola: Dover Publications, 2000 (cf. pp. 4, 74, 75).

[116] Ibrahimbegović A and Mamouri S. "Nonlinear dynamics of flexible beams in planar motion: Formulation and time-stepping scheme for stiff problems". In: *Computers and Structures*, 70(1): 1–22, 1999. DOI: 10.1016/S0045-7949(98)00150-3 (cf. pp. 36, 50).

[117] Ibrahimbegovic A. "On the choice of finite rotation parameters". In: *Computer Methods in Applied Mechanics and Engineering*, 149(1-4): 49–71, 1997. DOI: 10.1016/S0045-7825(97)00059-5 (cf. p. 64).

[118] Jacob B and Zwart HJ. *Linear Port-Hamiltonian Systems on Infinite-Dimensional Spaces*. Basel: Springer, 2012. DOI: 10.1007/978-3-0348-0399-1 (cf. p. 36).

[119] Janz A. “Structure-preserving space-time discretization in a mixed framework for multi-field problems in large strain elasticity”. PhD thesis. Karlsruher Institut für Technologie (KIT), 2019. DOI: 10.5445/KSP/1000093768 (cf. pp. 1, 4, 5).

[120] Jüngel A, Stefanelli U, and Trussardi L. “Two structure-preserving time discretizations for gradient flows”. In: *Applied Mathematics and Optimization*, 80: 733–764, 2019. DOI: 10.1007/s00245-019-09605-x (cf. p. 102).

[121] Karlton DP. *Naming things is hard*. Dec 4th, 2017. Blog: https://www.karlton.org/2017/12/naming-things-hard/, Accessed: Mar 2nd, 2026 (cf. p. 11).

[122] Kim JG and Kim YY. “A new higher-order hybrid-mixed curved beam element”. In: *International Journal for Numerical Methods in Engineering*, 43(5): 925–940, 1998. DOI: 10.1002/(SICI)1097-0207(19981115)43:5<925::AID-NME457>3.0.CO;2-M (cf. pp. 5, 6, 65).

[123] Kim S, Hsiao YH, Ren Z, Huang J, and Chen Y. “Acrobatics at the insect scale: A durable, precise, and agile micro–aerial robot”. In: *Science Robotics*, 10(98): eadp4256, 2025. DOI: 10.1126/scirobotics.adp4256 (cf. p. 2).

[C2] Kinon PL, Thoma T, Betsch P, and Kotyczka P. “Port-Hamiltonian formulation and structure-preserving discretization of hyperelastic strings”. In: *Proceedings of the 11th ECCOMAS Thematic Conference on Multibody Dynamics*. Lisbon, Portugal, 2023, pp. 1–10. DOI: 10.48550/arXiv.2304.10957 (cf. pp. 12, 36, 37, 41, 48, 64, 65, 69, 71, 77, 91, 113, 116, 127–130, 133, 135, 136, 138, 140).

[124] Kinon PL. *plkinon/ph_cosserat_rods*. GitHub. 2025 (cf. p. 83).

[125] Kinon PL. *plkinon/ph_cosserat_rods, v0.0.5*. Zenodo. 2025. DOI: 10.5281/zenodo.18007057 (cf. p. 83).

[126] Kinon PL. *plkinon/phdae_discrete_gradients, v1.0.0*. Zenodo. 2026. DOI: 10.5281/zenodo.15007241 (cf. p. 122).

[F2] Kinon PL and Bauer JK. *pydykit: A Python-based dynamics simulation toolkit, v0.0.6*. Zenodo. 2025. DOI: 10.5281/zenodo.14849865 (cf. p. 122).

[A2] Kinon PL, Betsch P, and Eugster SR. “Energy-momentum-consistent simulation of planar geometrically exact beams in a port-Hamiltonian framework”. In: *Multibody System Dynamics*, 2025. DOI: 10.1007/s11044-025-10087-9 (cf. pp. 11, 35, 64, 65, 69, 71, 74, 145).

[B3] Kinon PL, Betsch P, and Schneider S. “Structure-preserving integrators based on a new variational principle for constrained mechanical systems”. In: *Nonlinear Dynamics*, 111: 14231–14261, 2023. DOI: 10.1007/s11071-023-08522-7 (cf. pp. 102, 121, 124).

[A4] Kinon PL, Eugster SR, and Betsch P. “Mixed formulation and structure-preserving discretization of Cosserat rod dynamics in a port-Hamiltonian framework”. In: *Computer Methods in Applied Mechanics and Engineering*, 458: 118966, 2026. DOI: 10.1016/j.cma.2026.118966 (cf. pp. 11, 26, 63, 145).

[A3] Kinon PL, Morandin R, and Schulze P. “Discrete gradient methods for port-Hamiltonian differential-algebraic equations”. In: *Applied Numerical Mathematics*, 223: 45–75, 2026. DOI: 10.1016/j.apnum.2025.12.006 (cf. pp. 12, 22, 65, 91, 101, 103, 109, 110, 113, 117, 119, 146).

[C4] Kinon PL, Thoma T, Betsch P, and Kotyczka P. “Discrete nonlinear elastodynamics in a port-Hamiltonian framework”. In: *PAMM*, 23(3): e202300144, 2023. DOI: 10.1002/pamm.202300144 (cf. pp. 4, 7, 15, 16, 24, 37, 48, 65, 77, 91, 102, 107, 109, 113, 116, 128, 134, 135).

[A1] Kinon PL, Thoma T, Betsch P, and Kotyczka P. "Generalized Maxwell viscoelasticity for geometrically exact strings: Nonlinear port-Hamiltonian formulation and structure-preserving discretization". In: *IFAC-PapersOnLine*, 58(6): 101–106, 2024. DOI: 10.1016/j.ifacol.2024.08.264 (cf. pp. 12, 36, 37, 43, 48, 58, 64, 65, 71, 79, 81, 127, 130, 132, 136–138, 146).

[127] Kotyczka P and Lefèvre L. "Discrete-time port-Hamiltonian systems: A definition based on symplectic integration". In: *Systems & Control Letters*, 133: 104530, 2019. DOI: 10.1016/j.sysconle.2019.104530 (cf. pp. 5, 102, 107).

[128] Kotyczka P. *Numerical Methods for Distributed Parameter Port-Hamiltonian Systems*. Munich: TUM.University Press, 2019. DOI: 10.14459/2019md1510230 (cf. pp. 3, 4, 13, 32).

[129] Kotyczka P, Maschke B, and Lefèvre L. "Weak form of Stokes–Dirac structures and geometric discretization of port-Hamiltonian systems". In: *Journal of Computational Physics*, 361: 442–476, 2018. DOI: 10.1016/j.jcp.2018.02.006 (cf. p. 32).

[130] Krenk S. *Non-linear Modeling and Analysis of Solids and Structures*. Cambridge, New York: Cambridge University Press, 2009 (cf. p. 15).

[131] Kunkel P and Mehrmann V. "Discretization of inherent ODEs and the geometric integration of DAEs with symmetries". In: *BIT Numerical Mathematics*, 63: 29, 2023. DOI: 10.1007/s10543-023-00966-y (cf. p. 102).

[132] Kunkel P and Mehrmann V. *Differential-algebraic equations: Analysis and numerical solution*. 1st ed. Zurich: European Mathematical Society, 2006. DOI: 10.4171/017 (cf. pp. 105, 116).

[133] Lang H and Arnold M. "Numerical aspects in the dynamic simulation of geometrically exact rods". In: *Applied Numerical Mathematics*, 62(10): 1411–1427, 2012. DOI: 10.1016/j.apnum.2012.06.011 (cf. pp. 3, 35, 64, 91, 142).

[134] Lang H, Linn J, and Arnold M. "Multi-body dynamics simulation of geometrically exact Cosserat rods". In: *Multibody System Dynamics*, 25(3): 285–312, 2011. DOI: 10.1007/s11044-010-9223-x (cf. pp. 3, 35).

[B6] Latussek L, Kinon PL, and Betsch P. "Port-Hamiltonian multibody dynamics: Lagrangian formulation, consistent interconnection, structure-preserving simulation and index-reduction". In: *Multibody System Dynamics (under review)*, 2026. DOI: 10.48550/arXiv.2603.12841 (cf. pp. 23, 27, 111, 120, 142).

[135] Le Gorrec Y, Zwart H, and Maschke B. "Dirac structures and boundary control systems associated with skew-symmetric differential operators". In: *SIAM Journal on Control and Optimization*, 44(5): 1864–1892, 2005. DOI: 10.1137/040611677 (cf. pp. 4, 31, 33).

[136] Lee T. "Computational geometric mechanics and control of rigid bodies". PhD thesis. The University of Michigan, 2008 (cf. p. 5).

[137] Leimkuhler BJ and Reich S. *Simulating Hamiltonian Dynamics*. Cambridge, New York: Cambridge University Press, 2005. DOI: 10.1017/CBO9780511614118 (cf. pp. 13, 15).

[138] Leimkuhler BJ and Skeel RD. "Symplectic numerical integrators in constrained Hamiltonian systems". In: *Journal of Computational Physics*, 112(1): 117–125, 1994. DOI: 10.1006/jcph.1994.1085 (cf. pp. 5, 102).

[139] Leitz T, Almagro RTSM de, and Leyendecker S. "Multisymplectic Galerkin Lie group variational integrators for geometrically exact beam dynamics based on unit dual quaternion interpolation — no shear locking". In: *Computer Methods in Applied Mechanics and Engineering*, 374: 113475, 2021. DOI: 10.1016/j.cma.2020.113475 (cf. pp. 3, 5, 35).

[140] Lestringant C, Audoly B, and Kochmann DM. "A discrete, geometrically exact method for simulating nonlinear, elastic and inelastic beams". In: *Computer Methods in Applied Mechanics and Engineering*, 361: 112741, 2020. DOI: 10.1016/j.cma.2019.112741 (cf. pp. 3, 9, 65, 79).

[141] Leyendecker S, Betsch P, and Steinmann P. "Objective energy-momentum conserving integration for the constrained dynamics of geometrically exact beams". In: *Computer Methods in Applied Mechanics and Engineering*, 195(19-22): 2313–2333, 2006. DOI: 10.1016/j.cma.2005.05.002 (cf. pp. 3, 5, 35, 36, 64).

[142] Leyendecker S, Marsden J, and Ortiz M. "Variational integrators for constrained dynamical systems". In: *ZAMM - Journal of Applied Mathematics and Mechanics / Zeitschrift für Angewandte Mathematik und Mechanik*, 88(9): 677–708, 2008. DOI: 10.1002/zamm.200700173 (cf. pp. 5, 102).

[143] Leyendecker S, Betsch P, and Steinmann P. "The discrete null space method for the energy-consistent integration of constrained mechanical systems. Part III: Flexible multibody dynamics". In: *Multibody System Dynamics*, 19(1-2): 45–72, 2008. DOI: 10.1007/s11044-007-9056-4 (cf. pp. 3, 64).

[144] Linn J, Lang H, and Tuganov A. "Geometrically exact Cosserat rods with Kelvin-Voigt type viscous damping". In: *Mechanical Sciences*, 4(1): 79–96, 2013. DOI: 10.5194/ms-4-79-2013 (cf. pp. 3, 79, 80, 128).

[145] Ljukovac S and Ibrahimbegovic A. "Control for (highly) flexible geometrically exact 2D Reissner beam by energy shaping of distributed port-Hamiltonian system". In: *Multibody System Dynamics*, 2026. DOI: 10.1007/s11044-025-10139-0 (cf. p. 143).

[146] Ljukovac S, Ibrahimbegovic A, and Husic MC. "Nonlinear dynamics and control of Reissner's 2D geometrically exact beam by distributed port-Hamiltonian system". In: *International Journal for Numerical Methods in Engineering*, 126(16): e70103, 2025. DOI: 10.1002/nme.70103 (cf. p. 143).

[147] Lohmayer M, Capobianco G, and Leyendecker S. "Exergetic port-Hamiltonian systems for multibody dynamics". In: *Multibody System Dynamics*, 65(2): 305–333, 2025. DOI: 10.1007/s11044-024-10038-w (cf. pp. 4, 142).

[148] Macchelli A, van der Schaft AJ, and Melchiorri C. "Multi-variable port Hamiltonian model of piezoelectric material". In: *2004 IEEE/RSJ International Conference on Intelligent Robots and Systems (IROS)*. Sendai, Japan, 2004, pp. 897–902. DOI: 10.1109/IROS.2004.1389466 (cf. p. 3).

[149] Macchelli A. "Port-Hamiltonian formulation of simple macro-economic systems". In: *52nd IEEE Conference on Decision and Control*. Firenze, Italy, 2013, pp. 3888–3893. DOI: 10.1109/CDC.2013.6760483 (cf. p. 3).

[150] Macchelli A. "Stabilisation of a nonlinear flexible beam in port-Hamiltonian form". In: *IFAC Proceedings Volumes*, 46(23): 412–417, 2013. DOI: 10.3182/20130904-3-FR-2041.00115 (cf. p. 64).

[151] Macchelli A and Melchiorri C. "Modeling and control of the Timoshenko beam. The distributed port Hamiltonian approach". In: *SIAM journal on control and optimization*, 43(2): 743–767, 2004. DOI: 10.1137/S0363012903429530 (cf. pp. 4, 36, 64).

[152] Macchelli A, Melchiorri C, and Stramigioli S. "Port-based modeling of a flexible link". In: *IEEE Transactions on Robotics*, 23(4): 650–660, 2007. DOI: 10.1109/TRO.2007.898990 (cf. pp. 4, 6, 36, 64, 65).

[153] Macchelli A, Melchiorri C, and Stramigioli S. "Port-based modeling and simulation of mechanical systems with rigid and flexible links". In: *IEEE Transactions on Robotics*, 25(5): 1016–1029, 2009. DOI: 10.1109/TRO.2009.2026504 (cf. pp. 4, 6, 142).

[154] Marino E. “Locking-free isogeometric collocation formulation for three-dimensional geometrically exact shear-deformable beams with arbitrary initial curvature”. In: *Computer Methods in Applied Mechanics and Engineering*, 324: 546–572, 2017. DOI: 10.1016/j.cma.2017.06.031 (cf. p. 65).

[155] Marino E, Kiendl J, and De Lorenzis L. “Isogeometric collocation for implicit dynamics of three-dimensional beams undergoing finite motions”. In: *Computer Methods in Applied Mechanics and Engineering*, 356: 548–570, 2019. DOI: 10.1016/j.cma.2019.07.013 (cf. p. 83).

[156] Marsden JE and West M. “Discrete mechanics and variational integrators”. In: *Acta Numerica*, 10: 357–514, 2001. DOI: 10.1017/S096249290100006X (cf. pp. 5, 102).

[157] Marsden JE and Ratiu TS. *Introduction to Mechanics and Symmetry: A Basic Exposition of Classical Mechanical Systems*. 2nd ed. New York: Springer, 1999 (cf. p. 16).

[158] Maschke B and van der Schaft AJ. “Port-controlled Hamiltonian systems: Modelling origins and systemtheoretic properties”. In: *IFAC Proceedings Volumes*, 25(13): 359–365, 1992. DOI: 10.1016/S1474-6670(17)52308-3 (cf. pp. 3, 64).

[159] May M and Betsch P. “Galerkin-based time integration approaches to rigid body dynamics in terms of unit quaternions”. In: *Multibody System Dynamics*, 2025. DOI: 10.1007/s11044-025-10093-x (cf. pp. 102, 143).

[160] McLachlan RI, Quispel GRW, and Robidoux N. “Geometric integration using discrete gradients”. In: *Philosophical Transactions of the Royal Society A: Mathematical, Physical and Engineering Sciences*, 357(1754): 1021–1045, 1999. Ed. by Budd C and Iserles A. DOI: 10.1098/rsta.1999.0363 (cf. pp. 5, 7, 10, 107, 108, 116).

[161] Mehrmann V and Morandin R. “Structure-preserving discretization for port-Hamiltonian descriptor systems”. In: *IEEE 58th Conference on Decision and Control (CDC)*. Nice, France, 2019, pp. 6863–6868. DOI: 10.1109/CDC40024.2019.9030180 (cf. pp. 4, 5, 8, 22, 24, 37, 41, 47, 65, 71, 75, 81, 101–103, 105–107, 128, 129).

[162] Mehrmann V and Unger B. “Control of port-Hamiltonian differential-algebraic systems and applications”. In: *Acta Numerica*, 32: 395–515, 2023. DOI: 10.1017/S0962492922000083 (cf. pp. 3, 4, 8, 37, 41, 47, 65, 71, 75, 81, 91, 106).

[163] Meier C, Popp A, and Wall WA. “Geometrically exact finite element formulations for slender beams: Kirchhoff-Love theory versus Simo-Reissner theory”. In: *Archives of Computational Methods in Engineering*, 26(1): 163–243, 2019. DOI: 10.1007/s11831-017-9232-5 (cf. p. 35).

[164] Mönch M and Marheineke N. “Commutator-based operator splitting for linear port-Hamiltonian systems”. In: *Applied Numerical Mathematics*, 210: 25–38, 2025. DOI: 10.1016/j.apnum.2024.12.007 (cf. pp. 5, 102).

[165] Morandin R. “Modeling and numerical treatment of port-Hamiltonian descriptor systems”. PhD thesis. Technische Universität Berlin, 2023. DOI: 10.14279/depositonce-19826 (cf. pp. 3, 4, 23, 106, 107, 110, 117).

[166] Moreschini A, Mattioni M, Monaco S, and Normand-Cyrot D. “Discrete port-controlled Hamiltonian dynamics and average passivation”. In: *58th IEEE Conference on Decision and Control (CDC)*. Nice, France, 2019, pp. 1430–1435. DOI: 10.1109/CDC40024.2019.9029809 (cf. pp. 7, 102).

[167] Moreschini A, Monaco S, and Normand-Cyrot D. “Dirac structures for a class of port-Hamiltonian systems in discrete time”. In: *IEEE Transactions on Automatic Control*, 69(3): 1999–2006, 2024. DOI: 10.1109/TAC.2023.3313327 (cf. p. 107).

[168] Myhr HN and Eidnes S. “Derivative-free discrete gradient methods”. In: *Journal of Computational Dynamics*, 11(3): 256–273, 2024. DOI: 10.3934/jcd.2024004 (cf. pp. 5, 143).

[169] Nishida G and Yamakita M. “A higher order Stokes-Dirac structure for distributed-parameter port-Hamiltonian systems”. In: *Proceedings of the 2004 American Control Conference*. Boston, USA, 2004, pp. 5004–5009. DOI: 10.23919/ACC.2004.1384643 (cf. p. 4).

[170] Nishida G and Sakamoto N. “Port-based modeling of magnetohydrodynamics equations for Tokamaks”. In: *IEEE International Conference on Control Applications*. Yokohama, Japan, 2010, pp. 842–847. DOI: 10.1109/CCA.2010.5611289 (cf. p. 3).

[171] Ortega R, van der Schaft AJ, Maschke B, and Escobar G. “Interconnection and damping assignment passivity-based control of port-controlled Hamiltonian systems”. In: *Automatica*, 38(4): 585–596, 2002. DOI: 10.1016/S0005-1098(01)00278-3 (cf. pp. 64, 91, 143).

[172] Öttinger HC. “GENERIC integrators: Structure preserving time integration for thermodynamic systems”. In: *Journal of Non-equilibrium Thermodynamics*, 43(2): 89–100, 2018. DOI: 10.1515/jnet-2017-0034 (cf. p. 102).

[173] Paynter HM. *Analysis and Design of Engineering Systems*. Cambridge: The M.I.T. Press, 1961 (cf. p. 3).

[174] Pfefferkorn R. “EAS elements for solid mechanics — Mesh distortion insensitive and hourglassing-free formulations with increased robustness”. PhD thesis. Karlsruher Institut für Technologie (KIT), 2023. DOI: 10.5445/KSP/1000154549 (cf. p. 4).

[175] Philo N. *Micrograph of hook and loop fastener, (Velcro like)*. Wikipedia: https://commons.wikimedia.org/wiki/File:Micrograph_of_hook_and_loop_fastener,(Velcro_like).jpg, Copyright: CC BY-SA 3.0. 2005 (cf. p. 2).

[176] Pian THH and Sumihara K. “Rational approach for assumed stress finite elements”. In: *International Journal for Numerical Methods in Engineering*, 20(9): 1685–1695, 1984. DOI: 10.1002/nme.1620200911 (cf. pp. 5, 142).

[177] Ponce C, Ramirez H, Le Gorrec Y, and Wu Y. “Constrained port-Hamiltonian modeling and structure-preserving discretization of the Rayleigh beam”. In: *IFAC-PapersOnLine*, 59(8): 108–113, 2025. DOI: 10.1016/j.ifacol.2025.08.075 (cf. pp. 4, 6, 64).

[178] Ponce C, Wu Y, Gorrec YL, and Ramirez H. “A systematic methodology for port-Hamiltonian modeling of multidimensional flexible linear mechanical systems”. In: *Applied Mathematical Modelling*, 134: 434–451, 2024. DOI: 10.1016/j.apm.2024.05.040 (cf. p. 138).

[179] Ponce C, Wu Y, Le Gorrec Y, and Ramirez H. “Port-Hamiltonian modeling of a geometrically nonlinear hyperelastic beam”. In: *IFAC-PapersOnLine*, 58(6): 309–314, 2024. DOI: 10.1016/j.ifacol.2024.08.299 (cf. pp. 4, 6, 36, 64).

[180] Ponce C, Wu Y, Le Gorrec Y, and Ramirez H. “A port-Hamiltonian framework for the modeling and FEM discretization of hyperelastic systems”. In: *Applied Mathematical Modelling*, 150: 116403, 2026. DOI: 10.1016/j.apm.2025.116403 (cf. p. 4).

[181] Rabier P and Rheinboldt W. “On impasse points of quasilinear differential-algebraic equations”. In: *Journal of Mathematical Analysis and Applications*, 181(2): 429–454, 1994. DOI: 10.1006/jmaa.1994.1033 (cf. p. 104).

[182] Ramirez H, Maschke B, and Sbarbaro D. “Irreversible port-Hamiltonian systems: A general formulation of irreversible processes with application to the CSTR”. In: *Chemical Engineering Science*, 89: 223–234, 2013. DOI: 10.1016/j.ces.2012.12.002 (cf. p. 3).

[183] Rashad R, Califano F, van der Schaft AJ, and Stramigioli S. “Twenty years of distributed port-Hamiltonian systems: A literature review”. In: *IMA Journal of Mathematical Control and Information*, 37(4): 1400–1422, 2020. DOI: 10.1093/imamci/dnaa018 (cf. pp. 3, 4, 36, 64, 127).

[184] Rashad R and Stramigioli S. “The port-Hamiltonian structure of continuum mechanics”. In: *Journal of Nonlinear Science*, 35(2): 35, 2025. DOI: 10.1007/s00332-025-10130-1 (cf. p. 4).

[185] Reddy JN. *Theory and Analysis of Elastic Plates and Shells*. 2nd ed. Boca Raton: CRC Press, 2006. DOI: 10.1201/9780849384165 (cf. p. 142).

[186] Reissner E. “On one-dimensional large-displacement finite-strain beam theory”. In: *Studies in Applied Mathematics*, 52(2): 87–95, 1973. DOI: 10.1002/sapm197352287 (cf. p. 8).

[187] Reissner E. “On one-dimensional finite-strain beam theory: The plane problem”. In: *Journal of Applied Mathematics and Physics (ZAMP)*, 23(5): 795–804, 1972. DOI: 10.1007/BF01602645 (cf. pp. 2, 35, 39, 64).

[188] Ren H, Fan W, and Zhu WD. “An accurate and robust geometrically exact curved beam formulation for multibody dynamic analysis”. In: *Journal of Vibration and Acoustics*, 140(1): 011012, 2018. DOI: 10.1115/1.4037513 (cf. p. 54).

[189] Renardy M and Rogers RC. *An Introduction to Partial Differential Equations*. 2nd ed. New York: Springer, 2004. DOI: 10.1007/b97427 (cf. pp. 28–30).

[190] Ringelnatz J. *Ich habe dich so lieb! Die schönsten Liebesgedichte von Joachim Ringelnatz*. Zürich: Diogenes, 2007.

[191] Rizzello G, Naso D, and Seelecke S. “A thermodynamically consistent port-Hamiltonian model for dielectric elastomer membrane actuators and generators”. In: *IFAC-PapersOnLine*, 50(1): 4855–4862, 2017. DOI: 10.1016/j.ifacol.2017.08.974 (cf. p. 142).

[192] Rodriguez CM. “Control and stabilization of geometrically exact beams”. PhD thesis. Friedrich-Alexander-Universität Erlangen-Nürnberg, 2022. DOI: 10.48550/arXiv.2202.07531 (cf. p. 64).

[193] Romero I and Armero F. “An objective finite element approximation of the kinematics of geometrically exact rods and its use in the formulation of an energy–momentum conserving scheme in dynamics”. In: *International Journal for Numerical Methods in Engineering*, 54(12): 1683–1716, 2002. DOI: 10.1002/nme.486 (cf. pp. 3, 5, 6, 9, 10, 64, 65, 67, 73, 74, 76, 93, 96).

[194] Romero I. “The interpolation of rotations and its application to finite element models of geometrically exact rods”. In: *Computational Mechanics*, 34(2), 2004. DOI: 10.1007/s00466-004-0559-z (cf. p. 64).

[195] Rucker DC and Webster III RJ. “Statics and dynamics of continuum robots with general tendon routing and external loading”. In: *IEEE Transactions on Robotics*, 27(6): 1033–1044, 2011. DOI: 10.1109/TRO.2011.2160469 (cf. pp. 3, 9, 64, 65, 81).

[196] Santos H, Pimenta P, and Moitinho De Almeida J. “Hybrid and multi-field variational principles for geometrically exact three-dimensional beams”. In: *International Journal of Non-Linear Mechanics*, 45(8): 809–820, 2010. DOI: 10.1016/j.ijnonlinmec.2010.06.003 (cf. pp. 5, 6, 65).

[197] Sato S. “Linear gradient structures and discrete gradient methods for conservative/dissipative differential-algebraic equations”. In: *BIT Numerical Mathematics*, 59(4): 1063–1091, 2019. DOI: 10.1007/s10543-019-00759-2 (cf. p. 102).

[198] Savin A. *Koblenz Seilbahn Wagen mit Bodenfenster*. Wikipedia: https://commons.wikimedia.org/wiki/File:Koblenz_Seilbahn_Wagen_mit_Bodenfenster.jpg, Copyright: CC BY-SA 3.0. 2012 (cf. p. 2).

[199] Schaller M, Philipp F, Faulwasser T, Worthmann K, and Maschke B. “Control of port-Hamiltonian systems with minimal energy supply”. In: *European Journal of Control*, 62: 33–40, 2021. DOI: 10.1016/j.ejcon.2021.06.017 (cf. p. 143).

[200] Schaller M, Zeller A, Böhm M, Sawodny O, Tarín C, and Worthmann K. "Energy-optimal control of adaptive structures". In: *at - Automatisierungstechnik*, 72(2): 107–119, 2024. DOI: 10.1515/auto-2023-0090 (cf. p. 143).

[201] Schulze P. *Structure-preserving time discretization of port-Hamiltonian systems via discrete gradient pairs*. Preprint. 2023. arXiv: 2311.00403v1 [math.NA] (cf. pp. 5, 7, 103, 107, 109, 128, 135).

[202] Shabana AA. "Flexible multibody dynamics: Review of past and recent developments". In: *Multibody System Dynamics*, 1(2): 189–222, 1997. DOI: 10.1023/A:1009773505418 (cf. pp. 2, 35).

[203] Simeon B. *Computational Flexible Multibody Dynamics: A Differential-Algebraic Approach*. Berlin, Heidelberg: Springer, 2013. DOI: 10.1007/978-3-642-35158-7 (cf. p. 2).

[204] Simo JC and Hughes TJR. *Computational Inelasticity*. New York: Springer, 1998. DOI: 10.1007/b98904 (cf. pp. 6, 9, 79, 81, 128, 130, 131, 135).

[205] Simo JC and Vu-Quoc L. "On the dynamics of flexible beams under large overall motions — The plane case: Part II". In: *Journal of Applied Mechanics*, 53(4): 855–863, 1986. DOI: 10.1115/1.3171871 (cf. pp. 53, 54).

[206] Simo JC and Rifai MS. "A class of mixed assumed strain methods and the method of incompatible modes". In: *International Journal for Numerical Methods in Engineering*, 29(8): 1595–1638, 1990. DOI: 10.1002/nme.1620290802 (cf. pp. 5, 142).

[207] Simo JC and Tarnow N. "The discrete energy-momentum method. Conserving algorithms for nonlinear elastodynamics". In: *Journal of Applied Mathematics and Physics (ZAMP)*, 43(5): 757–792, 1992. DOI: 10.1007/bf00913408 (cf. pp. 5, 102).

[208] Simo JC, Tarnow N, and Doblare M. "Non-linear dynamics of three-dimensional rods: Exact energy and momentum conserving algorithms". In: *International Journal for Numerical Methods in Engineering*, 38(9): 1431–1473, 1995. DOI: 10.1002/nme.1620380903 (cf. pp. 5, 64, 83).

[209] Simo J. "A finite strain beam formulation. The three-dimensional dynamic problem. Part I". In: *Computer Methods in Applied Mechanics and Engineering*, 49(1): 55–70, 1985. DOI: 10.1016/0045-7825(85)90050-7 (cf. pp. 2, 8, 35, 64, 69, 93).

[210] Simo J and Vu-Quoc L. "On the dynamics in space of rods undergoing large motions — A geometrically exact approach". In: *Computer Methods in Applied Mechanics and Engineering*, 66(2): 125–161, 1988. DOI: 10.1016/0045-7825(88)90073-4 (cf. p. 83).

[211] Simoes AA, Martín de Diego D, and Maschke B. *Discrete gradient methods for irreversible port-Hamiltonian systems*. Preprint. 2023. arXiv: 2303.08034v1 [math.NA] (cf. p. 102).

[212] Sonneville V, Cardona A, and Brüls O. "Geometrically exact beam finite element formulated on the special Euclidean group $SE(3)$". In: *Computer Methods in Applied Mechanics and Engineering*, 268: 451–474, 2014. DOI: 10.1016/j.cma.2013.10.008 (cf. p. 64).

[213] Stander N and Stein E. "An energy-conserving planar finite beam element for dynamics of flexible mechanisms". In: *Engineering Computations*, 13(6): 60–85, 1996. DOI: 10.1108/02644409610128418 (cf. pp. 5, 6, 36, 49–52, 55, 57).

[214] Steinbrecher A. "Numerical solution of quasi-linear differential-algebraic equations and industrial simulation of multibody systems". PhD thesis. Technische Universität Berlin, 2006. DOI: 10.14279/depositonce-1360 (cf. p. 104).

[215] Ströhle T and Betsch P. "A simultaneous space-time discretization approach to the inverse dynamics of geometrically exact strings". In: *International Journal for Numerical Methods in Engineering*, 123(11): 2573–2609, 2022. DOI: 10.1002/nme.6951 (cf. pp. 127, 138).

[216] Thoma T. “Energy-based numerical models for simulation and control of flexible mechanical systems”. PhD thesis. Technische Universität München, 2026 (cf. pp. 23, 33).

[217] Thoma T and Kotyczka P. “Explicit port-Hamiltonian FEM-models for linear mechanical systems with non-uniform boundary conditions”. In: *IFAC-PapersOnLine*, 55(20): 499–504, 2022. DOI: 10.1016/j.ifacol.2022.09.144 (cf. pp. 43, 73, 142).

[218] Thoma T and Kotyczka P. “Port-Hamiltonian FE models for filaments”. In: *IFAC-PapersOnLine*, 55(30): 353–358, 2022. DOI: 10.1016/j.ifacol.2022.11.078 (cf. pp. 4, 6, 26, 29, 36, 43, 64, 65, 73, 127, 128, 137–139, 142).

[219] Thoma T, Kotyczka P, and Egger H. “On the velocity-stress formulation for geometrically nonlinear elastodynamics and its structure-preserving discretization”. In: *Mathematical and Computer Modelling of Dynamical Systems*, 30(1): 701–720, 2024. DOI: 10.1080/13873954.2024.2397486 (cf. pp. 4, 6, 26, 36, 41, 65, 142, 143).

[220] Till J, Aloi V, and Rucker C. “Real-time dynamics of soft and continuum robots based on Cosserat rod models”. In: *The International Journal of Robotics Research*, 38(6): 723–746, 2019. DOI: 10.1177/0278364919842269 (cf. pp. 3, 9, 64, 65, 81).

[221] Trivedi M, Banavar R, and Maschke B. “Modeling of hybrid lumped-distributed parameter mechanical systems with multiple equilibria.” In: *IFAC Proceedings Volumes*, 44(1): 7696–7701, 2011. DOI: 10.3182/20110828-6-IT-1002.03070 (cf. pp. 4, 6).

[222] van der Schaft A. *L_2-Gain and Passivity Techniques in Nonlinear Control*. 3rd ed. Cham: Springer, 2017. DOI: 10.1007/978-3-319-49992-5 (cf. p. 14).

[223] van der Schaft AJ. “Port-Hamiltonian differential-algebraic systems”. In: *Surveys in Differential-Algebraic Equations I*. Ed. by Ilchmann A and Reis T. Berlin, Heidelberg: Springer, 2013, pp. 173–226. DOI: 10.1007/978-3-642-34928-7_5 (cf. pp. 4, 13, 17, 18, 20, 101, 105, 111).

[224] van der Schaft AJ and Jeltsema D. “Port-Hamiltonian systems theory: An introductory overview”. In: *Foundations and Trends® in Systems and Control*, 1(2-3): 173–378, 2014. DOI: 10.1561/2600000002 (cf. pp. 3, 4, 13–15, 17–19, 35, 101, 105).

[225] van der Schaft AJ and Maschke BM. “Hamiltonian formulation of distributed-parameter systems with boundary energy flow”. In: *Journal of Geometry and Physics*, 42(1-2): 166–194, 2002. DOI: 10.1016/S0393-0440(01)00083-3 (cf. pp. 4, 36, 40, 41, 64).

[226] van der Schaft AJ and Maschke B. “Fluid dynamical systems as Hamiltonian boundary control systems”. In: *Proceedings of the 40th IEEE Conference on Decision and Control (Cat. No.01CH37228)*. Vol. 5. Orlando, FL, USA: IEEE, 2001, pp. 4497–4502. DOI: 10.1109/CDC.2001.980911 (cf. p. 3).

[227] van der Schaft AJ and Maschke B. “A port-Hamiltonian formulation of open chemical reaction networks”. In: *Advances in the Theory of Control, Signals and Systems with Physical Modeling*. Ed. by Morari M, Thoma M, Lévine J, and Müllhaupt P. Berlin, Heidelberg: Springer, 2010, pp. 339–348. DOI: 10.1007/978-3-642-16135-3_27 (cf. p. 3).

[228] van der Schaft AJ and Maschke B. “Generalized port-Hamiltonian DAE systems”. In: *Systems & Control Letters*, 121: 31–37, 2018. DOI: 10.1016/j.sysconle.2018.09.008 (cf. pp. 4, 101, 142).

[229] van der Schaft AJ and Maschke B. “Dirac and Lagrange algebraic constraints in nonlinear port-Hamiltonian systems”. In: *Vietnam Journal of Mathematics*, 48(4): 929–939, 2020. DOI: 10.1007/s10013-020-00419-x (cf. p. 101).

[230] Verrier G, Haine G, and Matignon D. “Modelling and structure-preserving discretization of the Schrödinger as a port-Hamiltonian system, and simulation of a controlled quantum box”. In: *Geometric Science of Information*. Ed. by Nielsen F and Barbaresco F. Cham: Springer, 2023, pp. 392–401. DOI: 10.1007/978-3-031-38299-4_41 (cf. p. 3).

[231] Wackerfuß J and Gruttmann F. "A mixed hybrid finite beam element with an interface to arbitrary three-dimensional material models". In: *Computer Methods in Applied Mechanics and Engineering*, 198(27-29): 2053–2066, 2009. DOI: 10.1016/j.cma.2009.01.020 (cf. pp. 5, 65).

[232] Wagner W and Gruttmann F. "A robust non-linear mixed hybrid quadrilateral shell element". In: *International Journal for Numerical Methods in Engineering*, 64(5): 635–666, 2005. DOI: 10.1002/nme.1387 (cf. p. 4).

[233] Wang L, Wang Y, Recuero AM, and Shabana AA. "ANCF analysis of textile systems". In: *Journal of Computational and Nonlinear Dynamics*, 11(3): 031005, 2016. DOI: 10.1115/1.4031289 (cf. p. 2).

[234] Warsewa A, Böhm M, Sawodny O, and Tarín C. "A port-Hamiltonian approach to modeling the structural dynamics of complex systems". In: *Applied Mathematical Modelling*, 89: 1528–1546, 2021. DOI: 10.1016/j.apm.2020.07.038 (cf. pp. 4–6, 9, 36, 64).

[235] Wasmer P and Betsch P. "A projection-based quaternion discretization of the geometrically exact beam model". In: *International Journal for Numerical Methods in Engineering*, 125(20): e7538, 2024. DOI: 10.1002/nme.7538 (cf. pp. 3, 35, 54, 64, 74, 91, 142).

[236] Weeger O, Schillinger D, and Müller R. "Mixed isogeometric collocation for geometrically exact 3D beams with elasto-visco-plastic material behavior and softening effects". In: *Computer Methods in Applied Mechanics and Engineering*, 399: 115456, 2022. DOI: 10.1016/j.cma.2022.115456 (cf. pp. 3, 9, 65, 79).

[237] Willems JC. "Dissipative dynamical systems part I: General theory". In: *Archive for Rational Mechanics and Analysis*, 45(5): 321–351, 1972. DOI: 10.1007/BF00276493 (cf. pp. 14, 15).

[238] Witz J and Tan Z. "Rotary bending of marine cables and umbilicals". In: *Engineering Structures*, 17(4): 267–275, 1995. DOI: 10.1016/0141-0296(95)00025-3 (cf. p. 2).

[239] Woernle C. *Multibody Systems: An Introduction to the Kinematics and Dynamics of Systems of Rigid Bodies*. Berlin, Heidelberg: Springer, 2024. DOI: 10.1007/978-3-662-67262-4 (cf. p. 2).

[240] Wriggers P. *Nonlinear Finite Element Methods*. Berlin, Heidelberg: Springer, 2008. DOI: 10.1007/978-3-540-71001-1 (cf. p. 45).

[241] Yu X, Zwölfer A, and Mikkola A. "An efficient, floating-frame-of-reference-based recursive formulation to model planar flexible multibody applications". In: *Journal of Sound and Vibration*, 547: 117542, 2023. DOI: 10.1016/j.jsv.2022.117542 (cf. p. 56).

[242] Zhang R and Zhong H. "A quadrature element formulation of an energy-momentum conserving algorithm for dynamic analysis of geometrically exact beams". In: *Computers & Structures*, 165: 96–106, 2016. DOI: 10.1016/j.compstruc.2015.12.007 (cf. pp. 83–85).

[243] Zienkiewicz OC, Taylor RL, and Zhu JZ. *The Finite Element Method: Its Basis and Fundamentals*. 6th ed. Amsterdam, Boston: Elsevier, 2005 (cf. pp. 4, 44, 45).

[244] Zupan D and Saje M. "Finite-element formulation of geometrically exact three-dimensional beam theories based on interpolation of strain measures". In: *Computer Methods in Applied Mechanics and Engineering*, 192(49-50): 5209–5248, 2003. DOI: 10.1016/j.cma.2003.07.008 (cf. pp. 5, 6, 65).

[245] Zupan E and Zupan D. "On conservation of energy and kinematic compatibility in dynamics of nonlinear velocity-based three-dimensional beams". In: *Nonlinear Dynamics*, 95(2): 1379–1394, 2019. DOI: 10.1007/s11071-018-4634-y (cf. pp. 83, 84).

[246] Zwart H. "From Dirac structures to port-Hamiltonian partial differential equations, a tutorial introduction". In: *Entropy*, 28(3), 2026. DOI: 10.3390/e28030292 (cf. pp. 17, 28, 33).

[247] Zwart H and Mehrmann V. “Abstract dissipative Hamiltonian differential-algebraic equations are everywhere”. In: *DAE Panel*, 2, 2024. DOI: 10.52825/dae-p.v2i.957 (cf. pp. 128, 129).